

Quantum Chaos in the Delta Kicked Harmonic Oscillator

Graham Kells
B.Sc.



NUI MAYNOOTH

Ollscoil na hÉireann Mhá Nuad

Thesis presented for the degree of
Doctor of Philosophy

to the

Mathematical Physics Department
Faculty of Science
National University of Ireland, Maynooth

Research Supervisors
Prof. Daniel Heffernan
Dr. Jason Twamley

July 2005

To Jim and Margaret

Contents

1	Introduction	2
1.1	Classical Chaos and Quantum Chaos	2
1.1.1	Time Dependent Hamiltonians	5
1.2	Study outline	10
	References	13
2	The Classical System	16
2.1	Introduction	16
2.2	The delta kicked harmonic oscillator	18
2.2.1	The system in action-angle coordinates	23
2.3	General properties of the Classical System	25
2.3.1	Irrational frequency ratios	26
2.3.2	Rational frequency ratio, $1/R=1/4$	33
2.4	Diffusion properties of the $1/R=1/4$ system	37
2.4.1	Structure of the quasi-periodic islands	43
2.4.2	Structure in the accelerator modes	46
2.5	Conclusion	53
	References	54
3	The Quantum System	56
3.1	Introduction	56
3.2	The Fractional Order Fourier Transform and its relationship with the SHO	58
3.3	The Floquet operator for the kicked system	60
3.4	Quasi-energies and Stationary States	62
3.4.1	Tight-binding model	62
3.4.2	Translational Invariance	68
3.5	Eigenfunctions of the Fourier transform	77
3.5.1	The Dirac Delta Comb	79
3.5.2	Superpositions of Displaced Number States (SDNS).	81
3.5.3	Double Gaussian states	88
3.6	Conclusion	90
	References	92

4	Simulating the Quantum system on a computer	94
4.1	Introduction	94
4.2	Arrays as state vectors	95
4.3	The Discrete fractional Fourier Transform	102
4.4	The Fast Fourier Transform	107
4.5	The Fast Fractional Fourier Transform	108
4.6	Conclusion	111
	References	112
5	Compilation of Numerical Results	114
5.1	Introduction	114
5.2	Irrational frequency ratio $1/R = (\sqrt{5} + 1)/2$	116
5.2.1	Evolving Husimi Distributions	117
5.2.2	Mean energy and diffusion	119
5.2.3	Quantifying the quantum suppression	126
5.2.4	Stationary States: Irrational frequency ratio $1/R = (\sqrt{5} + 1)/2$	130
5.2.5	Quasi-Energy statistics	134
5.3	Numerical study with frequency ratio $1/R = 1/4$	141
5.3.1	Stationary States: $1/R = 1/4$	142
5.3.2	Mean energy growth with $1/R = 1/4$	152
5.3.3	Mean energy and \hbar : Ballistic islands	161
5.4	Conclusion	170
	References	173
6	Conclusion and perspectives	175
A	The Simple Harmonic Oscillator	178
A.1	The Simple Harmonic Oscillator	178
A.1.1	Energy-eigenvalue problem	180
A.1.2	Coherent States	183
	References	186
B	The Split Step Method	187
B.1	The Split Step Method	187
	References	188
C	Quasi-Probability Distributions	189
C.1	Quasi-probability Distributions	189
	References	191

List of Figures

2.1	Diagram showing the motion of a particle initially at $(q_0, p_0) = (1.5, 2.1)$. In this example $\mu = 2\pi$ and $1/R = 1/4$, giving $\theta = \omega_0 T = \pi/2$. Points are given a kick to their momentum and then rotated clockwise through $\pi/2$ where upon the process is repeated. The size of the kick depends sinusoidally on the particle's position . . .	24
2.2	Graphs showing Poincaré surface of sections with $1/R = (\sqrt{5} + 1)/2$ for various values of the kicking strength μ . We have set $k = 1$ in these calculations.	28
2.3	Diagram showing points $\hat{J} = M_\mu^N \hat{J}$. Outside this curve we have the orbit \hat{J}^+ on which all points are rotated counterclockwise by M_μ^N . Inside we have \hat{J}^- on which all points are rotated clockwise by M_μ^N . Below: Here we see the modified curve \hat{J}_ϵ which is only altered radially by the map M_ϵ^N	29
2.4	Diagram showing the formation of elliptic and hyperbolic stable points due to the Poincaré Birkhoff theorem	30
2.5	q - v - μ with $R = 2/(\sqrt{5} + 1)$. Every line crossing represents an exact resonance of some degree. The orbit eventually becomes chaotic with large μ . We have set $k = 1$ in these calculations	32
2.6	Rate of diffusion D - v - μ . Irrational frequency ratio, $1/R = (\sqrt{5} + 1)/2$. The numerical calculation was performed by taking 600 uniformly distributed particles in the phase plane window $q, p \in [-6\pi, 6\pi]$ setting $k = 1$ and then evolving for 400 discrete time steps at different μ	34
2.7	Graphs showing Poincaré surface of sections with $1/R = 1/4$ for various values of the kicking strength μ . We have set $k = 1$ in these calculations	38
2.8	D - v - μ for the rational frequency ratio $1/R = 1/4$. The numerical calculation was performed by taking 600 randomly distributed particles in the phase plane and evolving for 400 discrete time steps at different μ . We have set $k = 1$ in this calculation.	39
2.9	Examples of exact periodic points that exist when $\mu = \pi$ and $k = 1$.	40
2.10	The exact periodic points are surrounded by stable elliptical orbits. We set $\mu = \pi$ and $k = 1$ to generate this diagram.	41
2.11	Motion and energy of particle on an accelerator island. Note that the energy initially decreases but eventually increases.	42

2.12	Rough shape and position of some accelerator modes generated by setting $\mu \approx 6.38, k = 1$ and evolving a selection of randomly distributed points for a fixed time. The initial configuration of particles that have gained, after the fixed time, an energy greater than some large value are plotted in the figure.	43
2.13	Transition to chaos. We start with initial point $(\delta q_0, \delta p_0) = (0.3, 0)$ and plot the δq_n for the first 80 iterations for different values of μ . Note the break up of the orbit just after $\mu = \pi$	45
2.14	Detailed Poincaré surface of section of the quasi-periodic islands for the map \mathbf{Q}_μ , see (2.62)	46
2.15	Graphs showing structure of a ballistic island for various values of the kicking strength μ . These graphs are generated by operating on a group of randomly distributed points in the phase plane window $\delta q, \delta p \in [-0.5, 0.5]$ with (2.76). We can see here the stable elliptical structure that was invisible to us in Figure 2.12.	49
2.16	Diagrams detailing the motion of particles in the vicinity of the accelerator or ballistic islands	50
2.17	Plot of μ - v - δq over first 128 time steps. The initial starting values $(\delta q, \delta p)$ are $(\pm \cos^{-1}(2\pi/\mu) + 0.0000001, \mp \cos^{-1}(2\pi/\mu) + 0.0000001)$. The line in the graph represents where our analysis predicts the elliptical stable point to become unstable. The numerical calculation shows that our analysis appears to be correct.	53
3.1	The transfer matrix R_n can be used to iterate vectors a_n both left and right. Exponential growth in both directions is seen. We can match the values of the a_n in the center by carefully selecting energies	66
3.2	The condition for translational invariance is such that the r' component in the displacement operator $D_{r',s'}$, represented by the vectors, remains a multiple of $2\pi/k$ upon repeated operation of \mathcal{U}_0 . In the above examples $k = 1$. Figures (c) and (d) show situations where the translational invariance condition is upheld	73
3.3	Figure showing exact double Gaussian SFF and approximate double Hermite-Gauss SFF. In the (b) we used the Hermite-Gauss polynomial with $n = 2$. Compare these figures to Figure 5.23	91
4.1	The process of the Discrete Fourier transform.	100
5.1	Phase space diagrams of (a) a normally distributed classical ensemble superimposed on the Husimi distribution of a coherent state centered at $(q, p) = (5, 0)$ in the phase plane. Subsequent diagrams show the classical ensemble and quantum state at Phase space diagrams of a classical ensemble superimposed on the Husimi distribution of a quantum state at times (b) $n = 100$, (c)200 and (d)400 In these calculations we used $\hbar, k = 1$ and $\mu = 0.1$	118

5.2	Phase space diagrams of a classical ensemble superimposed on the Husimi distribution of a quantum state. Diagrams show states at times (a) $n = 0$, (b)400, (c)800 and (d)1600. In these calculations we used $\hbar = 0.25$, $k = 1$ and $\mu = 0.1$	118
5.3	Phase space diagrams of a classical ensemble superimposed on the Husimi distribution of a quantum state. Diagrams show states at times (a) $n = 0$, (b)100, (c)200 and (d)400. In these calculations we used $\hbar = 1$, $k = 1$ and $\mu = 0.5$	119
5.4	Phase space diagrams of a classical ensemble superimposed on the Husimi distribution of a quantum state. Diagrams show states at times (a) $n = 0$, (b)100, (c)200 and (d)400. In these calculations we used $\hbar = 1$, $k = 1$ and $\mu = 2$	120
5.5	Phase space diagrams of a classical ensemble superimposed on the Husimi distribution of a quantum state. Diagrams show states at times (a) $n = 0$, (b)10, (c)20 and (d)30. In these calculations we used $\hbar = 1$, $k = 1$ and $\mu = 4$	120
5.6	Initial value $(q, p) = (5, 0)$ evolved over 400 discrete steps with $\mu = 0.1$ and $k = 1$. Compare this figure with Figures 5.1 and 5.2. We used a Hilbert space of 2^{14} dimensions to do the quantum simulation.	122
5.7	Initial value $(q, p) = (5, 0)$, with $\mu = 0.5$, $\hbar = 1$ and $k = 1$. We use a discretised Hilbert space of 2^{14} dimensions to do the quantum simulation.	123
5.8	Initial value $(q, p) = (5, 0)$, with $\mu = 2.0$, $\hbar = 1$ and $k = 1$. We use a discretised Hilbert space of 2^{15} dimensions to do the quantum simulation.	124
5.9	Initial value $(q, p) = (5, 0)$, with $\mu = 2.0, \pi, 4.0, 6.0$, $\hbar = 1$ and $k = 1$. We use a discretised Hilbert space of 2^{14} dimensions to all simulations except part (d) where we used 2^{15} dimensions.	125
5.10	D -v- μ with $\hbar = 1/4$. We use a discretised Hilbert space of 2^{16} dimensions in all calculations	126
5.11	D -v- μ with $\hbar = 1/2$. We use a discretised Hilbert space of 2^{16} dimensions in all calculations	127
5.12	D -v- μ with $\hbar = 1$. We use a discretised Hilbert space of 2^{15} dimensions in all calculations	127
5.13	D -v- μ with $\hbar = 2$. We use a discretised Hilbert space of 2^{14} dimensions in all calculations	127
5.14	D -v- μ with $\hbar = 3$. We use a discretised Hilbert space of 2^{14} dimensions in all calculations	128
5.15	D -v- μ with $\hbar = 4$. We use a discretised Hilbert space of 2^{14} dimensions in all calculations	128
5.16	Suppression of Diffusion as a function of \hbar	130

5.17	Husimi Distributions of some stationary states of the kicked system U with irrational frequency ratio. $\hbar = 1$ and $k = 1$. We used a Hilbert space of 2^9 to generate these figures. The integer s labels the stationary states according to energy.	132
5.18	These graphs show how the energies of the stationary states changes as we vary \hbar and μ . The larger the value of μ the closed our eigenstates come to our idealised extended state represented by the line E_e	135
5.19	These graphs show how the energies of the stationary states changes as we vary \hbar and μ . The larger the value of μ the closed our eigenstates come to our idealised extended state represented by the line E_e	136
5.20	Quasi-Energy level statistics. In these figures we use $\mu = 0.5$ and we used a discretized Hilbert space of 3000 dimensions. If the effective KAM curves still exist in the classical system varying \hbar has little effect on the statistical distribution	139
5.21	Quasi-Energy level statistics. In these figures $\mu = 1.5$ and we used a discretised Hilbert space of 3000 dimension. As we reduce \hbar the distribution becomes more like P_W	139
5.22	Quasi-Energy level statistics. In these figures $\mu = 4$ and we used a discretised Hilbert space of 3000 dimensions. Agasin, as we reduce \hbar distribution becomes more like P_W	140
5.23	Plots showing quasi periodic behaviour of some stationary states with $k = 1$ and with $N = 2^8$. The resonance condition (3.61) is not fulfilled for these values of \hbar . Compare thse figures with those of Figure (3.3).	143
5.24	Stationary states in the position basis with $\hbar = \pi/2$ and $k = 1$. The quantum resonance condition (3.61) is fulfilled in these examples. .	144
5.25	Probabilty distributions of some stationary states of the kicked system in the position basis. For (a),(b),(c),(d),(e),(f) $\hbar = \pi/4, k = 1, N = 512$. In (g),(h),(i) $\hbar = \pi/16, k = 2, N = 512$. In (j),(k),(l) $\hbar = \pi/32, k = 1, N = 1024$	146
5.26	Husimi distributions of some stationary states of the kicked system corresponding to the distributions in Figure 5.25. For (a)-(f) $\hbar = \pi/4, k = 1, N = 512$. In (g),(h),(i) $\hbar = \pi/16, k = 2, N = 512$. In (j),(k),(l) $\hbar = \pi/32, k = 1, N = 1024$	147
5.27	Husimi distributions of stationary states with $\mu = \pi$ and $\hbar = 0.03$ superimposed over th classical quasi-periodic islands. In this diagram a Hilbert space of 2^{10} was used. The eigenstates can be visually seen to be approximate superpositions of the displaced Fock states. The quasi-energies of these states can be also shown to very close to the ones we predicted analytically.	149

5.28	Husimi distributions of stationary states near periodic islands with $\mu = \pi$ and $\hbar = \pi/128$. In this diagram a Hilbert space of 2^{10} was used. When \hbar is a fraction of π the stationary states which dictate the motion on classical period 1 islands are not localised. This is because they may have the same phase as stationary states centered primarily on the classical period 4 islands.	150
5.29	Husimi distributions of numerically calculated stationary states near classical accelerator modes with $\mu = 2\pi + 0.15$ and various resonant values of \hbar . In this diagram a Hilbert space of 2^{10} was used. Compare these figures to Figures 2.12 and 2.15	151
5.30	$\langle E_n \rangle$ -v- n , for various system parameters. $k = 1$ in all of the above plots.	153
5.31	Dependence of D_q and D_c on \hbar . For each specific value of \hbar we evolved the system over 400 time steps. For all of the above initial conditions there is effectively no classical diffusion, that is $D_c \approx 0$. The vertical lines in the graph represent where the main resonant modes are expected to occur.	155
5.32	Dependence of D_q and D_c on \hbar . In these examples for each specific value of \hbar we evolved the system over 200 time steps. The vertical lines in the graph represent the main resonant modes are expected to occur	156
5.33	Dependence of D_q and D_c on \hbar . The Figure shows that the quantum resonance effect is still very evident for values of μ where most of the phase plane is chaotic. Compare this figure to Figure 5.34	157
5.34	Dependence of β_q and β_c on \hbar . The curve αn^β is fitted to the energy -v- time graphs instead of the linear D . The parameter β is then plotted against \hbar . The peaks in Figures 5.33 are seen to be as a result of quadratic or near quadratic energy growth around quantum resonance.	159
5.35	D_q, D_c -v- \hbar for coherent states intially placed exactly on the classical period 1 stable islands. The quantum system can diffuse more easily than the classical emsemble. The red (classical) spikes serve to remind us that there is a small but finite probability that some particles in the classical ensemble will be placed outside the stable structure.	160
5.36	(a)-(h) E -v- n . (i)-(p) Final probability distribution in position basis after 40 iterations of the quantum map. We use a discretised Hilbert space of 2^{22} dimensions in all calculations	164
5.37	$\mu = 2\pi + 0.05$, (a)-(h) E -v- n . (i)-(p) Final probability distribution in position basis after 40 iterations of the quantum map. We use a discretised Hilbert space of 2^{22} dimensions in all calculations	166
5.38	$\mu = 6.349972$, (a)-(h) E -v- n . (i)-(p) Final probability distribution in position basis after 40 iterations of the quantum map. We use a discretised Hilbert space of 2^{22} dimensions in all calculations . . .	168

5.39	$\mu = 2\pi + 0.1$ (a)-(h) E - v - n . (i)-(p) Final probability distribution in position basis after 40 iterations of the quantum map. We use a discretised Hilbert space of 2^{22} dimensions in all calculations . . .	169
5.40	$\log_{10} \psi(q', 100) ^2$ versus q' with $\hbar = 2\pi/200$ and $\mu = 2\pi + 0.05$ after 100 iterations of the quantum map. There seems to be barrier that prevents tunneling to higher energy modes. However, it is not possible to rule out tunneling to higher energy modes altogether. .	170
C.1	Schematic showing the how the Wigner function may be calculated from the density matrix ρ . The matrix elements of the density matrix are inside the red square. All other highlighted squares are set to 0. We obtain the correct Wigner distribution by oversampling the highlighted squares by interpolation and then performing a FFT along the vectors indicated by the arrows.	191

List of Tables

5.1	Here we give some parameters characterising the quantum diffusion as a function of \hbar	129
5.2	Here we give some parameters of the quantum localisation as a function of \hbar and μ	140

Acknowledgments

There are many people to whom I owe a great deal of thanks. From both a personal and an academic standpoint I would like to sincerely thank both Jason and Danny, without whose knowledge, support and guidance this project could not have been completed. I wish to extend my sincere thanks to Derek, Mark, Aiveen, Joe, Billy, Derek, Barry, Deirdre, Vladimir, Anthony, Mang and Tony. Thanks for all your help and the all the laughs. Thank you Dimitri and Charles for patiently keeping the machine on my desk and running smoothly and thank you to Monica, Valerie and Marie for the smooth running of everything else.

On a purely personal level there are so many people who have helped and guided me safely through the last 4 years and who contributed in different but significant ways to this thesis. To Margaret, Jim, Pat, Dennis and Ciaran, I really do owe you everything. Thank you all so much. Special thanks to all my other relations especially Francis, Gerry, Claire and Brian.

To Laf, Vinny, Claireline, Dave, Sandrine, Grainne, Podge, Padraig, Annejulie, Mary, Ciaran, Ciara, Peter, Perrine, Tiffany, Trisha, to everybody at the book shop and canteen/coffee, to anyone I ever tutored, to anyone I played football with and finally to Martin and Fiona. Thank you all for everything!

Chapter 1

Introduction

1.1 Classical Chaos and Quantum Chaos

Depending on your point of view, all modern physics either comes from or leads back to Newton's contribution to classical mechanics. From the perspective of quantum mechanics there are many paths between the two theories but one of the end points always lies fixed somewhere near Newton's Principia. Of course modern quantum mechanics is most easily and effectively formulated using the classical language developed by Hamilton, Jacobi and Lagrange among others. It is always stressed however that these advancements contain no more extra physics than that highlighted back in 1687 by Isaac Newton.

The many ways that we have managed to connect classical to quantum physics are all referred to collectively as *the correspondence principle*. Among these is the connection between the uncertainty principle and the Poisson bracket notation. The principle also manifests itself in the relationship between Hamilton-Jacobi theory and Schrodinger's wave mechanics and the relationship between the Lagrangian and the Feynman's path integral. In all cases however, the correspondence principle means that we obtain classical mechanics from quantum mechanics in the classical, $\hbar \rightarrow 0$, limit. A problem arises however when one tries to reconcile the principle with what is now called chaos. To understand where the problem lies and where the theory of quantum chaos has come from, a brief historical discussion is perhaps in order.

It is Henri Poincaré who is credited with first recognizing the phenomena of chaos in 1913. He writes *'it may happen that small differences in the initial conditions produce very great ones in the final phenomena. A small error in the former will produce an enormous error in the latter. Prediction becomes impossible, and we have the fortu-*

itous phenomenon' [1]. At issue here was the stability of the solar system itself. Poincaré had been looking for regularity in the motion of a system of planets, to see if it could be written as the sum of a uniformly convergent series. Using his considerable computational abilities he succeeded in showing that regularity would not occur even in the simplest systems. He discovered that series used to describe the motion would often diverge because of small denominators appearing in the calculations. This was surprising because as far as anyone could tell the motion of the solar system was stable.

Around this time the quantum mechanical revolution was beginning to take over. The fundamental nature of the issues being analysed probably meant that the importance of the Poincaré's analysis was not recognised by many in the field. This not to say that the quantisation problems associated with nonlinearity in general were not appreciated. A multi-dimensional generalisation of the Wentzel-Kramer-Brillouin (WKB) approximation to quantum mechanics was suggested by Einstein in 1917 [2]. He clearly understood that the approach, now known as Einstein-Brillouin-Keller (EBK) quantization, would not work if the classical dynamics were non-integrable. The contributions of Van Vleck [3] and the path integral approach to quantum theory introduced by Feynman [4] would also play an important role in the subsequent development of periodic orbit theory and semi-classical physics. However, it is fair to say that quantum mechanical and non-linear issues were generally kept separate.

The solar system was still stable half a century later when contributions by Chirikov [5] * and the so called KAM theorem, developed between 1954 and 1968 in a series of papers by Kolmogorov, Arnol'd and Moser, illuminated this puzzling issue of stability [7–9]. It was explained that the series expansions that described the motion of these systems would remain convergent so long as the natural frequencies of the system's orbits were not resonant with each other [10]. These contributions stressed that while the notions of stability and regularity are similar, they are also fundamentally different. 'It shows that if one thinks of such systems as a struggle between order and disorder, order is more powerful than had been thought' [11].

The '*fortuitous*' sensitive dependence on initial conditions was rediscovered in 1963 by Lorenz [12]. This time, backed up by powerful computation machines, the discovery would effect drastic changes on our understanding of physics. It eventually led to the realisation that we were ill equipped to predict the long

*Also see the review [6]

time behaviour of the vast majority of physical systems. The apparent randomness observed in calculations had nothing to do with external noise (statistical physics deals with such issues remarkably well). The randomness and unpredictability comes from within what were thought to be well understood systems. To paraphrase Chernikov, this '*Stochasticity or chaos*' is '*understood as the occurrence of statistical dynamics in the absence of random forces*' [13].

In order to deal with chaos, concepts such as positive Liapouov exponents and fractal boundaries found their way into the literature. However, the idea of point like particles and exactly deterministic trajectories on which this new language was based could clearly not be reconciled with theory that now had the uncertainty principle as its corner stone. How could the idea of uncertainty in position and momentum be reconciled with the idea of sensitive dependence on initial conditions?

While the singular nature of the classical limit in the correspondence principle had always been a bit of a frustration to physicists, the emergence of chaos from obviously deterministic equations left many with the view that it represented a hole in our understanding of both quantum and classical mechanics. Interesting discussions on these problems of definition can be found in numerous texts, see [10,14–18] and the references therein. It is generally accepted however that these apparent contradictions are the result of conflicting mathematical frameworks and not something inherent in the physical world.

The term *quantum chaos* or *quantum chaology* is now understood to mean the study of quantum systems whose classical counterparts display the properties associated with classical chaos. This pragmatic approach is now adopted by the majority in the field. This means however, that what are called *signatures of quantum chaos*, that is the quantum manifestations of classical chaos, are now what must be identified and examined.

Many of the signatures now applied in the field were already in use describing other aspects of complexity in quantum theory. For example, *random matrix theory* was already well established as a means of understanding the complicated processes going on inside atomic nuclei. The theory describes the statistical properties of the eigenvalues of complicated and unknowable Hamiltonians by essentially allowing the matrix elements of the Hamiltonian be random [19]. The eigenvalue repulsion that was associated with these complicated processes is also seen to be evident in the numerical calculations of *quantum chaotic* systems.

The problem of quantizing ergodic systems has also taken a giant leap for-

ward with the introduction of the Gutzwiller trace formula, see [20–22]. The new approach, built upon the ideas of Van Vleck and the path integral approach to quantum theory, allowed for the effective quantization of certain complicated systems through the knowledge of the classical systems periodic orbits alone. These trace formulae are especially adept at dealing with what has been dubbed *hard chaos*. This is when there are no stable periodic orbits anywhere in the system.

Despite these advances, there are still limits to the complexities of the systems that can be analysed. While this may seem obvious it means that researchers in quantum chaos have had to be selective about the types of system they attempt to understand. We can summarise the most important properties:

- Implicitly, the classical system should display some chaos. However, the system should be also easy to model and therefore it is essential that there are only a few variables of the motion.
- It must also be possible to numerically solve the quantum mechanical equations of motion. In many ways, this is perhaps the most restrictive requirement. Many seemingly straightforward Hamiltonians require an enormous computational effort to solve the corresponding Schrödinger equation.
- Finally, and most importantly, these systems should be open to experimental verification.

One popular system used in the study of quantum chaos is that of the 2 dimensional billiard with non-linear boundary conditions. The problem is classically simple to analyse since changes in direction and velocity of the particle can depend only on the angle of collision with the boundary. These types of systems display *hard* chaos and are therefore especially suited to the trace formula approach mentioned above. The requirement that the systems be relatively easy to numerically model is also fulfilled. Most importantly the system also lends itself to easy experimental probing albeit in an unexpected way. The equations of motion for the billiard system are identical to Maxwell's equations describing the EM-field inside a microwave resonator [22].

1.1.1 Time Dependent Hamiltonians

Another important set of 'simple' systems are those with non-linear Hamiltonians. These systems are generally understood to display what is known as *weak*

chaos. This means they can display both chaotic and stable dynamics depending on the initial configuration of the system. The existence in the classical system of integrable and chaotic dynamics means that there must exist a boundary between the two. These systems are therefore key to understanding the transition from regular to chaotic dynamics. In most classical cases this transition to chaos can be understood through the correct application of the KAM theorem mentioned above, see [23–25]. However, understanding the quantum mechanics of the transition is still an area of active research.

An important subgroup of nonlinear dynamical systems are those that are subject to time-dependent external forces. Unfortunately, while this time dependence is relatively easy to examine experimentally, it can be very difficult to model the quantum system numerically. However, a special type of model known as a periodically kicked system provides a welcome compromise. These systems generally display the *weakly chaotic* properties required and have numerous other advantages besides.

The time dependence allows chaos to exist in systems that are essentially one dimensional. This makes things easier for everybody except the experimentalist. The classical equations of motion can be written in terms of an iterative mapping of the conjugate position and momentum variables. This allows one to easily plot the particles position and momentum at discrete time periods on the phase plane making up what is called a Poincaré surface of section. These diagrams can be a very powerful visual aid and can greatly help ones understanding of the the system dynamics.

The quantum mechanical versions of these problems are also much easier to model. The ‘kicking’ we refer to is generally regarded as being an instantaneous perturbation to the free evolution of the system. This means the quantum dynamics can be factorised into two separate operations. This is analogous to the way the classical system is examined only now matrix operations take the place of the iterative mapping.

The periodic time dependence also allows one to apply the what is called the Floquet theorem to the problem [26]. The eigenvectors of the Floquet operator are called the stationary states of the system. The eigenvalues associated with these stationary states can also be calculated and the results of random matrix theory can be employed here.

Using these techniques, and if the role of \hbar can reliably controlled, the numerical modeling of the quantum system can then be used to connect classical, semi-

classical and quantum results. The compromise is, as we have mentioned, that these systems are harder to test experimentally. However, significant improvements in quantum control in recent years have led to an impressive complement of experimental data.

1.1.1.1 The Kicked Rotor

One of the most widely studied kicked systems both classically and quantum mechanically is that of the kicked rotor. The iterative process that determines the Poincaré surface of section is called the *standard* or *Taylor-Greene-Chirikov* map [6,24]. The conjugate variables used are that of an angle and the conjugate angular momentum. Classically it obeys the KAM theorem and because one of its conjugate variables is cyclic it is relatively easy to simulate quantum mechanically [27].

This model is one of a few kicked systems that classically displays anomalous diffusion characteristics. The 'anomalous' generally refers to a rapid increase or decrease in the energy growth rate of an ensemble of classical particles [28,29]. Responsible for these sudden changes is a kind of classical resonance between the perturbation strength and the free motion of the rotor. These resonances manifest themselves as stable structures in the classical Poincaré surface of section or phase-map.

One of the more striking properties of the purely quantum system is that of dynamical localisation. Classically when all bounding KAM curves have broken up the statistical diffusion associated with chaos takes place. However, a quantum state represented in the unbounded angular momentum basis will initially begin to diffuse and spread out much like that of the classical ensemble. Oddly the quantum system eventually run into some kind of boundary [17,22,26,30]. This boundary is significant because it can be brought about only through quantum interference of the state with itself. The result has been explained by applying a tight-binding approximation to the model and the process is then understood as a kind of Anderson localisation for a time dependent system [31–33]. This remarkable property has implications in the field of quantum control and has been claimed as the explanation for the reduction of the microwave field ionization rate of hydrogen atoms [34]. This property has been verified experimentally by [35].

The quantum system also displays what has become known as chaos assisted tunneling. The tunneling refers to the ability of the quantum state, under certain

conditions, to tunnel through the classical KAM curves. This means a quantum state, localised in a certain region of phase space, has the ability to reach areas of the phase plane that are inaccessible to a classical particle. This property has been demonstrated experimentally with cold atoms in [36].

Another interesting effect is what is known as quantum resonance, see [27, 37]. Essentially it is the non-trivial dependence of the system on the quantum parameter \hbar . In particular it has been demonstrated that quadratic energy growth may occur within the system when \hbar is some fraction of 2π . Amazingly, these effects have also been demonstrated experimentally [38].

Other kicked systems are also known to display these properties. The kicked particle in a 1-dimensional infinite potential well being one notable example. This system is similar to the KR in two important ways. Firstly, both systems are known to obey the KAM theorem. This means the break up of periodic orbits under perturbation is well understood. Secondly, both systems are bounded in one of their conjugate variables. Namely the angle for the KR and position for the kicked particle in a box. An obvious question to ask is whether the unusual properties mentioned above are exclusive to these systems that are bounded in conjugate position space and obey the KAM theorem?

In order to answer this question we therefore study an alternative periodically kicked system. The kicked harmonic oscillator does *not* obey either of these criteria but nonetheless has been shown, under certain conditions, to display properties similar to those mentioned above. However, the fact that the KAM theorem does not apply in our case and the unbounded nature of the unperturbed system means that the kicked harmonic oscillator can also display a wide range of radically different behaviours.

1.1.1.2 The Kicked Harmonic Oscillator

The Kicked Harmonic Oscillator (KHO) is a system rooted in physical reality. The system was first proposed as a 2-dimensional model of charges moving in a homogeneous static magnetic field under the influence of an orthogonal time dependent propagating electric field [39]. However it has since been proposed as a model for electronic transport in semiconductor super-lattices [40,41] and for atom optic modeling using ion-traps [42]. However, the behaviour of the harmonic oscillator under periodic excitation or perturbation has extra significance for physics given the important role the unperturbed system plays in quantum optics and in our understanding of atomic physics.

This kicked system is radically different from other periodically kicked systems. Firstly, there are two distinct time scales. There is a natural frequency associated with the free oscillation as well as the frequency of the periodic kicking potential. The relative values of these frequencies, which we generally refer to by the ratio $1/R$, have enormous consequences on the behaviour of the system. We use this ratio to classify the system into two categories. The first category deals with the systems behaviour when R , and therefore the frequency ratio is, irrational. The second category deals with the system when the frequency ratio is a rational number.

The natural frequency of the Simple Harmonic Oscillator (SHO) remains constant regardless of the amplitude of the oscillations. This means that the KAM theorem, which usually describes the breakup of periodic orbits under perturbation, cannot be applied. This has profound consequences for the behaviour of the system when the frequency ratio is rational. Even the presence of an infinitesimally small kick means the spectacular organisation of the classical Poincaré phase plot into incredible crystal and quasi-crystal tiling patterns. This implies the instantaneous break up of an infinity of previously stable orbits. What's more, these patterns extend to all areas of the phase plane. The unstable orbits now form what is called a periodic or aperiodic stochastic web, depending on if the pattern is crystalline or quasi-crystalline. These webs mean that given the correct initial condition a particle under the tiniest of perturbations is free to move close to all regions of the phase plane [43,44].

Another feature of the classical model with rational frequency ratio is the existence under certain special resonant conditions of accelerator modes or islands. These modes allow for stable ballistic motion throughout the phase space and are the main reason behind what is called anomalous diffusion. There has been some previous analysis on the exact classical dynamics associated with these types of modes as well as some statistical analysis on general properties of the energy growth [45,46].

Both of these classical effects and many others besides will also be apparent in the quantum system if we make the quantum parameter \hbar small enough. How these effects manifest themselves in the eigensolutions of the quantum system however is an open question. In addition to these classical effects we must also account for the purely quantum contributions to the dynamics. We are speaking specifically of effects like quantum resonance and tunneling that have been shown analytically and numerically to exist [47–50].

The case with irrational frequency is interesting because for a non-KAM system it behaves very much like the kicked rotor. Under strong enough perturbation, in the classical system, there is the statistical diffusional dynamics associated with chaos and the energy growth rates can easily be predicted using elementary techniques. However, the quantum dynamics with the same parameters is radically different. Like the kicked rotor there is a strong theoretical and numerical case to be made for the existence of some sort of quantum suppression of the energy growth rates [49,52,53].

Of course one could never hope to give a complete review of the kicked oscillator, never mind quantum chaos, in an opening introduction. However, I have tried to explain some of the motivation behind the subject as a whole as well as trying to highlight where this study stands in relation to other aspects of the field. Much more material on quantum chaos and semi-classical physics can be found in [16,17,20–22,26].

1.2 Study outline

The thesis is constructed as follows. In chapter 2 we examine closely the classical system. We identify all the properties we are interested in and will later look for in the quantum system. With regard to much of the analysis I have tried where possible to provide alternative derivations to those found in the standard texts. Although the end results often correspond with those given in the literature I feel that the treatment given here is often more transparent. Included is an alternative explanation of the classical cell structure and the emergence of the web for any size perturbation. We also perform new analysis on the periodic islands and accelerator modes that occur under certain classical resonance conditions. In particular we identify the stability conditions associated with the classical ballistic islands responsible for anomalous diffusion. We also give considerable space to explaining the concept of energy growth of a classical ensemble.

In chapter 3 a detailed analysis of the quantum mechanics of the delta kicked oscillator is given. The approach is to define what is called the Fractional Fourier transform and show that it is, up to a phase, the evolution operator of the Simple Harmonic Oscillator (SHO). We supply most of the background material for this in appendix A.1. Through the definition it is then a simple task to write out the evolution operator for the perturbed system. These results are essential to

understanding the numerical model presented later.

The last few sections of the chapter are dedicated to the analytical analysis of the quantum system. We first review the tight binding approximation put forward by Frasca [52] and analysed by Engel [51]. This analysis best explains the concept of dynamical localisation when the system's frequency ratio is irrational. We comment briefly about the accuracy of this model and where it should break down.

We then review some of the analysis by Borgonovi and Rebuffini [49] on the translational invariance of the kicked system for $R = 3, 4, 6$ and concentrate particularly on the $R = 4$ case. The emphasis is placed on understanding the changes in the system's stationary state structure around values of \hbar associated with quantum resonance. This is done by examining what are called Self-Fourier functions (SFF's). We introduce three separate but related functional structures, all of which help illuminate particular processes occurring within the quantum dynamics.

Chapter 4 is dedicated to explaining thoroughly our numerical model. We begin with a brief introduction to the idea of representing a discrete quantum state as an array in computer memory. We then show how the relationship between the discrete Fourier transform (DFT) and the continuous Fourier transform (FT) can be used to effectively simulate continuous quantum systems on a discrete vector. Importantly we show how the parameter \hbar is controlled by the grid size and the coordinate boundary of the simulation.

The rest of the chapter is concerned with the technical details of the numerical algorithm. In particular we concentrate on explaining the concept of the discrete fractional Fourier transform (DFrFT). Since much of the notation used in explaining these concepts has been adopted with digital signal processing in mind we make a considerable effort to keep the notation as quantum mechanical as possible.

Chapter 5 is a compilation of the most relevant numerical simulations and observations. It is organised as follows. We first concentrate on the system with irrational kicking frequency ratio. We give some visual examples of the quantum and classical systems evolving in phase space. In this way we introduce the concept of comparing the evolution of a normally distributed classical ensemble and a quantum coherent state. We then show how the mean energies of both systems evolve in time and how with small \hbar they behave very similarly.

We perform a very detailed numerical analysis on the dynamical localisation effects seen in the quantum system and attempt to quantify this effect in terms of \hbar . While doing so we shall show that complete localisation of the quantum state only occurs for specific ranges of the perturbing kick and the quantum parameter \hbar . We then numerically calculate some of the systems stationary states and associated quasi-energies and perform some statistical analysis on this data. In particular we wish to discern if there is any grounds for believing that states become extended if the kick strength becomes large enough or if \hbar becomes small enough.

The numerical analysis of the $R = 4$ system is slightly different in approach. We are primarily interested in displaying some of the properties that have been predicted in chapter 3. We first look at the eigenstates of the systems Floquet operator. We wish to check if some of the unusual structures described in 3 are displayed by the numerically calculated eigenstates. We give special attention to the structure of the stationary states under parameters for which the classical system undergoes ballistic energy growth.

We then use our model to analyse thoroughly the effects that \hbar has on the energy growth rates. In particular we are interested in looking for the predicted increases in these rates due to quantum resonance. We examine the diffusion characteristics of quantum system when classical resonance effects are also present. We will then finally look for evidence that the quantum system can exploit classical and quantum resonance effects simultaneously to achieve super-ballistic energy growth.

We have tried to emphasise how underlying classical structures affect both the quantum dynamics and eigensolutions. One reason for this emphasis on the classical phase space structures is because of our development of the aforementioned numerical procedure which is based on the fractional Fourier transform. This has allowed us to analyse the quantum dynamics in much more detail than had previously been possible. This development and of course the constant development of better computers allows one, in the numerical simulations, to make \hbar so small as to be able to place a minimum uncertainty quantum state inside stable classical regions of the phase plane. As will be demonstrated, it is even possible to place states initially on the classical structures responsible for anomalous diffusion. This allows for a very direct and controlled examination of quantum effects around integrable and chaotic areas of the classical phase space.

References

- [1] H. Poincaré, *The foundation of science: science and method*, English version, the Science Press, Lancaster, PA, pg. 397 (1946).
- [2] A. Einstein, *Verh. Deut. Phys. Ges.* **19**, 82 (1917).
- [3] J. H. van Vleck, *Proc. Natl. Acad. Sci. USA* **14**, 178 (1928).
- [4] R. P. Feynman, *Space-time Approach to Non-relativistic Quantum Mechanics*, *Rev. Modern. Phys.* **20**, 367 (1948).
- [5] B. V. Chirikov, *The Passage of a Nonlinear System Through Resonance*, *Sov. Phys. Dokl* **4**, 253 (1959).
- [6] B. V. Chirikov, *A Universal Instability of Many-Dimensional Oscillator Systems*, *Phys. Rep.* **52**, 264 (1979).
- [7] A. N. Kolmogorov, *Dokl. Akad. Nauk. SSSR* **98**, 527 (1954) (An English version is given in R. Abraham, *Foundations of Mechanics* W. A. Benjamin, Appendix D, (New York, 1967).
- [8] V. I. Arnol'd, *Russ Math. Survey* **18**, 9;18 85 (1963).
- [9] J. Moser, *Nachr. Akad. Wiss. Gottingen II, Math. Phys. Kd* **1**, 1 (1968).
- [10] L. E. Reichl, *The Transition to Chaos in Conservative Classical Systems: Quantum Manifestations*, (Springer, New York, 1992)
- [11] B. B. Hubbard *The world according to wavelets* 2nd edition, (A K Peters, Natick , Massachusetts 1998).
- [12] E. N. Lorenz *Deterministic non-periodic flow*, *J. Atmos Sci*, **20** 130 (1963).
- [13] A. A. Chernikov, R. Z. Sagdeev, D. A. Usikov, M. Y. Zakharov and G. M. Zaslavsky, *Minimal chaos and stochastic Webs*, *Nature*, **326**, 559 (1987).
- [14] J. Ford, *Quantum Chaos, is there any?*, *Directions in Chaos*, Vol. II, edited by B.-L. Hao (World Scientific, Singapore, 1988), pp. 129-147.
- [15] M. V. Berry, *Quantum chaology, not quantum chaos*, *Physica Scripta* **40** 335, (1989).
- [16] M. Tabor *Chaos and integrability in nonlinear dynamics : an introduction*, (John Wiley and Sons, New York 1989).
- [17] E. Ott, *Chaos in dynamical systems*, (Cambridge University Press, Cambridge, 1993).
- [18] R. C. Hilborn, *Chaos and Nonlinear Dynamics :An introduction for scientists and engineers*, (Oxford University Press, Oxford, 1994).
- [19] M. L. Mehta, *Random Matrices*, 2nd rev. enl. ed. (New York, Academic Press, 1991).
- [20] M. C. Gutzwiller, *Chaos in Classical and Quantum Mechanics*, (Springer, New York, 1990).
- [21] M. Brack and R. K. Bhaduri, *Semiclassical physics*, (Addison and Wesley, Reading, 1997).
- [22] H. -J. Stöckman, *Quantum Chaos. An Introduction.*, (Cambridge University Press, Cambridge, 1999).
- [23] H. Goldstein *Classical Mechanics*, 2nd edition, (Addison-Wesley, 1980).

- [24] A. J. Lichtenberg and M. A. Leiberman, *Regular and Chaotic Dynamics*, 2nd edition (Springer-Verlag, New York, 1992)
- [25] J. V. Jose and E. J. Saletan *Classical Dynamics A Contemporary Approach* (Cambridge University Press, Cambridge, 2000).
- [26] F. Haake *Signatures of Quantum Chaos* vol. 54 of *Springer Series in Synergetics*, 2nd edition, (Springer-Verlag, Berlin, 2001).
- [27] F. M. Izrailev, *Simple models of Quantum Chaos: Spectrum and Eigenfunctions* *Physics Reports* **196**, 299 (1990).
- [28] Y. H. Ichikawa, T. Kamimura and T. Hatori *Stochastic diffusion in the standard map*, *Physica D* **29**, 247 (1987).
- [29] R. Ishizaki, T. Horita, T. Kobayashi and H. Mori, *Anomalous diffusion due to accelerator modes in the standard map*. *Prog. Theo. Phys*, **85**, 1013 (1991).
- [30] G. Casati, B. V. Chirikov, F.M Izraelev and J. Ford, *Stochastic behaviour of a quantum pendulum under a periodic perturbation*, in G. Casati and J. Ford, *Stochastic Behaviour in classical and Quantum Hamiltonian systems*, vol. 93 of *Lecture Notes in Physics*, 332. (Springer, Berlin 1979)
- [31] P. W. Anderson, *Absence of diffusion in certain in random lattices*. *Phys. Rev.* **109**, 1492 (1958).
- [32] P. W. Anderson, *Localized magnetic fields in metals*. *Phys. Rev.* **124**, 41 (1961).
- [33] D.R. Grempel, S. Fishman and R.E. Prange *Localization in an incommensurate potential: An exactly solvable model*. *Phys. Rev. Lett.* **49**, 833 (1982).
- [34] G. Casati, I. Guarneri and D. Shepelyansky, *IEEE J. Quantum Electron.* **24**, 1420 (1988).
- [35] M. G. Raizen, F. L. Moore, J. C. Robinson, C. F. Bharucha and B. Sundaram, *An experimental realization of the quantum delta kicked rotor*, *Quantum Semiclass. Opt.* **8**, 687 (1996).
- [36] A. Mouchet, C. Miniatura, r. Kaiser, B. Grémaud and D. Delande, *Chaos-assisted tunneling with cold atoms*, *Phys. Rev. E* **64**, 016221 (2001).
- [37] F. M. Izrailev and D. Shepelyanskii, *Theor. Math. Phys.* **43**, 553 (1980).
- [38] W. H. Oskay, D. A. Steck, V. Milner, B. G. Klappauf and M. Raizen, *Ballistic peaks at quantum resonance*, *Optics communications* **179**, 137 (2000).
- [39] G. M. Zaslavsky, M. Yu. Zakharov, R. Z. Sagdeev, D. A. Usikov and A. A. Chernikov, *Sov. Phys. JETP* **64**, 294 (1986).
- [40] T. M. Fromhold *et al.* *Effects of stochastic webs on chaotic electron transport in semiconductor superlattices* *Phys. Rev. Lett.* **87**, 046803 (2001).
- [41] T. M. Fromhold *et al.* *Chaotic electron diffusion through stochastic webs enhances current flow in superlattices* *Nature (London)* **428**, 726 (2004).
- [42] S. A. Gardiner, J. I. Cirac and P. Zoller *Quantum chaos in an ion trap; the delta kicked harmonic oscillator*. *Phys. Rev. Lett.* **79**, 4790 (1997)
- [43] G.M. Zaslavsky, R.Z. Sagdeev, D.A.Usikov, A.A. Chernikov, *Weak Chaos and Quasi-Regular Patterns*. (Cambridge nonlinear science series, Cambridge, 1991).

- [44] G.M. Zaslavsky *Physics of chaos in Hamiltonian systems*. (Imperial College Press, London, 1998)
- [45] M. V. Daly and D. M. Heffernan, *Dynamically enhanced chaotic transport*. *Chaos, Sol. & Fract.* **8**, 933 (1997).
- [46] G.M. Zaslavsky and B. A. Niyazov, *Fractional Kinetics and accelerator modes*. *Phys. Rep.* **283**, 73 (1997).
- [47] G. P. Berman, V. Yu. Rubaev and G. M. Zaslavsky, *The Problem of quantum chaos in the kicked harmonic oscillator*, *Nonlinearity* **4**, 543 (1991).
- [48] R. Lima and D. Shepelyansky *Fast Delocalization in a model of Quantum Kicked Rotor*, *Phys. Rev. Lett.* **67**, 1377 (1990).
- [49] F. Borgonovi and L. Rebuzzini, *Translational invariance in the kicked harmonic oscillator*, *Phys. Rev. E* **52**, 2302 (1995).
- [50] Go. Torres-Vega, Klaus B. Møller, and A. Zúñiga-Segundo, *Role that separatrices and stochastic webs play in quantum dynamics*, *Phys. Rev. A* **57**, 771 (1998).
- [51] M. Engel, *On Quantum chaos, Stochastic Webs and Localization in a Quantum Mechanical Kick system*. Ph. D Thesis, 2003.
- [52] M. Frasca, *Quantum kicked dynamics and classical diffusion*, *Physics Lett. A* **231**, 344 (1997).
- [53] G. Kells, J. Twamley and D. Heffernan, *Dynamical Properties of the delta kicked harmonic oscillator*, *Phys. Rev. E* **70**, 015203 (2004).

Chapter 2

The Classical System

2.1 Introduction

Kicked Hamiltonian systems are firmly established as prototypical models for studying chaos. Enormous effort has been spent examining models like the standard map and the kicked rotator. The study of kicked degenerate systems, those that do not obey the KAM theorem, have received less attention but display fascinating dynamical properties both classically and quantum mechanically. The Kicked Harmonic Oscillator (KHO) is an example of such a system. The system was originally proposed as a 2-dimensional model of charges moving in a homogeneous static magnetic field under the influence of an orthogonal time dependent propagating electric field [1]. It has also been proposed as a model for electronic transport in semiconductor super-lattices [2,3] and for atom optic modeling using ion-traps [4].

There are now a considerable number of papers dealing with the classical system and as we will see many ways to generalise the model. Specifically we will deal with the case where the kicking potential is the even cosine function which arises naturally from the derivation given below. However, it is very easy to classify this particular case among more general periodic kicking potentials. The general behaviour of the system for these potentials *can* be significantly different [5].

The system is most easily classified according to ratio between the perturbing frequency and the natural frequency of the oscillator. We deal with 2 general situations: (1) when the frequency ratio is irrational (2) when the ratio is rational.

In the irrational case describing the classical dynamics is relatively uncomplicated. In many ways the system behaves as though it obeys the KAM theorem.

When the perturbation or kick is small the majority of the system orbits remain intact and non-chaotic. We are primarily interested examining the energy growth of a statistical ensemble of particles when the perturbation has destroyed all stable orbits. Additional analysis on the diffusional properties of this system can be found in [14].

The dynamics of the classical system are much more difficult to describe when the natural frequency is some multiple of the perturbing frequency. In the particular cases of when the frequency ratio is $1/R = 1/3, 1/4, 1/6$ the perturbation organises the system's Poincaré surface of section into a cellular lattice. Between each cell there exists a web like structure containing a mesh of the systems unstable trajectories. This remarkable property means that a particle on the web is unbounded in position and momentum and could potentially go anywhere in the phase plane (except off the web) [6–8,12,13].

In the particular case with $R = 4$ and when the perturbation strength is within certain ranges the system also displays what is called *anomalous energy growth* or *anomalous diffusion*. These effects are due to a resonance between the natural motion of the free oscillator and the perturbation. These resonances manifest themselves in stable structures or islands inside the web. A particle can be repeatedly accelerated or remain localised depending on the type of structure it is on.

In this chapter we first derive the Hamiltonian for the delta kicked harmonic oscillator. We then use a simple canonical transform for to derive a general classical mapping that describes the discrete time evolution of the system.

In the irrational case we will apply a modified Poincaré Birkhoff theorem to explain the general dynamics and gradual breakup of the systems stable orbits. There are pronounced differences between the diffusion properties of the quantum and classical systems and for this reason we review the general diffusion properties of the classical system. This is a precursor for the subsequent quantum analysis where it will be demonstrated that there is some quantum process that restricts the diffusion.

In the rational case with $R = 4$ we firstly present analysis that describes the organisation of the Poincaré surface of section into the lattice like structure mentioned above. We then concentrate on examining the structures that are responsible for the anomalous spikes in the numerical simulations. We are primarily concerned with the stability and exact locations of such structures and to this end we derive several new results.

The interested reader can consult [15,16] and the review [6] for alternative ex-

positions on the classical dynamics of the kicked oscillator. Some of the derivations from [15,16] are also included below for clarity. A number of monographs that deal with the general properties of *weak chaos* and stochasticity in Hamiltonian systems also include discussions on the Kicked Harper Model (KHM) and the associated web map (WM) are also available [9,10]. Under certain conditions the KHO has been shown to be equivalent to the KHM [11]. This chapter concentrates specifically on the KHO although I will try to include results pertaining to the KHM and the WM where appropriate.

2.2 The delta kicked harmonic oscillator

The delta kicked harmonic oscillator was first proposed as a way of modeling the dynamics of a charged particle moving in a homogeneous static magnetic field and an orthogonal time dependent propagating electric field wave packet [9], that is

$$\vec{B} = B_0 \vec{e}_z, \quad (2.1a)$$

$$\vec{E}(q_x, t) = E_0 \sum_{m=-\infty}^{\infty} \sin(\bar{k}q_x - m\omega t) \vec{e}_x, \quad (2.1b)$$

where the constants B_0 , E_0 , \bar{k} and ω are all real. We use the term q_x to represent position in the x -direction. The summation can be rewritten using a variation of the Poisson sum rule. The Poisson sum formula is generally written as

$$\sum_{m=-\infty}^{\infty} \exp\left(-\frac{i2\pi tm}{a}\right) = a \sum_{n=-\infty}^{\infty} \delta(t - na) \quad (2.2)$$

However, because the sin function is odd we can also write this as

$$\sum_{m=-\infty}^{\infty} \cos\left(\frac{i2\pi tm}{a}\right) = a \sum_{n=-\infty}^{\infty} \delta(t - na). \quad (2.3)$$

Substituting (2.3) into (2.1b) gives

$$\sum_{n=-\infty}^{\infty} \sin(\bar{k}q_x - n\omega t) = \sin \bar{k}q_x \sum_{n=-\infty}^{\infty} \cos n\omega t = T \sin \bar{k}q_x \sum_{n=-\infty}^{\infty} \delta(t - nT), \quad (2.4)$$

where $a = T = 2\pi/\omega$ is the period. The total expression for the propagating \vec{E} field is given by

$$\vec{E}(q_x, t) = E_0 T \sin \bar{k} q_x \sum_{n=-\infty}^{\infty} \delta(t - nT) \vec{e}_x . \quad (2.5)$$

Writing it in this way shows that the propagating electric wave packet may also be interpreted as a standing sinusoidal wave that is switched on stroboscopically. Of course it is unreasonable to assume that a wave-packet made up of an infinite number of harmonics could ever be experimentally reproduced. However summations over a large number of harmonics very nearly produce this stroboscopic effect.

We are now in a position to write out the equations of motion [16]. The Newtonian equation of motion for a charged particle is given by

$$m\ddot{\vec{q}} = Q(\vec{E} + \dot{\vec{q}} \times \vec{B}) , \quad (2.6)$$

with $\vec{q} = q_x \vec{e}_x + q_y \vec{e}_y + q_z \vec{e}_z$ and Q is the charge of the particle. Using (2.1a) and (2.5) we can write for the components of \vec{q} :

$$m\ddot{q}_x = QB_0 \dot{q}_y + QE_0 T \sin \bar{k} q_x \sum_{n=-\infty}^{\infty} \delta(t - nT) , \quad (2.7a)$$

$$m\ddot{q}_y = -QB_0 \dot{q}_x , \quad (2.7b)$$

$$m\ddot{q}_z = 0. \quad (2.7c)$$

The motion of the particle in the q_z -direction is one of constant velocity. Integration of (2.7b) gives

$$m\dot{q}_y = -QB_0 q_x + c , \quad (2.8)$$

where c is a constant that can be set to zero by appropriate choice of the x -axis. By substituting this into (2.7a) we get

$$\ddot{q}_x + \omega_0^2 q_x = \frac{QE_0 T}{m} \sin \bar{k} q_x \sum_{n=-\infty}^{\infty} \delta(t - nT), \quad (2.9)$$

with $\omega_0 = QB_0/m$. This is the equation of motion for the delta kicked harmonic oscillator. It describes the motion of a particle in a harmonic potential that is periodically kicked by an impulsive force. This force is proportional, in this case, to $\sin \bar{k}q_x$. The resulting dynamics are easier to compute once we have found the corresponding Hamiltonian.

The Hamiltonian of a charged particle in an unspecified electromagnetic field is given by [17]

$$\mathcal{H}(\vec{q}, \vec{p}, t) = \frac{1}{2m} \left(\vec{p} - Q\vec{A}(\vec{q}, t) \right)^2 + Q\phi(\vec{q}, t) , \quad (2.10)$$

where \vec{p} and \vec{q} are the momentum and position vectors of the particles. Here again the parameter Q represents the charge of the particle and \vec{A} and ϕ are the vector and scalar potentials respectively. These potentials are related to the \vec{E} and \vec{B} fields through

$$\begin{aligned} \vec{B} &= \nabla \times \vec{A} , \\ \vec{E} &= -\nabla\phi - \frac{\partial\vec{A}}{\partial t} . \end{aligned} \quad (2.11)$$

The correct values for the \vec{E} (2.5), and \vec{B} (2.1a), fields are obtained by setting

$$\vec{A} = B_0q_x\vec{e}_y , \quad (2.12a)$$

$$\phi(\vec{q}, t) = \frac{E_0T}{\bar{k}} \cos \bar{k}q_x \sum_{n=-\infty}^{\infty} \delta(t - nT) . \quad (2.12b)$$

Substitution of these into the the general Hamiltonian,(2.10), gives

$$\mathcal{H}(\vec{q}, \vec{p}, t) = \frac{1}{2m} (p_x^2 + (p_y - QB_0q_x)^2 + p_z^2) + \frac{QE_0T}{\bar{k}} \cos \bar{k}q_x \sum_{n=-\infty}^{\infty} \delta(t - nT) . \quad (2.13)$$

We can see now that the Hamiltonian is invariant under translations in the q_y and q_z directions. This means that both p_z and p_y are constants of motion. The origins of each component may be adjusted so as to only leave terms p_x and q_x in the Hamiltonian. Setting p_z and p_y to zero means the the Hamiltonian can now be written in terms of x only

$$\mathcal{H} = \frac{p_x^2}{2m} + \frac{m\omega_0^2 q_x^2}{2} + \frac{QE_0T}{\bar{k}} \cos \bar{k}q_x \sum_{n=-\infty}^{\infty} \delta(t - nT) . \quad (2.14)$$

Introducing the canonical transformation $p_x = p\sqrt{m\omega_0}$ and $q_x = q/\sqrt{m\omega_0}$ and setting $\bar{k} = k\sqrt{m\omega_0}$ we can write this as

$$\mathcal{H}(q, p, t) = \mathcal{H}_0 + \mathcal{H}_1 = \frac{\omega_0}{2} (p^2 + q^2) + \bar{\mu} \cos kq \sum_{n=-\infty}^{\infty} \delta(t - nT) , \quad (2.15)$$

where $\bar{\mu} = \frac{QE_0T}{\sqrt{m\omega}k}$. The first part, \mathcal{H}_0 , is just the Hamiltonian of a free harmonic oscillator with a frequency of ω_0 . The period of such an oscillator is thus $T_0 = 2\pi/\omega_0$. The frequency of the kicking pulse is given by $\omega = 2\pi/T$. We define the *frequency ratio* as $1/R = \omega_0/\omega = \omega_0T/2\pi$.

We now show that the classical equations of motion for such a Hamiltonian are quite simple. We first deal with Hamilton's equations over the infinitesimal time when the delta kicking function is applied. We are allowed to ignore the time independent part of the Hamiltonian because of the infinitesimal nature of the delta kick. We write Hamilton's equations of motion for the kick as

$$\frac{dp}{dt} = -\frac{d\mathcal{H}}{dq} = -q + k\bar{\mu} \sin(kq) \sum_{n=-\infty}^{\infty} \delta(t - nT) , \quad (2.16a)$$

$$\frac{dq}{dt} = \frac{d\mathcal{H}}{dp} = p . \quad (2.16b)$$

We now integrate these over the n^{th} delta function kick:

$$\int_{p_n^-}^{p_n^+} dp = \int_{nT-\epsilon}^{nT+\epsilon} \left[-q + \mu \sin(kq) \sum_{n=-\infty}^{\infty} \delta(t - nT) \right] dt , \quad (2.17a)$$

$$\int_{q_n^-}^{q_n^+} dq = \int_{nT-\epsilon}^{nT+\epsilon} p dt , \quad (2.17b)$$

where $\mu = k\bar{\mu}$ and q_n^-, p_n^- refer to the values of q, p an infinitesimal time before the kick and q_n^+, p_n^+ refer to the values of q, p an infinitesimal time after the kick. The right hand side of (2.17) then becomes

$$\int_{p_n^-}^{p_n^+} dp = -2q_n^- \epsilon + \mu \sin(kq_n^-) , \quad (2.18a)$$

$$\int_{q_n^-}^{q_n^+} dq = 2p_n^- \epsilon , \quad (2.18b)$$

as the integral over the delta function picks out the value of $\mu \sin(kq)$ at the time nT . All the other terms now vanish as $\epsilon \rightarrow 0$ and we have a simple mapping for the kick:

$$p_n^+ = p_n^- + \mu \sin(kq_n^-) , \quad (2.19a)$$

$$q_n^+ = q_n^- \quad (2.19b)$$

The particle undergoes no change in position but has its momentum changed by a finite amount. However, the jump in the particle's momentum depends sinusoidally on its position.

We now concentrate on the time-*independent* part of the Hamiltonian. We write out Hamilton's equations of motion for the time independent part:

$$\frac{dp}{dt} = -\frac{d\mathcal{H}_0}{dq} = -\omega_0 q , \quad (2.20a)$$

$$\frac{dq}{dt} = \frac{d\mathcal{H}_0}{dp} = \omega_0 p . \quad (2.20b)$$

Substituting the second into the first we get

$$\ddot{q} + \omega_0^2 q = 0 . \quad (2.21)$$

The most general solution for such an equation is

$$q(t) = a \cos \omega_0 t + b \sin \omega_0 t . \quad (2.22)$$

Using (2.20b) we can also write

$$p(t) = -a \sin \omega_0 t + b \cos \omega_0 t . \quad (2.23)$$

Setting $t = 0$ we see the initial conditions $q(0) = a$ and $p(0) = b$. In this derivation we are going to assume that we first apply the kick and then let the oscillator evolve till just before the next kick. This means that we shall set the position and momentum at the time just after the kick to $q_n^+ = q(0) = a$ and $p_n^+ = p(0) = b$. Since, it takes a time $t = T$ to evolve the system from just after a kick to just before the next one can write for the free evolution between delta functions

$$q_{n+1}^- = q_n^+ \cos(\omega_0 T) + p_n^+ \sin(\omega_0 T) \quad , \quad (2.24a)$$

$$p_{n+1}^- = -q_n^+ \sin(\omega_0 T) + p_n^+ \cos(\omega_0 T) \quad . \quad (2.24b)$$

Substituting (2.19) into (2.24) we get

$$q_{n+1}^- = q_n^- \cos(\omega_0 T) + p_n^- \sin(\omega_0 T) + \mu \sin(kq_n^-) \sin(\omega_0 T) \quad ,$$

$$p_{n+1}^- = p_n^- \cos(\omega_0 T) - q_n^- \sin(\omega_0 T) + \mu \sin(kq_n^-) \cos(\omega_0 T) \quad . \quad (2.25)$$

This is the general map for the delta kicked harmonic oscillator. It says that a particle that has a phase space coordinate (q_n^-, p_n^-) just before a kick will have the coordinates (q_{n+1}^-, p_{n+1}^-) just before for the next kick. Once it is understood that we are referencing the time from just before each kick we can drop the '-' superscript on the coordinates to give,

$$\begin{aligned} q_{n+1} &= q_n \cos(\theta) + p_n \sin(\theta) + \mu \sin(kq_n) \sin(\theta) \quad , \\ p_{n+1} &= p_n \cos(\theta) - q_n \sin(\theta) + \mu \sin(kq_n) \cos(\theta) \quad . \end{aligned} \quad (2.26)$$

where $\theta = \omega_0 T$. Given an initial condition (q_0, p_0) we can easily calculate the exact coordinates of a particle at discrete times by repeatedly iterating this map. However, the general behaviour of (2.26) is perhaps easier understood through the separate mappings (2.19), (2.24) and a phase space diagram, Figure (2.1). The particle first receives discrete kick to it's momentum the magnitude of which varies sinusoidally with it's position. This is described by equations (2.19). After this the particle is free to oscillate as a normal harmonic oscillator until it receives it's next kick. The harmonic oscillation is described by equations (2.24) and is seen to be a clockwise rotation in the phase plane.

2.2.1 The system in action-angle coordinates

The harmonic oscillator is particularly easy to write in the Action-Angle (AA) coordinates of Hamilton-Jacobi theory, see [17,20]. We define the free part of the Hamiltonian as \mathcal{H}_0 , which, because of its time independence we may set equal to a constant energy E . That is

$$\mathcal{H}_0 = \frac{\omega_0}{2} (p^2 + q^2) = E \quad . \quad (2.27)$$

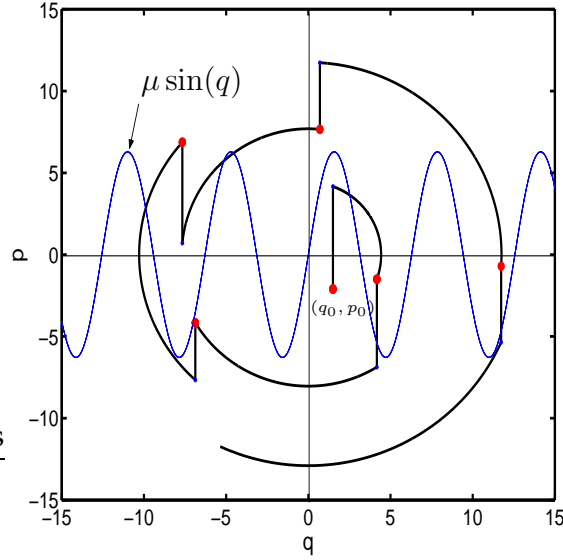


Figure 2.1. Diagram showing the motion of a particle initially at $(q_0, p_0) = (1.5, 2.1)$. In this example $\mu = 2\pi$ and $1/R = 1/4$, giving $\theta = \omega_0 T = \pi/2$. Points are given a kick to their momentum and then rotated clockwise through $\pi/2$ where upon the process is repeated. The size of the kick depends sinusoidally on the particle's position

The action J is defined to be

$$J = \frac{1}{2\pi} \oint p dq \quad , \quad (2.28)$$

and solving for $p(E, q)$ we have

$$J = \frac{1}{2\pi} \oint \left(\frac{2E}{\omega_0} - q^2 \right)^{\frac{1}{2}} dq \quad . \quad (2.29)$$

The substitution $q = \sqrt{2E/\omega_0} \sin \theta$ reduces the integral to

$$J = \frac{E}{\omega_0 \pi} \int_0^{2\pi} \cos^2 \theta d\theta \quad . \quad (2.30)$$

The integral of $\cos^2 \theta$ over a complete cycle is π so we have

$$\mathcal{H}_0 = E = \omega_0 J \quad . \quad (2.31)$$

So in our system the energy is exactly the action times the natural frequency of the oscillator. Hamilton's equations now give

$$\dot{\theta} = \frac{\partial \mathcal{H}_0}{\partial J} = \omega_0 . \quad (2.32)$$

and therefore

$$\theta = \theta_0 + \omega_0 t , \quad (2.33)$$

where θ_0 is the initial condition. Thus we have derived exactly the same picture as before. The action is represented by the constant vector $\frac{1}{2}(p^2 + q^2)$. The angle represents the rotation of that vector around the phase plane with time. In our system the period for one rotation is given by $T_0 = 2\pi/\omega_0$. We can finally write out q and p in terms of the action angle variables

$$\begin{aligned} q &= \sqrt{2J} \sin \theta , \\ p &= \sqrt{2J} \cos \theta . \end{aligned} \quad (2.34)$$

These ideas will be useful in the next section when we attempt to introduce a modified Poincaré Birkhoff theorem for the kicked system with an irrational frequency ratio.

2.3 General properties of the Classical System

The kicked harmonic oscillator is quite distinct from other widely studied kicked systems. The integrable part of this system, that is, the simple harmonic oscillator has the curious property that the frequency of oscillation remains constant regardless of the oscillation amplitude. This degeneracy of frequency prevents direct application of the theory of perturbed integrable systems otherwise known as the KAM theorem. An introduction to some of these ideas is supplied in the texts [17,19,20]. While this degeneracy allows for some unusual dynamics under certain exact conditions it does not necessarily imply that the dynamical behaviour of the KHO system is always different from other kicked systems.

The second distinguishing factor is the presence of two distinct time-scales in the system's Hamiltonian (2.14). Namely $T_0 = 2\pi/\omega_0$, which is the natural period of the simple harmonic oscillator and $T = 2\pi/\omega$, the period of time between kicks. It is the ratio between these times or frequencies that we use to classify the

system. We designate the frequency ratio $1/R = \omega_0/\omega = \omega_0 T/2\pi$. This means that the parameter $\theta = \omega_0 T$ completely control the frequency ratio $1/R$ e.g. $\theta = \pi/2 \implies 1/R = 1/4$. This frequency ratio is by far the best way to classify and order the system. We can break down the system's behaviour into two categories, (1) $1/R$ being rational and (2) $1/R$ being irrational.

We first present a general discussion on the properties of the irrational case. We introduce a modified Poincaré Birkoff theorem that helps explain the behaviour of the system as we change the kicking strength μ . We examine the structure of the Poincaré surface of section for a specific irrational case, $R = 2/(\sqrt{5}+1)$ and describe the eventual break up of the largest isolating orbits. We predict that for the most part the system with irrational frequency ratio should behave in a similar way to that of a KAM system. To conclude this section we then discuss how to effectively estimate the average rate of energy growth of the system once it is completely chaotic.

We shall also discuss some of the properties of the system for certain integer values of R , that is when the kicking frequency is resonant with the natural frequency of the system. One of the most interesting properties of these cases is the presence of a stochastic web that spans all of the the classical phase space. The values of R for which this crystalline structure appears can be seen to be related to the tessellation of the phase plane, where the values of $R = 3, 6$ represent filling (tiling) the plane with triangles and hexagons and $R = 4$ with squares [9,10,18]. A nice review of these particular cases can also be found in [16]. We will concentrate specifically on the $R = 4$ case and introduce some new analysis that explains the instantaneous ordering of the phase plane into lattices of elliptical and hyperbolic return points. Since the diffusional properties of this system with rational frequency ratio are somewhat unusual we leave the discussion of this to section 2.4.

2.3.1 Irrational frequency ratios

The harmonic oscillator is a degenerate system. This means that all particles, regardless of their initial conditions have exactly the same frequency of rotation about the phase space. It implies that if we were to take the Poincare surface of section at time intervals of some rational multiple of the natural frequency ω_0 then all points on the phase plane would be periodic. It is for this reason that the harmonic oscillator is called a non-KAM system. The KAM theorem says that under small perturbations to the integrable Hamiltonian nearly all non-degenerate

orbits of the integrable system survive. Since the orbits of the non-perturbed system are degenerate the theorem is said not to apply. In more mathematical terms we say that for the KAM theorem to be applicable the non-perturbed Hamiltonian must obey the non-degeneracy condition, that is

$$\left| \frac{\partial^2 \mathcal{H}_0(J)}{\partial J_k \partial J_l} \right| \neq 0, \quad (2.35)$$

where the Hamiltonian is written in action-angle coordinates (2.31). See [17,19,20] for more details. Clearly this is not true of our one dimensional system where, using (2.32)

$$\frac{\partial^2 \mathcal{H}_0(J)}{\partial J^2} = \frac{\partial \omega_0}{\partial J} = 0. \quad (2.36)$$

The KAM theorem, therefore, does not apply to the kicked oscillator. However, what happens if we were to look at the Poincaré surface of section at time intervals of some irrational multiple of the natural frequency ω_0 ? With the exception of the origin all points are now quasi-periodic. They will eventually return to a point infinitesimally close to some previous position but never exactly. These orbits now resemble the invariant tori which the KAM theorem says are stable (non-chaotic) under small perturbation. Fig (2.2) shows that this appears to be true. We are *not* saying that the KAM theorem applies in this case. We are only pointing out that when viewing the Poincaré surface of section on the correct time-scale we have what appear to be invariant non-resonant tori.

We can present a modified Poincaré Birkhoff theorem which describes the break up of all non-resonant tori under perturbation and the general descent into chaos. The modification is necessary because in the non-perturbed irrational system all particles regardless of their initial condition (action) have the same frequency of oscillation (2.36) and the Poincaré Birkhoff theorem given in most text books uses the fact that neighboring trajectories of the system have different frequencies of oscillation. However, with a slight modification we can apply essentially the same argument as that supplied in [19]. The mapping M_0 of the oscillator for simple harmonic motion (no perturbation) over time T can be written in action angle coordinates.

$$J_{n+1} = J_n, \quad (2.37)$$

$$\theta_{n+1} = \theta_n + T \text{ mod } 2\pi. \quad (2.38)$$

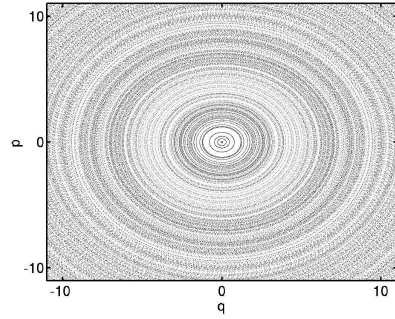
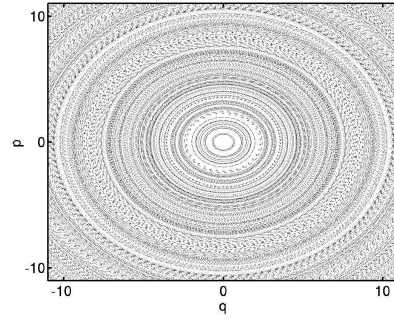
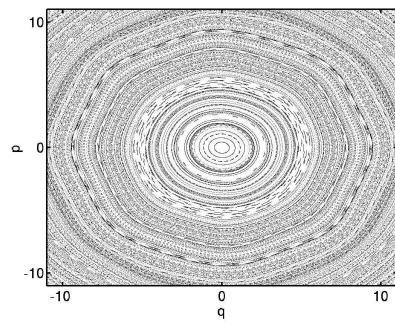
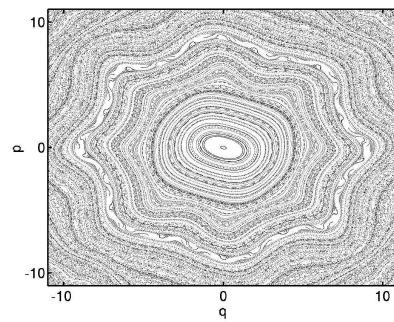
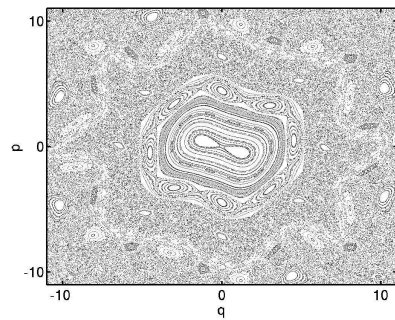
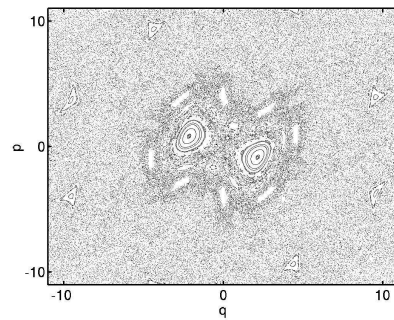
(a) $\mu = 0$ (b) $\mu = 0.01$ (c) $\mu = 0.1$ (d) $\mu = 0.5$ (e) $\mu = 1$ (f) $\mu = 2$

Figure 2.2. Graphs showing Poincaré surface of sections with $1/R = (\sqrt{5} + 1)/2$ for various values of the kicking strength μ . We have set $k = 1$ in these calculations.

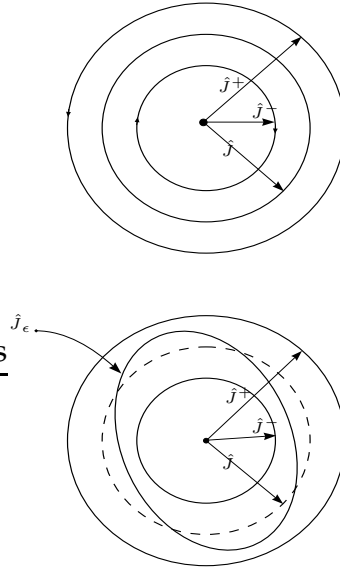


Figure 2.3. Diagram showing points $\hat{J} = \mathbf{M}_\mu^N \hat{J}$. Outside this curve we have the orbit \hat{J}^+ on which all points are rotated counterclockwise by \mathbf{M}_μ^N . Inside we have \hat{J}^- on which all points are rotated clockwise by \mathbf{M}_μ^N . Below: Here we see the modified curve \hat{J}_ϵ which is only altered radially by the map \mathbf{M}_ϵ^N

In this case T is an irrational multiple of 2π . In terms of the Poincaré surface of section where we plot points (J_n, θ_n) this means that no two values of θ_n will ever be the same. However, since the values of θ_n will densely fill the circle of radius J , different values of θ_n may become arbitrarily close. We now imagine the mapping under infinitesimal kicking strength μ . We call the perturbed map \mathbf{M}_μ and can be written as:

$$J_{n+1} = J_n + \mu g(J_n, \theta_n), \quad (2.39)$$

$$\theta_{n+1} = \theta_n + T + \mu h(J_n, \theta_n) \pmod{2\pi}. \quad (2.40)$$

where we have ignored the precise form of the kick. We have chosen μ to be so small that repeated iteration of the map effectively leaves $J_N = J_0$. The situation for the θ variable is somewhat different. Since with no perturbation and for some N , θ_N can be made infinitesimally close to θ_0 we can conceivably imagine a situation with infinitesimal μ where the $\mu h(J_n, \theta_n)$'s can be made to make up that difference exactly.

The remainder of the argument is very similar to the one presented in [19]. We have a curve $J = \hat{J}(\theta)$ on which all points return onto themselves under operation of \mathbf{M}_μ^N . Assuming that the functions g and h are continuous we can

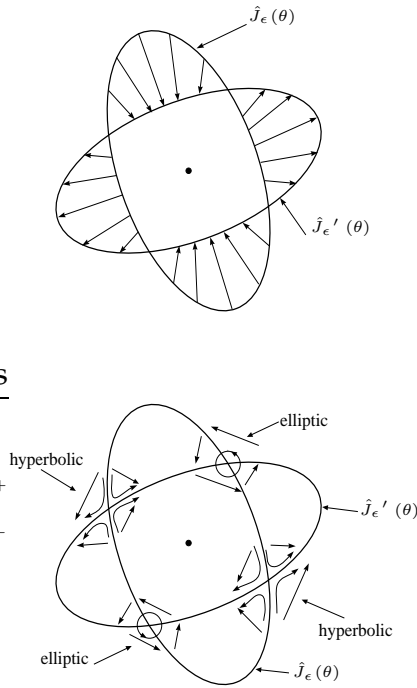


Figure 2.4. Diagram showing the formation of elliptic and hyperbolic stable points due to the Poincaré Birkhoff theorem

say that there exists a curve $J = \hat{J}^+$ for which all values of θ on that circle are rotated, say, anti-clockwise by M_μ^N and some curve $J = \hat{J}^-$ for which all points are mapped clockwise.* Lets say we increase the value of μ to $\epsilon = \mu + \eta$. The exact periodicity of θ_n on the original torus $\hat{J}(\theta)$ is now lost. However, suppose that η is sufficiently small so that a larger loop with always clockwise rotation and smaller loop with always anti-clockwise rotation still exist †. This means that somewhere in between these curves lies another continuous loop $\hat{J}_\epsilon(\theta)$ on which the value of θ returns exactly to itself upon operation of M_ϵ^N . See Figure 2.3.

Therefore the curve $\hat{J}_\epsilon(\theta)$ can only be altered in the radial direction under the map M_ϵ^N . Using the fact that the mapping must be area preserving we can now say that the curve $\hat{J}'_\epsilon(\theta)$ gotten by applying M_ϵ^N to all points on $\hat{J}_\epsilon(\theta)$ must also intersect $\hat{J}_\epsilon(\theta)$. See Figure 2.4 and compare it with Figure 2.2(e). From Figure 2.4 we see that the two curves can generally said to intersect an even number of times. The intersections are fixed points of either an elliptic or hyperbolic nature as can also be seen in figure.

It is debatable if what we have done here is acceptable. However, all arguments seem to be solid as long as we have continuity in the perturbing functions

*It is not important to our analysis which is which.

†They need not be exactly the same curves

g and h . It can be assumed that there exists certain conditions where the perturbation must push a particle into an exactly periodic orbit. Then it must follow from the continuity of g and h that there exists tori, inside and outside the periodic orbit, on which points are moved clockwise or counter-clockwise upon operation of the same perturbed map. All other arguments are exactly the same as the usual Poincaré Birkhoff Theorem.

As a consequence of the modified theorem we should see the break up of certain orbits as the perturbation pushes neighboring orbits into exact periodicity. If an orbit becomes exactly periodic then neighboring orbits will be nearly periodic and will turn into tori around these periodic points. As the perturbation is increased further these neighboring orbits may become exactly periodic and the orbit that was periodic is now forming the tori around this exactly periodic point.

We can show these effects with a numerical calculation. In Figure 2.5 we pick a point on the phase space and evolve for up to $n = 128$ for separate values of μ . We plot the 128 values of q on the y-axis against the different μ values on the x-axis. The exactly periodic points can be seen in the diamond shape pattern. Every line crossing represents an exact resonance of some degree. We see that as μ increases the dynamics of the particle can become chaotic over certain ranges. Eventually for large μ the particles dynamics will go completely chaotic.

Chaos results from the hetro-clinic tangles between the stable and unstable manifolds of the hyperbolic fixed point. This process is explained in detail in the text [19]. Eventually with large μ all tori will have broken apart to leave the whole phase plane chaotic. It is only with the break up of all the invariant tori that we can expect to see complete diffusion of particles in the phase plane.

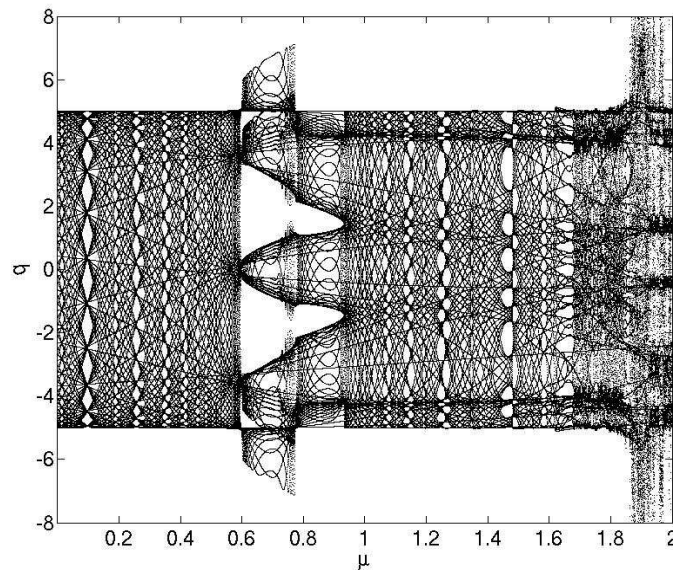
The average rate of diffusion D in this model is understood to be the mean rate of energy growth of a large ensemble over a long time. The energy of a particle as a function of n is given by

$$E_n = \frac{q_n^2 + p_n^2}{2} \quad (2.41)$$

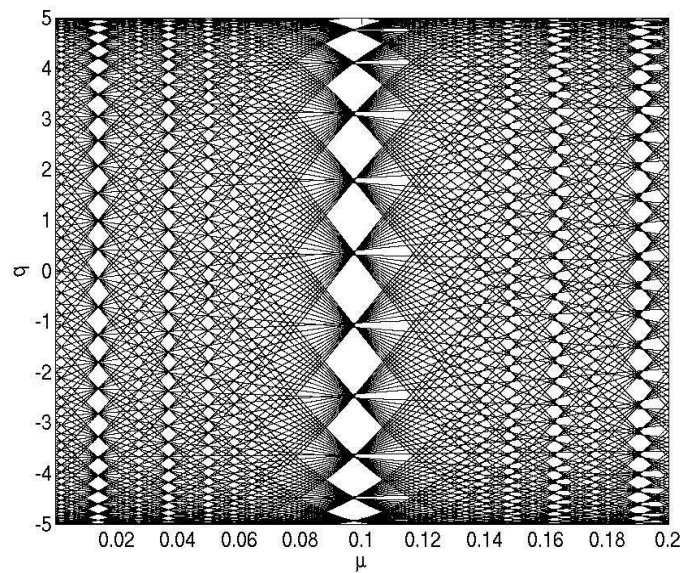
and the rate of linear energy growth or diffusion over a time 0 to n is defined as

$$D(\mu) = \frac{\langle E_n \rangle}{n} \quad (2.42)$$

Where the average is calculated over a large ensemble of randomly distributed particles or points on the phase space. To calculate D numerically we evolve over



(a) Initial value $(q, p) = (5, 0)$ evolved over 128 discrete time steps for different μ .



(b) On closer inspection additional resonances can be seen.

Figure 2.5. q - v - μ with $R = 2/(\sqrt{5}+1)$. Every line crossing represents an exact resonance of some degree. The orbit eventually becomes chaotic with large μ . We have set $k = 1$ in these calculations

a certain amount of time (the longer the better) and then fit a slope to the energy curve (2.41). It can be easily seen that any change in energy is as a result of the discrete kick given to the momentum term, see (2.19). This is because there is no change in energy associated with a simple rotation in the phase plane. The change in energy of one particle is thus given by

$$\Delta E = E_{n+1} - E_n = \frac{1}{2} (p_{n+1}^2 - p_n^2) = \frac{1}{2} (2p_n\mu \sin(kq_n) + \mu^2 \sin^2(kq_n)). \quad (2.43)$$

If we assume that the ensemble is evenly distributed along the q axis we may integrate q_n from 0 to $2\pi/k$, the period of the sin function, to get the average energy growth of the ensemble over one kick. That is,

$$\langle \Delta E \rangle = \frac{k}{2\pi} \int_0^{2\pi/k} \frac{1}{2} (2p_n\mu \sin(kq_n) + \mu^2 \sin^2(kq_n)) dq_n = \frac{\mu^2}{4}. \quad (2.44)$$

In the event of large μ and therefore completely chaotic dynamics where there are no isolating non-resonant tori we may say that this estimation is always roughly correct. Putting this into (2.42) we have

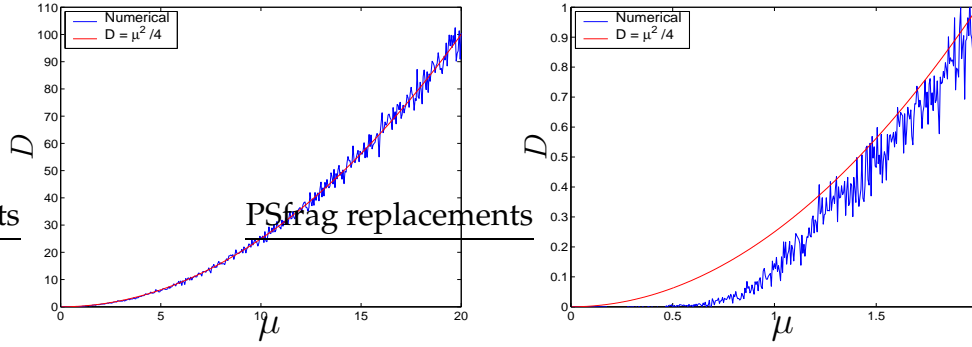
$$D(\mu) = \frac{\langle E_n \rangle}{n} = \frac{n \langle \Delta E \rangle}{n} = \frac{\mu^2}{4}. \quad (2.45)$$

The rate of this diffusion as a function of the perturbing parameter μ is calculated numerically and compared with the theoretical prediction in Figure 2.6. The results are, as predicted, in good agreement for large values of μ .

This concludes this section on the dynamics of the kicked oscillator with irrational frequency ratios. We have suggested that dynamics of this non-KAM system with irrational frequency ratios behaves in many respect like those of a KAM system. We see in the Poincaré surface of section, virtually impenetrable tori or barriers inside which the dynamics of the particle must remain. We also have the chaotic instability that follows from the break up of these invariant tori like in a KAM system. So we have the curious situation that the harmonic oscillator which is said to be a non-KAM system behaves very like a KAM system when the kicking frequency is incommensurate with the natural frequency of the oscillator.

2.3.2 Rational frequency ratio, $1/R=1/4$

It has already been mentioned that setting $\theta = \omega_0 T = \pi/2$ sets the frequency ratio $1/R$ to $1/4$. Substituting $\theta = \pi/2$ into (2.26) sets all cos terms to zero and all sin



(a) The approximation is quite good for large kick strengths

(b) The theoretical approximation is poor for $\mu < 2$. The approximation does not take into account the existence of the invariant tori

Figure 2.6. Rate of diffusion D -v- μ . Irrational frequency ratio, $1/R = (\sqrt{5} + 1)/2$. The numerical calculation was performed by taking 600 uniformly distributed particles in the phase plane window $q, p \in [-6\pi, 6\pi]$ setting $k = 1$ and then evolving for 400 discrete time steps at different μ .

terms to unity. This leaves the simple map

$$\begin{aligned} q_{n+1} &= p_n + \mu \sin(kq_n), \\ p_{n+1} &= -q_n. \end{aligned} \quad (2.46)$$

This mapping which we will refer to as \mathbf{Q}_μ displays some very interesting properties including the aforementioned stochastic web. It also displays some strange diffusional properties at certain values of the kick strength μ . We begin by referring again to equation (2.36) which says that the harmonic oscillator is not a system to which the KAM theorem can be applied. The surface of section picture for the kicked oscillator with $\mu = 0$ and $\theta = \pi/2$, see Figure 2.7(a), shows that all points on the phase plane will, after four iterations of the map \mathbf{Q}_0 , return to their original coordinates exactly. What happens after 4 iterations of \mathbf{Q}_μ with $\mu \neq 0$? The map \mathbf{Q}_μ^2 is calculated by twice iterating (2.46) to give

$$\begin{aligned} q_{n+2} &= p_{n+1} + \mu \sin(kq_{n+1}) = -q_n + \mu \sin(kp_n + k\mu \sin(kq_n)), \\ p_{n+2} &= -q_{n+1} = -p_n - \mu \sin(kq_n). \end{aligned} \quad (2.47)$$

The map \mathbf{Q}_μ^4 may then be calculated by twice iterating (2.47). We have

$$\begin{aligned}
q_{n+4} &= -q_{n+2} + \mu \sin(kp_{n+2} + k\mu \sin(kq_{n+2})), \\
p_{n+4} &= -p_{n+2} - \mu \sin(kq_{n+2}).
\end{aligned} \tag{2.48}$$

which after substituting (2.47) into (2.48) gives

$$\begin{aligned}
q_{n+4} &= q_n - \mu \sin(kp_n + k\mu \sin(kq_n)) \\
&\quad + \mu \sin(-kp_n - k\mu \sin(kq_n) + k\mu \sin(-kq_n + k\mu \sin(kp_n + k\mu \sin(kq_n)))) \\
p_{n+4} &= p_n + \mu \sin(kq_n) \\
&\quad - \mu \sin(-kq_n + k\mu \sin(kp_n + k\mu \sin(kq_n))).
\end{aligned} \tag{2.49}$$

We can now clearly see that if $\mu \neq 0$ exact periodicity, that is,

$$\begin{aligned}
q_{n+4} &= q_n, \\
p_{n+4} &= p_n,
\end{aligned} \tag{2.50}$$

always occurs if both kq_n and kp_n are integer multiples of π . This can also be written as:

$$\begin{aligned}
q_n &= \frac{m_q \pi}{k} \\
p_n &= \frac{m_p \pi}{k} \quad m_q, m_p = \dots -2, -1, 0, 1, 2 \dots
\end{aligned} \tag{2.51}$$

The introduction of the perturbation knocks the vast majority of orbits out of exact periodicity. However, we also see that, no matter how large we make μ , points obeying (2.51) will always be exact return points of \mathbf{Q}_μ^4 .

We now attempt some linear stability analysis on \mathbf{Q}_μ^4 for small values of μ . First note that in the immediate vicinity of $x = m\pi$ we may use the following Taylor expansion to approximate $\sin x$

$$\sin x \approx (-1)^m \left[(x - m\pi) - \frac{(x - m\pi)^3}{3!} + \frac{(x - m\pi)^5}{5!} - \dots \right] \tag{2.52}$$

When μ is extremely small we can approximate (2.49) with the expression

$$\begin{aligned} q_{n+4} &= q_n - 2\mu \sin(kp_n), \\ p_{n+4} &= p_n + 2\mu \sin(kq_n), \end{aligned} \quad (2.53)$$

as all other expressions inside the outermost sin functions are very small because μ is small and $|\sin x|$ is also small when x near $m\pi$. Using expression (2.52) we may approximate further around the points $(q_n, p_n) = (m_q\pi/k, m_p\pi/k)$. We can write to the first order

$$\begin{aligned} q_{n+4} &= q_n - 2\mu(-1)^{m_p}(kp_n - m_p\pi), \\ p_{n+4} &= p_n + 2\mu(-1)^{m_q}(kq_n - m_q\pi). \end{aligned} \quad (2.54)$$

From this we may find the Jacobian \mathbf{J} to first order

$$\mathbf{J} = \begin{pmatrix} \frac{\partial q_{n+4}}{\partial q_n} & \frac{\partial q_{n+4}}{\partial p_n} \\ \frac{\partial p_{n+4}}{\partial q_n} & \frac{\partial p_{n+4}}{\partial p_n} \end{pmatrix} = \begin{pmatrix} 1 & -2k\mu(-1)^{m_p} \\ 2k\mu(-1)^{m_q} & 1 \end{pmatrix} \quad (2.55)$$

It is the eigenvalues of the Jacobian \mathbf{J} that determine whether a point is stable or unstable [8]. Complex conjugate eigenvalues on the unit circle $\lambda_{1,2} = e^{\pm i\sigma}$ correspond to elliptic and therefore stable orbits. Real reciprocal eigenvalues $\lambda_2 = \lambda_1^{-1}$ correspond to hyperbolic periodic orbit and therefore the existence of unstable manifolds. The eigenvalues of the Jacobian are given by

$$|\mathbf{J} - \lambda\mathbf{I}| = 0. \quad (2.56)$$

which gives for the characteristic equation

$$\lambda^2 - 2\lambda + (1 + 4k^2\mu^2(-1)^{m_q+m_p}) = 0. \quad (2.57)$$

The solutions to this equation are

$$\lambda = 1 \pm k\mu\sqrt{-(-1)^{m_q+m_p}}. \quad (2.58)$$

Remembering that μ is small we can say the following:

- If $m_q + m_p$ is even then the eigenvalues $\lambda_{1,2}$ are complex $\lambda_{1,2} = 1 \pm ik\mu \approx e^{\pm ik\mu}$ and $(q, p) = (m_q\pi/k, m_p\pi/k)$ is a stable periodic point.
- If $m_q + m_p$ is odd then the eigenvalues $\lambda_1 = 1 + k\mu$ and $\lambda_2 = 1 - k\mu$ are approximately reciprocal and are real. Therefore $(q, p) = (m_q\pi/k, m_p\pi/k)$ is a unstable periodic point.

This describes a lattice with alternating stable and unstable points. Around the stable points are elliptical orbits encircling an ever greater area. Examining Figure 2.7 we see that at some point these orbits must end as they will eventually run into the unstable manifolds predicted above. In the same way as in the irrationally kicked system these hyperbolic fixed points and the manifolds that are connected to them generate the hetro-clinic tangles that are the cause of chaos. The chaos thus exists even for extremely small kick strengths. The hetro-clinic tangles inter-twine to form a chaotic net or web like structure that acts as a fractal like separatrix between points orbiting different elliptical stable points. This is the so called stochastic web and we see it must extend to infinity in all directions of the phase plane.

As μ gets larger the stochastic nature of the web becomes apparent. The web will eventually increase in size until nearly all of the non-resonant or orbiting tori have been destroyed. At nearly all values of the kicking strength above about $\mu \approx 4$ the phase space Poincaré surface of section seems to be completely chaotic. The quick analysis for the rate of diffusion for an ensemble of particles for the irrationally kicked oscillator would also seem to be in order here. See section 2.3.1. The value of D obtained before $D(\mu) = \frac{\mu^2}{4}$, is not bad for a first order estimate. However, we shall see in the next section that there is a periodic fluctuation about this central function $D(\mu)$ and that this periodic fluctuation is supplemented by a large delta like spike for certain values of the kick strength.

2.4 Diffusion properties of the 1/R=1/4 system

This section attempts to explain the phenomena of anomalous diffusion that occurs for certain values of kicking strength in the resonant system with frequency ratio of 1/4. We begin with a brief review of some classical results dealing with this particular setup and then examine the specific mechanisms that lead to these phenomena. This will hopefully give a more complete picture of the nature of the classical anomalous diffusion.

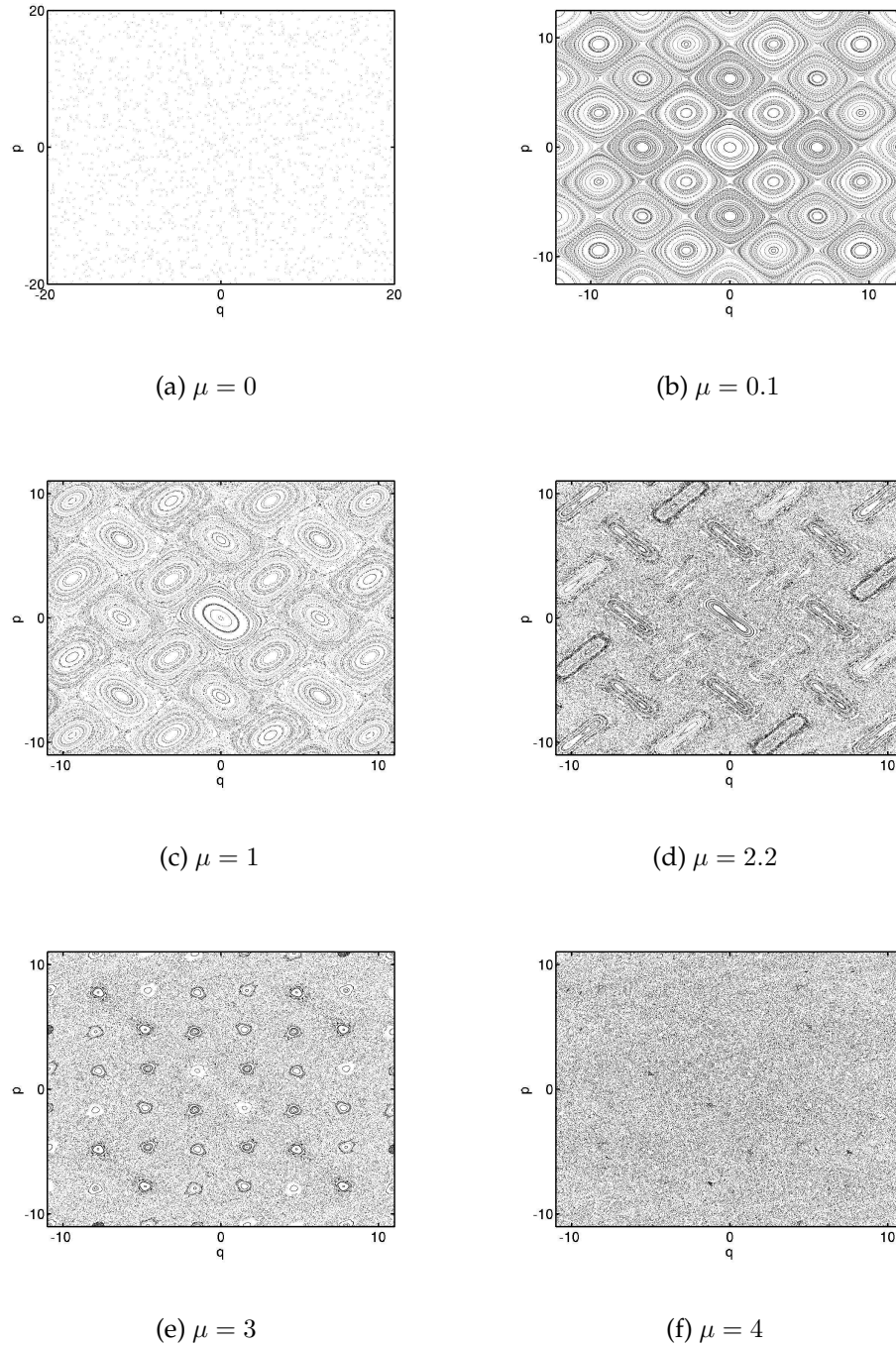
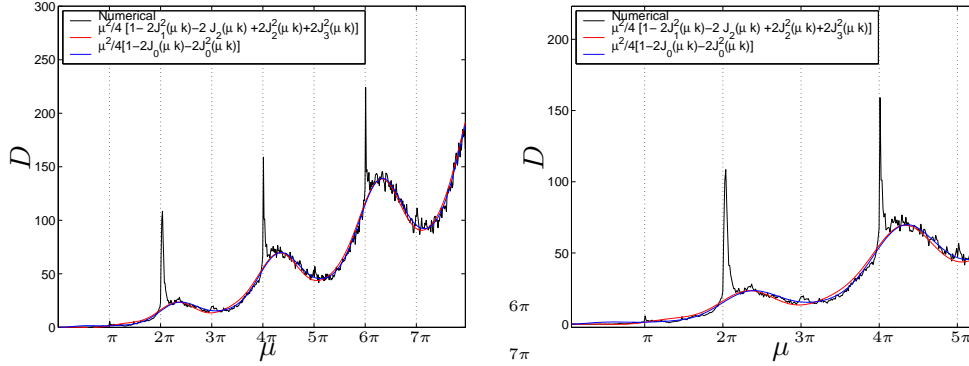


Figure 2.7. Graphs showing Poincaré surface of sections with $1/R = 1/4$ for various values of the kicking strength μ . We have set $k = 1$ in these calculations



(a) The theoretical approximations for $D(\mu)$ are quite good. However, they do not predict the large spikes occurring just after $\mu = 2m\pi$

(b) Here we zoom in on the first two spikes. They appear just after $\mu = 2m\pi$, with $m = 1, 2, \dots$

Figure 2.8. D -v- μ for the rational frequency ratio $1/R = 1/4$. The numerical calculation was performed by taking 600 randomly distributed particles in the phase plane and evolving for 400 discrete time steps at different μ . We have set $k = 1$ in this calculation.

The process of diffusion has been treated thoroughly for the kicked rotor or standard map [21–23]. A similar analysis to that in [21] can be applied to the kicked harmonic oscillator [15,24,25] with similar results. The rate of diffusion as a function of kick strength μ with was calculated to be

$$D = \frac{1}{4}\mu^2[1 - 2J_1^2(\mu k) - 2J_2 + 2J_2^2(\mu k) + 2J_3^2(\mu k)] . \quad (2.59)$$

An alternative analysis is provided in [26] and gives

$$D = \frac{1}{4}\mu^2[1 - 2J_0(\mu k) - 2J_0^2(\mu k)] . \quad (2.60)$$

In Figure 2.8 we compare these functions with the numerically calculated values of the diffusion coefficient. Setting $k = 1$ we get these values by evolving 600 hundred randomly distributed classical points in the range $q, p \in [-6\pi, 6\pi]$ over 400 time steps, fitting a line to its energy diffusion curve, and getting the slope for different values of μ . The results show that while being an extremely good fit for most kicking strengths neither analysis accounts for the sharp spikes that occur when the kicking strengths μ are just above a multiple of 2π . It is clear that some other process is working in conjunction with this average diffusion to create these large fluctuations in the rate of energy growth.

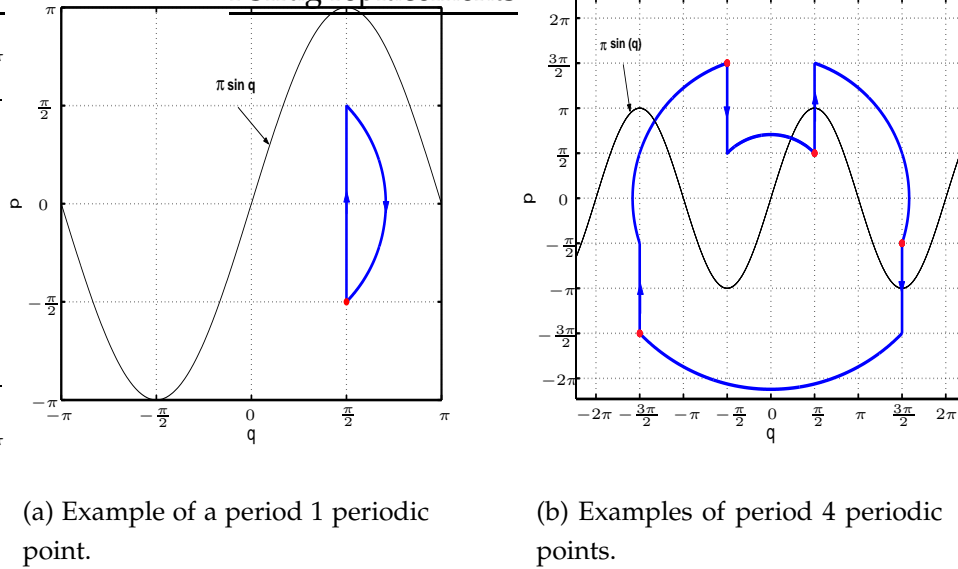
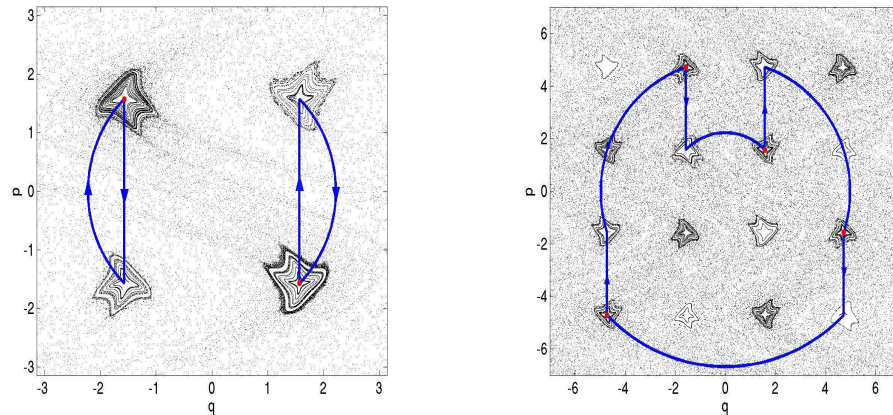


Figure 2.9. Examples of exact periodic points that exist when $\mu = \pi$ and $k = 1$

The large spikes in the numerical diffusion curves may be explained through the existence of stable *accelerator* islands. These islands are also called *ballistic* islands or modes. The troughs in the oscillating pattern in Figure 2.8 also have a stable structure associated with them and we shall refer to them as *periodic* or *quasi-periodic* islands. Both these types structures exist because at certain resonant values of the kicking strength both the kick and the rotation can be made to either cancel each other out or reinforce each other. We shall refer to the whole phenomenon as *anomalous diffusion* or *classical resonance*.

The processes forming these structures may best be discussed with the aid of a few specific examples. Let us first examine the system with a kicking strength equal to π and for simplicity we shall also set $k = 1$ for the remainder of the chapter. We start with a particle situated at $(\pi/2, -\pi/2)$ on the $q - p$ phase plane. We will assume that we first kick the particle and then apply the rotation that corresponds to the free evolution of the SHO. For the kick we may apply the map (2.19) which moves the particle up to the point $(\pi/2, \pi/2)$. For the free evolution (rotation) we use (2.24) with $\theta = \pi/2$, which brings the point back to where it started at $(\pi/2, -\pi/2)$, see Fig. 2.9(a). This is an example of what we will call a period 1 return point. Indeed we will see that a region of stability exists around such points whereby each operation of the map returns a points to somewhere in the same region.



(a) Example of a period 1 periodic point and the surrounding elliptical orbits.

(b) Examples of period 4 periodic points and the surrounding elliptical orbits.

Figure 2.10. The exact periodic points are surrounded by stable elliptical orbits. We set $\mu = \pi$ and $k = 1$ to generate this diagram.

Consider now the point $(\pi/2, \pi/2)$, using \mathbf{Q}_π , that is (2.26) with $\mu = \pi$, we calculate its trajectory through four successive mappings

$$(\pi/2, \pi/2) \rightarrow (3\pi/2, -\pi/2) \rightarrow (-3\pi/2, -3\pi/2) \rightarrow (-\pi/2, 3\pi/2) \rightarrow (\pi/2, \pi/2) . \quad (2.61)$$

These are exact period 4 return points. They are the center points of special stable regions of the phase plane. If a particle has initial conditions such that it lies somewhere in these regions it will return to that same region after 4 iterations of the map, see Fig. 2.9(b). The islands of stability can clearly be seen in the phase portraits in Figure 2.10. It is obvious from this simple analysis that particles on these particular points do not gain energy over time. It is however not so obvious what determines the stability of the neighboring region. We briefly discuss this stability issue in the next section.

We now turn our attention to the aforementioned *accelerator* islands or modes. These cannot be seen using a Poincaré surface of section like in Fig.2.10 for the simple reason that particles initially existing on these islands never return to the same region. In fact a particle on one of these islands will be passed from one island to another and, depending on the initial conditions, will result in a rapid

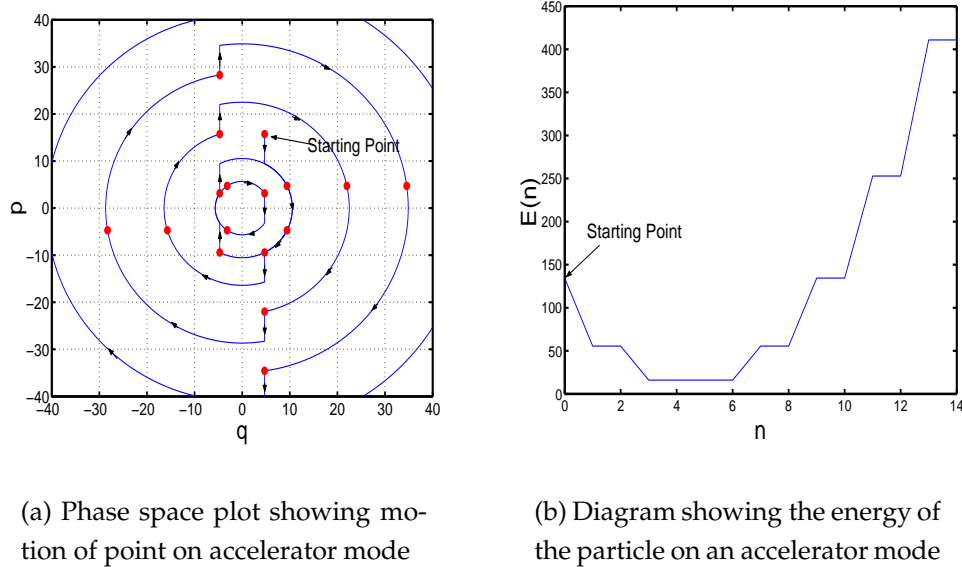
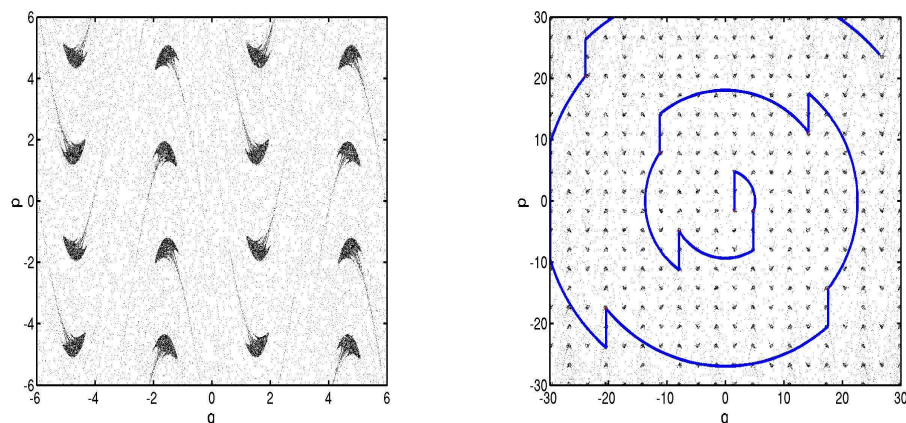


Figure 2.11. Motion and energy of particle on an accelerator island. Note that the energy initially decreases but eventually increases.

increase or decrease in a particle's energy under consecutive mappings. However, particles that initially lose energy will eventually reach a minimum energy level and then have its energy increase with each mapping. We again use a specific example to illustrate these processes. Setting $\mu = 2\pi$, $k = 1$ and starting with a particle at initial position $(3\pi/2, 10\pi/2)$ we plot the trajectory of the particle under the mapping and show the energy of the particle as calculated from $E = (q^2 + p^2)/2$ as a function of time or kick number n , see Fig. 2.11. For now it is only important to notice that over long enough times particles on these types of islands will increase in energy and move farther from the origin.

As mentioned already it is difficult to see any signatures of these structures in the phase portrait because of their diffusive nature. To get an idea of their shape and size we first try the simple technique of plotting on the phase plane the initial positions of particles that after a certain amount of time have been displaced by over a certain amount. Fig. 2.12 gives a good illustration of the shape, size and overall position of these islands near the origin. The distance the particle should have moved from its initial location depends on a number of factors such as the kicking strength and the number of kicks and is therefore somewhat arbitrary. Note that to generate these these figures we chose $\mu \approx 6.38 > 2\pi$. The reason for this will be discussed in section 2.4.2.



(a) The accelerator modes are distributed in a lattice over all phase space.

(b) The blue curve shows how a particle initially on an accelerator mode will quickly gain in energy.

Figure 2.12. Rough shape and position of some accelerator modes generated by setting $\mu \approx 6.38, k = 1$ and evolving a selection of randomly distributed points for a fixed time. The initial configuration of particles that have gained, after the fixed time, an energy greater than some large value are plotted in the figure.

2.4.1 Structure of the quasi-periodic islands

We noted earlier that both the quasi-periodic and accelerator islands exist because of an unusual resonance between the kicking and free evolution within the system. In this section we deal, in more detail, with the exact structure of the quasi-periodic modes. This is best done by examining the map \mathbf{Q}_μ (2.46), repeated here,

$$\begin{aligned} q_{n+1} &= p_n + \mu \sin(q_n) \\ p_{n+1} &= -q_n. \end{aligned} \tag{2.62}$$

where for simplicity we have set $k = 1$. Resonance then occurs when μ is some factor of the period of the sinusoidal function, which in this particular case is 2π . These quasi-periodic modes or islands are shown in Figure 2.10 when $\mu \approx \pi$. However, we will show these particular stable points, and their surrounding elliptical orbits exist for values of μ that are well lower than this. Examining the map (2.62), it is easy to see that a period one fixed point exists at $(q, p) = (0, 0)$ for all values of μ . By looking at the phase portraits in Figure (2.7) we notice

that somewhere around the value of $\mu \approx 2$ two new elliptic period 1 fixed points appear. The nature of the the motion that leads to these new points is exactly the same as we demonstrated in Figure 2.10. That is, around these points, the jump in momentum and free evolution or rotation cancel each other. We cast this in a new light by examining the map (2.62). We can see that the second line means that any period one solution must exist on the $p = -q$ line. Substituting this into the first line gives the implicit formula for the fixed point position coordinate which we call s_q .

$$2s_q = \mu \sin(s_q) \quad (2.63)$$

The trivial solution at $s_q = 0$ can easily be seen. Since the sinc function can't have values greater than unity we see that other solutions only exist for $\mu \geq 2$. We can also see that as $\mu \rightarrow \pi$ the coordinates of the elliptic stable points $(s_q, s_p) \rightarrow (\pi/2, -\pi/2)$ and $(-\pi/2, \pi/2)$ which is what we demonstrated numerically in the previous section.

We next deal with the question of the stability of these 'periodic' islands. We use the period one point at $(s_q, s_p) = (\pi/2, -\pi/2)$ in the second quadrant as a typical example. We first perform a coordinate transformation by letting

$$\begin{aligned} q &= s_q + \delta q , \\ p &= s_p + \delta p . \end{aligned} \quad (2.64)$$

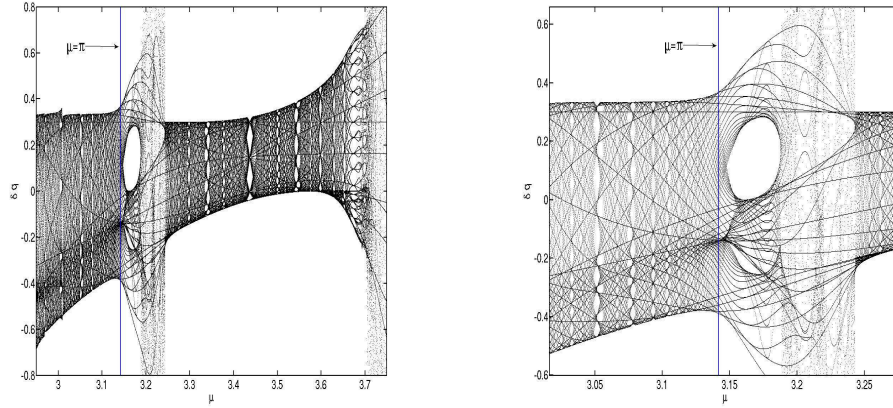
Substituting this into (2.62) gives

$$\begin{aligned} \delta q_{n+1} + s_q &= \delta p_n + s_p + \mu \sin(\delta q_n + s_q) , \\ \delta p_{n+1} + s_p &= -\delta q_n - s_q . \end{aligned} \quad (2.65)$$

If we put in the exact values of (s_q, s_p) we may write this as

$$\begin{aligned} \delta q_{n+1} &= \delta p_n - \pi + (\mu) \cos(\delta q_n) , \\ \delta p_{n+1} &= -\delta q_n . \end{aligned} \quad (2.66)$$

We can now perform some new analysis similar to that of section 2.3.1. We can see the brief transition to chaos as we move μ through π . Figure 2.13 shows this



(a) δq -v- μ . The plot contains the first 80 values of δq_n plotted against the kick strength μ .

(b) Here we examine the bifurcation at $\mu \approx \pi$ in more detail

Figure 2.13. Transition to chaos. We start with initial point $(\delta q_0, \delta p_0) = (0.3, 0)$ and plot the δq_n for the first 80 iterations for different values of μ . Note the break up of the orbit just after $\mu = \pi$.

strange bifurcation. Here we iterate forward 80 times from the starting position $(\delta q_0, \delta p_0) = (.3, 0)$ and repeat for different values of the μ . This bifurcation can also be viewed by looking at the phase space structure just before and after $\mu = \pi$. We plot these in Figure 2.14.

Interestingly, if we let $\mu = \pi + \Delta$ and Taylor expand the \cos term above, ignoring higher order terms, we may approximate the map (2.66) as

$$\begin{aligned} \delta q_{n+1} &= \delta p_n - \frac{\pi}{2}(\delta q_n)^2 + \Delta , \\ \delta p_{n+1} &= -\delta q_n . \end{aligned} \quad (2.67)$$

Since each new δp is gotten only from the previous δq we can write the whole map as a simple nonlinear recurrence relation:

$$\delta q_{n+1} = -\frac{\pi}{2}\delta q_n^2 - \delta q_{n-1} + \Delta . \quad (2.68)$$

Most of the structures and chaotic effects of the full map are still apparent in this simpler map. It serves to emphasise the fact that the most complex structures observed in chaos often have extremely simple relationships as their building

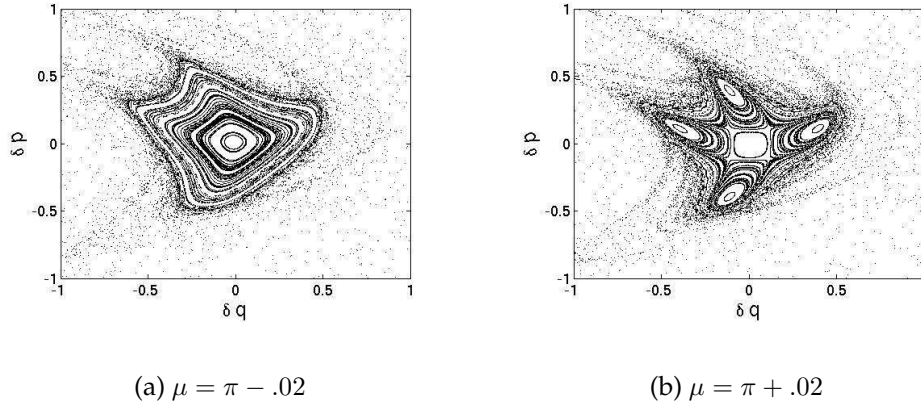


Figure 2.14. Detailed Poincaré surface of section of the quasi-periodic islands for the map Q_μ , see (2.62)

blocks. It is here we leave the discussion of these stable elliptical islands. We just mention that the same type of structures emerge again at $\mu = 3\pi, 5\pi, \text{etc.}$ through the same simple process. We also point out that we have only dealt with modes of period 1. The period 4 modes mentioned at the top of this section are formed in essentially the same way and therefore have an identical structure.

2.4.2 Structure in the accelerator modes

As we have mentioned the anomalous spikes seen in the diffusion curve for Q_μ , see Figure 2.8, for specific ranges of μ can be explained by the existence of stable ballistic or accelerator structures in the phase plane. We showed in section 2.4 that these islands appear because at the specific values of the kick strength μ the rotation and kicking operations of Q_μ act in such a way as to reinforce each other and rapidly change the energy of a particle on one of the islands.

The broad topic of anomalous diffusion and the accelerator modes is treated in the review [28]. This review touches on aspects of anomalous diffusion in the KHO but from the perspective of the Kicked Harper Model (KHM) and its associated mapping, sometimes called the Web Map (WM). For more details on this system the reader should consult the texts [9,10]. The web map is often written as

$$\begin{aligned} u_{n+1} &= v_n , \\ v_{n+1} &= -u_n - K \sin v_n , \end{aligned} \tag{2.69}$$

where K is used to represent the kick strength. However, it can be mapped directly to Q_μ , (2.46), by setting our parameter $k = 1$ and using the simple transformations

$$\begin{aligned} v &= q , \\ u &= -p , \\ \mu &= -K . \end{aligned}$$

Using the WM, analysis on the self similarity of the phase space structure near the ballistic islands has been done using fractional kinetics in [27] and reviewed in [10]. A 'magic' value of the kick strength $\mu = 6.349972$, where the stickiness of the modes is a maximum, is calculated. The terms stickiness and self similarity refer to the fractal nature of the boundary that seem to trap unstable orbits within them for unusually long times.

In this section we present our own analysis that allows us to calculate the exact positions of the accelerator islands and perform linear stability analysis on them. As mentioned already it is not as easy to see any structure in the accelerator modes using the mapping (2.46), so instead we derive a new map from the reference frame of a particle on an accelerator island. We first perform the KHO mapping twice, see (2.47)

$$\begin{aligned} p_{n+2} &= -p_n - \mu \sin(q_n) , \\ q_{n+2} &= -q_n + \mu \sin(p_n + \mu \sin(q_n)) . \end{aligned} \quad (2.70)$$

We now pick a starting point that we know to be on the center of an accelerator island, namely $(q_n, p_n) = (5\pi/2, 7\pi/2)$ (it doesn't matter which one). Substituting these values into (2.70) and setting $\mu = 2\pi, k = 1$ we get

$$\begin{aligned} p_{n+2} &= -7\pi/2 - 2\pi \sin(5\pi/2) = -11\pi/2 , \\ q_{n+2} &= -5\pi/2 + \mu \sin(7\pi/2 + 2\pi \sin(5\pi/2)) = -9\pi/2 . \end{aligned} \quad (2.71)$$

Notice that the new values of q and p are the negative of the old values minus 2π . This means of course that if we were to add 2π to each one and rotate π around the origin we would be back where we had started. Performing this addition and rotation on the map (2.70) gives

$$\begin{aligned}
p_{n+2} &= p_n + \mu \sin(q_n) - 2\pi , \\
q_{n+2} &= q_n - \mu \sin(p_n + \mu \sin(q_n)) - 2\pi .
\end{aligned} \tag{2.72}$$

or

$$\begin{aligned}
p_{n+2} &= p_n + \mu \sin(q_n) - 2\pi , \\
q_{n+2} &= q_n - \mu \sin(p_{n+2}) - 2\pi .
\end{aligned} \tag{2.73}$$

The next step is to make a coordinate transformation so that we put what we call the center of the island at the origin. We make the substitution like before using the coordinates given above $(s_q, s_p) = (5\pi/2, 7\pi/2)$. We set

$$\begin{aligned}
q &= s_q + \delta q , \\
p &= s_p + \delta p ,
\end{aligned} \tag{2.74}$$

and substitute this into (2.73) to get

$$\begin{aligned}
\delta p_{n+2} &= \delta p_n + \mu \sin(\delta q_n + 5\pi/2) - 2\pi , \\
\delta q_{n+2} &= \delta q_n - \mu \sin(\delta p_{n+2} + 7\pi/2) - 2\pi .
\end{aligned} \tag{2.75}$$

We may finally write out in the simple form

$$\begin{aligned}
\delta p_{n+2} &= \delta p_n + \mu \cos(\delta q_n) - 2\pi , \\
\delta q_{n+2} &= \delta q_n + \mu \cos(\delta p_{n+2}) - 2\pi .
\end{aligned} \tag{2.76}$$

This mapping will now track points that are initially on the accelerator island at $(s_q, s_p) = (5\pi/2, 7\pi/2)$ and perform the correct transformation so that they appear near the origin. We could have derived a general map for all the different modes but that would be unnecessary for our purposes. We can now use our new map to examine the structure and stability properties of these accelerator modes. Some Poincaré surfaces of section of these accelerator modes can be seen in Fig. 2.15. What is striking from these pictures is the complete lack of a stable accelerator mode when $\mu < 2\pi$. Even if $\mu = 2\pi$ the island is not very large and could not be regarded as stable. It is however when $\mu > 2\pi$ that we actually see

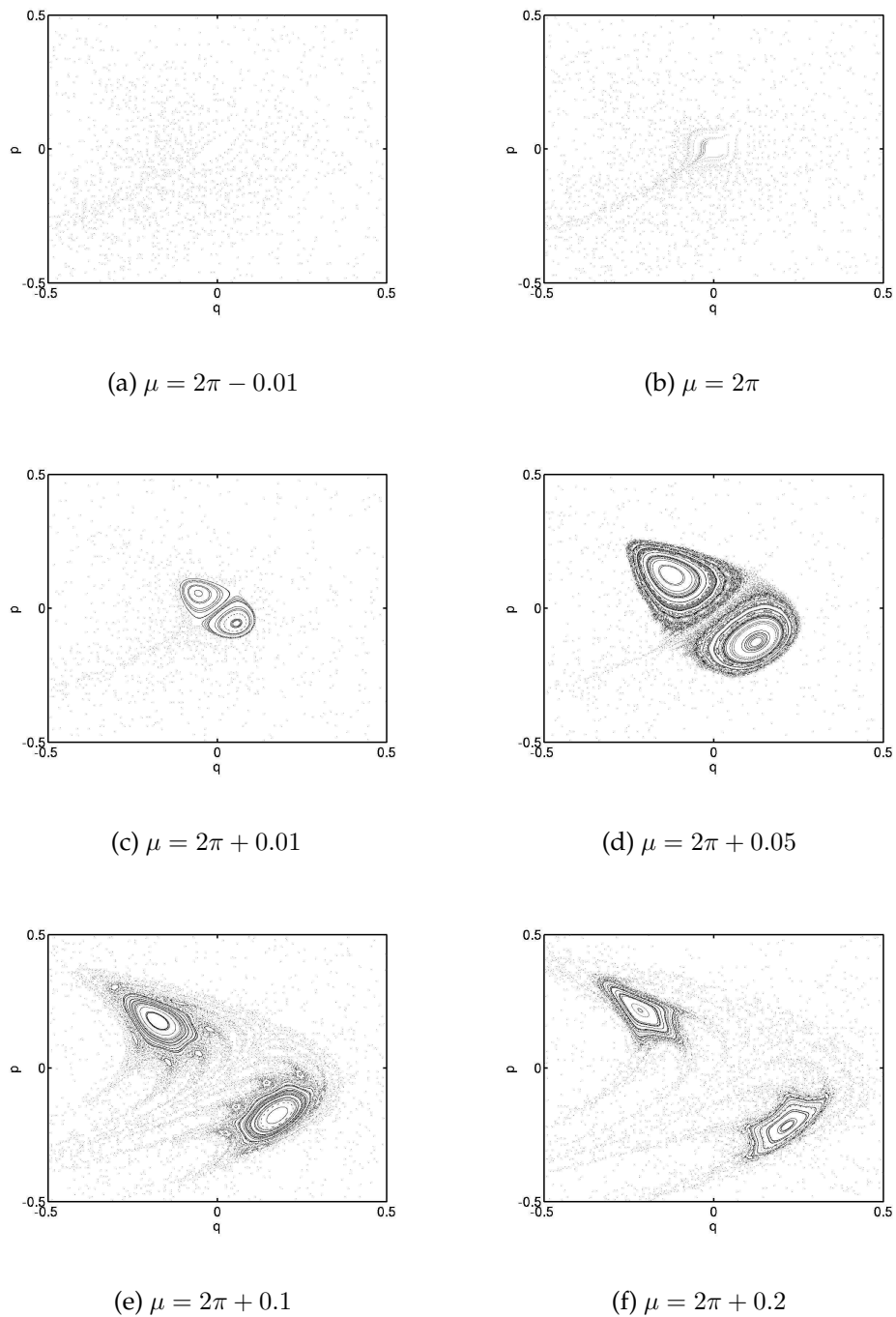


Figure 2.15. Graphs showing structure of a ballistic island for various values of the kicking strength μ . These graphs are generated by operating on a group of randomly distributed points in the phase plane window $\delta_q, \delta_p \in [-0.5, 0.5]$ with (2.76). We can see here the stable elliptical structure that was invisible to us in Figure 2.12.

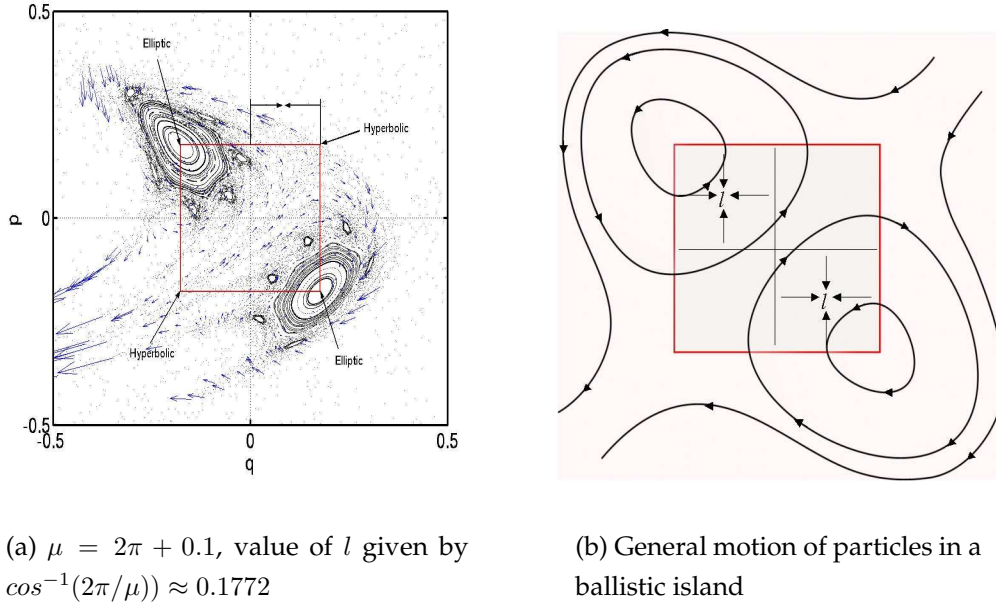


Figure 2.16. Diagrams detailing the motion of particles in the vicinity of the accelerator or ballistic islands

the real structure of the mode. We see the existence of two main islands that grow as we initially move away from exact resonance. Analysis of individual points in these islands show that they remain on the same island through each operation. It is important to remember however, that in creating the map (2.73), we used two iterations of the kicked harmonic oscillator map and therefore in reality a particle will move back and forth between the 2 distinct stable structures as it moves from accelerator mode to accelerator mode.

We can analyse this further by plotting the 'velocity' vectors of each point along with the Poincaré surface of section. See Figure 2.16(a). This clearly shows the existence of four return points. The two elliptic points already mentioned and two hyperbolic points. Using (2.76) and setting the conditions for exact periodicity, $\delta p_{n+2} = \delta p_n$ and $\delta q_{n+2} = \delta q_n$, we may write the periodic points of the new map as

$$\bar{\delta q} = \pm l = \pm \cos^{-1} \left(\frac{2\pi}{\mu} \right) \quad (2.77)$$

and

$$\bar{\delta p} = \pm l = \pm \cos^{-1} \left(\frac{2\pi}{\mu} \right). \quad (2.78)$$

For either of these to have real values we know that the argument of the \cos^{-1} function must be $\leq |1|$. This explains why we see no sign of this anomalous diffusion until $\mu \geq 2\pi$, see Figures 2.15(a) and 2.15(b). Referring forward again to Figures 2.16(a) we see that the corners of the red rectangle in each figure represent the exact location of the return points. Figure 2.16(b) represents the typical flow of particles inside one of these accelerator islands. Of course, *this* flow represents the motion of particles over two separate operations of the kicked harmonic oscillator map in addition to a shift and a rotation.

We can perform some linear stability analysis on the mapping (2.76). We first find the Jacobian :

$$\mathbf{J} = \begin{pmatrix} \frac{d\delta q_{n+2}}{d\delta q_n} & \frac{d\delta q_{n+2}}{d\delta p_n} \\ \frac{d\delta p_{n+2}}{d\delta q_n} & \frac{d\delta p_{n+2}}{d\delta p_n} \end{pmatrix} = \begin{pmatrix} \frac{\partial\delta q_{n+2}}{\partial\delta q_n} + \frac{\partial\delta q_{n+2}}{\partial\delta p_{n+2}} \frac{\partial\delta p_{n+2}}{\partial\delta q_n} & \frac{\partial\delta q_{n+2}}{\partial\delta p_{n+2}} \frac{\partial\delta p_{n+2}}{\partial\delta p_n} \\ \frac{\partial\delta p_{n+2}}{\partial\delta q_n} & \frac{\partial\delta p_{n+2}}{\partial\delta p_n} \end{pmatrix}. \quad (2.79)$$

This gives

$$\mathbf{J} = \begin{pmatrix} 1 + \mu^2 \sin(\bar{\delta}p) \sin(\bar{\delta}q) & -\mu \sin(\bar{\delta}p) \\ -\mu \sin(\bar{\delta}q) & 1 \end{pmatrix}. \quad (2.80)$$

when we evaluate this at the maps fixed points. If we make the substitution $\bar{p} = \mu \sin(\bar{\delta}p)$ and $\bar{q} = \mu \sin(\bar{\delta}q)$ we may write \mathbf{J} as

$$\mathbf{J} = \begin{pmatrix} 1 + \bar{q}\bar{p} & -\bar{p} \\ -\bar{q} & 1 \end{pmatrix}. \quad (2.81)$$

As before, it is the eigenvalues of the Jacobian \mathbf{J} that determine whether a point is stable or unstable [8]. Complex conjugate eigenvalues on the unit circle $\lambda_{1,2} = e^{\pm i\sigma}$ correspond to elliptic and therefore stable orbits. Real reciprocal eigenvalues $\lambda_2 = \lambda_1^{-1}$ correspond to hyperbolic periodic orbit and therefore the existence of unstable manifolds. The eigenvalues of the Jacobian are given by

$$|\mathbf{J} - \lambda\mathbf{I}| = 0. \quad (2.82)$$

This works out to give

$$\lambda^2 - \lambda(\bar{q}\bar{p} + 2) + 1 = 0, \quad (2.83)$$

whose exact eigenvalues are

$$\lambda_{1,2} = \frac{1}{2} \left(2 + \bar{q}\bar{p} \pm \sqrt{4\bar{q}\bar{p} + \bar{q}^2\bar{p}^2} \right) \quad (2.84)$$

The eigenvalues are always real if \bar{q} and \bar{p} have the same sign and complex if the signs of \bar{q} and \bar{p} are different and their absolute values are less than 2. The condition for the existence of the elliptic points is then

$$|\bar{q}| = |\bar{p}| = \mu \sin(\bar{\delta}q) = \mu \sin(\cos^{-1}(2\pi/\mu)) < 2. \quad (2.85)$$

We are now in a position to write out the general stability condition for the accelerator modes. Remembering that the periodic points only occur when $\mu \geq 2\pi$ and noting that $\sin(\cos^{-1}(2\pi/\mu)) = \sqrt{\mu^2 - (2\pi)^2}/\mu$ we can say that the island has stable return points when μ is in the range $2\pi < \mu < \sqrt{(2\pi)^2 + 4}$.

If we recognise that the procedure used to derive the map (2.76) can also be used to derive maps for the accelerator islands with $\mu \geq 2n\pi$ we can write down the generic stability condition for different n as

$$2n\pi < \mu < \sqrt{(2n\pi)^2 + 4}. \quad (2.86)$$

This compares nicely the stability condition for accelerator modes in the standard map or kicked rotor [22,23]. In that model the stability condition is $2n\pi < \mu < \sqrt{(2n\pi)^2 + 16}$. Indeed (2.86) easily explains why the anomalous diffusion peaks in Figure 2.8 become thinner as we increase the value of μ or n . We can numerically check our value for $n = 1$ by picking starting points $(\delta q, \delta p) = (\pm l + 0.0000001, \mp l + 0.0000001)$, where $l = \cos^{-1}\left(\frac{2\pi}{\mu}\right)$ and evolve the map (2.76) over 128 discrete timesteps. The points should remain stable and bounded until we approach this special value of μ . This is exactly what we see in Figure 2.17.

We shall end our analysis of the classical system here. We are now in a position to see the importance of a detailed study of the classical diffusion, especially in the case dealing with accelerator modes. In the chapter 5 our most effective method for examining how these classical resonant effects manifest themselves in the quantum dynamics is to place a coherent state on one of the modes. However as we've just seen we must be very careful about what kicking strength μ we use and the exact placement of the state if we want to observe anomalous diffusion over long time scales.

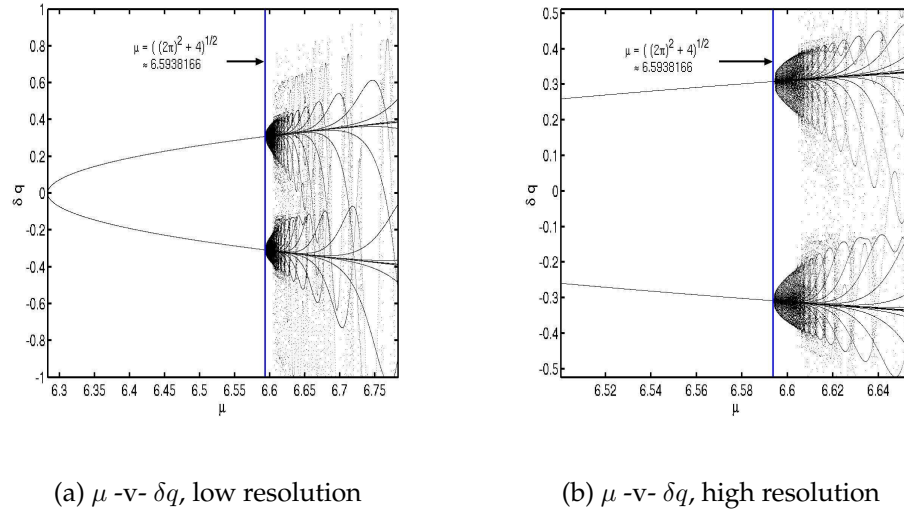


Figure 2.17. Plot of μ -v- δq over first 128 time steps. The initial starting values $(\delta q, \delta p)$ are $(\pm \cos^{-1}(2\pi/\mu) + 0.0000001, \mp \cos^{-1}(2\pi/\mu) + 0.0000001)$. The line in the graph represents where our analysis predicts the elliptical stable point to become unstable. The numerical calculation shows that our analysis appears to be correct.

2.5 Conclusion

This concludes this chapter on the classical delta kicked harmonic oscillator. We have analysed the general behaviour of the system for two particular situations namely irrational frequency ratios and the rational frequency ratio $1/4$. The main goal of this chapter was to provide solid analysis on the classical system so that we could reliably compare it against quantum simulations later on. In particular we concentrated on the diffusion characteristics of the system.

We tried to give a simple explanation for the diffusion characteristics of the irrational system including the break up of the binding tori under large perturbation. This is essential for later on when we attempt to quantify the quantum mechanical suppression of the energy growth rates or diffusion.

In the system with rational frequency ratio $1/4$ we first tried to explain the general behaviour of the system under infinitesimal perturbation. We then concentrated on the actual dynamic processes that give rise to the sharp anomalous spikes in the energy growth rates. In particular we showed that the structures appear because of resonance between kicking frequency and the strength of the kick. We performed some stability analysis on the accelerator modes and showed that the ranges of stability follow the same pattern as those of the kicked rotor

(KR). This analysis is essential later on when we try to study the quantum mechanical behaviour around these types of structures.

References

- [1] G. M. Zaslavsky, M. Yu. Zakharov, R. Z. Sagdeev, D. A. Usikov and A. A. Chernikov, *Sov. Phys. JETP* **64**, 294 (1986).
- [2] T. M. Fromhold *et al.* *Effects of stochastic webs on chaotic electron transport in semiconductor superlattices* *Phys. Rev. Lett.* **87**, 046803 (2001).
- [3] T. M. Fromhold *et al.* *Chaotic electron diffusion through stochastic webs enhances current flow in superlattices* *Nature* **428**, 726 (2004).
- [4] S. A. Gardiner, J. I. Cirac and P. Zoller *Quantum chaos in an ion trap; the delta kicked harmonic oscillator.* *Phys. Rev. Lett.* **79**, 4790 (1997)
- [5] I. Dana and M. Amit, *Phys. Rev. E*, **51**, R2731 (1995)
- [6] G. M. Zaslavsky, R.Z. Sagdeev, D.A.Usikov, A.A. Chernikov, *Minimal chaos, stochastic webs, and structures of quasi-crystal symmetry*, *Sov. Phys. Usp.* **31**, 887 (1988)
- [7] A. J. Lichtenberg and B. P. Wood, *Phys. Rev. A*, **39** 2153 (1989)
- [8] A. J. Lichtenberg and M. A. Lieberman, *Regular and Chaotic Dynamics*, 2nd edition (Springer-Verlag, New York 1992)
- [9] G.M. Zaslavsky, R.Z. Sagdeev, D.A.Usikov, A.A. Chernikov, *Weak Chaos and Quasi-Regular Patterns*, (Cambridge nonlinear science series, Cambridge 1991).
- [10] G.M. Zaslavsky, *Physics of chaos in Hamiltonian systems*, (Imperial College Press, London, 1998)
- [11] I. Dana, *Phys. Rev. Lett.*, **73**, 1609 (1994).
- [12] J. H. Lowenstein, *Parameter dependence of stochastic layers in a quasi-crystalline web*, *Chaos* **1**, 473 (1991)
- [13] J. H. Lowenstein, *Interpolating Hamiltonians for a stochastic-web map with quasi-crystalline symmetry*, *Chaos* **2**, 413 (1992).
- [14] G. Schmerla, P. Jung and F. Moss, *Diffusion on the chaotic web of a Hamiltonian oscillator with incommensurate forcing*, *Phys. Rev. A* **45**, 5462 (1992).
- [15] M. V. Daly, *Classical and Quantum chaos in a non-linearly kicked harmonic oscillator*, Ph. D Thesis, (1994).
- [16] M. Engel, *On Quantum chaos, Stochastic Webs and Localization in a Quantum Mechanical Kick system*, Ph. D Thesis, (2003).
- [17] H. Goldstein, *Classical Mechanics*, 2nd edition, (Addison-Wesley, Reading, 1980).
- [18] G. P. Berman, V. Yu. Rubaev and G. M. Zaslavsky, *The problem of the of quantum chaos in the kicked harmonic oscillator* *Nonlinearity* **4**, 543 (1991).
- [19] E. Ott, *Chaos in dynamical systems*, (Cambridge University Press, Cambridge, 1993).

- [20] J. V. Jose and E. J. Saletan, *Classical Dynamics A Contemporary Approach*, (Cambridge University Press, Cambridge, 2000).
- [21] Rechester A. B. & White R. B., *Calculation of Turbulent Diffusion for the Chirikov-Taylor Model*, Phys. Rev. Lett. **44**,1586 (1980) .
- [22] Y. H. Ichikawa, T. Kamimura and T. Hatori *Stochastic diffusion in the standard map*, Physica D **29**, 247 (1987).
- [23] R. Ishizaki, T. Horita, T. Kobayashi and H. Mori, *Anomalous diffusion due to accelerator modes in the standard map*, Prog. Theo. Phys, **85**, 1013 (1991).
- [24] M. V. Daly and D. M. Heffernan, *Chaos in a resonantly kicked oscillator*, J. Phys. A: Math. Gen. **28**, 2515 (1995).
- [25] M. V. Daly and D. M. Heffernan, *Dynamically enhanced chaotic transport*, Chaos, Sol. & Fract. **8**, 933 (1997).
- [26] V. V. Afanasiev, A. A. Chernikov, R. Z. Sagdeez and G. M. Zaslavsky, Phys. Lett. A **144**, 229 (1990).
- [27] G.M. Zaslavsky and B. A. Niyazov, *Fractional Kinetics and accelerator modes*, Phys. Rep. **283**, 73 (1997).
- [28] G.M. Zaslavsky, *Chaos, fractional kinetics and anomalous transport*, Phys. Rep. **371**, 461 (2002).

Chapter 3

The Quantum System

3.1 Introduction

In the last chapter we dealt with various aspects of the classical systems dynamics using both analytical and numerical techniques. This chapter however, is concerned with what can be said about the quantum system through analytical analysis alone. Subsequent chapters deal with the numerical procedures used to analyse the problems and of course the results of that analysis.

The problem of quantum chaos in the delta kicked harmonic oscillator was first studied in [1]. The paper concentrated in particular on cases where the classical phase space displayed a crystalline structure and the stochastic web. That is when the frequency ratio was $1/3$, $1/4$ and $1/6$.

The paper pointed to the translational invariance of the R^{th} power of the system's evolution operator when the frequency ratio in the problem is $1/R = 1/3, 1/4, 1/6$. This aspect of the problem was built upon by Borgonovi and Rebuffini to show the existence of a quantum resonance condition that manifested itself in the quadratic energy growth of an evolving quantum state [2]. Other purely quantum properties of the system have also been demonstrated. In particular in the ability of the quantum system, under certain parameters, to tunnel between classical separatrices much like the quantum kicked rotor (KR) [3].

As we have mentioned the symmetrical Kicked Harper Model (KHM) can be exactly related to the kicked harmonic oscillator (KHO) with $R = 4$ [4]. Significant progress toward analysing the eigensolutions to generalised kicked Harper models has been made, see [5–7] and the references therein. In particular it has been proved in the latter paper that, in the symmetric case where the KHM and KHO are identical, the spectrum of the Floquet operator is continuous.

The situation for the system when the frequency ratio is irrational has also attracted some attention. In particular it has been shown by Frasca that the system, like the KR can be mapped onto a tight-binding model [8–10]. The importance of this result means that the phenomena known as dynamical localisation (the quantum suppression of diffusion) may also exist in this model. This chapter proceeds as follows. We first define what is called the fractional Fourier transform. We show that, up to a phase, it is identical to the evolution operator of the harmonic oscillator in the position basis. From here it is a simple task to calculate the Floquet operator for the system over one time period. This analysis is essential to understanding the numerical procedures outlined in chapter 4.

The remainder of the chapter deals with the quasi-energies and stationary states of the kicked system. We first deal with the tight-binding approximation of the system with irrational frequency ratios and the consequences for the system's behaviour. The original analysis is due to Frasca [8] and has been analysed in more detail by Engel [10]. We review most of this work and also place our own upper bound on the validity of the approximation.

Next we deal with the analysis due to Borgonovi and Rebuzzini dealing with translational invariance when $R = 3, 4, 6$ [2]. The results have also been re-derived by Engel [10]. We repeat how the condition for quantum resonance is arrived at and its relation to one and two parameter translation groups. We do not include the argument that predicts quadratic energy growth when the resonance condition is fulfilled and linear energy growth when it is not. Instead our own work concentrates on the specific structure of the systems stationary states when $R = 4$. In particular we note the discretised and extended nature of such states in the position basis when the same resonance condition is fulfilled.

As a consequence of these results and of some of the surprising numerical results on quantum resonance documented in chapter 5, the remainder of the chapter deals specifically with analysing eigenstates of the Fourier transform. These are also called self Fourier functions (SFF's). In particular we deal with the Dirac comb function, superpositions of displaced number (Fock) states and a hybrid function that is strikingly similar to some of the numerically calculated stationary states of the kicked system. From these we try to construct an alternative basis in which the resonance phenomena demonstrated in chapter 5 can be explained.

3.2 The Fractional Order Fourier Transform and its relationship with the SHO

The Fourier transform relationship between a wavefunction in the position representation and the momentum representation is derived in nearly all introductory textbooks to quantum mechanics, and we give it here in the form found in [11]:

$$\psi(q') \equiv \langle q' | \psi \rangle = \int_{-\infty}^{\infty} \langle q' | p' \rangle \langle p' | \psi \rangle dp' = \frac{1}{\sqrt{2\pi\hbar}} \int_{-\infty}^{\infty} \exp\left(\frac{ip'q'}{\hbar}\right) \phi(p') dp' \quad , \quad (3.1)$$

and similarly

$$\phi(p') \equiv \langle p' | \psi \rangle = \int_{-\infty}^{\infty} \langle p' | q' \rangle \langle q' | \psi \rangle dq' = \frac{1}{\sqrt{2\pi\hbar}} \int_{-\infty}^{\infty} \exp\left(-\frac{ip'q'}{\hbar}\right) \psi(q') dq' \quad , \quad (3.2)$$

where we have used the completeness of the momentum and position bases and the transformation function

$$\langle p' | q' \rangle = \frac{1}{\sqrt{2\pi\hbar}} \exp\left(-\frac{ip'q'}{\hbar}\right) = \langle q' | p' \rangle^* \quad . \quad (3.3)$$

These relationships are well known and they form the back bone to what is called the split-step method, see appendix B, for numerically approximating the time evolution of certain quantum systems. The symmetry between q and p representations however also hints at a more general relationship between these operations and the simple harmonic oscillator (SHO). The relationship was made explicit in 1980 by Namias with the introduction of the Fractional Fourier Transform of which the ordinary Fourier transforms of (3.1) and (3.2) are just a special case.

It is well known that the Hermite-Gauss (HG) polynomials, (A.33), as well as being the energy eigenfunctions of the SHO Hamiltonian, are also eigenfunctions of the Fourier transform. Eigenfunctions of this type are often called Self Fourier Functions (SFF's). The Fourier eigenvalue equation, for a function $u_n(q')$, is given by

$$\mathcal{F}_{-\frac{\pi}{2}} u_n(q') = e^{-in\frac{\pi}{2}} u_n(q') \quad , \quad (3.4)$$

where

3.2: The Fractional Order Fourier Transform and its relationship with the SHO⁵⁹

$$\mathcal{F}_{-\frac{\pi}{2}} u_n(q') = \frac{1}{\sqrt{2\pi\hbar}} \int_{-\infty}^{\infty} \exp\left(-\frac{ip'q'}{\hbar}\right) u_n(q') dq' . \quad (3.5)$$

Namias defines the Fractional Fourier Transform in terms of the same Hermite-Gauss functions. That is

$$\mathcal{F}_{-\theta} \langle q'|n \rangle = e^{-in\theta} \langle q'|n \rangle , \quad (3.6)$$

where we have written the HG functions in Dirac notation. That is $u_n(q') = \langle q'|n \rangle$. From a quantum mechanical point of view it is easily seen that this is also, up to a constant phase, the eigenvalue equation for the evolution operator of the SHO. Operating with the $\mathcal{U}_0(T)$, (A.11), on the ket $|n\rangle$ and multiplying from the left with the bra $\langle q'|$ we have

$$\langle q'|e^{-i\frac{\theta}{2}}e^{-iN\theta}|n\rangle = e^{-i\frac{\theta}{2}}e^{-in\theta} \langle q'|n \rangle . \quad (3.7)$$

In the position basis the state of the quantum system after evolving for a time T is given by

$$\langle q'|\psi(T)\rangle = \langle q'|\mathcal{U}_0(T)|\psi(0)\rangle = e^{-i\frac{\theta}{2}} \sum_{n=0}^{\infty} e^{-in\theta} \langle q'|n\rangle \langle n|\psi(0)\rangle . \quad (3.8)$$

Using the eigenvalue equations above this can simply be written

$$\langle q'|\psi(t)\rangle = e^{-i\frac{\theta}{2}} \sum_{n=0}^{\infty} e^{-in\theta} \langle q'|n\rangle \langle n|\psi(0)\rangle = e^{-i\frac{\theta}{2}} \mathcal{F}_{-\theta} \langle q'|\psi(0)\rangle . \quad (3.9)$$

or

$$\psi(q', t) = e^{-i\frac{\theta}{2}} \mathcal{F}_{-\theta} \psi(q', 0) . \quad (3.10)$$

Here we have written out explicitly the relationship between the Fractional Fourier Transform and the Floquet operator of the Simple Harmonic Oscillator. This is the same result as the one given in [12]. However it was derived in a different way. Indeed from our perspective it hardly passes for a derivation at all. The Fractional Fourier Transform is the evolution operator of the SHO because it is defined as such.

We will give details on the exact form of this operator in the next chapter. We expand upon the definition (3.6) given above to give more details on how to actually perform such a transform numerically. We will also demonstrate that there exists Fast Fractional Fourier Transforms (FFFT's) analogous to the ordinary Fast Fourier Transforms (FFT's) introduced by [13]. We will use these algorithms to numerically simulate the kicked quantum system very efficiently.

3.3 The Floquet operator for the kicked system

One might wonder why we bother work in the position basis at all. After all, the simple harmonic oscillator is diagonal in the Fock (number) state basis. The reason lies in the fact that the kicking potential term in the kicked system is a function of position and is therefore not diagonal in the number basis. To numerically evolve the system like this would have to involve a matrix-vector multiplication. This is never efficient and would place huge demands on both computer speed and memory. However, using the results from the last section, we can write out the Floquet operator for the kicked system in a very straight-forward way.

The state vector for the system must obey the Schrödinger equation , that is

$$i\hbar \frac{\partial}{\partial t} |\psi(t)\rangle = \mathcal{H} |\psi(t)\rangle . \quad (3.11)$$

We now integrate this equation over the kicking potential from $t_1 = nT - \epsilon$ to $t_2 = nT + \epsilon$ using the Hamiltonian given in (2.15),

$$i\hbar \int_{|\psi(t_1)\rangle}^{|\psi(t_2)\rangle} \frac{d|\psi(t)\rangle}{|\psi(t)\rangle} = \int_{t_1}^{t_2} \frac{\omega_0}{2} (p^2 + q^2) dt + \int_{t_1}^{t_2} \bar{\mu} \cos kq \sum_{n=-\infty}^{\infty} \delta(t - nT) dt . \quad (3.12)$$

We note here that the Hamiltonian \mathcal{H} and q and p are now understood to be operators. Performing the intergation we have

$$|\psi(t_2)\rangle = \exp\left(-\frac{i}{\hbar} \omega_0 \epsilon (p^2 + q^2)\right) \exp\left(-\frac{i}{\hbar} \bar{\mu} \cos(kq)\right) |\psi(t_1)\rangle , \quad (3.13)$$

which reduces to

$$|\psi(nT+)\rangle = \mathcal{U}_1 |\psi(nT)-\rangle \equiv \exp\left(-\frac{i}{\hbar} \bar{\mu} \cos(kq)\right) |\psi(nT)-\rangle , \quad (3.14)$$

when $\epsilon \rightarrow 0$. Here $t_1 = nT^-$ is the time just before the n^{th} kick and $t_2 = nT^+$ is the time just after. At all other times the dynamics of the system are that of a simple harmonic oscillator. We can thus use (3.10) to write out the unitary operator that evolves the system from just after one kick to just before the next kick, that is, over a time of length $t = T$:

$$|\psi((n+1)T)^-\rangle = \mathcal{U}_0 |\psi(nT)^+\rangle = e^{-i\frac{\theta}{2}} F_{-\theta} |\psi(nT)^+\rangle, \quad (3.15)$$

with $\theta = \omega_0 T$. If we substitute (3.14) into (3.15) we get the unitary operation that evolves the system from just before one kick to just before the next kick

$$\langle q' | \psi((n+1)T)^-\rangle = \langle q' | \mathcal{U} | \psi(nT)^-\rangle \equiv e^{-i\frac{\theta}{2}} F_{-\theta} e^{-i\mu \cos(kq')/k\hbar} \langle q' | \psi(nT)^-\rangle. \quad (3.16)$$

The operator \mathcal{U} is called the system's Floquet operator. We may also write the above relation in functional form, that is

$$\psi(q', (n+1)T)^- = e^{-i\frac{\theta}{2}} F_{-\theta} e^{-i\mu \cos(kq')/k\hbar} \psi(q', nT)^-. \quad (3.17)$$

We will see in the following chapters how this result allows us to numerically analyse the kicked quantum system in great detail. We may now approximate the wavefunction in the position basis as numbers in an array. The state can now be evolved in time, regardless of θ , by operations that do not include matrix multiplications. It will allow us to accurately examine how the system evolves over longer times than has previously been possible in the literature. This computational speed up is possible because of the existence of numerical procedures known as the Fast Fractional Fourier Transform (FFFT) and Fast Fourier Transform (FFT). We will see that the procedures also have an added advantage because a matrix can be found that performs the discrete fractional Fourier Transform. We can then numerically calculate the unitary matrix that approximates \mathcal{U} . This allows us to numerically study the system's stationary states and quasi-energies discussed in the next section. Some technical matters associated with the FFT and FFFT algorithms are also outlined in chapter 4.

3.4 Quasi-energies and Stationary States

A more complete understanding of the quantum dynamics entails finding the eigenvectors and eigenvalues of the Floquet operator. In the particular case of the delta kicked oscillator finding exact analytical expressions from the system's eigenfunctions and eigenvalues has not yet been done. However, using various properties of the Hamiltonian we have been able to say a great deal about these eigenvectors. We first present an important analytical result that hints at stationary states of a localised nature when the frequency ratio is irrational [8]. We then turn our attention to the stationary states of the system with rational frequency ratios. In particular we include most of the argument of translational invariance first shown by Borgonovi and Rebuffini [2] and expanded upon by Engel [10]. The phenomena known as quantum resonance is also addressed and we include an original Fourier type analysis on the structure of the systems stationary states at and near these resonant values of \hbar .

3.4.1 Tight-binding model

In this section the argument initially put forward by Frasca is presented [8]. We shall also include some new analysis due Engel [10]. The general idea is to map the irrationally kicked system to a tight-binding model which we can then be said to display Anderson type localisation properties [9,17,18]. In light of our numerical results, see chapter 5, we also include our own simple analysis which places a limit to the validity of the tight-binding approximation.

Beginning with relations (3.15), (3.14) and (A.3) we write out the Floquet operator $\mathcal{U} = \mathcal{U}_0 \mathcal{U}_1$ for the KHO in the number basis,

$$\mathcal{U} = \exp\left(-i\left(N + \frac{1}{2}\right)\theta\right) \exp\left(-i\mu \cos(\beta(a^\dagger + a))/k\hbar\right) . \quad (3.18)$$

where $\theta = \omega_0 T$ and $\beta = k\sqrt{\hbar/2}$ and as always $\mu = k\bar{\mu}$. The eigenvalue equation for this operator is

$$e^{-i\frac{\theta}{2}} \exp(-iN\theta) \exp\left(-i\mu \cos(\beta(a^\dagger + a))/k\hbar\right) |\Psi\rangle = e^{-i\Omega} |\Psi\rangle , \quad (3.19)$$

where Ω are the quasi-energies. We then define $A = (\mu/k\hbar) \cos(\beta(a^\dagger + a))$ and introduce the operator W as

$$W = -\tan(A/2) \ , \quad (3.20)$$

or equivalently

$$e^{-iA} = \frac{1 + iW}{1 - iW} \ . \quad (3.21)$$

Substituting 3.21 into 3.19 and rearranging we get

$$(1 + iW)e^{-i(\theta(N+1/2)-\Omega)}|\Psi\rangle = (1 - iW)|\Psi\rangle \ . \quad (3.22)$$

We set $C = (\theta(N + 1/2) - \Omega)$ and bring every thing to one side

$$[e^{-iC} - 1 + iWe^{-iC} + iW]|\Psi\rangle = 0 \ . \quad (3.23)$$

Introducing $|\bar{\Psi}\rangle = (1 + e^{-iC})|\Psi\rangle$ we can rewrite (3.23) as

$$\frac{e^{-iC} - 1}{e^{-iC} + 1}|\bar{\Psi}\rangle + iW\frac{e^{-iC} + 1}{e^{-iC} + 1}|\bar{\Psi}\rangle = 0 \ , \quad (3.24)$$

and we can now write

$$-i\tan(C/2) - i\tan(A/2)|\bar{\Psi}\rangle = 0 \ . \quad (3.25)$$

Dividing all across by $-i$ reduces this to

$$(D + W)|\bar{\Psi}\rangle = 0 \ , \quad (3.26)$$

with

$$W = \tan[A/2] = \tan[(\mu \cos(\beta(a^\dagger + a))/2\hbar] \ , \quad (3.27)$$

and

$$D = \tan[C/2] = \tan[(\theta(N + 1/2) - \Omega)/2] \ . \quad (3.28)$$

Expanding $|\bar{\Psi}\rangle$ in the Fock state basis we have

$$\begin{aligned} (D + W)|\bar{\Psi}\rangle &= \sum_{n=0}^{\infty} |n\rangle [\langle n|D|\bar{\Psi}\rangle + \langle n|W|\bar{\Psi}\rangle] \\ &= \sum_{n=0}^{\infty} \langle n|D|\bar{\Psi}\rangle |n\rangle + \sum_{m,n}^{\infty} \langle n|W|m\rangle \langle m|\bar{\Psi}\rangle |n\rangle . \end{aligned} \quad (3.29)$$

Equating coefficients for each ket $|n\rangle$ we get

$$D_n \langle n|\bar{\Psi}\rangle + \sum_{n \neq m} W_{nm} \langle m|\bar{\Psi}\rangle = \epsilon \langle n|\bar{\Psi}\rangle , \quad (3.30)$$

where $\epsilon = -W_{nn}$ and

$$D_n = \tan[(\theta(n + 1/2) - \Omega)/2] . \quad (3.31)$$

Once we have reduced the problem to the tight binding form in (3.30) we may apply an argument first introduced by [9]. The argument has been used to explain the very obvious dynamical localisation observed in the quantum version of the kicked rotor. We proceed with an argument similar to the ones presented in [10,15,16].

The essential idea is that the kicked system is mapped on to a tight-binding model that has been used to successfully to describe electronic motion in solid state systems. The model predicts that the electronic eigenfunctions are extended or spread out only if there is a high degree of regularity in the position of the atoms. However if there is some disorder in the systems, what is know known as Anderson localisation occurs [17,18]. It should however be mentioned here that to make the connection between the kicked harmonic oscillator and the tight-binding model requires quite a few approximations and there are many open questions regarding its validity. We will highlight these as we go along.

Assume that the matrix W has only values w along its secondary diagonals (we will see later that this is not really the case). In the solid state model this is equivalent to saying that the electron only interacts with three atoms at any one time, the one it's directly over and two on either side. We can then write (3.30) as

$$w \langle n+1|\bar{\Psi}\rangle + w \langle n-1|\bar{\Psi}\rangle + D_n \langle n|\bar{\Psi}\rangle = \epsilon \langle n|\bar{\Psi}\rangle . \quad (3.32)$$

This can also be written in the matrix form

$$\begin{pmatrix} a_{n+1} \\ a_n \end{pmatrix} = R_n \begin{pmatrix} a_n \\ a_{n-1} \end{pmatrix} , \quad (3.33)$$

where R is the transfer matrix

$$R_n = \begin{pmatrix} \frac{\epsilon - D_n}{w} & -1 \\ 1 & 0 \end{pmatrix} , \quad (3.34)$$

and

$$a_n = w \langle n | \bar{\Psi} \rangle . \quad (3.35)$$

Components of a state vector at the start of a chain can be used via the matrices R_n to obtain components of state vectors at the end of the chain. That is,

$$\begin{pmatrix} a_{N+1} \\ a_N \end{pmatrix} = R \begin{pmatrix} a_1 \\ a_0 \end{pmatrix} . \quad (3.36)$$

where

$$R = R_N R_{N-1} \dots R_1 . \quad (3.37)$$

We can see here that the components a_{N+1} and a_N are determined by the components a_1 and a_0 and the matrix R . Similarly we could write

$$\begin{pmatrix} a_{n-1} \\ a_n \end{pmatrix} = R_n \begin{pmatrix} a_n \\ a_{n+1} \end{pmatrix} , \quad (3.38)$$

and use the transfer matrix R to get components a_{n-1} and a_n from components a_{n+N-1} and a_{n+N} to their right.

The matrices R_n can be classified as unimodular. A unimodular matrix is defined as a real square matrix A with determinant $\det(A) = +1$ [19]. We can now apply a theorem due to Furstenberg about random unimodular matrices M_i [20]. The theorem states that under general conditions

$$\lim_{Q \rightarrow \infty} \frac{1}{Q} \text{Tr} M_Q M_{Q-1} \dots M_2 M_1 \equiv \lambda > 0 . \quad (3.39)$$

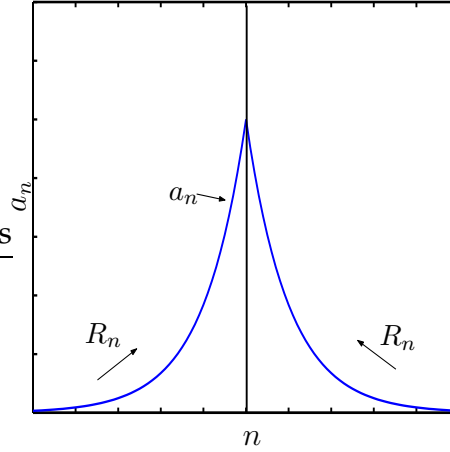


Figure 3.1. The transfer matrix R_n can be used to iterate vectors a_n both left and right. Exponential growth in both directions is seen. We can match the values of the a_n in the center by carefully selecting energies

What this means in the present context is that if we can say that the values $\epsilon - D_n$ are random then the unimodular matrix $R = R_N R_{N-1} \dots R_1$ has two eigenvalues $\exp(\pm N\lambda)$. This implies that for almost all starting coefficients a_1, a_0 the wavefunction will grow exponentially to the left and right. However it has been shown [21–23] that the wavefunctions when iterated from both sides can be made to match up somewhere in the center by carefully selecting the energies. See Figure 3.1.

In this particular case, with simplified off diagonal terms, the argument for localisation depends on the randomness of the D_n term in the matrices R_n . Examining the term D_n , (3.31), we see it is a simple trigonometric function of the Fock number n . How the function behaves as n changes depends intimately on the parameter $\theta = \omega_0 T$. Thus if θ is a rational multiple of 2π then D_n is periodic, and could not be said to contain any randomness whatsoever. However, if T is an irrational multiple of 2π the function D_n can not display the same kind of exact periodicity as in the rational case. Indeed the function never repeats exactly as we increase n . It is conjectured that under these conditions D_n behaves as a pseudo-random number generator [9]. We can assume Furstenberg's theorem applies in this case and we can claim to have explained localisation.

It must be now mentioned however that nowhere in the above discussion did we mention the role of \hbar . We know that in the classical limit that the quantum system should diffuse at the same rate as the classical one. Since \hbar does not

appear in D_n , it's pseudo-randomness, or lack of, has nothing to do with connecting classical and quantum systems. This is not to say that this does not play a role in the localisation of the quantum system, it only says that it cannot explain why the quantum system should diffuse when \hbar gets small and, as we will see later, when the kicking strength μ gets large. Indeed, careful examination of W_{mn} , (3.27), shows that reducing \hbar and increasing μ affect the structure of the matrix W in a very similar way. We will now show that by examining the structure of W_{mn} for different values of \hbar and μ that a tight-binding model only applies when values of $\mu/2\hbar$ are below a critical value. We steady our argument first by using some of Engel's analysis [10]. Starting with (3.27)

$$W_{mn} = \langle m | \tan[(\mu \cos(\beta(a^\dagger + a)))/2\hbar] | n \rangle , \quad (3.40)$$

and using expression (A.3) and the completeness relation in the position basis

$$I = \int_{-\infty}^{\infty} dq' |q'\rangle \langle q'| , \quad (3.41)$$

we get

$$\begin{aligned} W_{mn} &= \int \int dq' dq'' \langle m | q' \rangle \langle q' | \tan[(\mu \cos(kq)/2\hbar] | q'' \rangle \langle q'' | n \rangle , \\ &= \int dq' \langle m | q' \rangle \tan[\mu \cos(kq')/2\hbar] \langle q' | n \rangle , \\ &= C_{nm} \frac{1}{\sqrt{\pi\hbar}} \int dq' \tan \left[\frac{\mu \cos(kq')}{2\hbar} \right] H_m \left(\frac{q'}{\sqrt{\hbar}} \right) H_n \left(\frac{q'}{\sqrt{\hbar}} \right) \exp \left(-\frac{q'^2}{\hbar} \right) , \end{aligned} \quad (3.42)$$

where the limits of iteration are $\pm\infty$, H_n represents the n^{th} Hermite polynomial and $C_{nm} = 1/(2^{n+m} m! n!)$. We can say quite lot about this integral with little effort. First we note that the term $\tan(\mu \cos(\sqrt{\hbar}x)/2\hbar)$ is even. This means that if the total integrand is odd if $m + n$ is an odd number and even otherwise. Therefore

$$W_{nm} = 0 , \quad m + n = \text{odd} . \quad (3.43)$$

Immediately this shows that this could not be a tight-binding model in the usual sense as neighboring Fock states are not connected and that $W_{n,n-2} \neq W_{n+2,n}$. It is possible however to construct an alternative model where every second Fock

state is connected and with different transfer matrices for left and right iteration. These aspects of the problem and more are discussed in detail by Engel [10] where, as well as this, the value of the integral (3.42) for small μ/\hbar is calculated to be approximately

$$|W_{m,m+2n}| \approx \frac{\mu}{2\hbar} \frac{1}{\sqrt{m!e^m}} \left(\frac{27e^2\hbar^2}{64n} \right)^{n/2}. \quad (3.44)$$

The essential point in his analysis is that the absolute values of the matrix elements W_{mn} decay faster than exponentially with distance from the diagonal. He then shows how a more complicated tight-binding model than the one discussed above can then be created. However, the same qualified conclusion can be made, that is that the quasi-eigenstates are localised if the D_n term displays pseudo-randomness.

To show how the tight-binding analysis breaks down we turn our attention to the case where μ/\hbar can take on any value. Note that $|\tan(n\pi/2)| = \infty$ and therefore that the integrand in (3.42) may contain delta function spikes once $\mu/\hbar > \pi$. Even a numerical analysis of such an integral is nontrivial. For our purposes it suffices to say that there is nothing to suggest rapid decay in the size of the integral $|W_{m,m+n}|$ as n gets large. In this way we may place limits on the range for which the tight-binding approximation is applicable. This conclusion squares nicely with both the correspondence principle (the wavefunction should diffuse with time as $\hbar \rightarrow 0$) and the numerical simulations in section 5.2.2 that show that, while there seems to be always some suppression of the energy growth rates, there is no complete dynamical localisation for large perturbation strengths.

3.4.2 Translational Invariance

In this subsection we outline an argument put forward by Borgonovi and Rebuzzini [2]. The basic idea is to show that under certain conditions the Floquet operator for the kicked harmonic oscillator commutes with a specific displacement operator. If this is established we can then make some very general statements about the eigenvectors of the total Floquet operator \mathcal{U} . However, we first introduce some simple group theory [24,25]

Theorem1: If, in a vector space \mathcal{E} , A and B are two operators that commute with each other, then every degenerate eigensubspace of A is globally invariant under B , and vice versa.

Proof: Let $|\psi_n\rangle$ be the eigenvectors of A with eigenvalues a_n . If A and B commute we can write

$$A(B|\psi_n\rangle) = BA|\psi_n\rangle = Ba_n|\psi_n\rangle = a_nB|\psi_n\rangle . \quad (3.45)$$

That is, $B|\psi_n\rangle$ is also an eigenvector of A with eigenvalue a_n . From here there are two possibilities:

(1) a_n is non-degenerate In this case $|\psi_n\rangle$ and $B|\psi_n\rangle$ must be the same state, which means that $|\psi_n\rangle$ is an eigenvector of B also:

$$B|\psi_n\rangle = b_n|\psi_n\rangle . \quad (3.46)$$

(2) a_n is degenerate

The eigenvectors of $a_n \{|\psi_n^j\rangle\}_{j=1,\dots,g_n}$ form an orthonormal basis of the degenerate eigensubspace \mathcal{E}_n of \mathcal{E} . The expression $A(B|\psi_n^j\rangle) = a_nB|\psi_n^j\rangle$ still applies but there is no need for $|\psi_n^j\rangle$ and $B|\psi_n^j\rangle$ to be parallel. The vector need only be a superposition of eigenstates spanning the degenerate subspace \mathcal{E}_n . That is,

$$B|\psi_n^j\rangle = \sum_{k=1}^{g_n} c_{nj}^k |\psi_n^k\rangle . \quad (3.47)$$

We next introduce the displacement operator:

$$D_{r,s} = \exp\left(\frac{i}{\hbar}(sq - rp)\right) = \exp(za^\dagger - z^*a) = D(z) , \quad (3.48)$$

with $z = 1/\sqrt{2\hbar}(r + is)$. Recall now that the Floquet operator of our system is given by

$$\mathcal{U} = \mathcal{U}_0 \mathcal{U}_1 = \exp\left(\frac{-i}{\hbar} \mathcal{H}_0 T\right) \exp\left(\frac{-i}{k\hbar} \mu \cos(kq)\right) . \quad (3.49)$$

Operating on a ket with the displacement operator has the effect of shifting the vector by $r\hat{i} + s\hat{j}$ in the phase plane. We now want to see the effect the displacement operator has on the Floquet operator for the kicked oscillator. We first see it's effect on the kicking operator \mathcal{U}_1

$$\begin{aligned} D_{s,r} \mathcal{U}_1 &= \exp\left(\frac{i}{\hbar}(sq - rp)\right) \exp\left(-\frac{i}{k\hbar} \mu \cos(kq)\right) \\ &= \exp\left(-\frac{i}{k\hbar} \mu \cos(k(q+r))\right) \exp\left(\frac{i}{\hbar}(sq - rp)\right) . \end{aligned}$$

So we see that the two operators commute if r is a multiple of $2\pi/k$. The next step is to see how the displacement operator effects the free evolution operator for the oscillator. To do this we will need to use a well known theorem about non-commuting operators [11].

Theorem2: If A and B are two non-commuting operators and ζ is a parameter, then, if n is an integer,

$$e^{\zeta A} B^n e^{-\zeta A} = (e^{\zeta A} B e^{-\zeta A})^n , \quad (3.50)$$

and,

$$e^{\zeta A} F(B) e^{-\zeta A} = F(e^{\zeta A} B e^{-\zeta A}) . \quad (3.51)$$

We are now in a position to write

$$\begin{aligned} D(z) \mathcal{U}_0 &= \exp(za^\dagger - z^* a) \mathcal{U}_0 , \\ &= \mathcal{U}_0 \mathcal{U}_0^\dagger \exp(za^\dagger - z^* a) \mathcal{U}_0 , \\ &= \mathcal{U}_0 \exp(z \mathcal{U}_0^\dagger a^\dagger \mathcal{U}_0 - z^* \mathcal{U}_0^\dagger a \mathcal{U}_0) , \\ &= \mathcal{U}_0 \exp(ze^{i\omega_0 T} a^\dagger - z^* e^{-i\omega_0 T} a) , \end{aligned} \quad (3.52)$$

where we have used (A.16) and (3.51). We can simplify the expression to

$$D_{s,r}\mathcal{U}_0 = D(z)\mathcal{U}_0 = \mathcal{U}_0 D(z') = \mathcal{U}_0 D_{s',r'} \quad , \quad (3.53)$$

with

$$\begin{aligned} z' &= ze^{i\theta} \quad , \\ r' &= r \cos \theta - s \sin \theta \quad , \\ s' &= r \sin \theta + s \cos \theta \quad . \end{aligned}$$

with $\theta = \omega_0 T$. So as \mathcal{U}_0 moves through the displacement operator it, in a manner of speaking, rotates it in a clockwise direction through the angle given by θ . The new displacement operator now shifts a quantum state along a new rotated direction. The displacement operator therefore moves through the total Floquet operator as

$$\begin{aligned} D_{s,r}\mathcal{U} &= D_{s,r}\mathcal{U}_0\mathcal{U}_1 \\ &= \mathcal{U}_0 D_{s',r'}\mathcal{U}_1 \\ &= \mathcal{U}_0\mathcal{U}'_1 D_{s',r'} \quad , \end{aligned}$$

where

$$\mathcal{U}'_1 = \exp\left(\frac{-i}{k\hbar}\mu \cos(k(q+r'))\right) \quad . \quad (3.54)$$

Now, if we were to move the displacement operator through a succession of operators \mathcal{U}^R under certain conditions we can see that the operators $D_{s,r}$ and \mathcal{U}^R commute. We can write this out explicitly

$$\begin{aligned} D_{s_1,r_1}\mathcal{U}^R &= \mathcal{U}_0\mathcal{U}'_1 D_{s_2,r_2}\mathcal{U}^{R-1} \\ &= \left[\prod_{j=1}^R \mathcal{U}_0 \exp\left(\frac{-i}{k\hbar}\mu \cos(k(q+r_j))\right) \right] D_{s_R,r_R} \quad . \end{aligned} \quad (3.55)$$

with

$$\begin{aligned}
z_j &= z e^{ij\theta}, \\
r_j &= r \cos j\theta - s \sin j\theta, \\
s_j &= r \sin j\theta + s \cos j\theta.
\end{aligned}$$

The conditions, explained in [2,10] are that firstly $\cos \theta \in \mathbb{Q}$, that is that the cosine of the angle of rotation θ is a rational number. Secondly, the angle θ itself must be a rational multiple of 2π . That is, $\theta = 2\pi/R$. This condition is only met if $R \in R_c = \{1, 2, 3, 4, 6\}$. We can explain this answer in geometrical terms in perhaps an easier way. The value of the term r'_j in D_{s_j, r_j} must remain a multiple of $2\pi/k$ as we rotate it through successive fixed angles (move it through \mathcal{U}_0). This must be so if it is to commute with the kicking operator \mathcal{U}_1 . This condition can only be met if we choose rotation angles $\theta = \{2\pi, 2\pi/2, 2\pi/3, 2\pi/4, 2\pi/6\}$. The last three of these situations, with $k = 1$, are illustrated in Figure 3.2(c) and 3.2(d) below along with some other examples where the operators cannot be made to commute. In the figure we represent the translation operator with a vector. It can clearly be seen that in the $1/R = 1/4$ case the condition can only be satisfied if both the s and r component of the displacement operator are integer multiples of $2\pi^*$. That is if

$$s = 2\pi n_s/k, \quad (3.56)$$

$$r = 2\pi n_r/k, \quad n_s, n_r \in \mathbb{Z}. \quad (3.57)$$

We next need to examine the group properties of the displacement operators themselves. Consider the two displacement operators D_{s_1, r_1} and D_{s_0, r_0} . Using the Baker Cambell Hausdorff formula [11] we can find out under what conditions two separate displacement operators commute. Some quick analysis shows that

$$[D_{s_1, r_1}, D_{s_0, r_0}] = 2i \sin \left(\frac{s_1 r_0 - s_0 r_1}{2\hbar} \right) D_{s_1+s_0, r_1+r_0}. \quad (3.58)$$

The two operators will then only commute when the sin term vanishes. In the particular case with $R = 4$ we see that this can happen in two ways. Substituting $s_1 = 2\pi n_{s_1}/k$, etc. into the above equation and dividing by $2i$, we have

*It is worth mentioning here that the specific shape of the kicking potential need only be periodic for the statements above to be true. This analysis then applies to all periodic kicking potentials and all kick strengths.

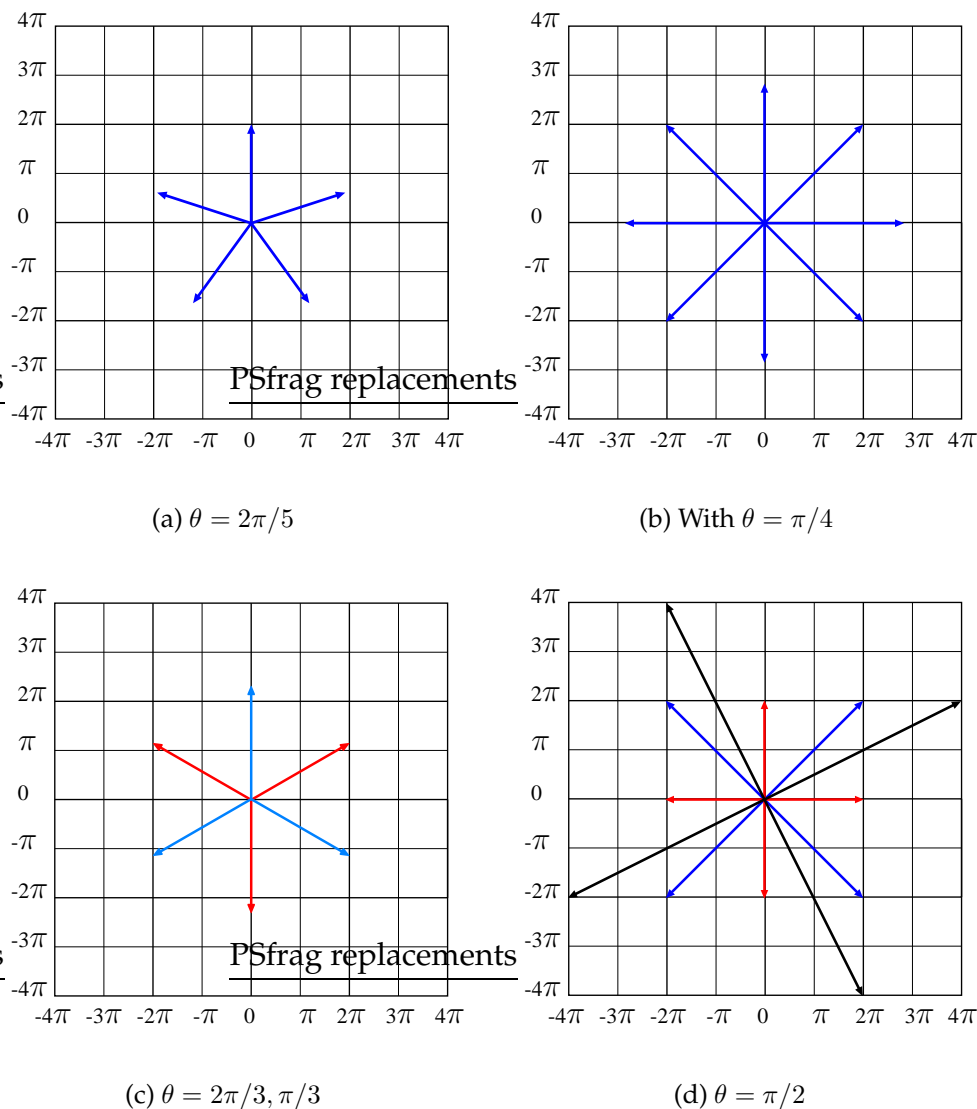


Figure 3.2. The condition for translational invariance is such that the r^l component in the displacement operator D_{r^l, s^l} , represented by the vectors, remains a multiple of $2\pi/k$ upon repeated operation of \mathcal{U}_0 . In the above examples $k = 1$. Figures (c) and (d) show situations where the translational invariance condition is upheld

$$\sin \left(\frac{2\pi^2}{k^2 \hbar} (n_{s_1} n_{r_0} - n_{s_0} n_{r_1}) \right) = 0 . \quad (3.59)$$

The first type of solution occurs when $n_{s_1} n_{r_0} = n_{s_0} n_{r_1}$ or $P = n_{s_1}/n_{r_1} = n_{s_0}/n_{r_0}$. The condition is only satisfied when the two displacements D_{s_1, r_1} and D_{s_0, r_0} are along the same direction (quadrature) in the phase plane. This corresponds to a one parameter commutative group since the directions of the translations can all be specified by the parameter P [10].

Another possibility occurs because $n_{s_1}, n_{r_0}, n_{s_0}$ and n_{r_1} are all integers. If

$$\hbar = \frac{2\pi}{k^2 n'} , \quad n' \in \mathbb{Z} , \quad (3.60)$$

then the group of translation defined by the two parameters, $2\pi n_s$ and $2\pi n_r$, is commutative. This symmetry has no analog in the classical system and in generally referred to as quantum resonance. It should be noted that

$$\hbar = \frac{2\pi m'}{k^2 n'} , \quad n', m' \in \mathbb{Z} , \quad (3.61)$$

also allows for the commutation of different displacement operators. The condition for commutation between different operators is thus

$$\frac{n'}{m'} (n_{s_1} n_{r_0} - n_{s_0} n_{r_1}) = l , \quad l, n', m' \in \mathbb{Z} . \quad (3.62)$$

In the texts [2,10] the authors now go on to present an argument estimating the decay rate of the Husimi distribution at a given phase point (q, p) . The decay rate of the the distribution at one point is shown to be inversely proportional to spread of the whole distribution. The energy of the state can then easily be shown to be proportional to the spread of the distribution.

The results are remarkable. The rate of energy growth with no quantum resonance is predicted to be linear in time or with time step n . That is,

$$\langle E \rangle_n \sim n . \quad (3.63)$$

With resonant \hbar the system is predicted to behave radically different over long times. The rate of energy growth is predicted , in this case, to be quadratic. That is,

$$\langle E \rangle_n \sim n^2 . \quad (3.64)$$

It should again be stressed that these growth rates are only valid when n is large. This makes sense because over short time-scales the quantum system and classical system have similar growth rates. The predictions are confirmed numerically by both authors although a detailed analysis of the \hbar dependence of the diffusion curve was not given. We shall attempt this in section 5.3.2.

In my own analysis I have concentrated more on understanding what specific consequences 1 parameter and 2 parameter translational invariance may have on the Floquet operator's eigenvectors. We return to the theorem stated at the start of the section. The theorem does not say anything about the class of operators we are dealing with and can therefore be applied to the unitary matrices \mathcal{U} and $D_{r,s}$.

Suppose now we have the displacement operators $D_{r,s}$ and it commutes with \mathcal{U}^4 . We can say that any non-degenerate eigenstate of \mathcal{U}^4 is still an eigenstate after it has been displaced by $D_{r,s}$ where $r, s = 2n\pi/k$ for integer n . More generally it implies that in this case any degenerate subspace will remain invariant under the translation $D_{r,s}$.

When the operators commute we may also apply the theorem in the opposite direction. This means that degenerate subspaces of the operator $D_{r,s}$ are also invariant under operation of \mathcal{U}^4 . In order to see what this means we first examine the operations of the translation operators $D_{0,r}$ and $D_{s,0}$ on q and p eigenkets:

$$\begin{aligned} D_{0,r}|q'\rangle &= \exp\left(-\frac{i}{\hbar}rp\right)|q'\rangle = |q' + r\rangle , \\ D_{0,r}|p'\rangle &= \exp\left(-\frac{i}{\hbar}rp\right)|p'\rangle = \exp\left(-\frac{i}{\hbar}rp'\right)|p'\rangle , \end{aligned} \quad (3.65)$$

and

$$\begin{aligned} D_{s,0}|q'\rangle &= \exp\left(\frac{i}{\hbar}sq\right)|q'\rangle = \exp\left(\frac{i}{\hbar}sq'\right)|q'\rangle , \\ D_{s,0}|p'\rangle &= \exp\left(\frac{i}{\hbar}sq\right)|p'\rangle = |p' + s\rangle . \end{aligned} \quad (3.66)$$

Suppose we set r to $2m'\pi/k$, clearly every $|p'\rangle$ is still an eigenket of this translation operator and, as one, has a distinct eigenvalue depending on the value of

p' . However, it is clear that an infinity of other kets $|p''\rangle$ also share this same eigenvalue. The degenerate subspace is then, by definition, the set of kets $|p''\rangle$ where

$$\frac{p' - p''}{k\hbar} 2m'\pi = 2n'\pi , \quad (3.67)$$

$$l = p' - p'' = k\hbar \frac{n'}{m'} , \quad n', m' \in \mathbb{Z} . \quad (3.68)$$

This is just a simple kind of Fourier analysis. The result tells us that if an operator is exactly periodic (translationally invariant) in the position basis then it must be discrete in the momentum basis and vice versa. *Theorem 1* then tells us that if an initial state is constructed in a degenerate subspace of $D_{0,r}$ then it must remain there under operation of \mathcal{U}^4 . The same argument can be applied to positions kets using the $D_{s,0}$ operator.

The idea of quantum resonance occurs when we try to see if it is possible for the degenerate subspaces of say $D_{0,r}$ to be also invariant under some other displacement operator, say $D_{s,0}$. However, if a degenerate subspace of $D_{0,r}$ is also to be $2\pi/k$ periodic in the momentum basis, a necessary condition for commutation with \mathcal{U}_A , then the difference between neighboring kets $|p'\rangle$ and $|p''\rangle$ has to be some fraction of $2\pi/k$. That is

$$l = p' - p'' = \frac{2\pi m''}{kn''} , \quad n'', m'' \in \mathbb{Z} . \quad (3.69)$$

Comparing (3.67) and (3.69) we again get the condition

$$\hbar = \frac{2\pi m}{k^2 n} , \quad n, m \in \mathbb{Z} , \quad (3.70)$$

with $m = m'm''$ and $n = n'n''$. This is the same two parameter resonance condition we had before. Suppose we have a non-degenerate eigenstate of \mathcal{U}^4 , we are saying that when quantum resonance occurs both the eigenstate and its Fourier Transform must be *periodic*. This statement also implies that both the original eigenstate and its Fourier transform must also be *discrete*. Indeed, since the 2 parameter group dependence implies that eigenstates could be translationally invariant along more than 2 directions we can infer that when the state is viewed from this quadrature basis it could be simultaneously periodic and discrete also.

We can speculate on what effect the one parameter group dependence has on the non-degenerate eigenstates of \mathcal{U}^4 . Remember the operator \mathcal{U}^4 can commute

with any displacement operator $D_{r,s}$ provided that $r, s = 2m\pi/k$. However, the individual displacement operators can only commute with each other provided they act along the same phase space quadrature. This means that the eigenvector that is translationally invariant in one direction cannot be translationally invariant in the other. From the perspective of the above analysis we can say that periodicity in one quadrature implies discretisation when represented in the perpendicular quadrature, that is on taking the Fourier transform. In the absence of quantum resonance simple Fourier analysis implies that the discretisation cannot be $2\pi/k$ periodic. In the next section we attempt to clarify this situation by examining the stationary states of the single \mathcal{U} operator using more established methods of Fourier analysis.

3.5 Eigenfunctions of the Fourier transform

In section 3.2 we emphasised how the Hermite-Gauss polynomials, also called number or Fock states, form the eigenbasis of both the simple harmonic oscillator and the Fourier transform. Indeed we showed how this basis was used to define the now familiar Fractional Fourier Transform. In particular we showed that the Fourier transform, up to phase, evolved any state forward $1/4$ of one natural oscillation period of the SHO. In the kicked system we made the choice to first kick the system and then apply the free evolution or Fourier Transform. We could just as easily have applied the Fourier transform and then the kicking operator. The eigenvalue equation for the first case can be written simply as

$$\mathcal{U}_0 \mathcal{U}_1 = V_1 D V_1^\dagger, \quad (3.71)$$

where V_1 are the original eigenvectors and D is the diagonal matrix containing the eigenvalues. Applying \mathcal{U}_0^\dagger to the left and \mathcal{U}_0 to the right we have

$$\mathcal{U}_1 \mathcal{U}_0 = \mathcal{U}_0^\dagger V_1 D V_1^\dagger \mathcal{U}_0. \quad (3.72)$$

We see that we the new system has the same eigenvalues as the system with operators in reverse order and with the eigenvectors $V_0 = \mathcal{U}_0^\dagger V_1$. In the case where the frequency ratio is just $1/4$, \mathcal{U}_0^\dagger is just the inverse Fourier transform. The reason we have emphasised this is because the kicking operator \mathcal{U}_1 being unitary and diagonal in the position basis can only adjust the phase of a state at

a particular position q' . Therefore the probability density of the quantum state can only be affected by the simple harmonic evolution operator \mathcal{U}_0 . This allows one to study the eigenvector properties of this model in a direct way that is not possible in most other kicked systems because the total evolution operator, in other kicked systems, *cannot* be factored into just two operations in the same basis. For the KHO however, eigenstates of the total Floquet operator \mathcal{U} must have the same *probability distribution* as certain eigenstates of the simple harmonic evolution operator \mathcal{U}_0 . That is, in the KHO, we can always say

$$|\mathcal{U}_0\Psi(q')| = |\Psi(q')| \quad , \quad (3.73)$$

where $\Psi(q')$ refers to some stationary state of the total Floquet operator \mathcal{U} . We can therefore gain significant information about the total kicked system by only studying the different types of eigenfunctions of operator \mathcal{U}_0 . The main aim of this section is therefore to show how, by analysing some of the eigenfunctions of the free evolution operator, we may gain a new perspective on certain localisation and resonance phenomena in the kicked system as a whole.

We begin first by analysing some eigenfunctions of the operator \mathcal{U}_0 with $\theta = \pi/2$ which as we have shown is, up to a phase, just the Fourier Transform. This corresponds to the search of what are defined as Self Fourier Functions (SFF's). The best known eigenfunctions of the Fourier Transform are the Hermite Gauss polynomials $u_n(q')$ or Fock states introduced in section A.1.1. Indeed it was from these functions that Namias [12] defined the fractional Fourier transform. Since superpositions of eigenfunctions with the same eigenvalue are also valid eigenfunctions we can easily see the infinity of possible functions that are valid. The situation appears even more daunting when we consider the relatively recent short paper by Caola [26] showing how any arbitrary function $\psi(q')$ can be used to construct a SFF. The simple result effectively says that the function

$$\Psi(q') = \psi(q') + \mathcal{F}\psi(q') + \mathcal{F}^2\psi(q') + \mathcal{F}^3\psi(q') \quad , \quad (3.74)$$

with \mathcal{F} the Fourier transform operator, must be a SFF. The paper by Lohmann and Mendlovic shows, among other things, that the functional structure given above is a necessary condition for the function $\Psi(q')$ to be a SFF [27]. Some of the other better known examples of SFF's are the functions [28]

$$1/\cosh(q\sqrt{\pi/2}), \quad \left| \frac{q}{\sqrt{2\pi}} \right|^{-1/2}. \quad (3.75)$$

However, we begin our analysis with the SFF that has become known as the Dirac comb.

3.5.1 The Dirac Delta Comb

We first introduce the Dirac delta comb. It is also called the Dirac delta train or the Dirac impulsion train. We define it as

$$\langle q' | III_l \rangle = III_l(q') = \sum_{n=-\infty}^{\infty} \delta(q' - nl). \quad (3.76)$$

The Fourier transform of this function is another Dirac train. This means that if a state is a Dirac train in the position basis then it will also be a Dirac train in the momentum basis. From the active transformation perspective we can say that if a Dirac train is a state of the harmonic oscillator in say the position basis, then after time $T_0/4$ it will have evolved into another Dirac train. We can show this by using (3.2). We have

$$\begin{aligned} \mathcal{F} III_l(q') &= \frac{1}{\sqrt{2\pi\hbar}} \int_{-\infty}^{\infty} \exp\left(-\frac{iq'p'}{\hbar}\right) III_l(q) dq' \\ &= \frac{1}{\sqrt{2\pi\hbar}} \int_{-\infty}^{\infty} \exp\left(-\frac{iq'p'}{\hbar}\right) \sum_{n=-\infty}^{\infty} \delta(q' - nl) dq' \\ &= \frac{1}{\sqrt{2\pi\hbar}} \sum_{n=-\infty}^{\infty} \exp\left(-\frac{ip'nl}{\hbar}\right), \end{aligned} \quad (3.77)$$

where \mathcal{F} is understood to be the ordinary Fourier transform. That is with $\theta = \pi/2$. Using the by now familiar Poisson sum formula

$$\sum_{n=-\infty}^{\infty} \exp\left(-\frac{i2\pi q'n}{a}\right) = a \sum_{m=-\infty}^{\infty} \delta(q' - ma), \quad (3.78)$$

with $l/\hbar = 2\pi/a$ we have

$$\mathcal{F} III_l(q') = \frac{\sqrt{2\pi\hbar}}{l} III_{\frac{2\pi\hbar}{l}}(p'). \quad (3.79)$$

This expresses the reciprocal relationship between periodicity in the conjugate spaces but more importantly from the active transformation point of view they show how the delta train evolves over $1/4$ of one revolution by simply setting $p' = q'$. We can clearly see that the train of delta functions becomes an exact eigenstate of the Fourier transform and hence is an exact eigenstate of the operator \mathcal{U}_0 only when we set

$$l = \sqrt{2\pi\hbar} . \quad (3.80)$$

This important property of the comb function can be used to construct more complicated functions which also display this property. We will discuss this in section 3.5.3. Using expression 3.80 we can illuminate the process of quantum resonance further by requiring that the comb function to have $2\pi/k$ periodic along, say either the position or momentum basis. Since the kicking operation \mathcal{U}_1 can only change the phase along the function we must require that the distances between spikes when viewed in this direction are some fraction of $2\pi/k$. That is

$$l = \frac{n}{m} \frac{2\pi}{k} , \quad n, m \in \mathbb{Z} . \quad (3.81)$$

Equating equations (3.80) and (3.81) give us the same quantum resonance condition that we have already worked out above using the translational invariance of the system. That is

$$\hbar = \frac{2\pi m^2}{k^2 n^2} , \quad n, m \in \mathbb{Z} . \quad (3.82)$$

This result tells us that states like that in (3.79) could only be used to construct an eigenbasis for the system when the quantum resonance condition applies. This has consequences for the nature of the solutions when there is no quantum resonance. The kicking operator being unitary and diagonal in the position basis can only adjust the phase of a state at a particular position q' and therefore the probability density of the quantum state can only be affected by the Fourier transform operation. This suggests again that stationary states of the total Floquet operator \mathcal{U} cannot be periodic in both the position and momentum basis in the absence of quantum resonance.

The comb function is also very useful from a numerical point of view. Indeed it is this function that perhaps gives us the most obvious link between the con-

tinuous Fourier transform (CFT) and the Discrete Fourier Transform (DFT) that we shall speak of in detail in chapter 4. This link is explained clearly in [35].

Using these ideas a generalised DFT can be created. This has been successfully used to analyse the eigenvalue structure of the Kicked Harper Model (KHM). In particular it has been shown that if $\hbar = 2\pi/N$ then the continuous problem can be analysed discretely using matrices of order N [29]. In the same paper it was also shown that the Lanczos diagonalisation procedure can be easily applied to this model. Recently, using this generalised DFT technique the topological properties of the eigenvalues of the KHM with $\hbar = \pi$ have been analytically examined [30].

The KHM is very similar to the kicked oscillator with frequency ratio $1/4$. One can transform the KHO into the KHM by alternating between 2 different kick strengths and consecutively applying the Fourier Transform and its inverse. It would therefore be possible to use these techniques on the KHO. However, commitments to our own lines of inquiry do not permit us to include such analysis at this time.

3.5.2 Superpositions of Displaced Number States (SDNS).

In this section, motivated largely by the structure of the numerically calculated eigenstates in section 5.3.1, we examine types of states which we unimaginatively call superpositions of displaced Fock or number states (SDNS). Many of properties of displaced Fock states are examined in [31–33]. However, we have been unable to find any information in the literature on the construction and properties of superpositions.

We therefore begin our analysis by recalling the equation, A.55, for a coherent state centered at $(q, p) = (r, s)$ on the phase plane. We repeat it here for ease of reference.

$$\langle q' | \alpha \rangle = \left(\frac{1}{\pi \hbar} \right)^{1/4} \exp \left[-\frac{q'^2}{2\hbar} + \sqrt{\frac{2}{\hbar}} \alpha q' - \frac{1}{2} |\alpha|^2 - \frac{1}{2} \alpha^2 \right], \quad (3.83)$$

with $\alpha = (r + is)/\sqrt{2\hbar}$. We could also write this as

$$\langle q' | \alpha \rangle = \left(\frac{1}{\pi \hbar} \right)^{1/4} \exp \left[-\frac{q'^2}{2\hbar} + \frac{q'}{\hbar} (r + is) - \frac{r}{2\hbar} (r + is) \right]. \quad (3.84)$$

Consider now the displacement operator

$$D_{s,r} = \exp\left(\frac{i}{\hbar}(sq - rp)\right) \quad (3.85)$$

$$= \exp\left(\frac{is}{\hbar}q\right) \exp\left(-\frac{ir}{\hbar}p\right) \exp\left(\frac{-isr}{2\hbar}\right) \quad (3.86)$$

$$= \exp\left(-\frac{ir}{\hbar}p\right) \exp\left(\frac{is}{\hbar}q\right) \exp\left(\frac{isr}{2\hbar}\right) , \quad (3.87)$$

acting on a number state (A.33), which we again repeat here for simplicity,

$$u_n(q') = \langle q'|n\rangle = \left(\frac{1}{(\pi\hbar)^{1/2}2^n n!}\right)^{1/2} \exp\left(\frac{-q'^2}{2\hbar}\right) H_n\left(\frac{q'}{\sqrt{\hbar}}\right) . \quad (3.88)$$

We can then write the whole operation as

$$D_{s,r}u_n(q') = \exp\left(\frac{isr}{2\hbar}\right) \langle q' | \exp\left(-\frac{ir}{\hbar}p\right) \exp\left(\frac{is}{\hbar}q\right) | n\rangle \quad (3.89)$$

$$= \exp\left(\frac{isr}{2\hbar}\right) \langle q' - r | \exp\left(\frac{is}{\hbar}q\right) | n\rangle \quad (3.90)$$

$$= \exp\left(\frac{isr}{2\hbar}\right) \exp\left(\frac{is}{\hbar}(q' - r)\right) \langle q' - r | n\rangle . \quad (3.91)$$

Using (3.88) and rearranging we can simplify this to

$$D_{s,r}u_n(q') = \left(\frac{1}{(\pi\hbar)^{1/2}2^n n!}\right)^{1/2} \exp\left(\frac{-q'^2}{2\hbar} + \frac{q'}{\hbar}(r + is) - \frac{r}{2\hbar}(r + is)\right) H_n\left(\frac{q' - r}{\sqrt{\hbar}}\right) . \quad (3.92)$$

Note that as expected this displaced Fock state reduces to expression (3.84) when $n = 0$. These displaced states are no longer eigenstates of the operator \mathcal{U}_0 except in the trivial case of a full revolution. This state evolves under \mathcal{U}_0 as

$$\mathcal{U}_0 D_{s,r} u_n(q') = D_{s',r'} \mathcal{U}_0 u_n(q') = e^{-i\theta/2} e^{-in\theta} D_{s',r'} u_n(q') , \quad (3.93)$$

where

$$r' = s \sin(\theta) + r \cos(\theta) , \quad (3.94)$$

$$s' = s \cos(\theta) - r \sin(\theta) . \quad (3.95)$$

We have used (3.53) and (3.54) in this calculation. This means that in terms of phase space the displaced Fock state simply rotates around the origin and picks up a phase of $e^{-i\theta/2}e^{-in\theta}$. Consider now the superposition of displaced Fock states under the operation \mathcal{U}_0

$$\mathcal{U}_0 S = \mathcal{U}_0 (D_1 + D_2 + \dots + D_m) u_n(q') , \quad (3.96)$$

with $D_1 = D_{s_1, r_1}$, $D_2 = D_{s_2, r_2}$ etc.. If we have a closed cyclic relationship between the group D_m such that

$$\mathcal{U}_0 D_1 = D_2, \mathcal{U}_0 D_2 = D_3, \dots, \mathcal{U}_0 D_m = D_1 . \quad (3.97)$$

We see that this superposition of displaced Fock states must also be an eigenstate of the operator $\mathcal{U}_0(\theta)$. There are n such superpositions Q_1, Q_2, \dots, Q_n for the case with frequency ratio $1/R$ or $\theta = 2\pi/R$. The superpositions for $R = 4$ are

$$Q_1 = D_1 + D_2 + D_3 + D_4 , \quad (3.98)$$

$$Q_2 = D_1 - iD_2 - D_3 + iD_4 , \quad (3.99)$$

$$Q_3 = D_1 - D_2 + D_3 - D_4 , \quad (3.100)$$

$$Q_4 = D_1 + iD_2 - D_3 - iD_4 , \quad (3.101)$$

or if we let $Q = [Q_1, Q_2, Q_3, Q_4]^T$ and $D = [D_1, D_2, D_3, D_4]^T$,

$$Q = F_4 D , \quad (3.102)$$

where F_4 is the 4×4 discrete Fourier matrix. In the general situations the coefficients that we use to make up the linear superposition can be gotten from the F_m matrix, where

$$F_m = e^{-i2\pi \frac{(j-1)(k-1)}{m}} = e^{-i\theta(j-1)(k-1)} , \quad (3.103)$$

for $j, k = 0, 1, 2, \dots, m-1$ and $i = \sqrt{-1}$. More details on the DFT are given in section 4.4. The general eigenvalue equation is therefore given by

$$\mathcal{U}_0(\theta) Q_m = e^{im\theta} Q_m . \quad (3.104)$$

These superpositions of Fock states are of exactly the form given in (3.74). We have only needed however to define how the operator \mathcal{U}_0 or Fourier transform acts on the displacement operator. Indeed, we can see without much thought that using the fractional Fourier transform it is possible to define a much more general expression to that of (3.74).

A general expression for the overlap between displaced Fock states can be found, see [31–33] and the references therein. Here we give the relationship without derivation

$$\begin{aligned} \langle m, \alpha_2 | n, \alpha_1 \rangle = & (-1)^{(m-n)} \left(\frac{n!}{m!} \right)^{\frac{1}{2}} (\alpha_2 - \alpha_1)^{(m-n)} \mathcal{L}_n^{m-n}(|\alpha_2 - \alpha_1|^2) \\ & \times \exp\left(-\frac{1}{2}|\alpha_1|^2 - \frac{1}{2}|\alpha_2|^2 + \alpha_2^* \alpha_1\right) \end{aligned} \quad (3.105)$$

However, it is remarkable fact that the superpositions of the displaced Fock states described above are almost all orthogonal. To show this analytically is quite tedious. Let us examine the scalar product $\langle m | Q_1^\dagger Q_1 | n \rangle$, we have in the $R = 4$ case

$$\langle m | Q_1^\dagger Q_1 | n \rangle = \langle m | (D_1^\dagger + D_2^\dagger + D_3^\dagger + D_4^\dagger)(D_1 + D_2 + D_3 + D_4) | n \rangle . \quad (3.106)$$

Expanding this out gives

$$\langle m | Q_1^\dagger Q_1 | n \rangle = \langle m | D_1^\dagger D_1 + D_1^\dagger D_2 + D_1^\dagger D_3 + D_1^\dagger D_4 \dots \quad (3.107)$$

$$+ D_2^\dagger D_1 + D_2^\dagger D_2 + D_2^\dagger D_4 + D_2^\dagger D_4 \dots \quad (3.108)$$

$$+ D_3^\dagger D_1 + D_3^\dagger D_2 + D_3^\dagger D_3 + D_3^\dagger D_4 \dots \quad (3.109)$$

$$+ D_4^\dagger D_1 + D_4^\dagger D_2 + D_4^\dagger D_4 + D_4^\dagger D_4 | n \rangle . \quad (3.110)$$

It is interesting that all these scalar products will sum to zero except in the case when $m - n = 4l$, for integer l . This is not a great surprise but is frustrating nonetheless because it tells us that these superpositions do not form a completely orthonormal basis.

Despite this, we can use these types of states to perform some very simple analysis on the whole kicked system. To this end we ask the what conditions must be imposed on these superposition states if we are to also make them *approximate* eigenstates of the total Floquet operator \mathcal{U} ? The kicking operator \mathcal{U}_1 , (3.14), can be approximated around $kq = n'\pi$ using a Taylor series, that is

$$\begin{aligned}
\mathcal{U}_1 = \exp\left(-\frac{i}{\hbar}\bar{\mu}\cos(kq)\right) &= \exp\left(-\frac{i}{k\hbar}\mu\cos(kq)\right) \\
&= \exp\left((-1)^{n'+1}\frac{i}{k\hbar}\mu\left[1 - \frac{(n'\pi - kq)^2}{2} + \dots\right]\right) .
\end{aligned} \tag{3.111}$$

Now suppose we act on the state $\langle q'|n\rangle$ with the approximated kicking operator. We have

$$\mathcal{U}_1\langle q'|n\rangle \approx \langle q'|n\rangle \exp\left(-\frac{i\mu}{k\hbar}\right) \exp\left(\frac{i\mu k}{2\hbar}q'^2\right) . \tag{3.112}$$

Clearly the first exponential is just a phase. The second exponential depends on q'^2 . We could make the effect negligible however by simply reducing k . More interesting however would be if we made the \hbar term small and the μ term even smaller. Reducing the value of the \hbar decreases the width of the number state. If μ is made even smaller the effect of the q dependence of the second term on the phase of the coherent state is practically nothing. So if μ is significantly smaller than \hbar we can say that lower energy Fock states are approximate eigenvectors of the quantum kicking operator. That is

$$\mathcal{U}_1 u_n(q') = e^{-i\Omega} u_n(q') , \tag{3.113}$$

with quasi-energy $\Omega = \mu/k\hbar$. As we have already said this number state is also the an eigenvector of the SHO Hamiltonian and therefore is also an eigenvector of the unitary operator \mathcal{U}_0 regardless of the time over which we apply it. Using 3.7 we can write out the eigenvalue equation for kick and free evolution as

$$\mathcal{U} u_n(q') = \mathcal{U}_0 \mathcal{U}_1 \langle q'|n\rangle \approx e^{-i\theta/2} e^{-i\Omega} u_n(q') , \tag{3.114}$$

for low energy number states. How low depends on the relationship between \hbar and μ .

Suppose instead of the ordinary Fock state we apply the kicking operation on to a superposition of these displaced states. If the same phase is to be applied to each separate displaced Fock state we must impose the condition that $r_1 - r_2 = 2n'\pi/k$. That is, the r values in the displacement operators must separated by a multiple of $2\pi/k$. This condition is the same as that given in [2] and described in

terms of vectors in the last section, see Figure 3.2. The allowed non trivial angles are therefore $\theta = \{2\pi/3, 2\pi/4, 2\pi/6\}$.

In the case of frequency ratio $1/4$ the condition implies that $s_1 - s_2 = 2n'\pi/k$ also. This means that only displaced Fock states whose centers can be connected by jumping a distance $D = 2\pi/k$ can be part of the same superposition.

With this established we can now ask if it is possible to connect up the SDFS structure with that of the Dirac comb structure examined in section 3.5.1. We attempt this by summing up all the displaced number states connected by jumps $2\pi/k$ along the q or p axis. To do this we first look at (3.92) and set, for the moment, $r = 0$. If we sum over all values of $s = 2m\pi/k$, with $m = [-\infty \dots -2, -1, 0, 1, 2, \dots \infty]$, we have

$$\psi_n(q') = \langle q' | \psi \rangle_n = C \exp\left(\frac{-q'^2}{2\hbar}\right) H_n\left(\frac{q'}{\sqrt{\hbar}}\right) \sum_{m=-\infty}^{\infty} \exp(i2m\pi q'/k\hbar) \quad (3.115)$$

$$= C \exp\left(\frac{-q'^2}{2\hbar}\right) H_n\left(\frac{q'}{\sqrt{\hbar}}\right) \sum_{m'=-\infty}^{\infty} \delta(q' - m'k\hbar), \quad (3.116)$$

where m and m' are integers and we have used Poisson's sum formula again in the last equality. What we have then is in a set of discretely sampled Hermite polynomials. The sampling rate is controlled completely by \hbar and so approaches the continuous function as $\hbar \rightarrow 0$. Since we required earlier that \hbar be very small, so as to limit the width of the Fock states, we may apply the same result at values of $r = 2n\pi/k$, with $n = [-\infty \dots -2, -1, 0, 1, 2, \dots \infty]$, also. While this establishes a general connection between the structures of the Dirac comb and the SDNS it is by no means rigorous and there are many unanswered questions. Nevertheless, the results above show that both constructions can under certain conditions give similar looking functions.

We may use superpositions of displaced number states to do some simple analysis on the stationary states responsible for anomalous diffusion or classical resonance, see sections 2.4.1 and 2.4.2. We begin first by examining the quasi-periodic islands. We shall choose again the simple case of a period one mode. We noted that these 2 modes occurs around the points $(\pi/2, -\pi/2)$ and $(-\pi/2, \pi/2)$ because of an exact cancellation between the rotation operator and the kick operator. We again use the technique of placing a displaced Fock state on the actual island and let \hbar get very small.

Note that the function $\cos(kq)$, near values of $m\pi/2$, with odd values of m , can be expanded to first order as

$$\cos(kq) = \sin(m\pi/2)(m\pi/2 - kq). \quad (3.117)$$

The kicking operator \mathcal{U}_1 around $q = 2m\pi/k$ may be then be approximated by

$$\mathcal{U}_1 = \exp\left(\frac{-i\mu}{\hbar k} \cos(kq)\right) \approx \exp\left(\frac{-i\mu}{\hbar k} \sin(m\pi/2)(m\pi/2 - kq)\right). \quad (3.118)$$

It is a simple task then to examine the effect of this operation on a displaced Fock state. In the position basis we write

$$\begin{aligned} \mathcal{U}_1 D_{s,r} u_n(q') &= C H_n\left(\frac{q' - r}{\sqrt{\hbar}}\right) \exp\left(\frac{-q'^2}{2\hbar} + \frac{q'}{\hbar}(r + i(s + \mu \sin(m\frac{\pi}{2})))\right) \\ &\times \exp\left(-\frac{r}{2\hbar}(r + i(s + \mu \sin(m\frac{\pi}{2})))\right) \exp\left(\frac{i\mu \sin(m\frac{\pi}{2})}{2\hbar}(r - \frac{m\pi}{k})\right), \end{aligned} \quad (3.119)$$

where $C = \left(\frac{1}{(\pi\hbar)^{1/2} 2^n n!}\right)^{1/2}$. We now evaluate the effect of this operation on a number state placed at the center of one of the quasi periodic modes. We now replace r in (3.120) to displace the state to the position coordinates where the classical anomalous islands would exist. We have

$$\begin{aligned} \mathcal{U}_1 D_{s,m\frac{\pi}{2}} u_n(q') &= C H_n\left(\frac{q' - m\pi/2}{\sqrt{\hbar}}\right) \exp\left(\frac{-q'^2}{2\hbar} + \frac{q'}{\hbar}(m\frac{\pi}{2} + i(s + \mu \sin(m\frac{\pi}{2})))\right) \\ &\times \exp\left(-\frac{m\pi}{4\hbar}(m\frac{\pi}{2} + i(s + \mu \sin(m\frac{\pi}{2})))\right) \exp\left(i\frac{\mu|m|\pi}{2\hbar} 1 - \frac{2}{k}\right). \end{aligned}$$

For simplicity we set $k = 1$ to get

$$\begin{aligned} \mathcal{U}_1 D_{s,m\frac{\pi}{2}} u_n(q') &= C H_n\left(\frac{q' - m\pi/2}{\sqrt{\hbar}}\right) \exp\left(\frac{-q'^2}{2\hbar} + \frac{q'}{\hbar}(m\frac{\pi}{2} + i(s + \mu \sin(m\frac{\pi}{2})))\right) \\ &\exp\left(-\frac{m\pi}{4\hbar}(m\frac{\pi}{2} + i(s + \mu \sin(m\frac{\pi}{2})))\right) \exp\left(-i\frac{\mu|m|\pi}{4\hbar}\right) \end{aligned} \quad (3.120)$$

We see then that applying the kicking operator just gives the number state a kick to momentum. This kick has a magnitude given by μ . In chapter 2 we showed how, on the period 1 and period 4 quasi-periodic islands, the rotation

induced by the SHO evolution cancels out the kicking operation. Using (3.93) we see that the quantum SHO operator, \mathcal{U}_0 , in the $R = 4$ case, rotates the displaced number states around the origin picking up a phase of $e^{-in\pi/2}e^{i\pi/4}$. It is easy to see then these Fock states initially displaced to either $(q, p) = (\pi/2, -\pi/2)$ and $(-\pi/2, \pi/2)$ are approximate stationary states of the system when with $\mu = \pi$. We write this out explicitly as:

$$\mathcal{U}_0\mathcal{U}_1D_{-\frac{\pi}{2}, \frac{\pi}{2}}u_n(q') \approx e^{i\Omega}D_{-\frac{\pi}{2}, \frac{\pi}{2}}u_n(q') \quad , \quad (3.121)$$

where $\Omega = -\pi^2/4\hbar - (n + 1/2)\pi/2$.

In a similar manner the period 4 modes can be also be examined. The phase picked up over the complete cycle is given by $\Omega = -2\pi^2/\hbar - (n + 1/2)2\pi$. We have showed that there are only two period 1 classical resonant islands in chapter 2. This means that these eigenfunctions, of the form above, centered on the period 1 periodic islands *cannot* have the same eigenvalues as the period 4 resonance modes if \hbar is not resonant with 2π . This would seem to imply that these *approximate* eigenstates of the total kicked operator are localised and continuous. We present some examples of numerically calculated eigenstates to back up this claim in section 5.3.1.1.

Of course the situation is different when dealing with the accelerator modes. In keeping with our classical analysis, if we put a displaced Fock state on the accelerator island at $(q, p) = (5\pi/2, 7\pi/2)$. Operating twice with the full map with $\mu = 2\pi$ should move the state to $(-9\pi/2, -11\pi/2)$ picking up a phase of $\exp(\frac{-i}{4\hbar}(10\pi^2 + 14\pi^2)) = \exp(-i6\pi^2/\hbar)$. What is important to note here is the behaviour of the phase being picked up. In all cases except for when \hbar is some fraction of 2π , a different phase will be picked up upon each operation of the kick. This poses some interesting problems when it comes to trying to numerically isolate and study the stationary states responsible for this anomalous diffusion. We discuss these problems briefly in sections 5.3.1.1, 5.3.1.2 and 5.3.3.

3.5.3 Double Gaussian states

In chapter 5 we detail the results of many of the numerical simulations we have performed. In one of the most surprising results we show that the magnitude of \hbar need only be near a resonant value for a near quadratic energy growth rates to occur 5.3.2. We have shown in the previous two sections how this quantum resonance can imply both discrete and periodic stationary states. We have also

showed how one can use superpositions of number states to approximate the KHO's stationary states around elliptical structures in classical phase space.

In this section we shall examine some functional structures that can be constructed by convolving and multiplying certain aperture functions with the Dirac comb function. These functions have the property that they can be, under certain conditions, exact self Fourier transforms (SFF's). We will show that these functions can provide an alternative link between the superpositions of displaced number states and the Dirac comb function. We speculate that these functions could potentially be used to describe a quantum mechanism that would explain the oscillating quantum resonance patterns observed in our numerical calculations in section 5.3.2.1.

To this end we introduce the function first analysed thoroughly by Corcoran and Pasch [34]. We start by stating the well known fact that one Gaussian will always become another Gaussian under Fourier transform but there is an uncertainty relation between the widths in each function. That is, the Fourier transform of a Gaussian G_a becomes another Gaussian $G_{1/a}$. Explicitly

$$\mathcal{F}C \exp\left(-\frac{q'^2}{a2\hbar}\right) = D \exp\left(-\frac{q'^2 a}{2\hbar}\right) \quad (3.122)$$

where C and D are constants which are trivial to work out. Note that as in the limit of very large or very small a we have the delta function and a constant as the Fourier transform pair. When $a = 1$ we retain the exact SFF.

Consider now the function

$$Z = G_a(q') * (III_l(q')G_{1/a}(q')) \quad (3.123)$$

where $III(q')$ is the Dirac comb, (3.79) and $*$ represents one-dimensional convolution. An interesting property of this construction is that it is unimportant whether the multiplication or convolution is computed first [34]. We have then by the convolution theorem, [28,35]

$$\mathcal{F}[G_a(q') * [III_l(q')G_{1/a}(q')]] = \mathcal{F}G_a(q')[\mathcal{F}III_l(q')G_{1/a}(q')] \quad (3.124)$$

$$= \mathcal{F}G_a(q')[\mathcal{F}[III_l(q')] * \mathcal{F}[G_{1/a}(q')]] \quad (3.125)$$

$$= G_{1/a}(q')[III_{\frac{\sqrt{2\pi\hbar}}{l}}(q') * G_a(q')] \quad (3.126)$$

which by the unusual property mentioned above is the original function Z provided that we set $l = \sqrt{2\pi\hbar}$. See Figure 3.3(a). It is not hard to see that this type of function could be generalised even further by using Hermite-Gauss polynomials to replace the simple Gaussian function. In these cases however the constructed function is only an approximate SFF. See again [34] and Figure 3.3(b).

We see that the function Z also has the property that under certain conditions $a = 0, \infty$ it becomes exactly the Dirac comb function. What's more is that in the cases where a is not quite 0 or ∞ this function must eventually tail off. This is precisely the property we need to try and explain some of the oscillating quantum resonance patterns in section 5.3.2.1. States that are very nearly infinite and very nearly periodic would provide a very easy explanation for the near quadratic energy growth found around quantum resonance. We shall also see in section 5.3.1 that the numerically predicted eigenvectors of the system resemble closely those shown in Figure 3.3. This is hardly conclusive proof of course but it hints at the possibility that a related hybrid basis could provide a platform from which one could successfully examine the system as it moves away from exact quantum resonance.

Of course there are a number of problems with using these functions. Most obviously they are not orthogonal in their current form. In addition to this is the fact that the limiting parameter $a \rightarrow 0, \infty$ bears no resemblance to the quantum resonance condition. There is also the problem that the distances between the spikes in the Dirac Comb must be some fraction of $2\pi/k$ before and after Fourier transformation. As we have already showed this only happens when the exact resonance condition is fulfilled. Perhaps however, some link between the parameters l and a could be found that would help rectify this problem. It is quite possible of course that this problem and indeed the orthonormality problem may not have a solution. However I believe, at the very least, that this approach is worthy of further study.

3.6 Conclusion

This concludes the analytical study of the quantum delta kicked harmonic oscillator. The system as been analysed thoroughly for the situations of irrational frequency ratio $1/R = (\sqrt{5} + 1)/2$ and the rational case of $1/R = 1/4$.

A new approach to the problem, using the Fractional Fourier Transform has been highlighted. The study of the Fractional Fourier Transform has over re-

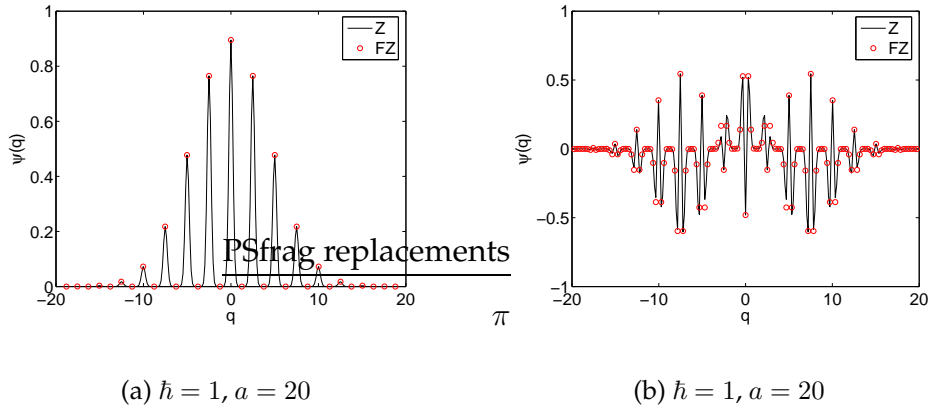


Figure 3.3. Figure showing exact double Gaussian SFF and approximate double Hermite-Gauss SFF. In the (b) we used the Hermite-Gauss polynomial with $n = 2$. Compare these figures to Figure 5.23

cent years grown considerably and has undoubtedly many more contributions to make to this particular model. It was not possible however to do justice to this, now huge, body of work and also provide the necessary analysis on the quantum chaotic aspects of the thesis. Therefore, the approach initially taken in this chapter was to only provide the simple connection between the SHO and the fractional Fourier transform. This analysis will also be used in the next chapter to explain the inner workings of our new numerical approach.

With regard to the analysis of the kicked quantum system the chapter has concentrated mostly on what can be said about the structure of the systems stationary states. With irrational frequency ratio it was shown, using the arguments of [8,10], how a map to a tight-binding approximation can be used to explain dynamical localisation under certain conditions. It was stressed however that this approximation could only be valid when the parameter $\mu/\hbar < \pi$. This fact will be demonstrated numerically in chapter 5.

The analysis of the system with rational frequency ratio $1/R = 1/4$ also concentrated on the structure of the Floquet operators stationary states. The original analysis on the translational invariance of the problem and some of the consequences were mentioned [2]. In particular we how one and two parameter translational groups were related to quantum resonance and briefly explained the effects this has on the rate of energy growth in the evolving system.

From this platform we then explained how translational invariance and in particular the two parameter group also led to discretised and extended eigen-

states in the position and momentum basis. This connection was then further emphasised through the discussion of three different types of Self Fourier functions (SFF's). Firstly we discussed the Dirac comb SFF. This was easily shown to be a very important basis for the system in exact quantum resonance. The analysis on the Dirac comb is also essential to understanding the link between the the kicked oscillator and much of the recent analysis on the kicked Harper model.

Next we dealt with the idea of using superpositions of displaced Fock states as an alternative basis for the system although it could not be made orthonormal. We used this idea to approximate some of the systems eigenstates. This approach was also used in the analysis of stationary states responsible for classical resonance.

Finally we dealt with the convolution of a double Hermite-Gauss structure with the Dirac comb to construct an approximate SFF. While this analysis could only give a qualitative explanation for the oscillating resonance patterns in section 5.3.2 I feel that the numerically calculated stationary states are reason to believe that this type of an analysis may eventually lead to a more satisfactory solution.

References

- [1] G. P. Berman, V. Yu. Rubaev and G. M. Zaslavsky, *The problem of the of quantum chaos in the kicked harmonic oscillator* Nonlinearity **4**, 543 (1991).
- [2] F. Borgonovi and L. Rebuzzini, *Translational invariance in the kicked harmonic oscillator*, Phys. Rev. E **52**, 2302 (1995).
- [3] Go. Torres-Vega, Klaus B. Møller, and A. Zúñiga-Segundo, *Role that separatrices and stochastic webs play in quantum dynamics*, Phys. Rev. A **57**, 771 (1998).
- [4] I. Dana, *Kicked Harper models and kicked charge in a magnetic field*, Phys. Lett. A **197**, 413 (1995).
- [5] R. Artuso, G. Casati and D. Shepelyansky, *Fractal spectrum and anomalous diffusion in the kicked Harper model*, Phys. Rev. Lett. **68**, 3826 (1992).
- [6] I. Dana, *Extended and localized states of generalized kicked Harper models*, Phys. Rev. E **52**, 466 (1995).
- [7] I. Guarneri and F. Borgonovi, *Generic properties of a class of translational invariant quantum maps*, J. Phys. A: Math. Gen **26**, 119 (1993).
- [8] M. Frasca, *Quantum kicked dynamics and classical diffusion*, Physics Lett. A **231**, 344 (1997).
- [9] D.R. Grempel, S. Fishman and R.E. Prange, *Localization in an incommensurate potential: An exactly solvable model*, Phys. Rev. Lett. **49**, 833 (1982).
- [10] M. Engel, *On Quantum chaos, Stochastic Webs and Localization in a Quantum Mechanical Kick system*, Ph. D Thesis (2003)

- [11] W. H. Louisell, *Quantum statistical properties of radiation* (Wiley & Sons 1990).
- [12] V. Namias, *The Fractional Order Fourier Transform and its Application to Quantum Mechanics*, J. Inst. Maths Applies **25**, 241 (1980).
- [13] J. W., Cooley, J.W. Tukey, *An Algorithm for Machine computation of Complex Fourier Series*. Mathematics of Computation, **19**, 297 (1965).
- [14] M. D. Feit, J.A. Fleck, Jr., and A. Steiger, J. Comput. Phys. **47**, 412 (1982).
- [15] F. Haake *Signatures of Quantum Chaos* vol. 54 of *Springer Series in Synergetics*, 2nd edition, (Springer-Verlag, Berlin, 2001).
- [16] H. -J. Stöckman, *Quantum Chaos. An Introduction*, (Cambridge University Press, Cambridge 1999).
- [17] P. W. Anderson, *Absence of diffusion in certain in random lattices*, Phys. Rev. **109**, 1492 (1958).
- [18] P. W. Anderson, *Localized magnetic fields in metals*. Phys. Rev. **124**, 41 (1961).
- [19] <http://mathworld.wolfram.com/UnimodularMatrix.html>
- [20] H. Furstenberg, *Non-commuting random products*, Trans. Am. Math, Soc. **108**, 377 (1963).
- [21] R. E. Borland, *The nature of the electronic states in disordered one-dimensional systems*. Proc. Roy. Soc. Londo A **274** 529 (1963).
- [22] F. Delyon, Y.-E Lévy and B. Souillard, *Anderson Localization for one- and quasi-one-dimensional systems*. J. Stat. Phys. **41**, 375 (1985).
- [23] F. Delyon, Y.-E Lévy and B. Souillard, *Approach à la Borland to multidimensional localization*, Phys. Rev. Lett. **55**, 618 (1985).
- [24] J. F. Cornwell, *Group Theory in Physics*, (Academic Press Limited, California, 1997).
- [25] O. Pfister, *Group representation theory and quantum physics*, Lecture notes, Physics Dept, University of Virginia, (2003).
- [26] M. J. Caola, *Self-Fourier functions* J. Phys. A: Math. Gen. **24**, L1143 (1991).
- [27] A. W. Lohmann and D. Mendlovic, *Self-Fourier objects and other self-transform objects* J. Opt. Soc. Am. A **9**, 2009 (1992).
- [28] R. N. Bracewell, *The Fourier Transform and its applications* (McGraw-Hill, USA, 1978).
- [29] R. Ketzmerick, K. Kruse and T. Geisel *Efficient diagonalization of kicked quantum systems*, Physica D **131**, 247 (1999).
- [30] I. I. Satija, *Topological singularities and transport in the kicked Harper model*, Phys. Rev. E **71**, 05621 (2005).
- [31] K. E. Cahill and R. J. Glauber, Phys. Rev. **177**, 1857 (1969); K. E. Cahill and R. J. Glauber, Phys. Rev. **177**, 1883 (1969)
- [32] S. M. Roy and V. Singh, Phys. Rev. D **25**, 3413 (1982).
- [33] F.A.M. de Oliveira, M.S. Kim, P.L. Knight and V. Bužek, *Properties of displaced number states* Phys. Rev. A **41**, 2645 (1990).
- [34] C. J. Corcoran and K. a. Pasch *Self-Fourier functions and coherent laser combination*, J. Phys. A:Math Gen. **37**, L461 (2004)
- [35] J. F. James, *A students guide to Fourier Transforms*, (Cambrigde University Press 1995)

Chapter 4

Simulating the Quantum system on a computer

4.1 Introduction

Computers now play a pivotal role in the study of all but the most simplistic physical systems. Indeed we demonstrated in chapter 2 that the analytical study of classical chaos must ultimately be tested against numerically computed examples. This computational dependence is even more evident in the study of complicated quantum systems. The Schrödinger equation can be very difficult to solve even in seemingly trivial situations. However, the data array structures used by most computational languages can be used quite easily to represent finite dimensional Hilbert spaces. In this case quantum states and operators are ideally represented as finite complex vectors and matrices.

However, the situation becomes more complicated when the Hilbert space on which we wish work is continuous and/or infinite. In these situations some sort of approximation and/or truncation is required. In cases where there are few analytical results the numerical procedures behind the simulation becomes almost as important as the mechanisms behind the actual continuous problem .

This chapters aims to first clarify the relationship between the continuous system and its discretised approximation. The emphasis is placed in particular in understanding the relationship between the size of our approximate Hilbert space and the value of quantum parameter \hbar . This is established using the well known connection between the continuous Fourier transform (FT) and its discrete counterpart the Discrete Fourier Transform (DFT). A simple relationship between \hbar , the spatial length L of our simulation and the number of discrete sampling

points N can then be derived. This then establishes limits on the ability of the DFT to accurately simulate the continuous problem.

Next the Discrete Fractional Fourier Transform (DFFT) is introduced. It is shown how the transform is defined in terms of a the discrete *Harper* equations [1]. The solutions to which are exactly the Hermite-Gauss polynomials in the continuous limit [8]. We include many of the technical details behind the construction and ordering of this basis, taking special care to include the quantum parameter \hbar at all times.

The remainder of the chapter is used to define the numerical procedures behind what is known as the Fast Fractional Fourier Transform (FFFT). To do this we analyse the well known Fast Fourier Transform (FFT) procedure. This can be used to evolve our kicked system when the frequency ratio is the rational $1/R = 1/4$. However it is also used to perform the digital convolutions necessary in for the FFFT.

4.2 Arrays as state vectors

The Dirac notation provides an easy way to visualise most quantum systems. We start off with a state $|\psi\rangle$ which may be viewed as a vector. The dimension of this vector depends the type of system and it's appearance, like all vectors, depends on which direction you look at it from. One way of looking at a quantum system is through the Fock state basis. Using the completeness relation we may expand out the a state in the Fock state basis:

$$|\psi\rangle = \sum_n |n\rangle \langle n|\psi\rangle . \quad (4.1)$$

Once written in this way we can write each vector as an array. By definition the basis kets $|n\rangle$ are orthogonal. We write them in vector form as

$$|0\rangle = \begin{pmatrix} 1 \\ 0 \\ \cdot \\ \cdot \\ 0 \end{pmatrix} \quad |1\rangle = \begin{pmatrix} 0 \\ 1 \\ \cdot \\ \cdot \\ 0 \end{pmatrix} \quad \dots \quad |n\rangle = \begin{pmatrix} 0 \\ 0 \\ \cdot \\ \cdot \\ 1 \end{pmatrix} . \quad (4.2)$$

From (4.1) we can see that the state $|\psi\rangle$ can be written in the Fock state basis as the array

$$|\psi\rangle = \begin{pmatrix} \langle 0|\psi\rangle \\ \langle 1|\psi\rangle \\ \cdot \\ \cdot \\ \langle n|\psi\rangle \end{pmatrix} . \quad (4.3)$$

Since the Fock state basis is infinite it is necessary to truncate the basis so that it may be stored on a computer. The situation is a little more complicated than this when dealing with continuous position and momentum representations. In the similar way to before, any arbitrary ket $|\psi\rangle$ may be expanded in these basis, that is

$$|\psi\rangle = \int_{-\infty}^{\infty} |q'\rangle \langle q'|\psi\rangle dq' = \int_{-\infty}^{\infty} |p'\rangle \langle p'|\psi\rangle dp' . \quad (4.4)$$

On close inspection of the above equation we should notice that it is not possible to write out the basis vectors $|q'\rangle$ or $|p'\rangle$ in the same way as we do for the Fock basis (4.2). No matter how we truncate the limits of the integral it is impossible to store all the values of a continuous function on a computer. It is therefore necessary to discretise the basis in a manner that allows us to still obtain highly accurate results. We do this by first recalling the Fourier transform relationship between wave-functions written in the position and momentum basis, (3.1) and (3.2). We will make the jump from continuous space to discretised space by requiring that a similar relationship be valid using discrete wavefunctions and the Discrete Fourier Transform (DFT).

We define the column vector $\phi[k]$, to be the DFT of an input column vector $\psi[n]$ of length N , that is

$$\phi[k] = \frac{1}{\sqrt{N}} \sum_{j=1}^N \psi[j] \exp(-i2\pi(k-1)(j-1)/N) , \quad 1 \leq k \leq N , \quad (4.5)$$

with the inverse transform defined as

$$\psi[j] = \frac{1}{\sqrt{N}} \sum_{k=1}^N \phi[k] \exp(i2\pi(k-1)(j-1)/N) , \quad 1 \leq j \leq N . \quad (4.6)$$

Sometimes it will be useful to view these transformations in matrix notation. For that purpose we define the matrix

$$F_{-\frac{\pi}{2}}[j, k] = e^{-i2\pi\frac{(j-1)(k-1)}{N}} \equiv \omega^{(j-1)(k-1)} , \quad (4.7)$$

for $j, k = 1, 2, \dots, N$. We can use this to write (4.5) and (4.6) as

$$\phi[k] = \frac{1}{\sqrt{N}} F_{-\frac{\pi}{2}} \psi[j] , \quad (4.8)$$

and

$$\psi[j] = \frac{1}{\sqrt{N}} F_{-\frac{\pi}{2}}^\dagger \phi[k] = \frac{1}{\sqrt{N}} F_{\frac{\pi}{2}} \phi[k] . \quad (4.9)$$

Careful comparison of (3.1) with (4.5) leads to some important results. We want to associate $\psi(q')$ with $\psi[j]$ and $\phi(p')$ with $\phi[k]$. This means that we must find relationships between the q', p' and j, k variables. To this end we must assume that q' and p' have a finite range which we define to be L^* . The value for L can be arrived at in the following way. Equating the expressions inside the exponentials in (3.1) and (4.5) we arrive at the following equation

$$\frac{2\pi(k-1)(j-1)}{N} = \frac{p'q'}{\hbar} . \quad (4.10)$$

There are N values of $(k-1)$ and $(j-1)$ to be distributed equally along the length L . Setting $(k-1), (j-1) = N$ and $p', q' = L$ and rearranging we get

$$L = \sqrt{2\pi\hbar N} . \quad (4.11)$$

This is extremely important. It will allow us set up a grid system specific to any \hbar we choose. If we wish to simulate a larger wavefunctions all we need to is increase the sampling rate or number of grid points N . It should be noted that it is customary to use $N = 2^s, s = 1, 2, 3, \dots$ as it makes the fast Fourier transform

*The advantage of, in chapter 2, using a canonical transform that leaves q' and p' symmetrical can be seen quite easily here. If this was not the case we would have to define separate ranges L_q, L_p for q' and p' respectively. The more general relationship $L_q L_p = 2\pi\hbar N$ could then be used along with more complicated normalisation relations. Having L_p and L_q symmetrical is essential for our purposes however because we wish to use the DFT as an active transformation on our discrete position basis.

algorithms considerably more efficient, see section 4.4. We can now define arrays $q[j]$ and $p[k]$ as discrete approximations to the continuous axes q' and p' ,

$$q[1, \dots, N] = p[1, \dots, N] = \left[\frac{-L}{2}, \frac{-L}{2} + l, \frac{-L}{2} + 2l, \dots, 0, \dots, \frac{L}{2} - 2l, \frac{L}{2} - l \right], \quad (4.12)$$

where $l = L/N$. The discrete wavefunctions $\psi[j]$ and $\phi[k]$ are thus defined in terms of $q[j]$ and $p[k]$. For example, $\psi[j]$ is now the value of the discrete wavefunction at the position given in the array $q[j]$.

To perform the actual DFT we must first perform a shifting operation to the arrays. To see why note that the situation where $j, k = 1$ should coincide with the situation where $p', q' = 0$. This is because the argument in the exponentials should be zero in both circumstances. This is important when actually performing a DFT and is achieved by taking the second half of the array $q[j]$ or $p[k]$ and placing it in front of the first half. This sets $q[1]$ and $p[1]$ to be zero. The ranges $-L/2 \rightarrow L/2 - l$ are chosen to make sure that there is a value of exactly 0 at $q[1]$ and $p[1]$ [†]. We call this shift the *fftshift* and denote the shifted arrays as $q_s[j], p_s[k], etc.$

Note that $q_s[j]$ and $p_s[k]$ are not used in the actual DFT calculation but since $\psi[j]$ and $\phi[k]$ are supposed to be functions of $q[j]$ and $p[k]$ these must be also shifted in the same way to get the correct results. After the DFT calculation has been performed we may apply the same shift operation to get the arrays running from negative to positive again.

At the heart of this method lies the fact that the DFT can effectively simulate the continuous Fourier transform provided the continuous signal is adequately sampled. We then established the relationship between \hbar , the range of position or momentum L and the number of sampling points or grid size N (4.11). What this means numerically is that if we have a fixed space L , in which we represent our quantum state, and we decrease the value of \hbar , that is bring it closer to the classical regime, we must increase the number of grid points N . Increasing the number of sampling points N in the discretised wavefunction means that the wavefunction now contains more information. Since L is fixed as we decrease \hbar the wavefunction is allowed to contain finer detail and look more complicated. This is, in the end, just another way of expressing Heisenberg's uncertainty principle. As a direct result of these factors we see that the finite memory in a CPU means that we can only make \hbar so small.

[†]Of course they could just as easily be defined from $-L/2 + l \rightarrow L/2$ but in this case the shifting operation to put the zero in the first array position would be different.

To illustrate the discretising procedure and the consistency of the results we shall perform a fast Fourier transform on a discretely sampled eigenfunction of the simple harmonic oscillator. From (A.33)) we write

$$u_2(q') = \langle q'|2\rangle = \left(\frac{1}{(\pi\hbar)^{1/2}2^2 2!} \right)^{1/2} \exp\left(\frac{-q'^2}{2\hbar}\right) H_2\left(\frac{q'}{\sqrt{\hbar}}\right) . \quad (4.13)$$

Setting $\hbar = 1$ and writing out H_2 explicitly we have

$$u_2(q') = \left(\frac{1}{(\pi)^{1/2}8} \right)^{1/2} e^{-\frac{q'^2}{2}} [4q'^2 - 2] . \quad (4.14)$$

we set $N = 2^7 = 128$ and use (4.11) to give $L = \sqrt{2\pi 128} \approx 28.46982\dots$ and $l = L/N = 0.22242\dots$. From (4.12) the arrays $q[j]$ and $p[j]$ are

$$q[j] = p[j] = -L/2 + j \times l \approx -14.23491 + j \times 0.22242 . \quad (4.15)$$

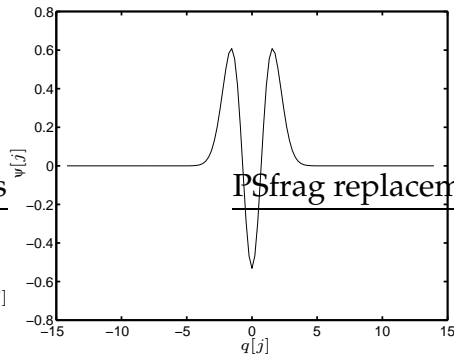
Using these reference points we can now calculate a discrete function $u_2(q[j])$ which we plot against the $q[j]$ array, see Figure 4.1(a). We first check that the properties of this state are correct. To check the wavefunctions is normalised we can perform the elementary numerical integration to get

$$C = \int_{-\infty}^{\infty} dq \Psi^*(q) \Psi(q) \approx l \sum_{j=1}^N \psi[j]^* \psi[j] = 1.0000000 \dot{} , \quad (4.16)$$

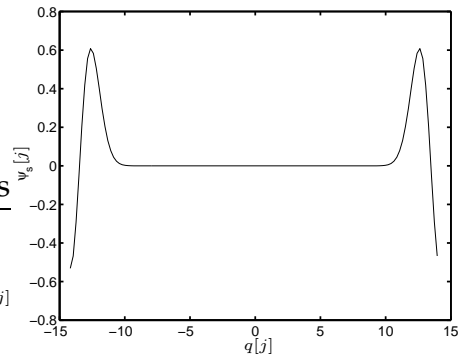
where the zeros continue to the sixteenth decimal place. We now take the second half of the array and place it before the first, see Figure 4.1(b). With the vector or array correctly shifted we can now operate on it with the DFT operation (4.5), resulting in Figure 4.1(c). Finally we perform the shifting operation again to obtain the correctly transformed wavefunction, see Figure 4.1(d). We can see that this is so if we examine (3.4), with $n = 2$ to get

$$F_{-\pi/2} u_2(q') = e^{-i2\frac{\pi}{2}} u_2(q') = -u_2(q') . \quad (4.17)$$

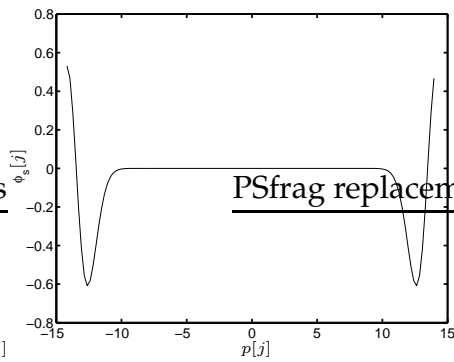
Using the elementary summation to again perform the numerical integration shows the final state to be also normalised to unity to the sixteenth decimal. In the figure, once we had performed the transform, we changed the label on the x -axis to $p[j]$. This was to emphasise the passive way of viewing the Fourier



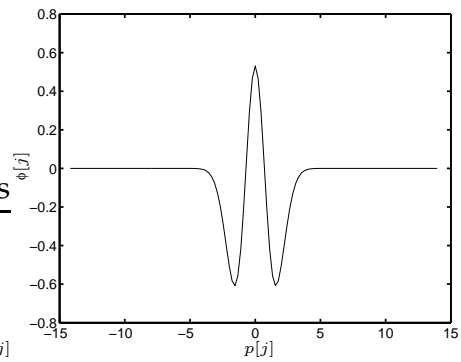
(a) Discrete wavefunction in the position basis



(b) Shifted wavefunction in the position basis



(c) Fourier Transform of shifted wavefunction



(d) Fourier Transform of Discrete wavefunction

Figure 4.1. The process of the Discrete Fourier transform.

Transform. The transformed function can be viewed as the same state vector but in the momentum representation. This idea now allows us to check the energy of the discretised wavefunction. The expectation value of the energy is, in Dirac notation

$$E = \frac{\omega_0}{2} \langle \psi | p^2 + q^2 | \psi \rangle, \quad (4.18)$$

where $|\psi\rangle$ is the state in no particular basis. Inserting the completeness relations for momentum and position we get

$$\begin{aligned} E &= \frac{\omega_0}{2} \left(\int_{-\infty}^{\infty} dp' \langle \psi | p^2 | p' \rangle \langle p' | \psi \rangle + \int_{-\infty}^{\infty} dq' \langle \psi | q^2 | q' \rangle \langle q' | \psi \rangle \right) \\ &= \frac{\omega_0}{2} \left(\int_{-\infty}^{\infty} dp' \phi^*(p') p'^2 \phi(p') + \int_{-\infty}^{\infty} dq' \psi^*(q') q'^2 \psi(q') \right). \end{aligned} \quad (4.19)$$

$$\approx \frac{\omega_0 l}{2} \left(\sum_{j=1}^N \phi^*[j] p^2[j] \phi[j] + \sum_{j=1}^N \psi^*[j] q^2[j] \psi[j] \right) \approx 2.5000000 \omega_0, \quad (4.20)$$

again with the zeros recurring till the sixteenth decimal place. This agrees with the theoretical energy for $|n\rangle$ with $\hbar = 1$, see (A.26).

For the specific value $n = 2$ the vector obtained by discretising the continuous Hermite Gauss polynomial $u_2(q')$ is, to a high degree of accuracy, an eigenfunction of the DFT matrix. We can quickly show that this is not always the case for larger values of n . It is known that the probability distributions $|u_n(q')|^2$ have a maximum roughly at the turning point of a classical particle. This becomes more obvious at higher energies $E_n = \hbar\omega_0(n + 1/2)$. As we move beyond the classical turning point the quantum probability distribution rapidly approaches 0. The classical turning points of a particle of energy E_n are easily found by setting $E_n = \omega_0 q^2/2$ and therefore exist at $q_{max} = |\sqrt{2E_n/\omega_0}| = |\sqrt{2\hbar(n + 1/2)}|$. This means that a grid space of at least $L = 2|\sqrt{2\hbar(n + 1/2)}|$ is needed to display the function $u_n(q')$ correctly. However, we already have a condition for L in terms of the size of the matrix space N and \hbar , (4.11). Comparing of the two conditions gives

$$n = \frac{\pi N}{4} - \frac{1}{2}. \quad (4.21)$$

Using a grid N we can, at most, accurately discretise the first n Hermite Gauss functions. While the vectors $u_n(q[j])$ are in general extremely good approximations for the eigenvectors of the DFT we can clearly see that this is not always the

case. In the next section we set about finding the exact set of eigensolutions for the DFT. It is this set of solutions that are used to defined the Discrete Fractional Fourier Transform (DFFT).

4.3 The Discrete fractional Fourier Transform

In section 3.2 we showed how, in the position basis, the Floquet operator for the SHO and the operator called the Fractional Fourier transform were, up to a phase, one and the same. In this section we will extend this relationship to the discretised basis $q[j]$ introduced above. The following discussion is based largely on the text [1], written in particular for the signal processing field. However, we have tried to maintain the Dirac notation and the variable \hbar throughout. The relationship between signal processing and quantum mechanics has been a productive one for both fields. The Wigner and Husimi distributions, see section C.1, have also many applications in signal processing.

In what follows we define the discretised Hamiltonian matrix in terms of difference equations used for differentiating discrete functions. The eigenvectors of this matrix can are then used to define a discrete Fourier transform.

The momentum operator p is defined in the position basis as

$$\langle q' | p | \psi \rangle = \frac{\hbar}{i} \frac{\partial}{\partial q} \langle q' | \psi \rangle = \frac{\hbar}{i} \frac{\partial}{\partial q} \psi(q') . \quad (4.22)$$

Likewise the position operator in the momentum basis

$$\langle p' | q | \psi \rangle = -\frac{\hbar}{i} \frac{\partial}{\partial p'} \langle p' | \psi \rangle = -\frac{\hbar}{i} \frac{\partial}{\partial p'} \phi(p') . \quad (4.23)$$

The Hamiltonian \mathcal{H}_0 , written in the position basis, is then

$$\mathcal{H}_0 = \frac{\omega_0}{2} (p^2 + q^2) = -\hbar^2 \frac{\partial}{\partial q'} + q^2 . \quad (4.24)$$

We have showed in section A.1.1 that the eigenfunctions of this equation are the Hermite Gauss polynomials $u_n(q')$ with eigenvalues $E_n = \hbar\omega_0(n+1/2)$. We define the discrete operator p_l as

$$\langle q' | p_l | \psi \rangle = \frac{\hbar}{i} \frac{\langle q' + l/2 | \psi \rangle - \langle q' - l/2 | \psi \rangle}{l} , \quad (4.25)$$

and p_l^2 as

$$\langle q' | p_l^2 | \psi \rangle = -\frac{\hbar^2}{l^2} [\langle q' + l | \psi \rangle - 2\langle q' | \psi \rangle + \langle q' - l | \psi \rangle] , \quad (4.26)$$

which we can write in the notation given before as

$$\langle q[n] | p_l^2 | \psi \rangle = -\frac{\hbar^2}{l^2} [\langle q[n+1] | \psi \rangle - 2\langle q[n] | \psi \rangle + \langle q[n-1] | \psi \rangle] , \quad (4.27)$$

where $q[n]$ is given by (4.12) and (4.11). This technique forms the basis of implicit schemes for evolving the Schrödinger equation [2]. A discrete Hamiltonian operation can then be defined as

$$\langle q[n] | H_0 | \psi \rangle = -\frac{\hbar^2}{2l^2} [\langle q[n+1] | \psi \rangle - 2\langle q[n] | \psi \rangle + \langle q[n-1] | \psi \rangle + \langle q[n] | q^2 | \psi \rangle] . \quad (4.28)$$

This Hamiltonian is then used to evolve the wavefunction forward in discrete units of time τ using a discrete Schrödinger equation

$$\frac{i\hbar}{\tau} \langle q' | \psi(t + \tau) \rangle - \langle q' | \psi(t) \rangle = \langle q' | H_0 | \psi(t) \rangle . \quad (4.29)$$

However we are only interested in the discrete form of the actual Hamiltonian. The matrix form of H_0 is tridiagonal, that is

$$\langle q[n] | H_0 | q[m] \rangle = \frac{\hbar^2}{2l^2} \begin{bmatrix} 2\frac{l^2}{\hbar^2}q[1]^2 + 2 & -1 & 0 & \cdots & 0 & -1 \\ -1 & 2\frac{l^2}{\hbar^2}q[2]^2 + 2 & -1 & \cdots & 0 & 0 \\ \vdots & \vdots & \vdots & \ddots & \vdots & \vdots \\ -1 & 0 & 0 & \cdots & -1 & 2\frac{l^2}{\hbar^2}q[n]^2 + 2 \end{bmatrix} \quad (4.30)$$

However, this matrix representation of the Hamiltonian does not have all the properties we are looking for. Most importantly, when it has been fftshifted, it does not commute with the DFT matrix and therefore does not have the same basis eigenvectors.

Notice now that in the simple derivation above the q and p operators are not treated the same. The p_l^2 operator is some sort of difference operation operating on the discretised function. The operator approaches the continuous operator p^2 as we make l smaller. The q^2 operator, however, is exactly the continuous

operator, albeit operating on discretised function. As a solution to this we present an argument found in [1]. For more details on these matters see [3–8].

We first define q_l^2 in terms of a difference equation in discretised momentum space and try to work out its exact form in terms of position space. From (4.23) and (4.26) it can be seen that the discrete operator q_l^2 can also be written as

$$\langle p' | q_l^2 | \psi \rangle = -\frac{\hbar^2}{l^2} [\langle p' + l | \psi \rangle - 2\langle p' | \psi \rangle + \langle p' - l | \psi \rangle] . \quad (4.31)$$

or

$$\langle p[n] | q_l^2 | \psi \rangle = -\frac{\hbar^2}{l^2} [\langle p[n+1] | \psi \rangle - 2\langle p[n] | \psi \rangle + \langle p[n-1] | \psi \rangle] . \quad (4.32)$$

An interesting comparison can be made of the discrete and continuous operators by using the displacement operator defined in (3.48). We have

$$D_{r,s} = \exp\left(\frac{i}{\hbar}(s\hat{q} - r\hat{p})\right) . \quad (4.33)$$

The operator $D_{0,s}$ has the following effect on the bra $\langle p' |$:

$$\langle p' | D_{0,s} = \langle p' | \exp\left(\frac{i}{\hbar}s\hat{q}\right) = \langle p' - s | . \quad (4.34)$$

if $s = l$ we can write in the discrete notation

$$\langle p[n] | D_{0,s} = \langle p[n] | \exp\left(\frac{i}{\hbar}s\hat{q}\right) = \langle p[n-1] | . \quad (4.35)$$

Using this idea we can write (4.31) as

$$\begin{aligned} q_l^2 \langle p' | \psi \rangle &= -\frac{\hbar^2}{l^2} [e^{-isq/\hbar} + e^{isq/\hbar} - 2] \langle p' | \psi \rangle \\ &= -\frac{\hbar^2}{l^2} [2 \cos(lq/\hbar) - 2] \langle p' | \psi \rangle . \end{aligned} \quad (4.36)$$

Dividing both sides by the function $\langle p' | \psi \rangle$ we can write

$$q_l^2 = -\frac{\hbar^2}{l^2} [2 \cos(lq/\hbar) - 2] = q^2 + O(l^2/\hbar^2) . \quad (4.37)$$

Where in the last step we expanded the cosine term in a Taylor expansion. Suppose that we now substitute the operator q_l^2 written in (4.37) for the operator q^2 in (4.28), we are left with

$$\langle q' | H_0 | \psi \rangle = -\frac{\hbar^2}{2l^2} [\langle q' - l | \psi \rangle + 2(\cos(lq'/\hbar) - 2)\langle q' | \psi \rangle + \langle q' + l | \psi \rangle] \quad (4.38)$$

To change to the discrete notation we again set $q' = q[j] = -L/2 + (j - 1) \times l$ $j = 1, 2, \dots, N$ and therefore the fftshifted array is $q_s[j] = [0, l, 2l, \dots, L/2 - l, -L/2 - L/2 + l, \dots - l]$. Remembering that $l = L/N = \sqrt{2\pi\hbar/N}$ we can finally write

$$\begin{aligned} \langle q_s[j] | H_0 | \psi \rangle &= \sum_k \langle q_s[j] | H_0 | q_s[k] \rangle \langle q_s[k] | \psi \rangle \\ &= -\frac{\hbar N}{4\pi} [\langle q_s[k - 1] | \psi \rangle + 2(\cos(2\pi(k - 1)/N) - 2)\langle q_s[k] | \psi \rangle + \langle q_s[k + 1] | \psi \rangle] \end{aligned} \quad (4.39)$$

The sum above is of course just a matrix multiplication. It is possible to write the matrix $H_0[j, k] = \langle q_s[j] | H_0 | q_s[k] \rangle$ as

$$H_0 = -\frac{\hbar N}{4\pi} \begin{bmatrix} 2 & 1 & 0 & \cdots & 0 & 1 \\ 1 & 2\cos(\frac{2\pi}{N}) - 4 & 1 & \cdots & 0 & 0 \\ 0 & 1 & 2\cos(\frac{2\pi^2}{N}) - 4 & \cdots & 0 & 0 \\ \vdots & \vdots & \vdots & \ddots & \vdots & \vdots \\ 1 & 0 & 0 & \cdots & 1 & 2\cos(\frac{2\pi(N-1)}{N}) - 4 \end{bmatrix} \quad (4.40)$$

The matrix multiplies the column vector $\psi(q_s) = \langle q_s[k] | \psi \rangle$ representing a state vector written in the discretised and fftshifted position basis. This Hamiltonian matrix $H_0[j, k]$ does commute with the DFT. It is interesting that by introducing what many would call an inaccuracy into the Hamiltonian we somehow end up with the correct matrix Hamiltonian. However, it makes sense from a symmetrical point of view. The Harmonic oscillator is in every way symmetrical with respect to the p and q representations. It is strangely logical that we should require the same symmetry in the discretised version, even if that means introducing another approximation.

The matrix above is sometimes called *Harpers matrix* and its associated eigenvalue equation (4.40) is called *Harpers equation*. The equation has many applications in areas of physical science. It has been associated with Bloch electron problems and some authors have associated it with Mathieu equations and Sturm-Liouville problems [1]. Detailed discussions on these matters can be found in [5–7].

The commutation of the Harper matrix with the DFT matrix means they share a common set of eigenvectors which we refer to as $v_n[j] = \langle q_s[j] | n \rangle$. Above we found numerical evidence that at least one of these eigenvectors, when shifted correctly, approach the discretely sampled Hermite Gauss polynomials referred to above as $u_n(q[j])$. For studies examining the differences between these two sets of functions as we increase the size of the vector space and, consequently, the overall ability of the DFT to simulate the continuous transform and evolution operator \mathcal{U}_0 of the SHO see [8] and references therein.

It is also possible to calculate the discrete matrix H_0 to higher orders. Indeed such a matrices also commute with the DFT matrix and the eigensolutions would also be even better approximations to the Hermite Gauss polynomials $u_n(q)$. We will not discuss these matters here but a brief discussion on this matter is given in [1].

The eigensolutions to the matrix H_0 in (4.40) can found by standard numerical techniques for solving tridiagonal systems. The set of eigenvectors is not necessarily unique. In order to proceed some complicated classification and re-ordering procedures must be carried out. For a discussion on these techniques see [1]. With the vector V correctly ordered, that is with $V = v_1[q] \dots v_N[q]$, one way to define the discrete fractional Fourier transform matrix (DFrFT) is by spectral decomposition. That is,

$$F_\theta = V D V^\dagger \quad . \quad (4.41)$$

where D has the eigenvalues $\exp(i(n-1)\theta)$ along it's diagonal. Using this definition of the transform we can now simulate the evolution matrix of the simple harmonic oscillator. In our matrix notation, with $\theta = \omega_0 t$, we can write

$$\langle q_s[j] | \psi(t) \rangle = e^{-i\frac{\theta}{4}} \sum_k \langle q_s[j] | F_{-\theta} | q_s[k] \rangle \langle q_s[k] | \psi(0) \rangle \quad . \quad (4.42)$$

Since the kicking operator matrix U_1 is already diagonal in the position basis, we can, using the fftshifted position basis $q_s[j]$, write it as the diagonal matrix

$$U_1 = \text{diag} \left[\exp \left(\frac{-i\bar{\mu} \cos(q_s[j])}{\hbar} \right) \right] = \text{diag} \left[\exp \left(\frac{-i\mu \cos(q_s[j])}{k\hbar} \right) \right] \quad , \quad (4.43)$$

where we have used (3.14). The discretised and fftshifted Floquet operator for the total kicked system with with $\theta = \omega_0 t$ is thus given by

$$U = U_0 U_1 = e^{-i\frac{\theta}{4}} F_{-\theta} \text{diag} [\exp(-i\mu \cos(q_s[j])/k\hbar)] \quad . \quad (4.44)$$

The matrix U written in this way is easy to calculate and offers an ideal way to numerically analyse the systems eigenvalues and eigenvectors for different frequency ratios. However, we are as always limited by memory storage and CPU speed in this respect. Nonetheless it is an extremely powerful tool and can be used to search for various signatures of chaos while also checking many of the analytical predictions. The real power of this particular technique comes when we want to evolve a discretised vector $\psi[j]$. We can use the fast Fourier transform and a technique known as the Fast Fractional Fourier transform to accurately evolve the vector with out ever having to store a matrix. It allows the user to examine the system for longer times and with more accuracy than have previously been possible.

4.4 The Fast Fourier Transform

The Fast Fourier Transform (FFT) was introduced by Cooley and Tukey in 1965 [11]. The process is possibly best illustrated by actually examining the the Fourier Transform matrix [12,13]. In the last section we defined the $N \times N$ matrix operator $F = F_{-\frac{\pi}{2}}$ as

$$F_N = e^{-i2\pi \frac{(j-1)(k-1)}{N}} \equiv \omega^{(j-1)(k-1)} \quad , \quad (4.45)$$

for $j, k = 1, 2, \dots, N$ and $i = \sqrt{-1}$. The subscript is used for the moment to illustrate the size of the matrix. The matrix F_2 is given by

$$F_2 = \begin{bmatrix} 1 & 1 \\ 1 & i^2 \end{bmatrix} \quad , \quad (4.46)$$

and the F_4 matrix is given by

$$F_4 = \begin{bmatrix} 1 & 1 & 1 & 1 \\ 1 & i & i^2 & i^3 \\ 1 & i^2 & i^4 & i^6 \\ 1 & i^3 & i^6 & i^9 \end{bmatrix} \quad , \quad (4.47)$$

which may be factorised into

$$F_4 = \begin{bmatrix} 1 & & & \\ & 1 & & \\ & & i & \\ & & & -i \end{bmatrix} \begin{bmatrix} 1 & 1 & & \\ & 1 & i^2 & \\ & & & 1 & 1 \\ & & & & 1 & i^2 \end{bmatrix} \begin{bmatrix} 1 & & & \\ & & & 1 \\ & & 1 & \\ & & & 1 \end{bmatrix} . \quad (4.48)$$

In general we may write

$$F_{2N} = \begin{bmatrix} I_N & D_N \\ I_N & -D_N \end{bmatrix} \begin{bmatrix} F_N & 0_N \\ 0_N & F_N \end{bmatrix} \begin{bmatrix} \text{even} - \text{odd} \\ \text{shuf fle} \end{bmatrix} . \quad (4.49)$$

where I_n is the $N \times N$ identity matrix and D_N is the diagonal matrix with entries $1, \omega, \dots, \omega^N$. It can now be seen that

$$\begin{bmatrix} F_N & & & \\ & F_N & & \\ & & & \\ & & & \end{bmatrix} = \begin{bmatrix} I_{\frac{N}{2}} & D_{\frac{N}{2}} & & \\ I_{\frac{N}{2}} & -D_{\frac{N}{2}} & & \\ & & I_{\frac{N}{2}} & D_{\frac{N}{2}} \\ & & I_{\frac{N}{2}} & -D_{\frac{N}{2}} \end{bmatrix} \begin{bmatrix} F_{\frac{N}{2}} & & & \\ & F_{\frac{N}{2}} & & \\ & & F_{\frac{N}{2}} & \\ & & & F_{\frac{N}{2}} \end{bmatrix} \begin{bmatrix} \text{Even} \\ \text{Odd} \\ \text{Shuf} \\ \text{-fle} \end{bmatrix} \quad (4.50)$$

In this way we can successively break down the original Fourier matrix into a series of simple, sparse matrices. These sparse matrices thus operate individually on the input vector. These operations need not be performed as matrix-vector multiplications but as simple reordering, multiplication and addition procedures. A cleverly written algorithm can perform a Fourier Transform on a vector in $O(N \log_2 N)$ operations compared to the $O(N^2)$ operations needed when operating with F_N matrix directly.

4.5 The Fast Fractional Fourier Transform

In this section we will try to give a brief overview of an algorithm used to calculate what is known as the Fast Fractional Fourier Transform (FFFT) [3,9,10]. The algorithm itself is quite complicated and the arguments presented will rely heavily on other material. This is unavoidable, many of the techniques used here were invented for specific use in digital signal processing which itself is a huge subject. We begin by placing the bra $\langle q' |$ on the left of (4.1). This gives

$$\langle q' | \psi \rangle = \sum_n^{\infty} \langle q' | n \rangle \langle n | \psi \rangle \quad (4.51)$$

or

$$\psi(q') = \sum_n^{\infty} a_n u_n(q') \quad (4.52)$$

where $a_n = \langle n | \psi \rangle$ and as usual the $u_n(q') = \langle q' | n \rangle$ represent the Hermite Gauss polynomials, see (A.33). Using the definition of the fractional Fourier transform (3.6) the effect of the operator \mathcal{F}_θ on $\psi(q')$ is

$$\langle q' | \mathcal{F}_\theta | \psi \rangle = \sum_n^{\infty} \langle n | \psi \rangle \langle q' | e^{iN\theta} | n \rangle = \sum_n^{\infty} \langle n | \psi \rangle e^{in\theta} \langle q' | n \rangle. \quad (4.53)$$

or

$$\mathcal{F}_\theta \psi(q') = \sum_n^{\infty} a_n e^{in\theta} u_n(q'). \quad (4.54)$$

Using the completeness relation in the position basis we can write these as

$$\langle q' | \mathcal{F}_\theta | \psi \rangle = \int_{-\infty}^{\infty} \sum_n^{\infty} \langle n | q'' \rangle \langle q'' | \psi \rangle e^{in\theta} \langle q' | n \rangle dq''. \quad (4.55)$$

Since the Hermite Gauss polynomials are real we may write this as

$$\mathcal{F}_\theta \psi(q') = \int_{-\infty}^{\infty} \sum_n^{\infty} u_n(q'') u_n(q') e^{in\theta} \psi(q'') dq''. \quad (4.56)$$

Using (A.33) this may be written as

$$\mathcal{F}_\theta \psi(q') = \frac{1}{\sqrt{\pi\hbar}} \int_{-\infty}^{\infty} \psi(q'') e^{\left(\frac{-(q'^2+q''^2)}{2\hbar}\right)} \sum_n^{\infty} \frac{e^{in\theta}}{2^n n!} H_n\left(\frac{\sqrt{q''}}{\hbar}\right) H_n\left(\frac{\sqrt{q'}}{\hbar}\right) dq''. \quad (4.57)$$

where H_n are the Hermite polynomials. We now use a formula due to Mehler to write the operation \mathcal{F}_θ as a simpler integration, see [14,15]. The formula says that the summation in the integration can be written as

$$\sum_{n=0}^{\infty} \frac{e^{in\theta}}{2^n n!} H_n\left(\frac{q''}{\sqrt{\hbar}}\right) H_n\left(\frac{q'}{\sqrt{\hbar}}\right) = \frac{1}{\sqrt{1 - e^{2i\theta}}} \exp\left[\frac{2q''q'e^{i\theta} - (q''^2 + q'^2)e^{2i\theta}}{\hbar(1 - e^{2i\theta})}\right]. \quad (4.58)$$

Substitution of this into (4.57) gives after some manipulation

$$\begin{aligned} \mathcal{F}_\theta \psi(q') &= \frac{e^{i(\frac{\pi}{4} - \frac{\theta}{2})}}{2\pi\hbar \sin \theta} \exp\left(-\frac{i}{2\hbar} q'^2 \cot \theta\right) \times \\ &\int_{-\infty}^{\infty} \exp\left(+\frac{iq''q'}{\hbar \sin \theta}\right) \exp\left(-\frac{i}{2\hbar} q''^2 \cot \theta\right) \psi(q'') dq''. \end{aligned} \quad (4.59)$$

The inverse of this transform is given as

$$\begin{aligned} \mathcal{F}_{-\theta} \psi(q') &= \frac{e^{-i(\frac{\pi}{4} - \frac{\theta}{2})}}{2\pi\hbar \sin \theta} \exp\left(+\frac{i}{2\hbar} q'^2 \cot \theta\right) \times \\ &\int_{-\infty}^{\infty} \exp\left(-\frac{iq''q'}{\hbar \sin \theta}\right) \exp\left(+\frac{i}{2\hbar} q''^2 \cot \theta\right) \psi(q'') dq''. \end{aligned} \quad (4.60)$$

It is the numerical calculation of these integrals that forms the basis of the Fast Fractional Fourier Transform algorithm. The basic idea is that through some clever sampling and interpolation techniques the integral can be estimated with a digital convolution [1,3]. The convolution theorem says that the convolution of two functions f and g can be performed with a number of Fourier transforms. That is

$$f * g = F_{\frac{\pi}{2}} \left[F_{-\frac{\pi}{2}}[f] F_{-\frac{\pi}{2}}[g] \right] \quad (4.61)$$

The discrete integral can therefore be performed using what are known in the signal processing field as chirp convolutions and multiplications. We can perform the convolutions using the FFT algorithm outlined in section 4.4. The whole algorithm can be therefore performed in $O(N \log N)$ time.

All this means that using these algorithms we can now evolve the discrete quantum system using (4.44) in $O(N \log N)$ time. This is significant improvement on the $O(N^2 \log N)$ time needed for the split step method, see section B.1. More importantly however is the fact that this method, like the Split step method, allows us to evolve the system without having to store any matrices in the computer memory. This will allow us to use vectors of incredible size to approximate

the continuous quantum state. It should be noted that this method, unlike the FFT which performs the DFT exactly, is only an estimation. However it can be regarded as being almost exact once the vector we are operating on has no significant values outside certain range. This is not a restrictive requirement because we are no longer required to store matrices and therefore can nearly always increase the boundary by increasing the effective grid size N .

There are two matlab algorithms available on the web for performing the fast fractional Fourier transform [16,17]. The first manipulates vectors with an even number of components. The second comes as part of a digital signal processing package and manipulates vectors with an odd number of components. A selection of web based resources can also be found at [18] and for an alternative but comprehensive review of the fractional Fourier transform see [19].

4.6 Conclusion

The main goal of this chapter was to explain the new Fractional Fourier Transform method, first demonstrated by ourselves [21], for evolving the delta kicked harmonic oscillator. The method is significantly faster and more effective than other techniques.

We have successfully explained the relationship between the truncated and discretised simulation and the continuous problem. Importantly we have showed explicitly how \hbar may be controlled through the spatial range L and the effective grid size or sampling frequency N of the simulation. A specific example demonstrates the accuracy and consistency of this method.

We then go on to show how the DFFT is related to a type of discrete Hamiltonian. This section shows the exact relationship between the number basis and our new method via *Harpers equations*.

The remaining sections are about trying to explain the reasons the method is so efficient. The main reason of course is the existence of FFT algorithms. Indeed, had we only wanted to examine the system with frequency ratio $1/R = 1/4$ there would not have been any need to go further. However, in order to generalise the problem to all frequency ratios and to show that most of the efficiency remained intact we also included an introduction to the FFFT algorithm we use later on.

In a chapter like this it is difficult to know how much information to include on what are now standard Digital Signal Processing techniques (DSP). However, there are many deep underlying connections between DSP and quantum me-

chanics that are often not highlighted. I would say this is to the detriment of both subjects and so have tried to write out some of these DSP results in the language of quantum mechanics. Of course there are always loose ends and therefore as many questions as answers. However, I feel that sufficient background material has been supplied to have a great deal of confidence in the numerical results this technique produces.

References

- [1] H. M. Ozaktas, Z. Zalevsky and M. A. Kutay, *The Fractional Fourier Transform with Applications in Optics and Signal Processing*. (Wiley & Sons, New York, 2000).
- [2] A. L. Garcia, *Numerical Methods for Physics*, 2nd edition, (Prentice Hall, New Jersey 2000). .
- [3] H. M. Ozaktas, O. Arikan, M. A. Kutay and G. Bozdagi, *IEEE Transactions on Signal Processing*, **44**, 2141 (1996).
- [4] N. M. Atakishiyev and S. K. Suslov, *Difference analogues of the harmonic oscillator*, *Teor. Mat. Fiz* **85**, 64 (1990).
- [5] Ç. Candon, *The Discrete Fractional Fourier Transform*, MS thesis, Bilkent University, Ankara (1998).
- [6] Ç. Candon, M. A. Kutay and H. M. Ozaktas, *The Discrete Fractional Fourier Transform*. *IEEE Int Conf Acoustics, Speech, Signal Processing*, IEEE 1713 (Piscataway, New Jersey, 1999).
- [7] Ç. Candon, M. A. Kutay and H. M. Ozaktas, *The Discrete Fractional Fourier Transform*, *IEEE Transactions on Signal Processing*, **46**, 3206 (2000).
- [8] L. Barker, C. Candan, T. Hakioglu, M. A. Kutay and H. M. Ozaktas, *The Discrete Harmonic oscillator, Harpers equation and the fractional Fourier transform*, *J. Phys. A: Math. Gen.* **33**, 2209 (2000).
- [9] D. H. Bailey and P. N. Swarztrauber, *The fractional Fourier transform and application*, *SIAM Review* **33** 389 (1991).
- [10] D. H. Bailey and P. N. Swarztrauber. *A fast method for the numerical evaluation of continuous Fourier and Laplace transforms*. *SIAM J. Sci. Comput.* **15**, 1105 (1994).
- [11] J. W., Cooley, J.W. Tukey, *An Algorithm for Machine computation of Complex Fourier Series*, *Mathematics of Computation* **19**, 297 (1965).
- [12] <http://mathworld.wolfram.com/FourierMatrix.html>.
- [13] B. B. Hubbard *The world according to wavelets* 2nd Edition, (A K Peters, Natick, Massachusetts 1998).
- [14] P. M. Morse and H. Feschbach, *Methods of Theoretical Physics* (McGraw-Hill, London, 1953).
- [15] V. Namias, *The Fractional Order Fourier Transform and its Application to Quantum Mechanics*, *J. Inst. Maths Applies* **25**, 241 (1980).
- [16] <http://www.ee.bilkent.edu.tr/~aldun/wileybook.html>.
- [17] <http://www.mathtools.net/files/net/dtfd.zip> .

- [18] Dr YangQuan Chen's FRFT Webpages ,<http://mechatronics.ece.usu.edu/foc/FRFT/>.
- [19] A. Bultheel, H. Martínez, *A shattered survey of the Fractional Fourier Transform*. Report TW337, Department of Computer Science, Katholieke Universiteit Leuven, April 2002;
<http://www.cs.kuleuven.ac.be/publicaties/rapporten/tw/TW337.abs.html>.
- [20] M. Engel, *On Quantum chaos, Stochastic Webs and Localization in a Quantum Mechanical Kick system*, Ph. D Thesis(2003).
- [21] G. Kells, J. Twamley and D. Heffernan, *Dynamical Properties of the delta kicked harmonic oscillator*, Phys. Rev. E **70**, 015203 (2004).

Chapter 5

Compilation of Numerical Results

5.1 Introduction

This chapter is a compilation of numerical results calculated using the procedure detailed in chapter 4. It is primarily a study of quantum chaos and as such tries to relate each simulation and calculation to the processes going on in the classical system under the same perturbation. Ultimately it is the study of the differences between the quantum and the classical systems.

The most powerful tool we have is the ability to numerically evolve a quantum wave-packet with unprecedented accuracy and efficiency. We use this to compare the dynamical evolution of a coherent state with that of the evolution of a normally distributed ensemble of classical particles. Where possible we will try to associate this evolution to a phase space representation, although this is not always feasible. A much easier way to compare classical and quantum dynamics is to plot the energy of the evolving state and the average energy of the classical ensemble against time.

A by-product of the new numerical method we have introduced is the ability to approximate the Floquet operator for the system as a large matrix. Using standard numerical diagonalisation techniques we can approximate, in the position representation, the stationary states of the KHO for any frequency ratio. We shall try where possible to compare the phase space representations of these eigenvectors to the Poincaré surface of section generated under the same perturbation. The diagonalisation procedure also returns the eigenvalues or quasi-energies of the Floquet matrix. We can then apply some of the results of *random matrix* theory to this data.

While the comparison between classical and quantum is paramount it is also

necessary to acknowledge analytical results pertaining to the specific system parameters under question. The results are therefore continually presented within the context of what was written in chapter 3.

The final factor we have taken into account in the presentation of these results is of course other numerical studies. There is already a considerable amount of numerical work available on the kicked harmonic oscillator. Numerical data on the quantum system with irrational frequency ratios is quite rare although specific examples can be found in [1,2]. A numerical study of the irrationally kicked system can also be found in [3].

The majority of previous numerical studies concentrate on rational frequency ratios $R = 3, 4, 6$ that give the crystalline structure in the classical phase plane. The case of $R = 4$ has had by far the most numerical studies performed on it. In particular see [1–5]. In the case of $R = 4$, the system is closely related to the symmetric Kicked Harper Model (KHM) [6]. This means that a wealth of numerical and analytical studies on the KHM can also be applied to the KHO. In particular the Lanczos method for finding the systems quasi-energies can be applied in the case with $R = 4$ [7]. It is for this reason that we do not include statistical analysis on the quasi-energies in this case. We briefly discussed the connection between the KHM and the KHO in section 3.5.1 .

Numerical work on the system with $R = 3, 6$ can also be found in [1,8] and data on the quasi-crystalline cases where R is any other integer can be found in [1–3,5,9]. As we have already explained we will not provide any numerical analysis for these frequency ratios although the numerical procedures work equally well in all these other cases.

The structure of this chapter is therefore as follows. We concentrate initially on the systems behaviour when the frequency ratio is the particular irrational value $1/R = (\sqrt{5} + 1)/2$. We first provide some comparative snapshots of the evolution of the system in the Husimi representation and the classical ensemble. The numerical model is then used to confirm the predictions of the tight-binding approximation, see section 3.4.1. Its invalidity for large μ and small \hbar is demonstrated.

We then analyse the mean energy of the quantum system and attempt to quantify this quantum suppression of the energy growth. We finally calculate the Floquet operator's eigenvectors and eigenvalues using standard LAPACK routines. The analysis we perform on stationary states and quasi-energies is designed to show that at least some of the stationary states will become quite broad

if μ is large and \hbar is small.

With frequency ratio $1/R = 1/4$ we start by analysing the stationary states of the system. We look for the discretisation associated with quantum resonance predicted in sections 3.4.2, 3.5.2. We also concentrate specifically on the types of stationary states that may be responsible for anomalous diffusion and classical resonance. As we explained we do not analyse the systems quasi-energies.

The last section is a comprehensive analysis of the quantum systems diffusional behaviour for different values of \hbar . Using our new numerical method we perform thousands of individual simulations in an attempt to see more clearly the effect quantum resonance has on the system. We shall also search for evidence that the quantum system with certain \hbar can exploit both the quantum and classical resonance effects simultaneously to achieve super ballistic energy growth .

5.2 Irrational frequency ratio $1/R = (\sqrt{5} + 1)/2$

In section 2.3.1 we numerically calculated the rate of energy growth or diffusion in the classical system as a function of μ for the irrational frequency ratio $1/R = (\sqrt{5} + 1)/2$. These numerical results showed a linear energy growth for all values of μ . This agreed very well with the analytically predicted result $D = \mu^2/4$ for μ larger than about 2, see Figure 2.6.

The quantum results are quite different. Studies into the rate of diffusion for the quantum system have shown that there is a distinct *suppression* of the rate of the diffusion which alludes to some sort of localisation mechanism present in the quantum dynamics [1–3,10]. This is similar to the case of the kicked rotor (KR) which displays complete localisation under certain conditions. It is generally accepted that the argument put forward by [11], linking the system with a tight-binding model that displays Anderson localisation [12–15] is correct. In section 3.4.1 we briefly described similar arguments first presented by [10] and expanded upon by [3] to map the kicked harmonic oscillator to a tight-binding model. We argued that the integral (3.42) was non-trivial once $\mu/\hbar > \pi$, involving integrations over delta like spikes and that this placed a limit on the range for which the tight binding approximation is accurate.

In this section we will catalog our numerical results for the irrationally kicked quantum system. We first present some Husimi distributions to compare the phase space distributions of a quantum state with that of an ensemble of classi-

cal particles at various stages of their evolution. We then show how the energy-time graph of different states for various initial states and various values \hbar and μ compares with the corresponding graph for a normally distributed classical ensemble. We examine the diffusion curve $D(\mu)$ for different values of \hbar and for different initial conditions against the corresponding classical graphs. Note that the classical graph should *resemble* that given in Figure 2.6. However in order to fairly compare classical and quantum evolutions we must use a normally distributed classical ensemble as opposed to the evenly distributed ensemble used in Figure 2.6.

Finally we will analyse some of the stationary states and quasi-energy statistics of the systems Floquet operator for various values of μ and \hbar . To the best of our knowledge no such attempt has been made before so the results are new and cannot be compared against previous studies.

5.2.1 Evolving Husimi Distributions

We begin by comparing the evolving classical ensemble with the evolving Husimi distribution. In Figures 5.1 and 5.2 we start with ensemble and coherent state centered at $(q, p) = (5, 0)$ and look at the classical and quantum distributions at different times. The distributions are quite similar for long evolution times. Quantum interference effects can be seen in (c) and (d) of both figures. In Figure 5.6 we plot the energy diffusion curves for these parameters. The classical and quantum curves are remarkably similar for long times. This reflects the lack of chaos in the classical system.

As we increase the value of μ the Poincaré surface of section for the classical system will get more complicated. See section 2.3.1 and in particular Figure 2.2. This finer detail means that the quantum distribution will typically not match the classical distribution. In Figure 5.3, with $\hbar = 1$ and $\mu = 0.5$ this becomes more apparent. However as we have already demonstrated the classical ensemble cannot diffuse because of the effective KAM curves that restrict the motion, see section 2.3.1. In Figure 5.7 we again plot energy versus time and see that there is still a large degree of correspondence between classical and quantum motion.

In order to see the classical ensembles energy grow we need to increase the value of the kick strength to $\mu \geq 2$. At this value, as can be seen from Figures 2.2 and 2.5, the classical motion is mostly chaotic. In Figure 5.4 we compare the classical and quantum distributions with $\mu = 2$ and $\hbar = 1$. We can see that the classical system has begun to diffuse. Visually it would seem that the quantum

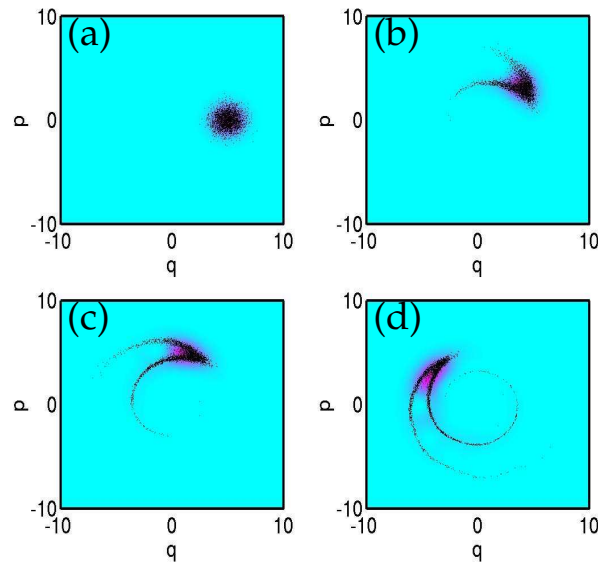


Figure 5.1. Phase space diagrams of (a) a normally distributed classical ensemble superimposed on the Husimi distribution of a coherent state centered at $(q, p) = (5, 0)$ in the phase plane. Subsequent diagrams show the classical ensemble and quantum state at Phase space diagrams of a classical ensemble superimposed on the Husimi distribution of a quantum state at times (b) $n = 100$, (c) 200 and (d) 400 In these calculations we used $\hbar, k = 1$ and $\mu = 0.1$

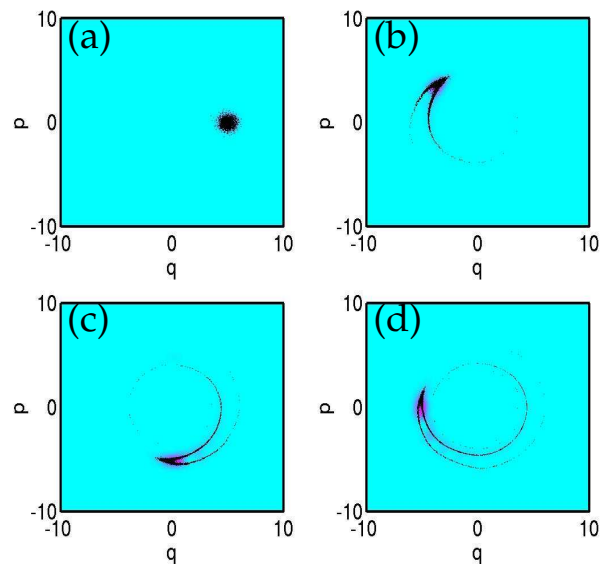


Figure 5.2. Phase space diagrams of a classical ensemble superimposed on the Husimi distribution of a quantum state. Diagrams show states at times (a) $n = 0$, (b) 400 , (c) 800 and (d) 1600 . In these calculations we used $\hbar = 0.25$, $k = 1$ and $\mu = 0.1$

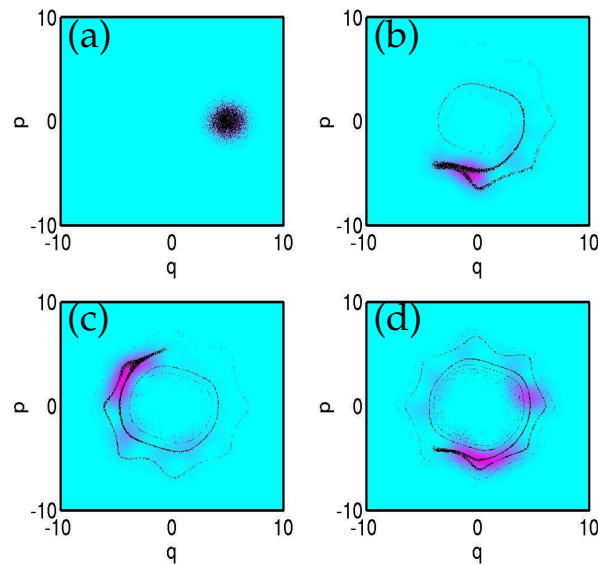


Figure 5.3. Phase space diagrams of a classical ensemble superimposed on the Husimi distribution of a quantum state. Diagrams show states at times (a) $n = 0$, (b) 100, (c) 200 and (d) 400. In these calculations we used $\hbar = 1$, $k = 1$ and $\mu = 0.5$.

system does not diffuse to the same extent as the classical system. In Figure 5.8 we have plotted out the energy time curve for these values of \hbar and μ for two different initial conditions. The curve confirms that the quantum system does not diffuse at the same rate as the classical ensemble. Indeed it could hardly be said to diffuse at all. We speak more on this in the next subsection.

Finally, for completeness we compare the classical and quantum distributions at various times with $\mu = 4$ and $\hbar = 1$, Figure 5.5. We can see that with these parameters the quantum state appears to diffuse. This diffusion or spreading of the wave-packet means that the quantum system quickly moves beyond the maximum range for which we can reliably compute the Husimi and Wigner distributions. However, even if we can only show the evolution of the Husimi distribution for a short time, the diffusive nature of the quantum dynamics is quite evident.

5.2.2 Mean energy and diffusion

In the last section we compared the Husimi distribution with the distribution of a classical ensemble after certain amount of time. Our method of calculating the Husimi and Wigner distributions only allowed us to view certain ranges of the quantum state accurately, see section C.1. However, we can easily obtain the

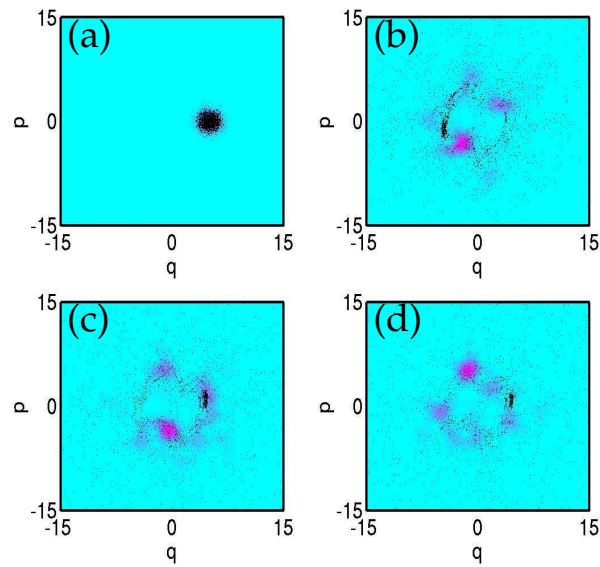


Figure 5.4. Phase space diagrams of a classical ensemble superimposed on the Husimi distribution of a quantum state. Diagrams show states at times (a) $n = 0$, (b) 100, (c) 200 and (d) 400. In these calculations we used $\hbar = 1$, $k = 1$ and $\mu = 2$.

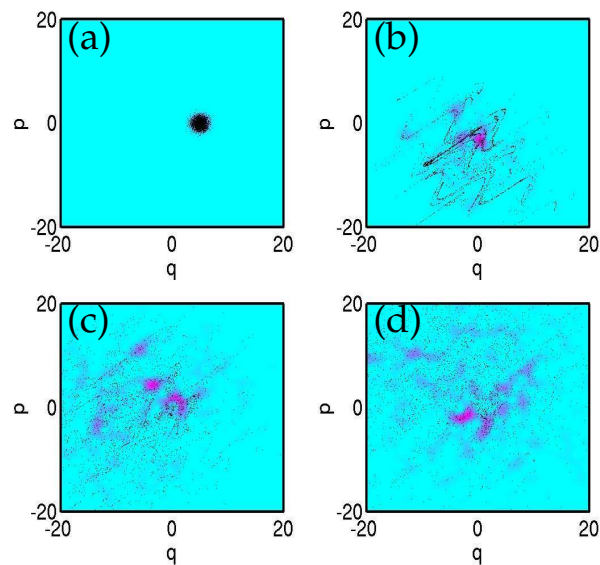


Figure 5.5. Phase space diagrams of a classical ensemble superimposed on the Husimi distribution of a quantum state. Diagrams show states at times (a) $n = 0$, (b) 10, (c) 20 and (d) 30. In these calculations we used $\hbar = 1$, $k = 1$ and $\mu = 4$.

energy expectation value of the quantum state and compare it to the mean energy of the classical ensemble. These expectation values provide a simple but effective measure of the spread of the wavefunction.

In section 3.3 we discussed how the Floquet operator for the kicked system could be said to be made out of a fractional Fourier transform and a simple diagonal operator. While in sections 4.3 and 4.5 we showed how the fractional Fourier transform could be applied to a discrete system. Using these methods we said we could calculate the actual Floquet matrix of our system up to a size of about 3000×3000 . We also said that we could effectively simulate, using the fast fractional Fourier transform, the evolution of the quantum system using an effective matrix size of about $10^6 \times 10^6$. We will give the results of many of these calculations and simulations in this section.

However we first would like to discuss what it means to evolve classical and quantum systems from similar initial conditions. We compare the evolution of coherent states and a normally distributed classical ensemble by examining the mean energy growth (diffusion) of both systems*. Quantum mechanically we measure the expectation value of the energy, which in Dirac notation is

$$E = \langle \psi | p^2/2 + q^2/2 | \psi \rangle. \quad (5.1)$$

Inserting the completeness relations for momentum and position we get

$$\begin{aligned} E &= \frac{1}{2} \left(\int_{-\infty}^{\infty} dp' \langle \psi | p^2 | p' \rangle \langle p' | \psi \rangle + \int_{-\infty}^{\infty} dq' \langle \psi | q^2 | q' \rangle \langle q' | \psi \rangle \right) \\ &= \frac{1}{2} \left(\int_{-\infty}^{\infty} dp' \Psi^*(p') p'^2 \Psi(p) + \int_{-\infty}^{\infty} dq' \Psi^*(q) q'^2 \Psi(q) \right). \end{aligned} \quad (5.2)$$

These integrations can be easily carried out to a large degree of accuracy using Simpson's rule. In this way we may compare at a glance the diffusion of the classical and quantum systems.

Now, starting with an initial classical ensemble and quantum coherent state at $(q, p) = (5, 0)$ we plot the energy of both systems as we evolve with $\hbar = 0.25$ and $\hbar = 1$ †. See Figure 5.6. The classical and quantum energies are very similar and

*The RMS spread in the classical ensemble is chosen to match the RMS spread of the initial quantum coherent state.

†Note that the value of \hbar seems to change the behaviour of the classical system. This is only as a result of the fact that we choose the width of the normally distributed ensemble to match the width of the coherent state.

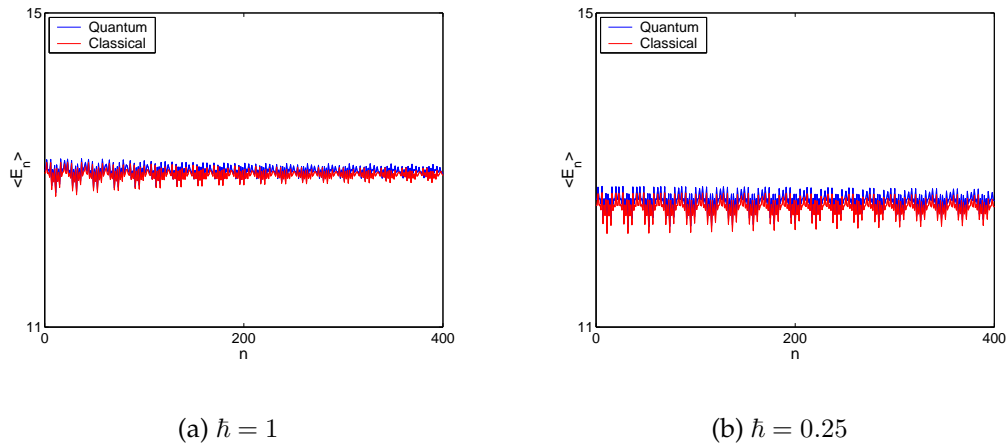


Figure 5.6. Initial value $(q, p) = (5, 0)$ evolved over 400 discrete steps with $\mu = 0.1$ and $k = 1$. Compare this figure with Figures 5.1 and 5.2. We used a Hilbert space of 2^{14} dimensions to do the quantum simulation.

there is no sustained energy growth in either the classical or quantum systems. Of course at this value of μ the classical system is still bounded by a multitude of effective KAM curves, see Figure 2.2.

Increasing the value of the kick strength to $\mu = 0.5$ the energies of quantum and classical systems grow less similar with longer times, see Figure 5.7. As we have already mentioned in the previous section this is because the classical trajectories get more complicated. The classical ensemble is still bounded in the phase plane by the effective KAM tori and, as before, there is no sustained energy growth in either system. We had concluded as much from our analysis of the Husimi distributions in the previous section, see Figure 5.3.

Increasing the kicking strength to $\mu = 2$ we finally see the difference between classical and quantum diffusion rates. The classical particles can now diffuse radially in the phase plane because there are no more bounding tori left to stop this energy growth. However, this is not the case for the quantum state which diffuses like the classical ensemble but then seems to reach a barrier of some kind. See the Figures 5.8(a) and 5.8(b). We can check if this suppression of the energy growth rate is due to some sort of quantum barrier, outside of which, the energy continues to grow. To do this we can perform a similar simulation but this time starting with an initial state centered much further from the origin. Figures 5.8(c) and 5.8(d) show this simulation with initial state placed at $(q, p) = (15, 15)$ in the phase plane. We clearly see that the energy growth in the quantum system is still

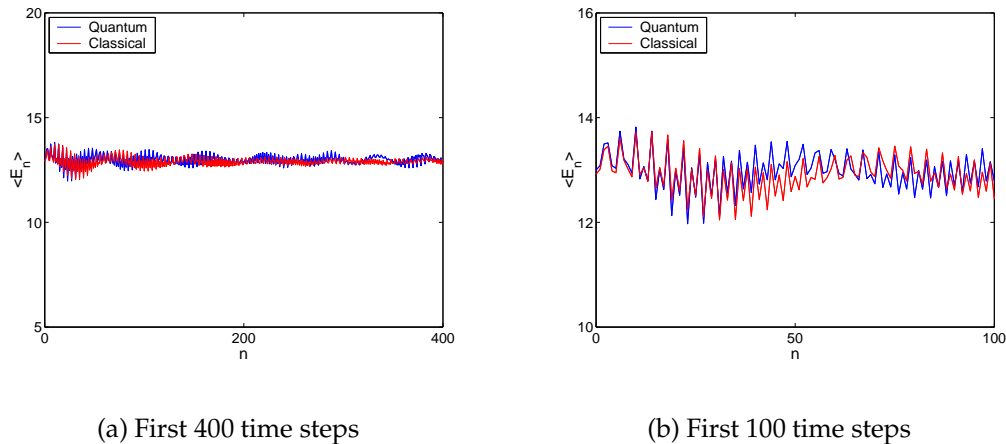


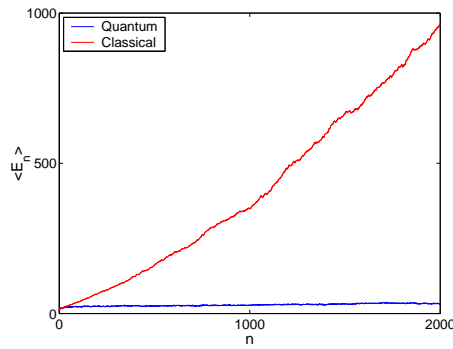
Figure 5.7. Initial value $(q, p) = (5, 0)$, with $\mu = 0.5$, $\hbar = 1$ and $k = 1$. We use a discretised Hilbert space of 2^{14} dimensions to do the quantum simulation.

significantly suppressed. This points to a process that occurs throughout phase space regardless of the initial phase coordinates of the coherent state.

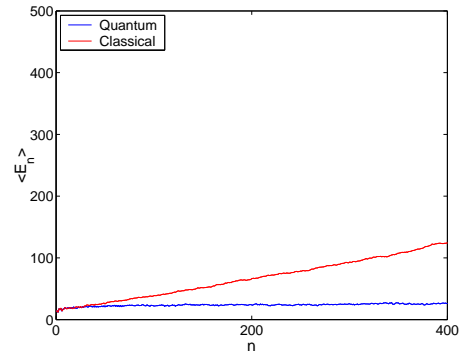
We give the quantum and classical energy-time plots with $(q, p) = (5, 0)$ and $\mu = [2.5, \pi, 4, 6]$ in Figure 5.9. In all cases there is sustained energy growth in the quantum system, however, this growth is always less than that of the classical system.

We now have considerable numerical evidence to support the idea that the quantum model experiences some sort of quantum suppression of its energy growth. In the next section we will attempt to quantify these effects. We are however, in a position to say with confidence that there exists a range of values for μ , for which the classical system can diffuse and the quantum system cannot. Above this range the quantum system experiences sustained energy growth but at a lesser rate than that of the classical system.

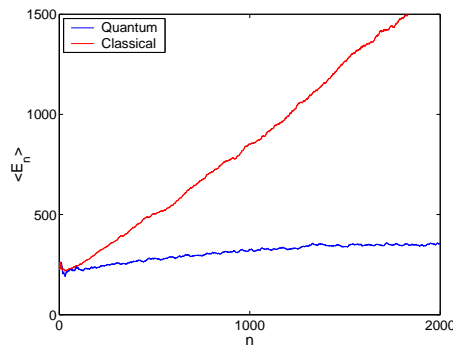
This agrees with what was said in section 3.4.1. There it was explained how the kicked oscillator with irrational frequency ratio could be mapped on to a kind of tight binding model. However we qualified this result by saying that the tight-binding assumption must break down once $\mu/\hbar > \pi$. Indeed the numerical evidence above shows delocalisation of the quantum system when the parameter is $\mu/\hbar = 2.5$. We stress that this delocalisation does not mean the tight-binding approximation is always invalid as there is clearly some sort of process working in the quantum system that suppresses the energy growth of the quantum state. It is still the best explanation we have.



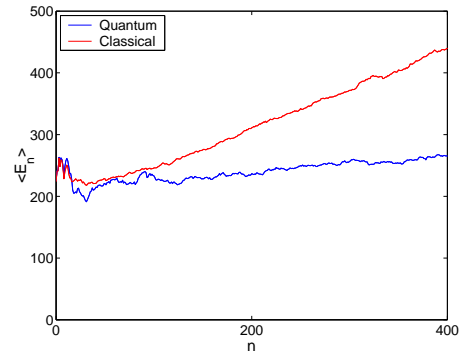
(a) Initial states are centered at $(5, 0)$, first 2000 iterations



(b) Initial states are centered at $(5, 0)$, first 400 iterations



(c) Initial states are centered at $(15, 15)$, first 2000 iterations



(d) Initial states are centered at $(15, 15)$, first 400 iterations

Figure 5.8. Initial value $(q, p) = (5, 0)$, with $\mu = 2.0$, $\hbar = 1$ and $k = 1$. We use a discretised Hilbert space of 2^{15} dimensions to do the quantum simulation.

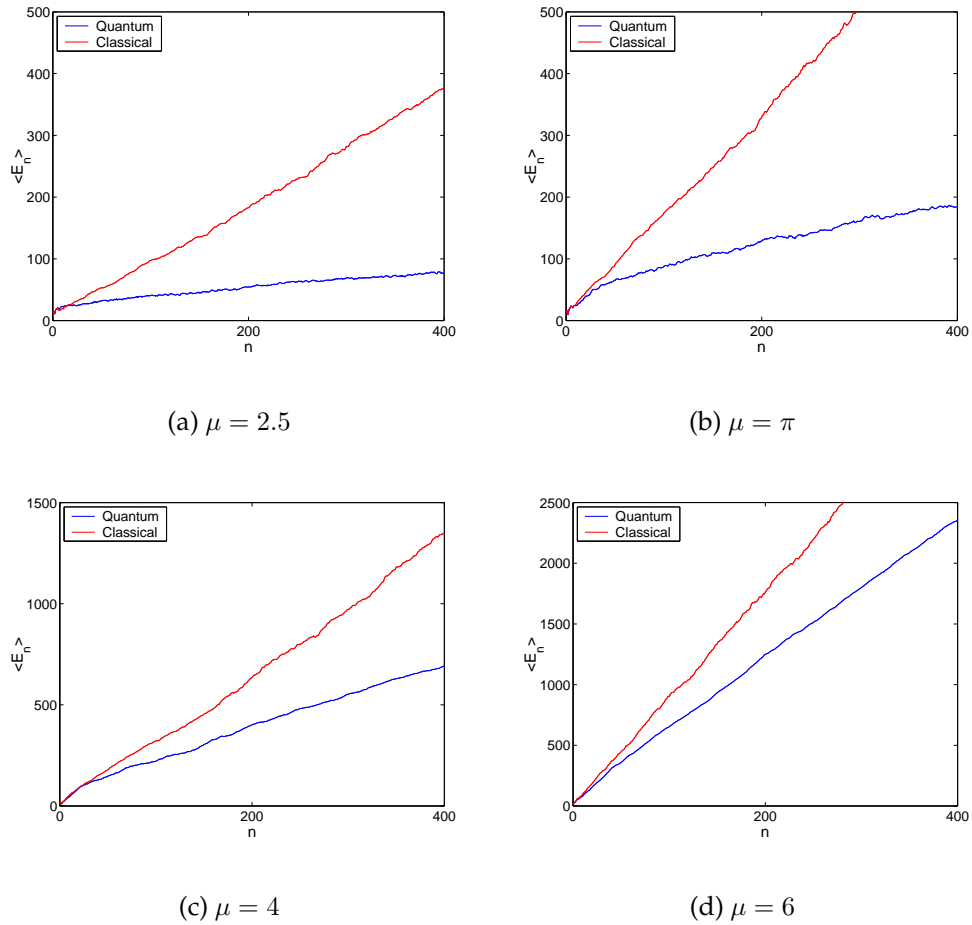


Figure 5.9. Initial value $(q, p) = (5, 0)$, with $\mu = 2.0, \pi, 4.0, 6.0$, $\hbar = 1$ and $k = 1$. We use a discretised Hilbert space of 2^{14} dimensions to all simulations except part (d) where we used 2^{15} dimensions.

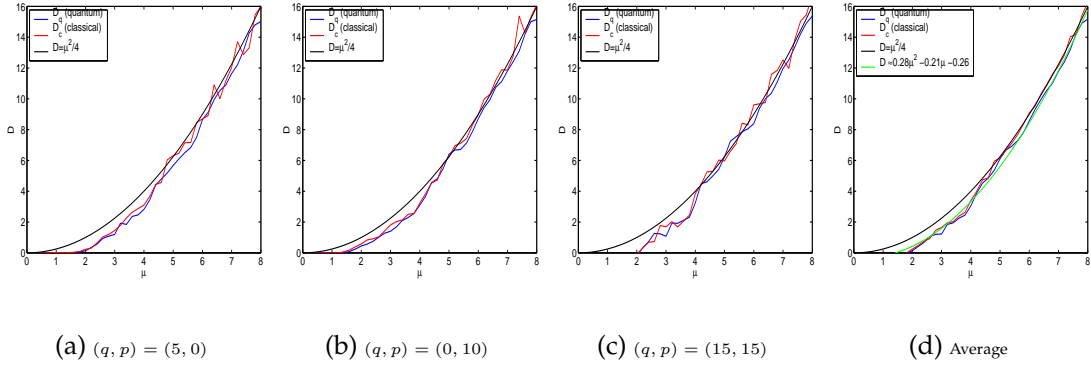


Figure 5.10. D - v - μ with $\hbar = 1/4$. We use a discretised Hilbert space of 2^{16} dimensions in all calculations

5.2.3 Quantifying the quantum suppression

In this section we will attempt to quantify the rate at which the the quantum energy growth is suppressed in relation to the classical system. We do this by calculating the quantum diffusion rate $D_q(\mu)$ analogous to the classical calculation plotted in Figure 2.6. This is a considerable task not least because in order to compare like with like we must use coherent states and normally distributed ensembles as our initial quantum and classical states.

To this end we shall perform the calculation with three separate initial conditions, that is $(q, p) = (5, 0), (0, 10), (15, 15)$. For each of the three initial conditions we then evolve the systems over 100 time steps for 40 different values of μ . That is from $\mu = 0.2$ to $\mu = 8.0$. To each of these curves we fit a slope giving us the discrete function $D_q(\mu) = \langle \psi_n | E | \psi_n \rangle / n$ for the quantum system and $D_c(\mu) = \langle E_n \rangle / n$ for the classical systems. See section 2.3.1.

The results are given in Figures 5.10- 5.15. Each figure contains the results for the three simulations and the average. The classical numerical curves generally fit the theoretical predicted curves $D = \mu^2/4$ calculated in section 2.3.1. As expected the numerically calculated quantum curve, $D_q(\mu)$, is nearly always less than the classical curve $D_c(\mu)$.

Using the polyfit function in matlab we can fit a second order polynomial of the form

$$D(\mu) = a_2\mu^2 + a_1\mu + a_0 \quad (5.3)$$

to the averaged D_q data. Interestingly the coefficient in front of the quadratic

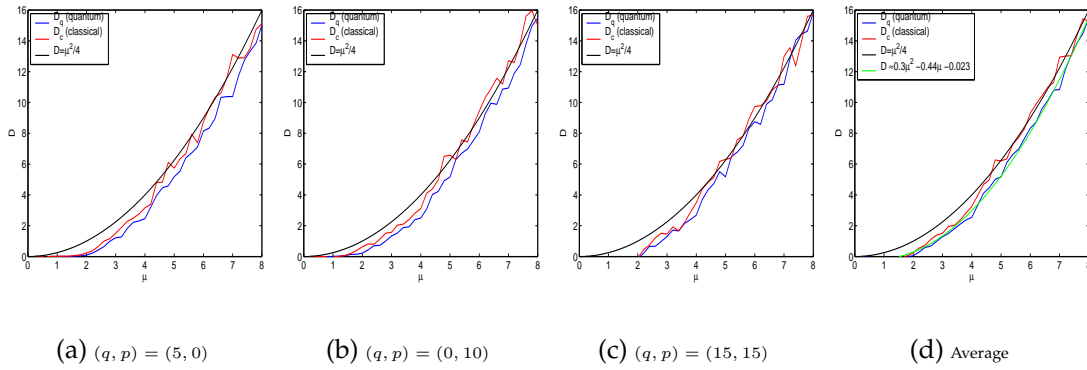


Figure 5.11. D -v- μ with $\hbar = 1/2$. We use a discretised Hilbert space of 2^{16} dimensions in all calculations

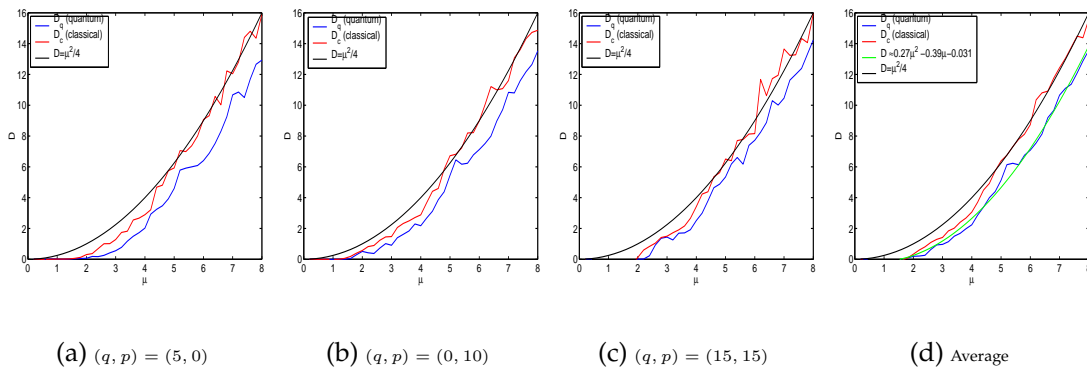


Figure 5.12. D -v- μ with $\hbar = 1$. We use a discretised Hilbert space of 2^{15} dimensions in all calculations

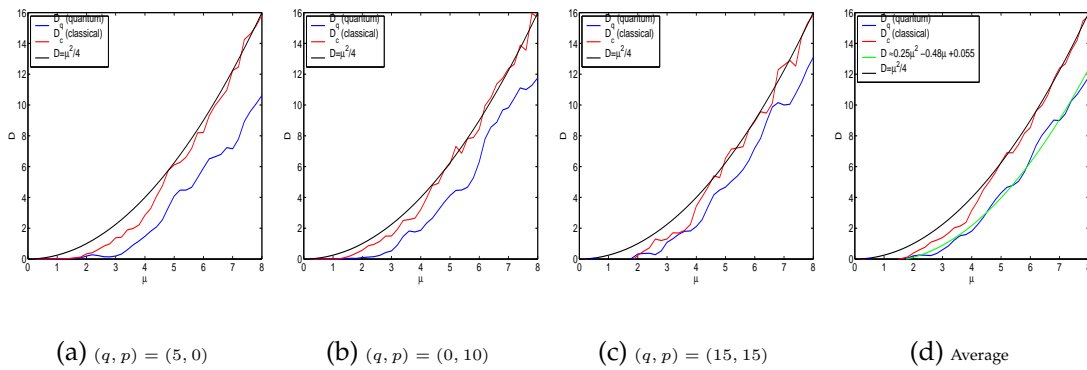


Figure 5.13. D -v- μ with $\hbar = 2$. We use a discretised Hilbert space of 2^{14} dimensions in all calculations

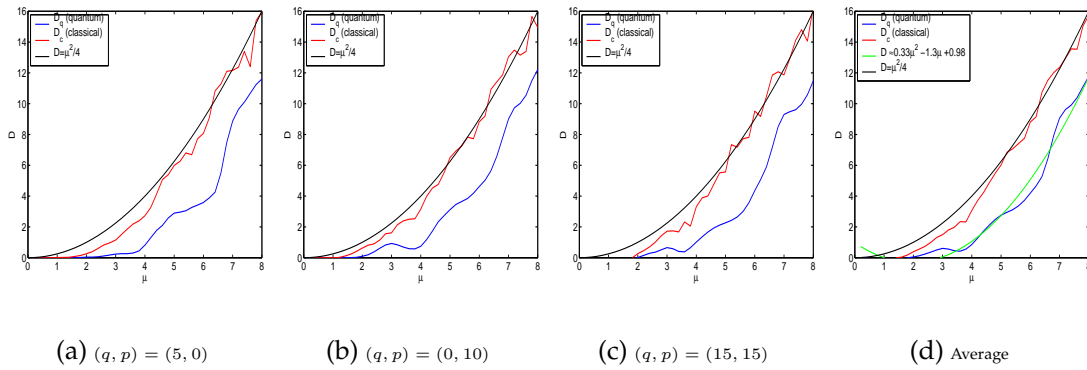


Figure 5.14. D - v - μ with $\hbar = 3$. We use a discretised Hilbert space of 2^{14} dimensions in all calculations

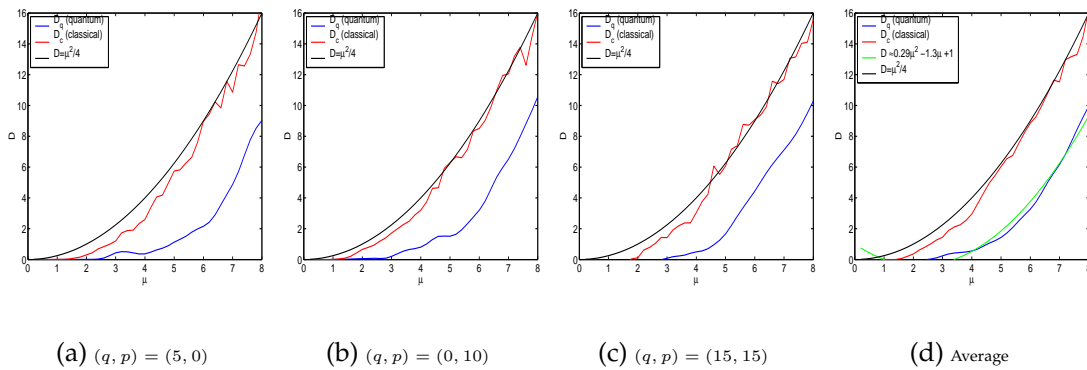


Figure 5.15. D - v - μ with $\hbar = 4$. We use a discretised Hilbert space of 2^{14} dimensions in all calculations

\hbar	$\langle \Delta D \rangle$	a_2	μ_0
0.25	0.1634	0.2771	1.4189
0.50	0.4010	0.2979	1.5277
1.00	0.9188	0.2663	1.5488
2.00	1.4921	0.2517	1.7667
3.00	2.2076	0.3304	2.9235
4.00	2.9926	0.2895	3.3901

Table 5.1. Here we give some parameters characterising the quantum diffusion as a function of \hbar .

term for all values of \hbar is close to the classical value of $1/4$, see Table 5.1. To get a quantitative number on the suppression in the diffusion of the quantum state we first average over all classical simulations. This gives us the curve $\langle D_c(\mu) \rangle$. We now average the difference between our quantum and classical curves for each value of \hbar . That is $\langle \Delta D \rangle$ where

$$\Delta D = \langle D_c(\mu) \rangle - D_q(\mu). \quad (5.4)$$

See Table 5.1 for these values. We plot the relationship between $\langle \Delta D \rangle$ and \hbar in Figure 5.16(a). There appears to be a linear relationship with between the values of \hbar and ΔD . We fit the straight line $f(\hbar) = 0.732\hbar + 0.057$ to our data. We see that the average difference between the classical and quantum energy time curves seem to have a linear dependence on \hbar . Of course this is only an average measure of a complicated process. Nonetheless it demonstrates that there is some dynamical process in the quantum model that suppresses diffusion and is perhaps linearly dependent on \hbar .

Another way of looking at this suppression is to ask at what parameter μ the quantum and classical system will begin to diffuse. To answer we again examine the second order polynomials fitted to the curves $D_q(\mu)$. We determine the roots of the equations and label the RHS root μ_0 . The results are tabulated in Table 5.1 and plotted in Figure 5.16(b), along with the classical value of μ_0 calculated in the same way from the curve $\langle D_c(\mu) \rangle$. The suppression as a function of \hbar is again obvious but the exact relationship between \hbar and the value of μ_0 is not.

We have achieved our aim of, to some degree, quantifying the rate of diffusion in the quantum system. Our analysis seems to suggest that the level of suppression may decrease linearly as $\hbar \rightarrow 0$. To say that this really is the case is another

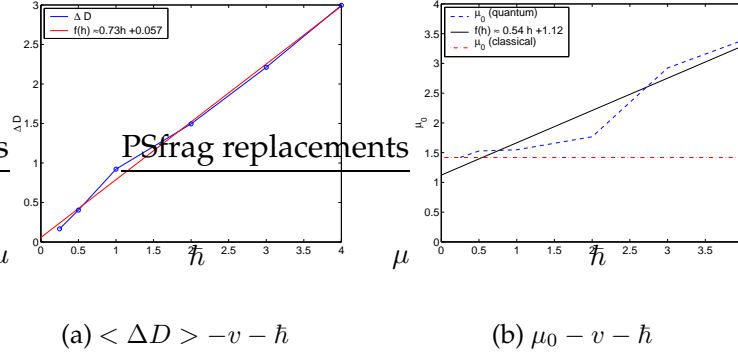


Figure 5.16. Suppression of Diffusion as a function of \hbar .

matter. Confidence in the validity of these results should be directly related to extent and accuracy of the simulation. It will always be possible to improve on these results.

We have examined between $\hbar = 0.25$ to $\hbar = 4$, using only 6 different values in this range. We have used 3 different initial conditions in each case which is hardly a reasonable sample size in a possible sample space of ∞^2 . We used 40 different values of μ and but only evolved 100 time-steps in each time.

At the same time this survey corresponds to 12,000 iterations for each value of \hbar and therefore 72,000 iterations overall. Considering that some of the calculations used effective grid sizes of $N = 2^{16} = 65636$ we can see the power of using the fractional Fourier transform method.

In the next section we analyse the eigenstates of the total Floquet operator \mathcal{U} , see (3.17) or (3.18) with the same irrational frequency ratio. To do this however we need to study the actual matrix operator. This will restrict the ranges of \hbar which we can study even more. However, as a way of illuminating the process of diffusion it is arguably more effective than the simple idea of evolving the system with different initial conditions.

5.2.4 Stationary States: Irrational frequency ratio $1/R = (\sqrt{5} + 1)/2$

In this section we examine the stationary states of the irrationally kicked harmonic oscillator and the properties of their associated quasi-energies. The main goal is, as in the previous section, to quantify the process of diffusion. More specifically we wish to shed light on the actual quantum process that restricts

the energy growth as we evolve the system. We begin by examining the Husimi distributions of some eigenstates for different values of μ and \hbar , using different matrix sizes where appropriate. We will see the remarkable relationship between these quasi-energy states and the classical phase space structure. We will also plot the energy of each of the stationary states for different values \hbar and μ . This will prove to be useful in explaining part of the diffusive process in the quantum regime. Finally we will analyse the quasi-energies of the system looking for signatures of quantum chaos. In particular we study the quasi-energy level spacing statistics for different parameters μ and \hbar .

In Figure 5.17 we superimpose the Poincaré surface of sections for different values of μ with the Husimi distributions of some of the stationary states computed with the same value of μ and \hbar . (As usual k is set to unity.) The most obvious characteristic of these figures is the structural similarity between the quantum quasi-probability distribution and the classical phase map. However, from our point of view, the most important observation is the very obvious difference between the distributions for $\mu = 0.1, 0.5, 1.5$ and those for $\mu = 6$. For the lower values of μ , the Husimi distributions to a certain extent still resemble those of Fock states. Even though the exact structure is disturbed slightly the ring like pattern around the origin is still evident. However when $\mu = 6$ there is a very different pattern to Husimi distributions. They are broad extended structures with significant values covering a much larger area of the phase plane. This is important for understanding the process of diffusion in the quantum system.

We denote the eigenkets of our Floquet operator \mathcal{U} as $|\psi_s\rangle$. That is

$$\mathcal{U}|\psi_s\rangle = e^{-i\Omega_s}|\psi_s\rangle \quad (5.5)$$

with the quasi-energies denoted by Ω . We can then easily write for the evolution of some state Ψ

$$\mathcal{U}|\Psi\rangle = \sum_{s=0}^{\infty} e^{-i\Omega_s}|\psi_s\rangle\langle\psi_s|\Psi\rangle. \quad (5.6)$$

where $s = 0$ represents the first and lowest energy eigenstate. This is so we can compare easily with number states. If our initial state $|\Psi\rangle$ is localised and of low energy, i.e a coherent state, we would expect that it to be made out of a superposition of some low energy stationary states, assuming they exist. To clarify, if for

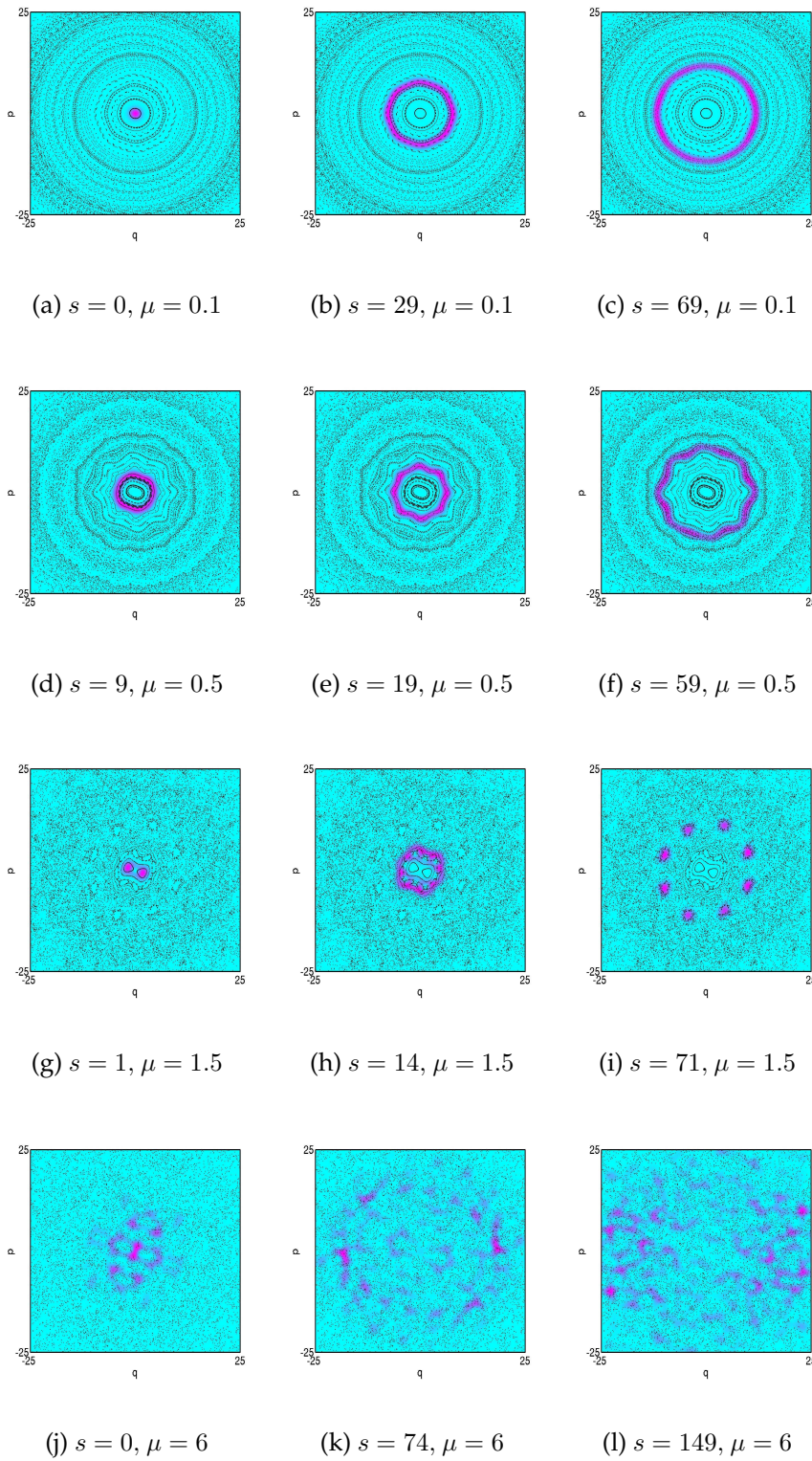


Figure 5.17. Husimi Distributions of some stationary states of the kicked system U with irrational frequency ratio. $\hbar = 1$ and $k = 1$. We used a Hilbert space of 2^9 to generate these figures. The integer s labels the stationary states according to energy.

instance the value of μ is very small we expect the Floquet eigenstates to be almost exactly those of the unperturbed harmonic oscillator, that is $|\Psi_s\rangle \sim |n\rangle$. A coherent state, written in the eigen-representation of the Floquet operator would be very similar to that of A.43. That is

$$|\alpha\rangle \approx e^{-1/2|\alpha|^2} \sum_{s=0}^{\infty} \frac{\alpha^s}{\sqrt{s!}} |\psi_s\rangle. \quad (5.7)$$

Therefore any subsequent evolution will take place only on this low energy subspace of the Floquet operator and we see no diffusion regardless of our quasi-energies.

However, when $\mu = 6$ we see the eigenstates are no longer localised. Consequently the initial coherent state must be a superposition of higher-energy Floquet eigenstates. Upon each operation of the Floquet operator each stationary state picks up a different phase and the initial interference between these extended states, which collectively makes a localised coherent state, disappears. Energy growth becomes very likely.

In section 3.4.1 we showed that the kicked oscillator can be mapped to a tight-binding model in the number representation. The tight binding mapping however only works for $\mu/\hbar < \pi$ and we have amassed considerable numerical evidence in the last section that suggest the quantum system diffuses if μ/\hbar gets large.

To get another perspective on the behaviour of the stationary states of the Floquet matrix U as we adjust μ and \hbar we examine the energies of the stationary states of the Floquet matrix \mathcal{U} . We have already established that with small values of μ the stationary states of the quantum system should resemble number states. We also noted that the stationary states seemed to be extended at $\mu = 6$ and showed that this was consistent with what we had already established. However, let us assume we have, in the truncated q and p basis, a completely extended state $|\psi_c\rangle$. A completely extended state would on average be a constant c in both position and momentum representations. Normalising in our truncated numerical basis between $-L/2$ and $L/2$ we get

$$\int_{-L/2}^{L/2} c^2 dq = \int_{-L/2}^{L/2} c^2 dp = c^2 L = 1 \quad (5.8)$$

and therefore $c = 1/\sqrt{L}$. The energy of this hypothetical state is given by

$$\langle \psi_c | E | \psi_c \rangle = \frac{\omega_0}{2} \langle \psi_c | p^2 + q^2 | \psi_c \rangle. \quad (5.9)$$

Inserting the completeness relations for momentum and position we get

$$\begin{aligned} E_e &= \frac{\omega_0}{2} \left(\int_{-\infty}^{\infty} dp' \langle \psi | p^2 | p' \rangle \langle p' | \psi \rangle + \int_{-\infty}^{\infty} dq' \langle \psi | q^2 | q' \rangle \langle q' | \psi \rangle \right) \\ &\approx \frac{\omega_0}{2} \frac{1}{L} \left(\int_{-L/2}^{L/2} dp' p'^2 + \frac{1}{L} \int_{-L/2}^{L/2} dq' q'^2 \right) \end{aligned} \quad (5.10)$$

$$\approx \frac{\omega_0}{2} \frac{1}{L} \left[\frac{p'^3}{3} + \frac{q'^3}{3} \right]_{-L/2}^{L/2} = \frac{\omega_0}{12} L^2 \quad (5.11)$$

Inserting our expression for L for the discretised basis, $L = \sqrt{2\pi\hbar N}$, (4.11), we could also write

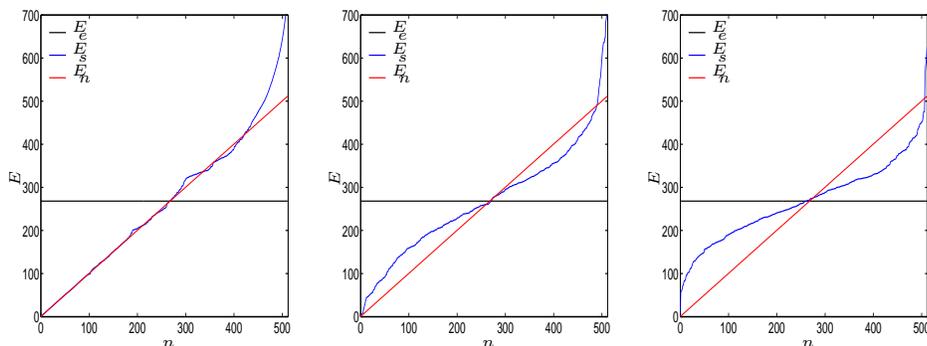
$$E_e = \hbar\omega_0\pi N/6. \quad (5.12)$$

In Figures 5.18 and 5.19 we plot the energy of the stationary states against $s = n$, for different μ and \hbar along with the line $E_n = \hbar\omega_0(n + 1/2)$ and the constant energy of a completely extended state E_e in our truncated basis. Note that the energies E_e and E_n are the equal when $n_e = \pi N/6 - 1/2 \approx \pi N/6$.

An interesting property of the numerical model can be seen here. Note how the higher energy E_s curve always seems to have an almost mirror image in the line E_e for all parameters. This suggests the discrete numerical system adjusts to keep the low energy and short time simulations performed in the last section nearly identical for different N . It is as if the higher energy eigenstates of the matrix are there solely to take up the energy slack from the lower energy states. All the errors introduced by discretising the system are compensated for by the higher energy terms but with the expense that these stationary states have no relation to classical system and indeed physical reality.

5.2.5 Quasi-Energy statistics

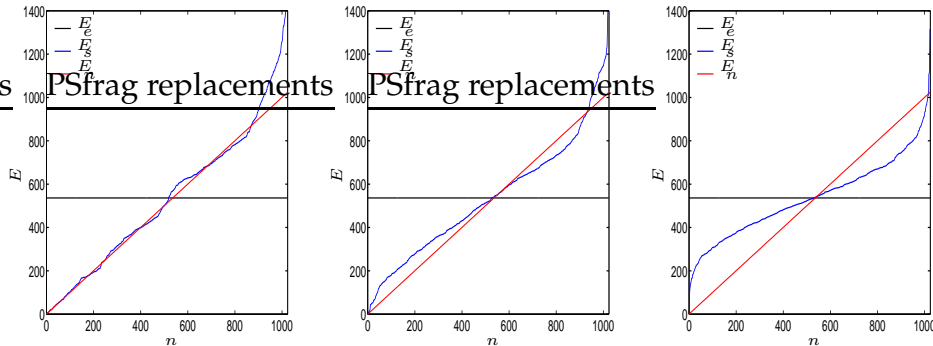
In this section we call upon the results of *random matrix theory* to perform some simple statistical analysis on the quasi-energy levels of the kicked system with irrational frequency ratio. Introductions to this topic can be found in [14,15]. A more rigourous discussion on these ideas can be found in [19].



(a) $\hbar = 1, \mu = 0.5,$
 $N = 2^9$

(b) $\hbar = 1, \mu = 3,$
 $N = 2^9$

(c) $\hbar = 1, \mu = 5,$
 $N = 2^9$



(d) $\hbar = 1, \mu = 1,$
 $N = 2^{10}$

(e) $\hbar = 1, \mu = 3,$
 $N = 2^{10}$

(f) $\hbar = 1, \mu = 5, N =$
 2^{10}

Figure 5.18. These graphs show how the energies of the stationary states changes as we vary \hbar and μ . The larger the value of μ the closed our eigenstates come to our idealised extended state represented by the line E_e .

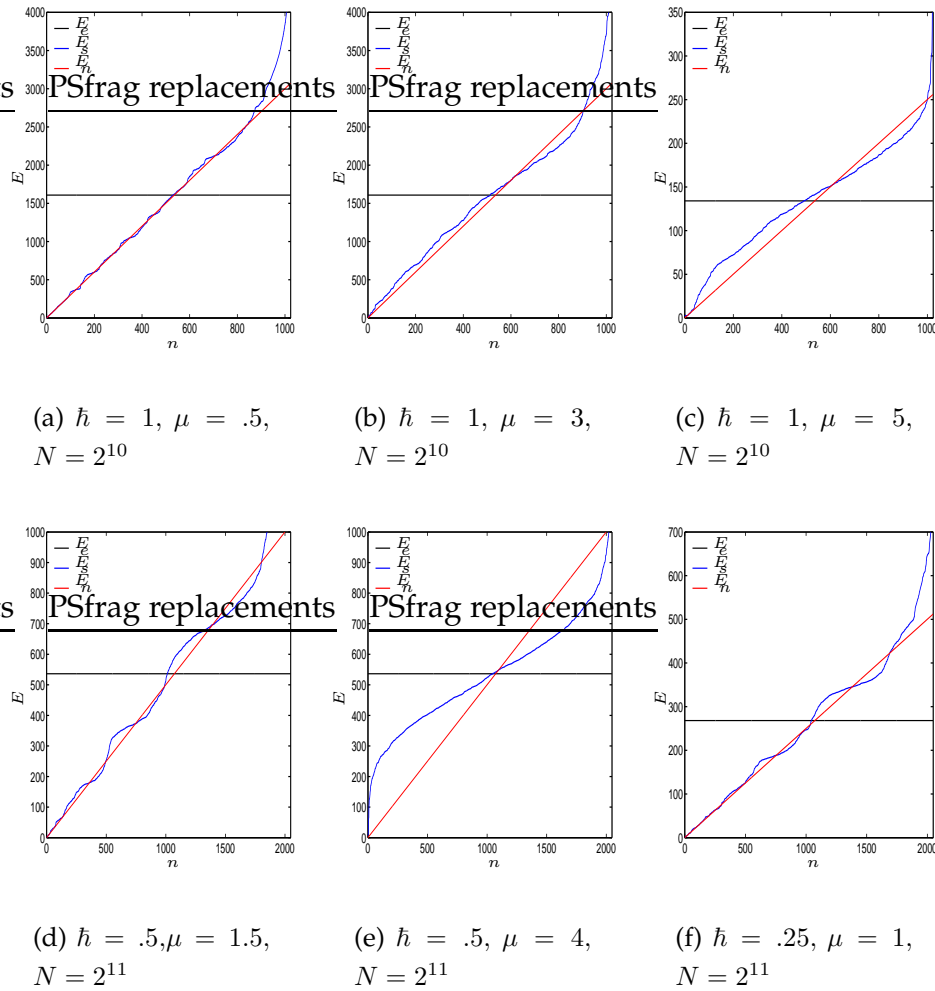


Figure 5.19. These graphs show how the energies of the stationary states changes as we vary \hbar and μ . The larger the value of μ the closed our eigenstates come to our idealised extended state represented by the line E_e .

The general idea behind the theory is that the statistical properties of the energy or quasi-energy levels of a system can be predicted very accurately even when practically none of the symmetries of the problem are known. If a classical system is integrable, the eigenvalues of the system's Hamiltonian or Floquet operator are generally randomly distributed. Calculating the differences between nearest eigenvalues and plotting results on a histogram generally we generally obtain what is called a Poissonian distribution.

On the other hand, a quantum system whose classical dynamics is known to be chaotic displays what is called energy/quasi-energy level repulsion. This means that the calculated energy levels tend not to be randomly distributed but for the most part lie some distance away from other eigenvalues. Interestingly, matrices whose elements are chosen from some random distribution, with some reasonable physical constraints, also have eigenvalues that seem to repel each other. The distribution pattern associated with these types of statistics is called a Wigner distribution pattern. These distribution patterns are regarded as being one of the most effective signatures of quantum chaos.

We can readily search for this signature using the quasi-energy data computed from the matrix \mathcal{U} . The Poissonian distribution is calculated to be [19],

$$P_P(s) = \exp(-s). \quad (5.13)$$

The Wigner, Gaussian Orthogonal Ensemble (GOE) distribution is given by [19],

$$P_W(s) = \frac{\pi}{2} s \exp\left(-\frac{\pi}{4} s^2\right) \quad (5.14)$$

In our case we will find that the eigenvalues generated rarely match either of these statistical distributions but is some kind of hybrid of them both. For this purpose we shall use three interpolation formulas that characterize these mixed statistics.

The Brody interpolation formula is defined as [16,17]

$$P_\alpha(s) = \gamma(\alpha + 1)s^\alpha \exp(-\gamma s^{\alpha+1}), \quad (5.15)$$

where $\gamma = \{\Gamma[(\alpha + 1)/(\alpha + 2)]\}^{\alpha+1}$. The distribution is normalised by construction and has mean spacing $\langle s \rangle = \int s P(s) ds = 1$. The Poisson distribution is gotten with $\alpha = 0$ and the Wigner distribution recovered with $\alpha = 1$.

Another interpolation formula was proposed by Israilev [18]. The distribution is

$$P_\beta(s) = A \left(\frac{\pi}{2}s\right)^\beta \exp \left[-\frac{\beta}{4} \left(\frac{\pi}{2}s\right)^2 - \left(\frac{2B}{\pi} - \frac{\beta}{2}\right) \frac{\pi}{2}s \right], \quad (5.16)$$

where the values of A and B are fixed by normalising the distribution and the condition that the mean spacing $\langle s \rangle$ is unity. The parameter β is particularly useful because it allows us to make a quantitative connection between quasi-energy statistics and the extended nature of the stationary states [16]. We will not attempt to analyse this here but this is due to the conjecture by Israilev that the repulsion parameter β is same as the parameter β_l used to measure what he calls 'entropy localisation length'.

We will also fit an interpolation formula that is just a simple weighted sum of both the Poisson and Wigner GOE distributions.

$$P_\delta = \delta P_W + (1 - \delta) P_P. \quad (5.17)$$

It is easy to see that this simple distribution also recovers the Poisson and Wigner distributions at $\delta = 0, 1$ respectively.

At $\mu = 0.5$ the effective classical KAM curves remain mostly intact and the quasienergy spacing distribution clearly displays the expected Poisson probability distribution even as we reduce the value of \hbar , see Figure 5.20.

When $\mu = 1.5$ there are almost no bounding KAM curves left in the classical regime. However, as shown in the last section the energy growth in the quantum system is still largely suppressed. We can see that by and large a Poissonian distribution still applies. However, as we make \hbar smaller we can see that there appears to be a slight shift towards a more Wigner like distribution and consequently some kind of quasienergy level repulsion, see Figure 5.21 .

Finally we move to a higher value of μ where the classical system is completely chaotic. We see that the quantum system still displays a somewhat mixed distribution, see Figure 5.22, for all values of \hbar considered. We have included a table of the parameters α, β and δ for the three mixed distributions, see table 5.2. As expected the parameters α, β and δ increase with increasing μ and decrease with increasing \hbar .

This concludes this section. Using the standard methods available to us we have briefly analysed the quasi-energy level spacing statistics for the Floquet op-

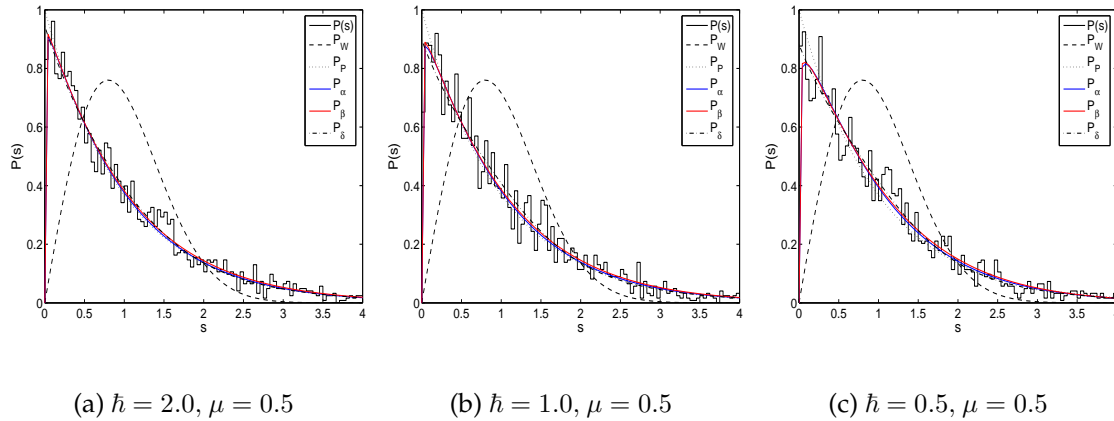


Figure 5.20. Quasi-Energy level statistics. In these figures we use $\mu = 0.5$ and we used a discretized Hilbert space of 3000 dimensions. If the effective KAM curves still exist in the classical system varying \hbar has little effect on the statistical distribution

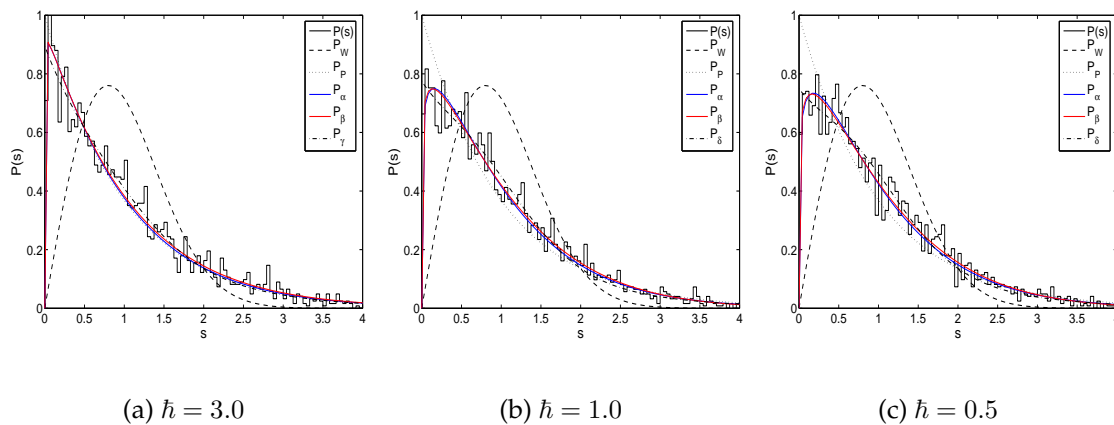


Figure 5.21. Quasi-Energy level statistics. In these figures $\mu = 1.5$ and we used a discretised Hilbert space of 3000 dimension. As we reduce \hbar the distribution becomes more like P_W .

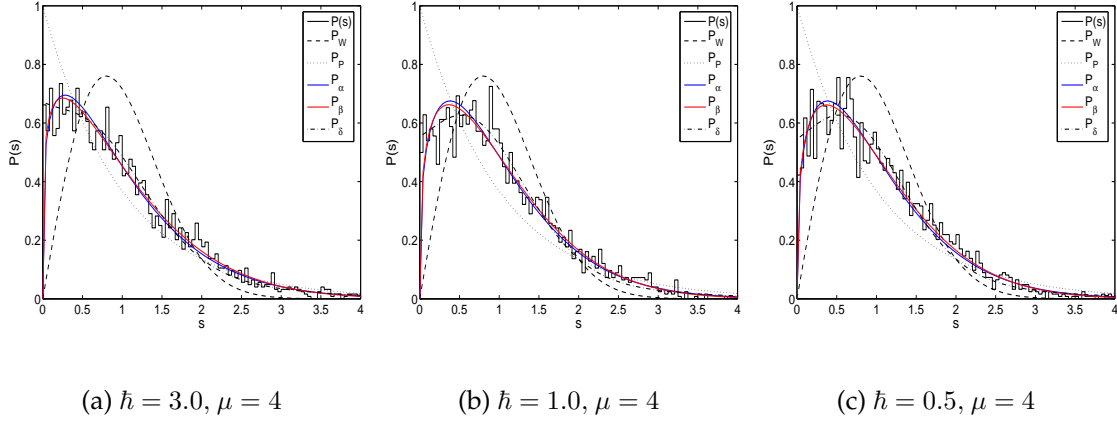


Figure 5.22. Quasi-Energy level statistics. In these figures $\mu = 4$ and we used a discretised Hilbert space of 3000 dimensions. As \hbar is reduced, the distribution becomes more like P_W .

\hbar	μ	α	β	δ
0.5	0.5	0.071	0.062	0.123
1.0	0.5	0.036	0.028	0.108
2.0	0.5	0.022	0.016	0.061
0.5	1.5	0.153	0.140	0.255
1.0	1.5	0.131	0.120	0.229
3.0	1.5	0.023	0.020	0.111
0.5	4.0	0.330	0.317	0.456
1.0	4.0	0.329	0.313	0.447
3.0	4.0	0.235	0.211	0.330

Table 5.2. Here we give some parameters of the quantum localisation as a function of \hbar and μ .

erator of one period of the kicked harmonic oscillator with irrational frequency ratios. We are not aware of any other published numerical data on this particular system. Our analysis strongly suggests the existence of a mixed (extended and localised) set of stationary states for this system as we reduce \hbar and increase the kicking strength μ . These deductions are in keeping with our earlier analysis on the quantum dynamics and the systems stationary states.

5.3 Numerical study with frequency ratio $1/R = 1/4$

In this section we attempt a numerical analysis of the kicked harmonic oscillator when the frequency ratio is $1/R = 1/4$ using the new FFT technique given in chapter 4. The general aim, as stated at the start of this chapter will be to compare and contrast classical and quantum systems as we vary the quantum parameter \hbar . In chapter 3 we found that for $1/R = 1/4$, as with the other cases with $1/R = 1/3, 1/6$, the parameter \hbar has an importance beyond its mere magnitude and therefore special attention to the small changes \hbar may have on the quantum dynamics.

The initial analysis will be on the general structure of the Floquet operators stationary states. We look to reconcile the numerical results with the analysis given in sections 3.4.2 and 3.5. Recall that as result of the translational invariance the eigenstates should made up of periodic trains of delta functions when the quantum resonance condition is fulfilled. We also speculated on the functional form of some of the eigenstates in the absence of quantum resonance. The aim is to show that these all these predictions are supported up by the numerical model.

Staying with the eigenstructure of the system we then select some examples of eigenstates centered primarily on the classical period 1 and period 4 modes. We show that when there is no quantum resonance the numerical model calculates completely localised and continuous stationary states over the classical islands. We shall also provide some examples of the effect quantum resonance has on stationary states existing primarily on the accelerator modes. We are unable to see these types of states in the absence of quantum resonance.

We then turn to straight forward evolution of the quantum system. We first provide some general comparisons of the quantum and classical energy growth to indicate the robustness of our model. However our main focus is on illuminating the effect that quantum resonance has on the energy growth rates. We plot the diffusion rates of the quantum system as a function of \hbar . We do this for

several different values of μ and initial positions. We do not aim to quantify the diffusion rates. We are more concerned with demonstrating that it is not necessary to have exact quantum resonance to see significant increases in the growth rates. We show also that this quantum resonance also effects the tunneling characteristics of the system and its ability to diffuse along the web structure.

We finally examine the energy growth rates of the evolving quantum system initially placed near the classical period 1 and ballistic islands. The new FFT numerical technique allows one us to reduce \hbar to a value where we can place a coherent state entirely within the stable classical structures. We can then note any major differences between the energy growth rates of the classical ensemble and the quantum state.

We are very interested in the idea that a state may tunnel from one of the islands through the chaotic sea to another. Particulary we are interested in detecting tunneling form one ballistic island to one of higher energy. Such a process would potentially mean that the quantum system could simultaneously exploit both the classically quadratic energy growth associated with the ballistic islands dealt with in chapter 2 and the quadratic energy growth associated with quantum resonance.

5.3.1 Stationary States: $1/R = 1/4$

In this section we provide some selected examples of the types of eigenstates numerically calculated from the numerical model given in chapter 4. We will not, as we did in the system with irrational kicking frequency, provide any analysis on the systems quasi-energy statistics. Considerable progress has been made in this respect using the Lanczos diagonalisation procedure for the kicked Harper model (KHM) [7].

We begin by displaying some simple plots of eigenstates when the quantum resonance condition is not fulfilled. Begining with $\hbar = 1.5$ and value of $\mu = 0.1$ we plot a few stationary states in the position basis in Figure 5.23. We see there seems to be some sort of periodicity to the stationary states. We draw attention now to the structural similarity between the generalised double Gaussian functions touched upon briefly in section 3.5.3 and these numerically calculated eigenstates. As we have already mentioned, the double Gaussian functions can be made into Dirac impulse or comb functions under certain conditions. However, we were unable to find a functional form that made this condition match with the quantum resonance condition at the time of writing.

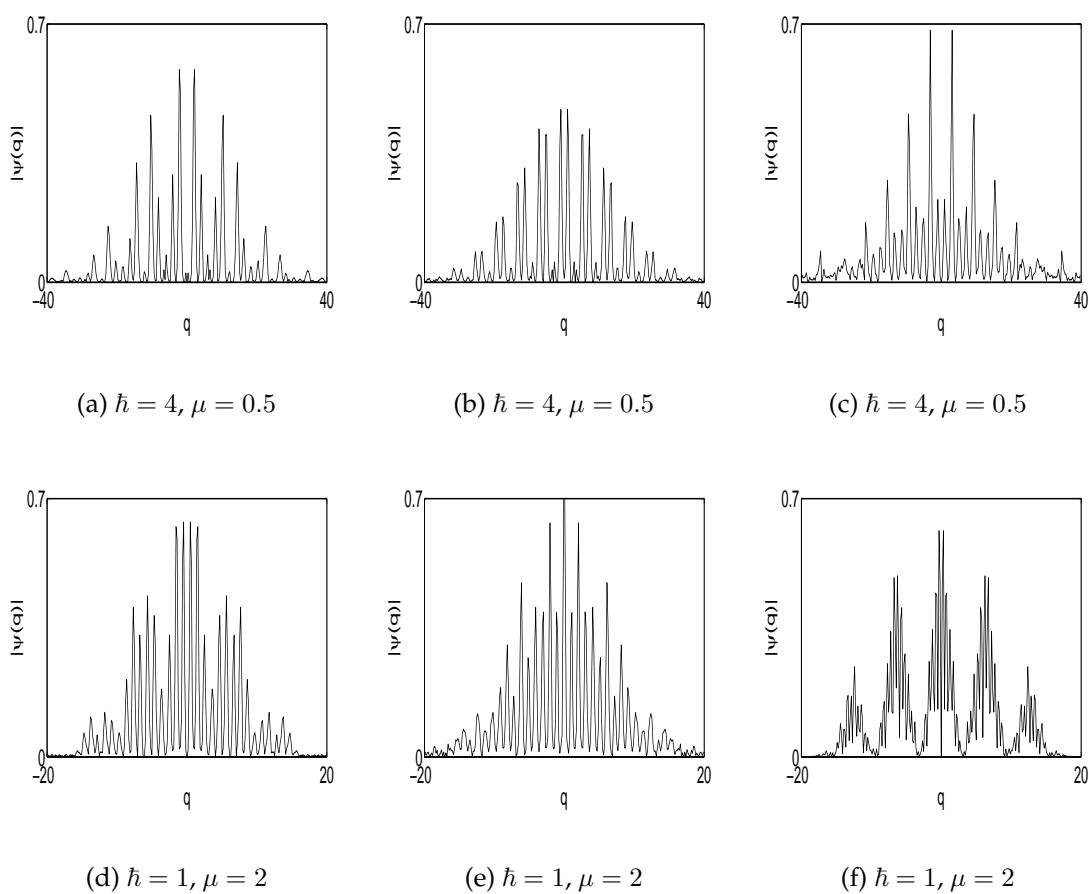


Figure 5.23. Plots showing quasi periodic behaviour of some stationary states with $k = 1$ and with $N = 2^8$. The resonance condition (3.61) is not fulfilled for these values of \hbar . Compare these figures with those of Figure (3.3).

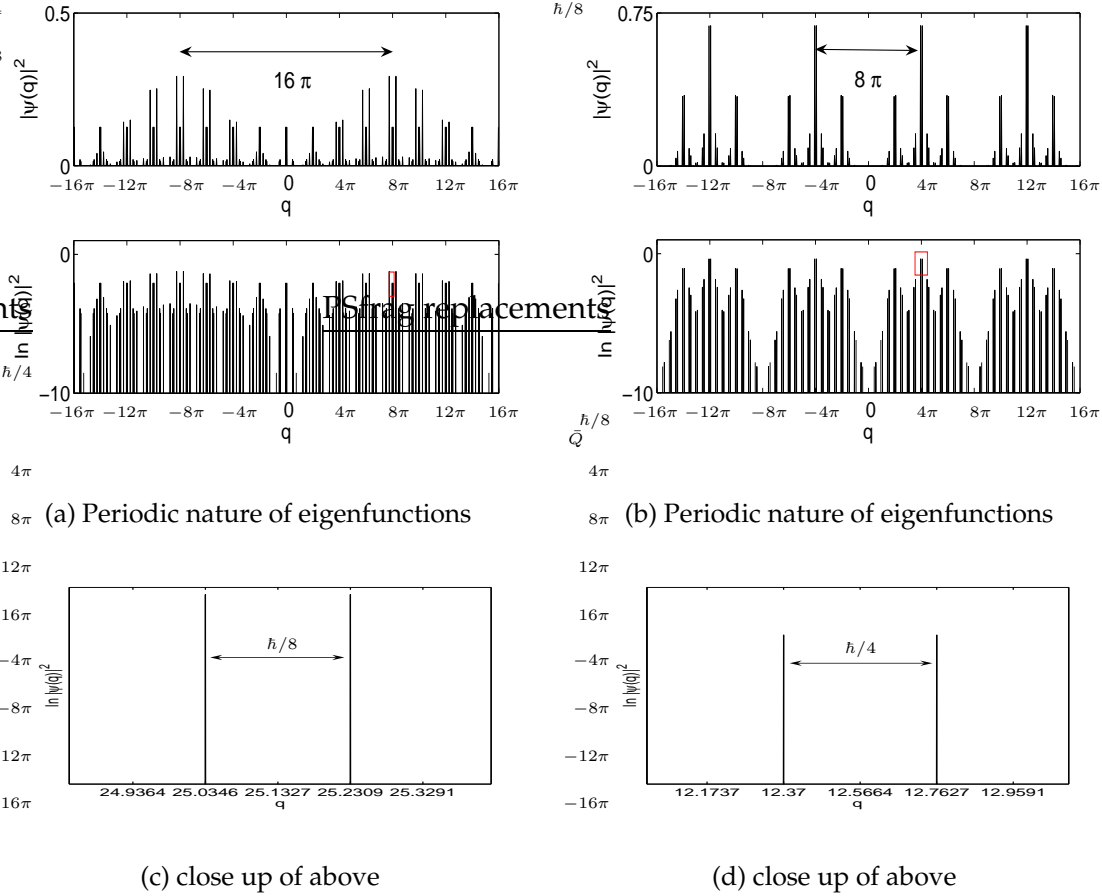


Figure 5.24. Stationary states in the position basis with $\hbar = \pi/2$ and $k = 1$. The quantum resonance condition (3.61) is fulfilled in these examples.

However, we can look for the delta function nature that our analysis suggests should occur when the resonance condition is fulfilled. We do this by setting $\hbar = \pi/2$ which with $N = 1024$ and $k = 1$ gives $l = \pi/32$ and $L = 32\pi$. In Figure 5.24 we have plotted 2 typical stationary states. The delta function nature of the states is very obvious. In the figure we have also focused in on two adjacent delta spikes and showed that they are both separated by the correct distance, see (3.67).

We give a selection of eigenfunctions for different parameters of μ , k , and resonant \hbar in Figure 5.25 and the corresponding Husimi phase space distributions in Figure 5.26. In particular we note the structure of the stationary states with small μ and \hbar . This is because they have been averaged over. In C.1 we discuss some of the problems that arise when computing Wigner and Husimi distributions of wavefunction when the resonance condition is and is not fulfilled. Note that in Figure 5.25(j) the stationary state appears to be continuous. However we must

accept the possibility that the sampling rate of the numerical model is not small enough to show the discrete nature of eigenfunctions.

5.3.1.1 Stationary states on periodic islands

We are also interested in the structure of the eigenstates when the classical system displays anomalous diffusion characteristics. We argued in section 3.5.2 that when $\mu = \pi$ and if \hbar is small enough we should be able to place displaced Fock states on the period one islands and they should retain their approximate shape (k is again set to unity). We also showed how to work out the phase picked up on one of the many period four islands. An important point here is to recognise that in order to get the delta functions to appear in our numerical eigenvector calculations we must set \hbar must then be some fraction of 2π , this means that in these particular situations the Fock states placed on the period 1 islands may pick up the same phase over 4 Floquet operations as Fock states on one of the period 4 islands, see section 3.5.2. If \hbar is not a multiple of π this cannot happen. We plot some stationary states computed for different values of \hbar around values of $\mu = \pi$ in Figures 5.27(d) and 5.28(d) below.

In Figure 5.27 we plot Husimi distributions of some stationary states where \hbar is not a fraction of 2π . We see that localised stationary states exist around period 1 islands. These states have different eigenvalues to stationary states with similar distributions around the period 4 islands.

The situation is different when \hbar is some fraction of 2π . We showed in section 3.5.2 that the a displaced Fock state on one of these islands approximates an eigenvalue of the system when \hbar gets very small. The quasisenergy of such a state was shown to approach $\Omega = -\pi^2/4\hbar - (n + 1/2)\pi/2$. Upon 4 operations of the Floquet operator the displaced Fock state would have picked up a phase given by $\exp(-i(\pi^2/\hbar - (n + 1/2)2\pi))$. We also calculated the phase picked up over a complete cycle by a displaced Fock state on a period 4 island to be $\exp(-i(2\pi^2/\hbar - (n + 1/2)2\pi))$. It is easy to see that these phases are the same if we set $\hbar = 2\pi m/n$, where n and m are integers. We show this situation in Figures 5.28.

Although the distributions above are only over a very limited phase space area imposed by using small \hbar they illustrate a very important point. Firstly to show that we have numerically found what appears to be a localised eigenstate if \hbar is not a fraction of 2π . However, in order to show this apparent localisation we had to choose a value of \hbar which would not display the delta function periodicity

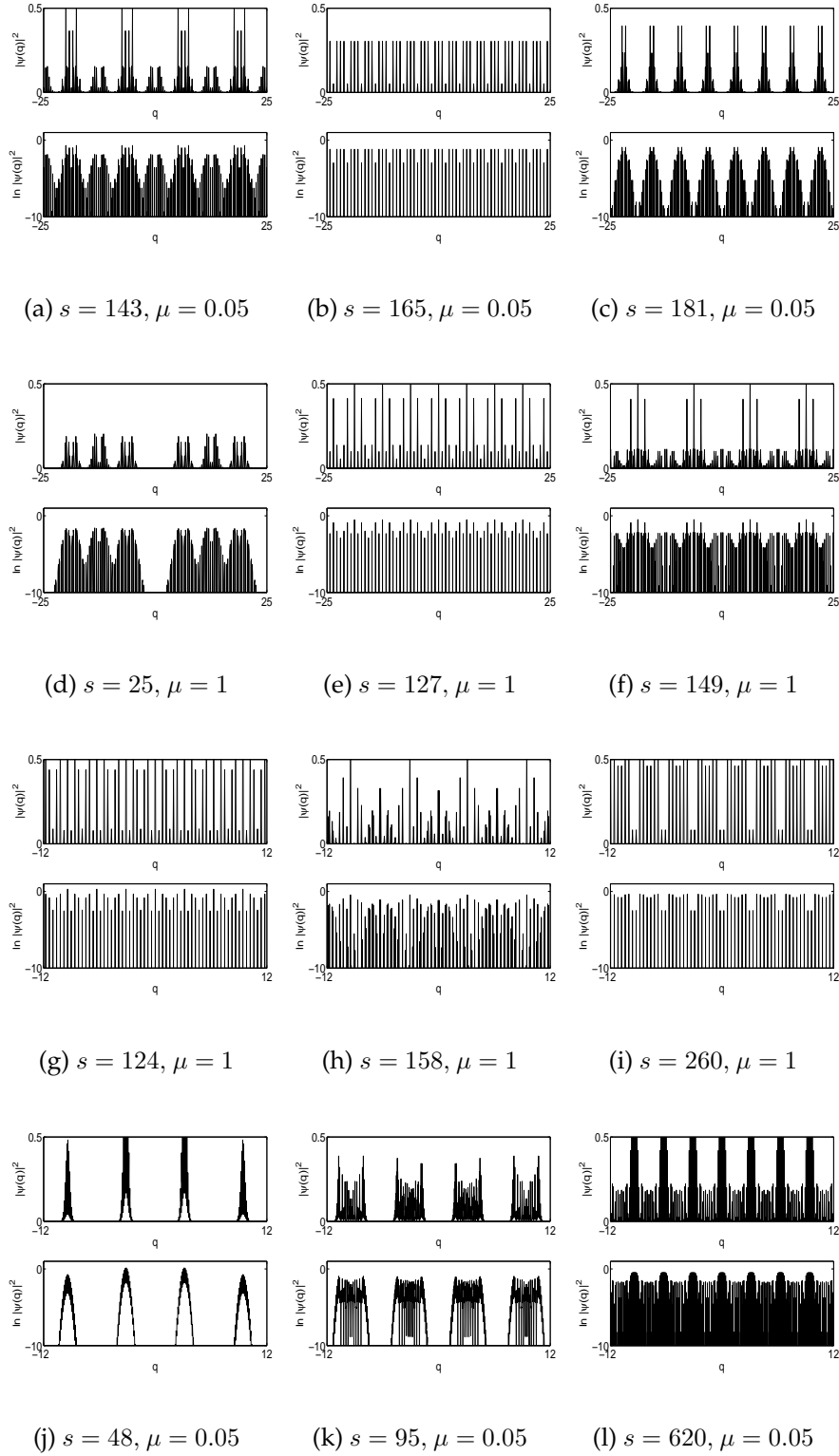


Figure 5.25. Probability distributions of some stationary states of the kicked system in the position basis. For (a),(b),(c),(d),(e),(f) $\hbar = \pi/4, k = 1, N = 512$. In (g),(h),(i) $\hbar = \pi/16, k = 2, N = 512$. In (j),(k),(l) $\hbar = \pi/32, k = 1, N = 1024$.

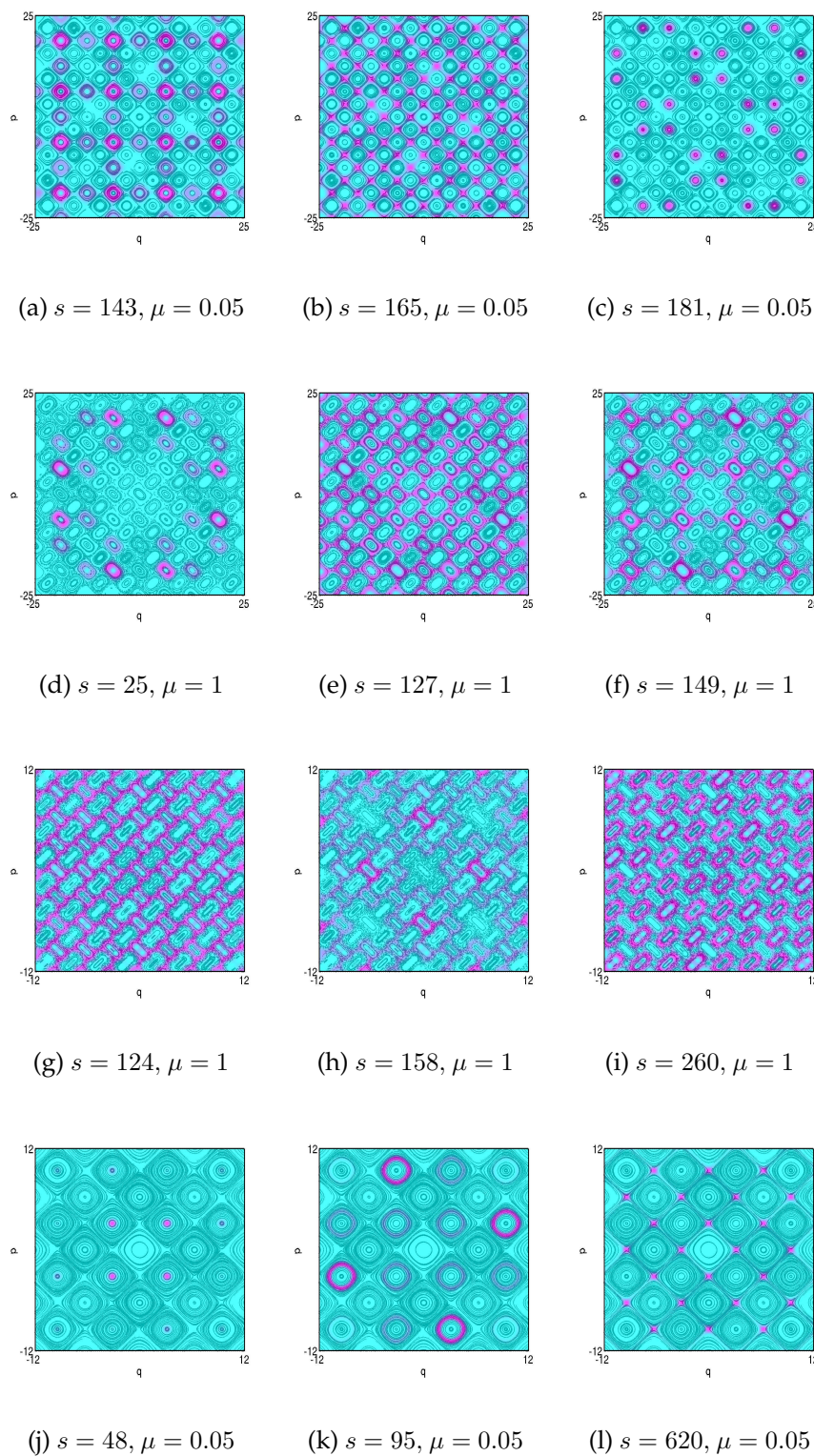


Figure 5.26. Husimi distributions of some stationary states of the kicked system corresponding to the distributions in Figure 5.25. For (a)-(f) $\hbar = \pi/4, k = 1, N = 512$. In (g),(h),(i) $\hbar = \pi/16, k = 2, N = 512$. In (j),(k),(l) $\hbar = \pi/32, k = 1, N = 1024$.

explained in sections 3.4.2 and 3.5.2. In section 5.3.2 we examine this issue further by evolving a wavepacket placed on these classical islands.

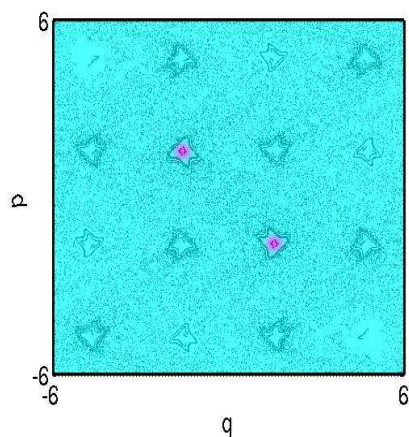
5.3.1.2 Stationary states on accelerator modes

We now search for any sign of the elusive accelerator modes. The fact that classical particles on these islands never return to the same vicinity leads us intuitively to say that there could be no stationary state existing entirely on one of these modes. However, in section 3.5.2 we discussed how a displaced Fock state placed at $q = m\pi/2$ picked up a phase of $\exp(-i\mu|m|\pi/4\hbar)$, therefore it is conceivable that when \hbar is some fraction of π certain states may pick up the same phase on each Floquet operation as they are transported from island to island. The aim of this section is therefore to provide examples of Husimi distributions of numerically calculated stationary states that exist mainly on the accelerator modes.

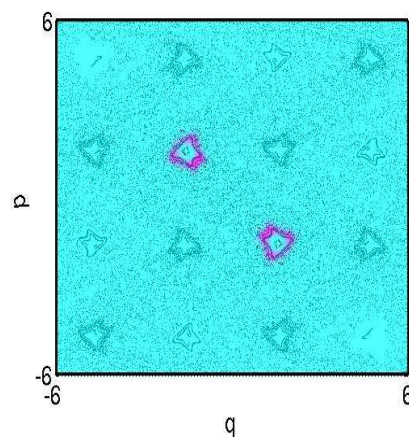
In Figure 5.29 we plot some Husimi distributions of stationary states for $\mu = 2\pi + 0.15$ and decreasing values of \hbar . We see that as expected the periodic nature of the stationary states is still present. Moreover, by comparing these figures with Figures 2.12 and 2.15 we can see that the Husimi distributions resemble the shape of the classical modes. This is very interesting. It shows that with a resonant \hbar sets of extended eigenstates centered primarily on the classical ballistic islands exist. We suggest therefore that these eigenstates are thus the primary modes of anomalous transport.

Upon each operation of the Floquet operator each of these states then picks up a different phase to interfere differently to create the ballistic motion from island to island. This leaves the possibility that the quantum system may be able to tunnel between different periodic and different accelerator modes. One aim of the next section will be to search for numerical evidence of such behaviour. With regards to the accelerator modes tunneling like this may lead to rates of anomalous diffusion that are greater than its classical counterpart. Indeed, as we have already mentioned in chapter 3, with frequency ratio of $1/4$, the rates of diffusion in the quantum system are routinely greater than that of its classical counterpart.

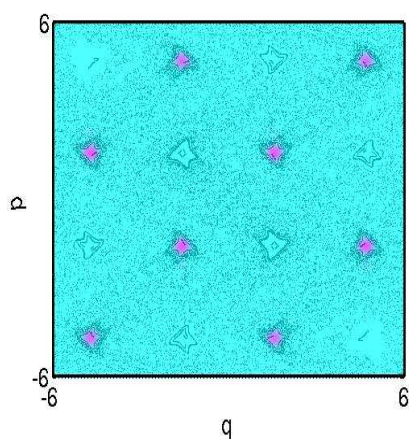
It is interesting that we have not found any of these striking phase space structures when \hbar is not a fraction of π . However, this does not mean that anomalous diffusion does not take place in these situations. We shall numerically demonstrate this in the next section.



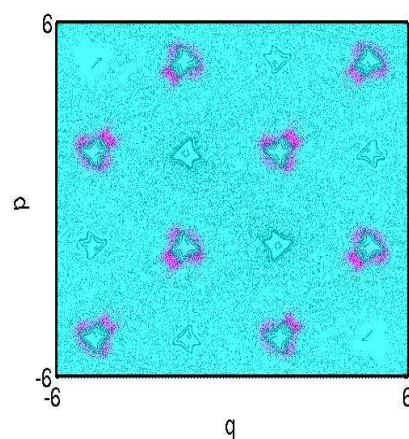
(a) This state is very similar to superposition of coherent states placed on classical period 1 islands.



(b) Another stationary state localised over the classical period 1 islands.

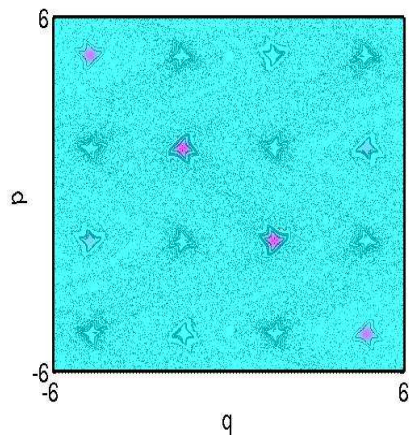


(c) This state is very similar to superposition of coherent states placed on classical period 4 islands.

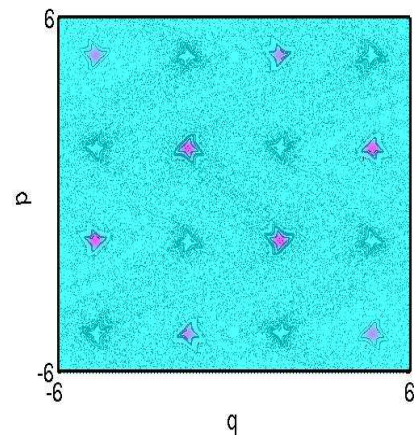


(d) Another Husimi distribution of a stationary state localised over the period 4 islands.

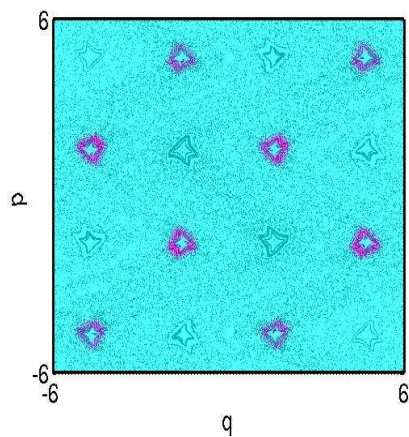
Figure 5.27. Husimi distributions of stationary states with $\mu = \pi$ and $\hbar = 0.03$ superimposed over the classical quasi-periodic islands. In this diagram a Hilbert space of 2^{10} was used. The eigenstates can be visually seen to be approximate superpositions of the displaced Fock states. The quasi-energies of these states can be also shown to very close to the ones we predicted analytically.



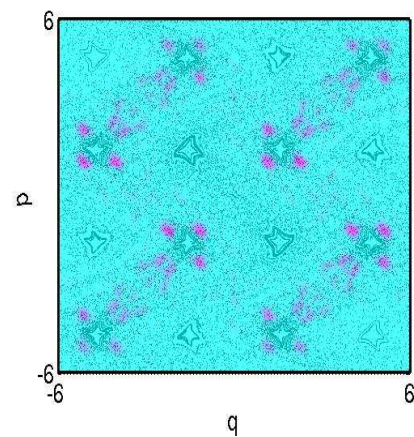
(a) Husimi distribution showing stationary state localised over both classical period 1 and period 4 islands.



(b) Another Husimi distribution showing stationary state localised over classical period 1 and period 4 islands.



(c) Distribution showing complicated nature of the systems stationary states at the KAM boundary in classical phase space



(d) Distribution showing a stationary state existing much farther out into the classical chaotic sea. The distribution still has some resemblance with the classical phase map.

Figure 5.28. Husimi distributions of stationary states near periodic islands with $\mu = \pi$ and $\hbar = \pi/128$. In this diagram a Hilbert space of 2^{10} was used. When \hbar is a fraction of π the stationary states which dictate the motion on classical period 1 islands are not localised. This is because they may have the same phase as stationary states centered primarily on the classical period 4 islands.

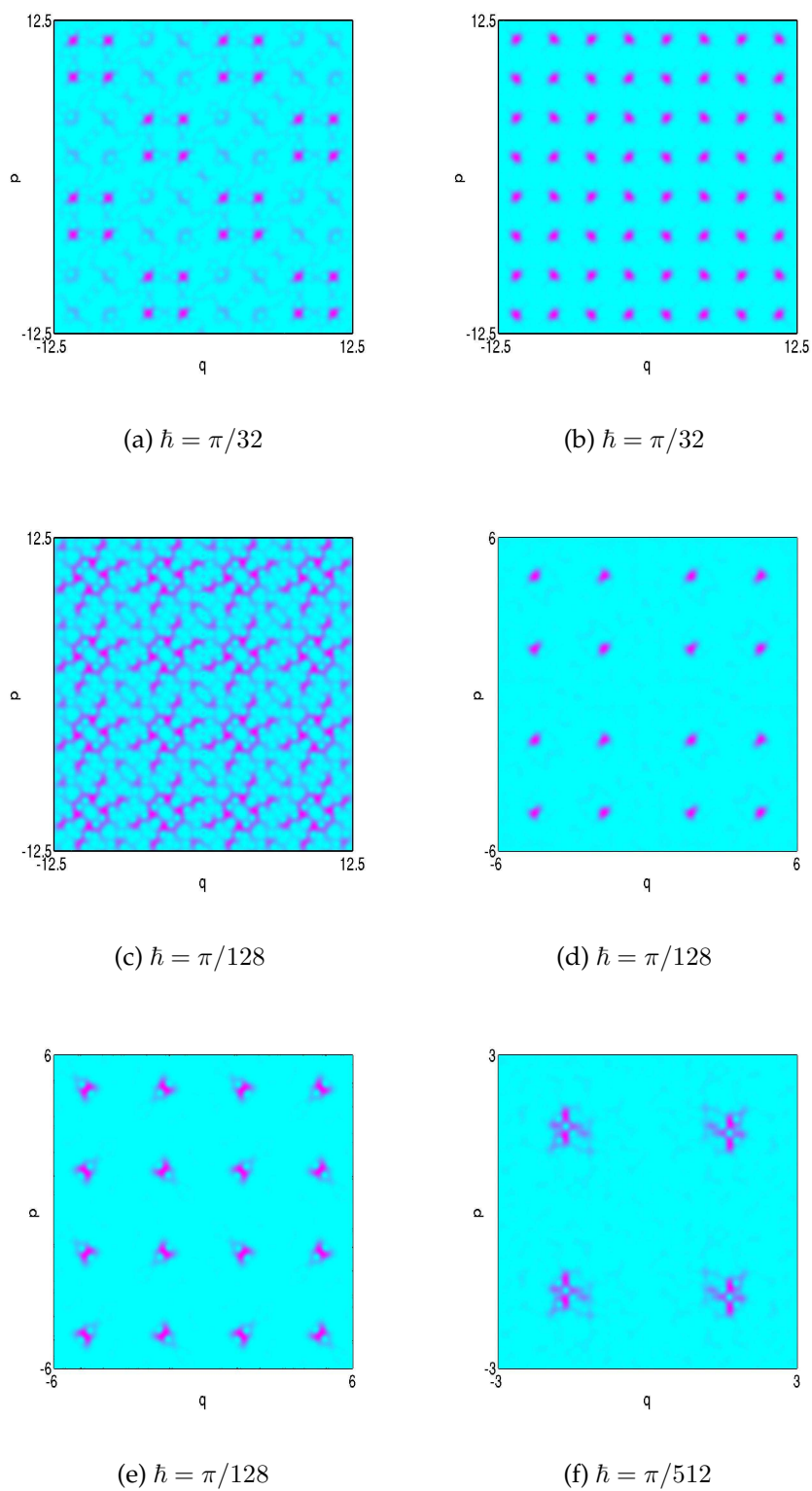


Figure 5.29. Husimi distributions of numerically calculated stationary states near classical accelerator modes with $\mu = 2\pi + 0.15$ and various resonant values of \hbar . In this diagram a Hilbert space of 2^{10} was used. Compare these figures to Figures 2.12 and 2.15

5.3.2 Mean energy growth with $1/R = 1/4$

The quantum kicked harmonic oscillator with frequency ratio $1/4$ displays some very interesting properties. Most notably is the idea of tunneling between areas of phase space that are classically isolated [1,4,5]. Although, not as striking as this there is also significant numerical evidence to suggest that the quantum system is also capable of exploiting the web structure to diffuse through phase space at a far greater rate than the classical system [2]. In the course of our calculations we shall provide examples of such effects but shall not study them specifically.

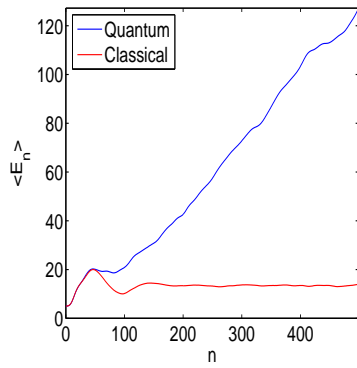
The main aim of this section see what effect, if any, resonant values of \hbar have on our simulations. In the chapter 3 we emphasised the fact that the stationary states of the Floquet operator at resonant frequencies ratio $1/4$ should be made up of periodic trains of delta functions when viewed from the position basis. We showed in the last section that these properties could only be picked up in the numerical calculations if \hbar was some fraction of π . In order to see what effect this has on the Energy - Time curves we plot the curves $D_q(\hbar)$ for fixed μ and a variety of different initial conditions. Any resonance effects should quickly make themselves known.

The rest of this section is concerned with examining the rates of diffusion of states initially near classically periodic and ballistic islands. In particular we will be looking for evidence of quantum tunneling between these islands. To do this we place the quantum states initially on classical stable and unstable points of these islands. A considerable effort was made in chapter 2 to find out where these were exactly.

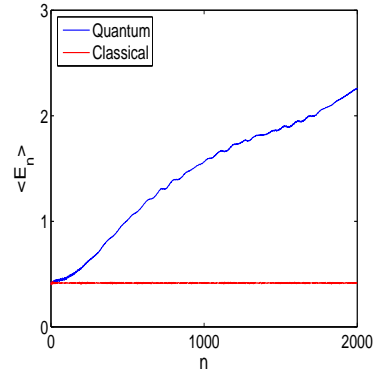
5.3.2.1 Mean energy growth and \hbar

In Figures 5.30 we plot some typical diffusion curves for different values of \hbar and μ for coherent states placed at different initial conditions. Linear energy growth does not always occur in these examples. Even so, fitting a line to each diffusion curve still serves as a useful measure of the systems energy growth over time. As well as this it has always been customary to measure the classical systems diffusion by finding the slope of the energy time graph. For comparative reasons we shall, for the most part, continue to measure diffusion rates in this way.

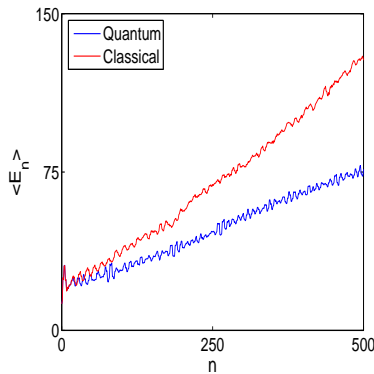
Figure 5.31(a) is a plot of the quantum diffusion $D_q(\hbar)$ for initial states centered on the classical stable point at the origin. Figure 5.31(b) is a similar plot but with the initial quantum state placed on an unstable point on the classical web.



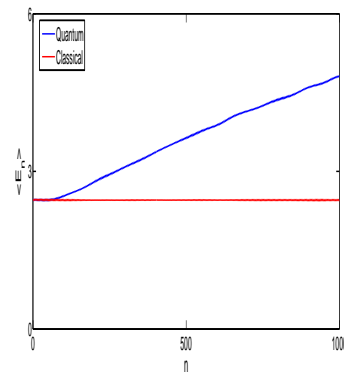
(a) $\hbar = 1, \mu = 0.5, (q, p) = (0, \pi), N = 2^{13}$



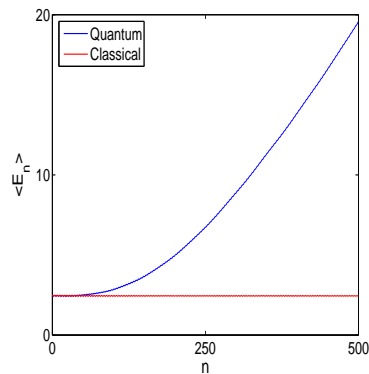
(b) $\hbar = 0.8, \mu = 0.4, (q, p) = (0, 0), N = 2^{13}$



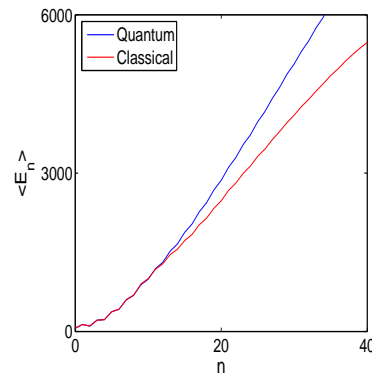
(c) $\hbar = 0.2, \mu = 2, (q, p) = (5, 0), N = 2^{16}$



(d) $\hbar = 0.0125, \mu = \pi, (q, p) = (\frac{\pi}{2}, \frac{\pi}{2}), N = 2^{17}$



(e) $\hbar = 0.0190, \mu = \pi, (q, p) = (\frac{\pi}{2}, \frac{\pi}{2}), N = 2^{19}$



(f) $\hbar = .01, \mu = 2\pi + .15, (q, p) = (5\pi/2, 5\pi/2), N = 2^{20}$

Figure 5.30. $\langle E_n \rangle - v \cdot n$, for various system parameters. $k = 1$ in all of the above plots.

In these examples the quantum wavefunction can spread out while the classical distribution is essentially bounded. The graph also shows the non-trivial dependence of the curve D_q on \hbar . There are significant jumps in the diffusion rates near where 2π is some rational multiple of \hbar . The spikes in the graphs represent where the quantum system displays quadratic energy growth with time. Numerical evidence of the quantum resonances was given in [1] along with qualitative theoretical explanation. A good review of this can also be found in [3]. It should be noted however that the theoretical explanations only holds in cases of exact resonance. Our numerical analysis suggests that the value of \hbar need only be nearly resonant for near quadratic energy growth to occur.

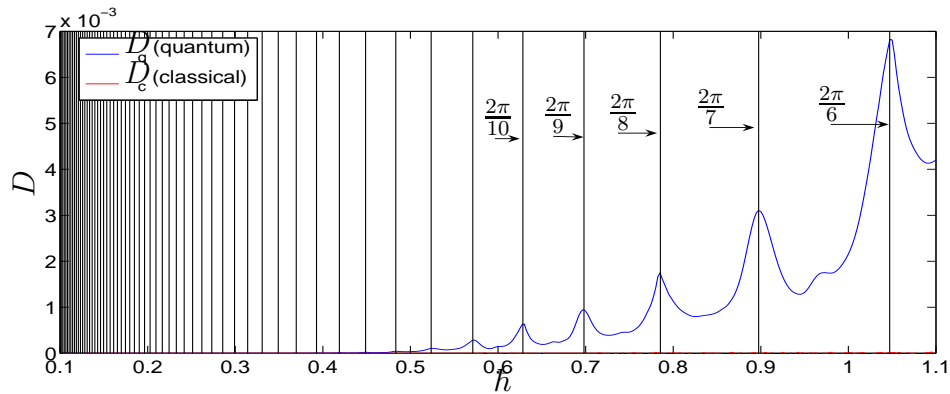
In Figures 5.32 and 5.33 we use values of μ and initial parameters where the classical system is able to diffuse and include the values of D_c calculated from the correctly distributed ensemble for different values \hbar^\ddagger . In all of the examples the same resonance effect is very obvious. The numerical results suggest that the quantum system generally diffuses more rapidly than the classical ensemble, though not always, see Figure 5.30(c).

It is important to note that in all of the above examples identical graphs were also generated with Hilbert spaces of different dimensions. The resonance effects are not specific to a particular choice N .

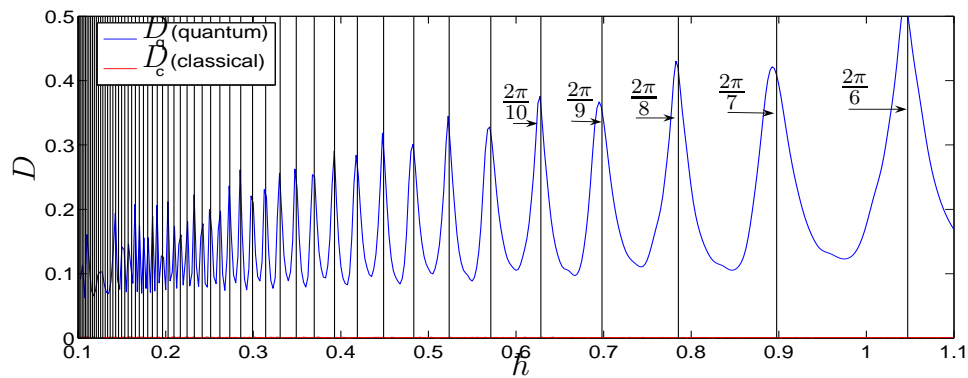
We finish this section by including two graphs demonstrating the smooth transition between quadratic to linear energy growth as \hbar moves between resonances. To this end we placed an initial state at $(q, p) = (5, 0)$ and evolved it over $n = 200$ time steps for various values of \hbar and with $\mu = 2$. A curve αn^β is then fitted to the last 100 time steps. We plot β vs \hbar in Figure 5.34(a). The last 100 time steps are used because the analysis of [1,3] requires that the quadratic and linear predictions for the systems energy growth rate for resonant and nonresonant \hbar only applies for large values of n . A similar simulation but with the initial state centered at $(q, p) = (0, 2)$, $\mu = 2$ and only evolved for 100 time steps is given in Figure 5.34(b). Only the last 50 time steps were used to fit to a curve αn^β . We also included a great deal more vertical lines at different values of $\hbar = 2\pi n/m$ in these figures to emphasise the many different resonant modes that the numerical model is capable of resolving.

The results are not altogether unexpected having already examined both situations in Figure 5.31. However they show that near quadratic energy growth can

[‡]Any \hbar dependence displayed classical curve is due solely to the width of the initial ensemble and has got nothing to do with the underlying dynamics.

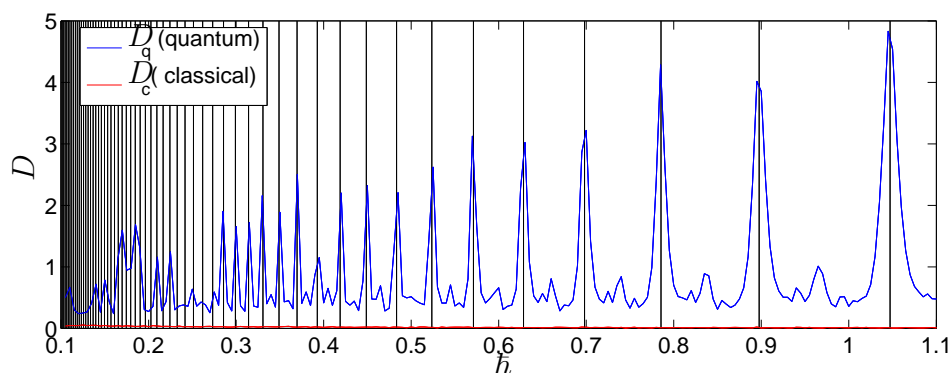


(a) Numerical calculation of $D(\hbar)$ for $\mu = 0.4$, $(q, p) = (0, 0)$ and $k = 1$. We have used 400 separate values of \hbar to generate this graph. A discretised Hilbert space of dimension 2^{12} was used in this calculation. The plot illustrates clearly the quantum tunneling effect.

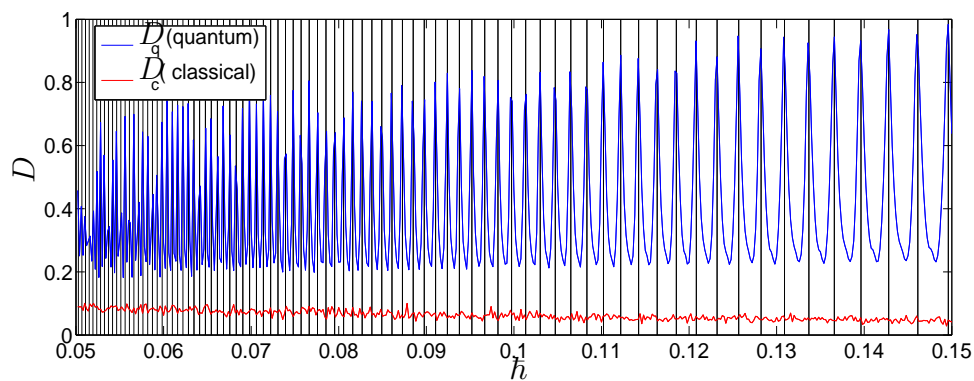


(b) Numerical calculation of $D(\hbar)$ for fixed $\mu = 0.3$, $(q, p) = (0, \pi)$, and $k = 1$. A discretised Hilbert space of dimension 2^{12} was used in this calculation. The quantum system seems to see the web structure at values of μ for which the classical web is infinitesimally thin

Figure 5.31. Dependence of D_q and D_c on \hbar . For each specific value of \hbar we evolved the system over 400 time steps. For all of the above initial conditions there is effectively no classical diffusion, that is $D_c \approx 0$. The vertical lines in the graph represent where the main resonant modes are expected to occur.

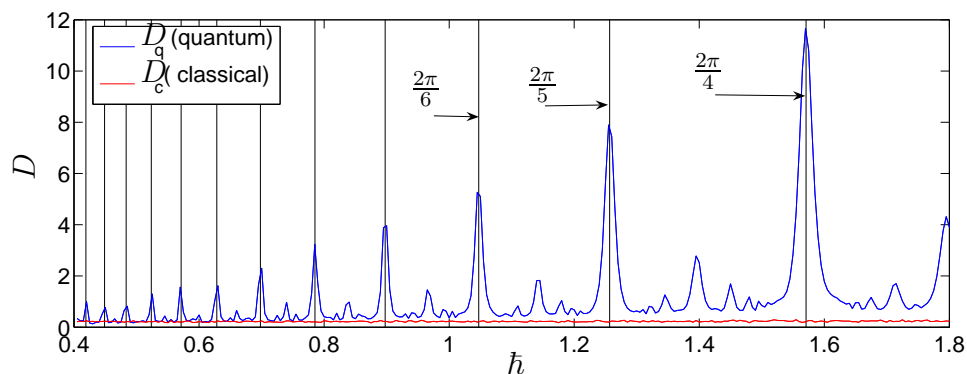


(a) Numerical calculation of $D_q(\hbar)$ for fixed $\mu = 1$, $(q, p) = (0, \pi)$. A discretised Hilbert space of dimension 2^{14} was used in this calculation.

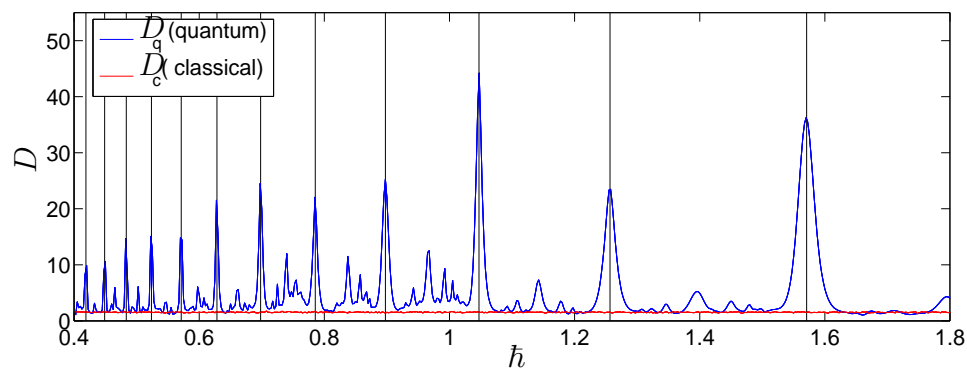


(b) Here we show the resonance effect is still in effect for smaller \hbar . A discretised Hilbert space of dimension 2^{18} was used in this calculation.

Figure 5.32. Dependence of D_q and D_c on \hbar . In these examples for each specific value of \hbar we evolved the system over 200 time steps. The vertical lines in the graph represent the main resonant modes are expected to occur



(a) $\mu = 2$, $(q, p) = (5, 0)$, $N = 2^{15}$. System was evolved for 200 time steps.



(b) $\mu = 4$, $(q, p) = (0, 2)$, $N = 2^{16}$. We evolved system over 100 timesteps

Figure 5.33. Dependence of D_q and D_c on \hbar . The Figure shows that the quantum resonance effect is still very evident for values of μ where most of the phase plane is chaotic. Compare this figure to Figure 5.34

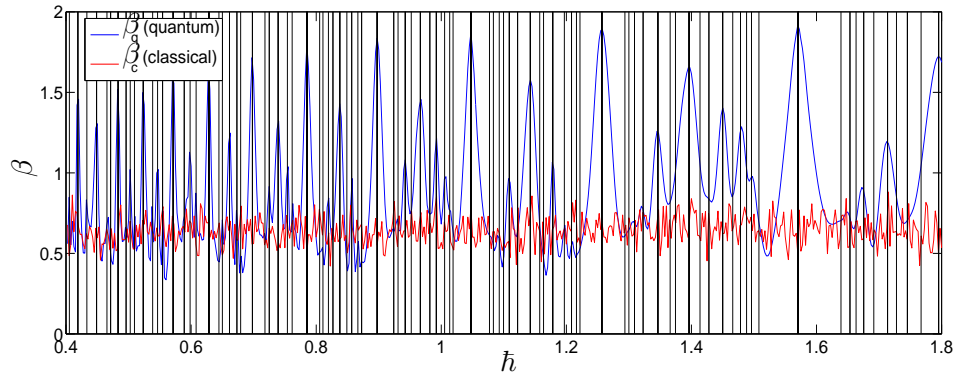
also occur near resonant values of \hbar . Surprisingly there is almost never any linear energy growth for nonresonant \hbar . In section 3.5 we suggested an explanation for this gradual resonance effect using the special double Gaussian SFF that under certain conditions becomes the completely extended Dirac comb function. However, we were not able at this time to find the correct form of the SFF so that this transition occurred at $\hbar = 2\pi n/m$.

5.3.2.2 Mean energy and \hbar : Period 1 islands

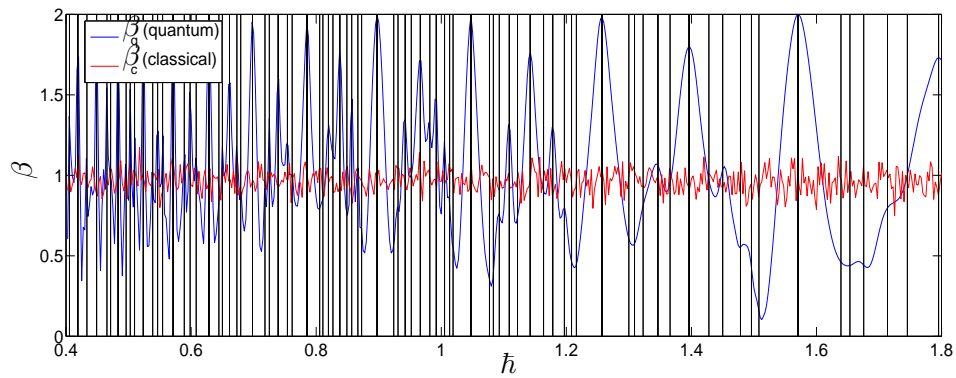
We now turn our attention to studying how the quantum system behaves when the classical system is undergoing anomalous diffusion. We begin with the numerically simpler problem of examining the quantum diffusion characteristics for states on the periodic islands. We concentrate on the period 1 islands located around $\pm(\pi/2, -\pi/2)$ in the phase plane, see section 2.4.1. In particular we shall examine how a coherent state evolves when placed inside the stable classical structure with $\mu = 3.14, \pi, 3.143$. The center of the coherent state each will be placed as the center of island, which is determined numerically from (2.63). The stable points thus have phase space coordinates of $(s_q, -s_q)$ with $s_q \approx 1.56999, \pi/2, 1.57149$. We evolve the system for some small values of \hbar (there are 500 in this calculation) over 150 time steps using a Hilbert space of 2^{16} . The results are shown in Figure 5.35.

At these tiny values of \hbar we can still see evidence that the quantum diffusion is for the most part greater than that of a classical ensemble. Examining the plots we see that at about $\hbar = 0.0125$ and $\hbar = 0.0190$ there are increases in the quantum diffusion rate above that of the classical rate. We examine the energy time curve for these particular parameters after 500 and 1000 time steps in Figures 5.30(d) and 5.30(e). We see this as clear evidence of tunneling.

However the spikes on the classical curve serve to remind us that there exists a finite probability at these values of \hbar that a small number the particles in the classical ensemble could be placed outside the bounding elliptical curves. The spikes can be interpreted as a classical particle undergoing Levy-type flights. This exposes a limitation in using a classical ensemble for studying the differences between the quantum and classical dynamics. However, there would appear to be no other reasonable way to do this. A classical Liouville probability distribution could not be accurately computed around these chaotic regions. It is tempting to explain the tunneling therefore as some sort of chaos assisted phenomena. However, we must remember previous results for which tunneling has



(a) $\mu = 2$, $(q, p) = (5, 0)$, $N = 2^{15}$. System was evolved for 200 time steps. The curve αn^β is fitted to the last 100 time steps



(b) $\mu = 4$, $(q, p) = (0, 2)$, $N = 2^{16}$. We evolved system over 100 timesteps. The curve αn^β is fitted to the last 50 time steps

Figure 5.34. Dependence of β_q and β_c on \hbar . The curve αn^β is fitted to the energy -v- time graphs instead of the linear D . The parameter β is then plotted against \hbar . The peaks in Figures 5.33 are seen to be as a result of quadratic or near quadratic energy growth around quantum resonance.

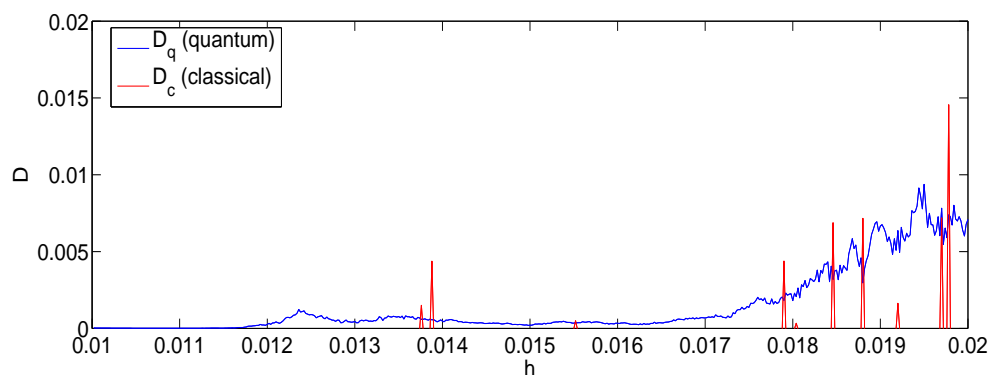
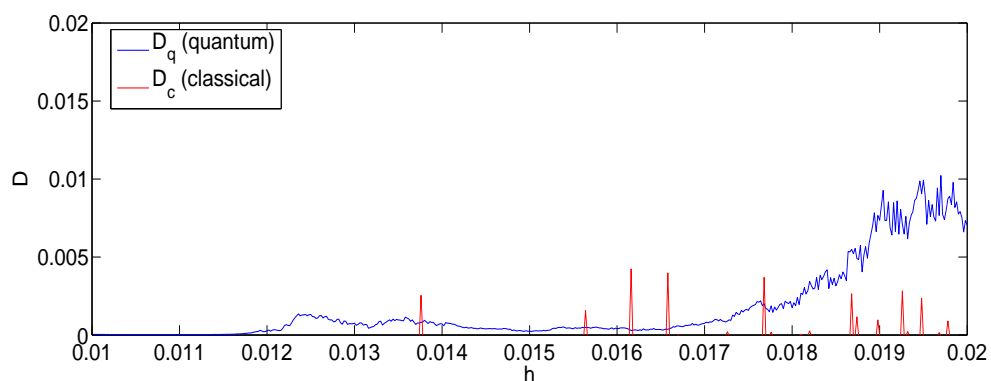
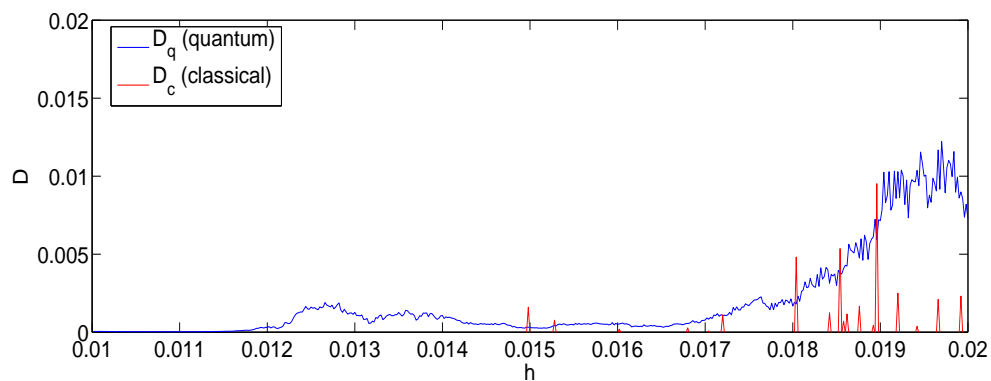
(a) $\mu = 3.14$ and $(q, p) \approx (1.56999, -1.56999)$ (b) $\mu = \pi$ and $(q, p) \approx (\pi/2, \pi/2)$ (c) $\mu = \pi$ and $(q, p) \approx (1.57149, -1.57149)$

Figure 5.35. D_q, D_c -v- \hbar for coherent states initially placed exactly on the classical period 1 stable islands. The quantum system can diffuse more easily than the classical ensemble. The red (classical) spikes serve to remind us that there is a small but finite probability that some particles in the classical ensemble will be placed outside the stable structure.

been displayed by the quantum system and while it being very unlikely that the classical ensemble would diffuse, see Figure 5.31(a). Indeed, the results of section 5.3.1.1 would even seem to suggest that tunneling in these cases has more to do with the periodic nature of the systems stationary states than stochasticity in the classical dynamics.

As for the question of whether quantum resonance plays a significant role we could point to the diffusion rate around $\hbar = 0.19$, Figure 5.35. However, it is not really possible to say if this is due to a particular resonance $\hbar = 2\pi/n'$ as the peak is broad enough to contain a number of different resonances. Nonetheless it is more evidence of tunneling between periodic islands. We examined the energy curve around this point in Figure 5.30(e). With a Hilbert space of 2^{19} dimensions we can see that the energy growth continues for at least 500 timesteps. It must be noted that at this value of \hbar some of the classical ensemble has a considerable chance of diffusing. It is therefore not possible to discount the possibility that the classical chaos plays some role in this type of diffusion.

In conclusion, there is considerable numerical evidence presented here to suggest the possibility of tunneling from between periodic islands with $\mu \approx \pi$. This agrees with our simple analysis in section 3.5.2. We were unable to see if quantum resonance significantly enhanced the tunneling rates because the values of \hbar used in these simulations are very small, and consequently the resonant values of \hbar are tightly packed together. We have also been unable to reach a conclusion on whether the tunneling is a consequence of the chaotic boundaries of the periodic islands or just a consequence of the natural periodicity in the classical phase space structure. A more detailed numerical analysis clearly required.

5.3.3 Mean energy and \hbar : Ballistic islands

In section 2.4.2 we discussed the exact mechanism responsible for the anomalous diffusion spikes shown in Figure 2.8. We analysed the stability and structure of these islands and it was made clear that the actual ballistic islands contained 2 primary stable structures. Exact expressions for the locations of these islands and the stability ranges were obtained. In the last section we examined the phenomena of quantum resonance and observed that significant increases in energy growth rates when the value of \hbar was near certain specific values. In an effort to illuminate the mechanisms responsible for this resonance we analysed some promising functional structures in section 3.5.

In this section we will compare and contrast the energy growth rates of a

quantum coherent state with a normal classical ensembles placed initially around a ballistic modes. We are particularly interested in confirming if the quantum system can exploit the classical and quantum mechanisms mentioned above to achieve super-ballistic energy growth.

It is necessary to demonstrate particular care in the following analysis. As was mentioned above the classical ballistic island is made up of 2 primary stable structures, see section 2.4.2. A particle inside one of the stable structures will jump over and back between islands upon each mapping. The analysis clearly showed then that somewhere between these islands lies an unstable chaotic region, the width of which depends on μ . Inside this region however exist a whole hierarchical of smaller less prominent modes. It is important in the analysis ahead that the precise placement and uncertainty of the quantum state be taken into account when interpreting the subsequent motion or dynamics. In particular we have to make \hbar small enough so as a coherent state should exist as much as possible inside the classical stable structure.

This is complicated even more because of the nature of ballistic motion in general. Once on a ballistic island the quantum state will rapidly move away from the phase-space origin. The evolving state will therefore reach the boundary, inside which we can accurately evolve the system, more rapidly than all of the other simulations we have documented.

In order to achieve any meaningful results the full power of the FFT technique must be used. We shall be using truncated Hilbert spaces of up to $N = 2^{22} = 4194304$ dimensions. At these sizes evolving the quantum state forward 1 time step takes typically 13s on 3GHz Pentium 4 processor with approximately 1GigaByte of RAM.

However, these time and space restrictions mean we will can only perform a few individual simulations with a few different initial conditions and parameters \hbar and μ . The results of the simulations will be therefore be presented in terms of individual energy - time graphs as opposed to the diffusion curves presented in the last section. To save space we will only present results of simulations where we have used resonant \hbar . We again stress that the sizes of the truncated Hilbert spaces have been carefully chosen so that boundary conditions *do not* play any significant role in the numerical results below.

We begin with simulations to check if the quantum system can see the anomalous islands at kick strength for which they do not exist classically. To this end we check for anomalous diffusion in the quantum system with $\mu = 2\pi - 0.05$,

see Figure 5.36. There is almost no difference between the classical and quantum short time evolution for the smaller small values of \hbar and therefore no sign of anomalous diffusion in either system. Note however with our largest value of \hbar , in Figures 5.36(d) that the quantum system experiences much more rapid growth. This can also be seen by comparing 5.36(l) with the other final states with smaller \hbar . This would not appear to be related to the anomalous islands. Notice the rapid decay of the probability distribution on the right hand side of Figures 5.36(i), 5.36(j) and 5.36(k).

We next examine the diffusion properties of the system with $\mu = 2\pi$. This is the value at which the classical anomalous diffusion has been shown to exist. As before we see a significant difference in the wavefunctions behaviour for the largest value of \hbar , see Figure 5.36(h). We also see that the rate of diffusion is much greater than when $\mu < 2\pi$ in all cases except with $\hbar = 2\pi/20$. In this case the quantum system hardly registers the change.

The logarithm of the wavefunction in the position basis reveals what appears to a an even more severe drop in the functions probability density on the right hand side, see Figures 5.36(i),5.36(j) and 5.36(k). This is interesting and seems to suggest that there is some kind of barrier preventing the quantum system diffusing in this direction. Analysis shows that this edge corresponds to where a classical particle placed on the island would be. It points to the possibility that there may be a significant barrier to faster than classical diffusion in this particular case.

We now turn our attention to values of μ for which there exists some stability in the structure of the ballistic islands, see Figures 5.37, 5.38 and 5.39. For each value of μ and \hbar we will run 2 simulations. One with the initial state centered at the center of the island and one on one of the two stable points worked out in section 2.4.2

We choose $\hbar = 2\pi/1400, 2\pi/800, 2\pi/200, 2\pi/20$ and $\mu = 2\pi + .05, 6.349972, 2\pi + 0.1$. The middle value of μ being the value where the classical system displays the most self similarity [20,21]. We plot two energy - time graphs for each setting of \hbar and μ , one for each initial condition. Also included are the corresponding plots of the wavefunctions probability distribution after 40 time steps.

We first consider the situation when $\mu = 2\pi + 0.05$. The structure of the classical island for this parameter is shown in Figure 2.15. With $\hbar = 2\pi/1400$ we see that within the time limits that we can view the system the classical and quantum diffusion curves are almost identical, see Figure 5.37(a) and 5.37(e). We can see

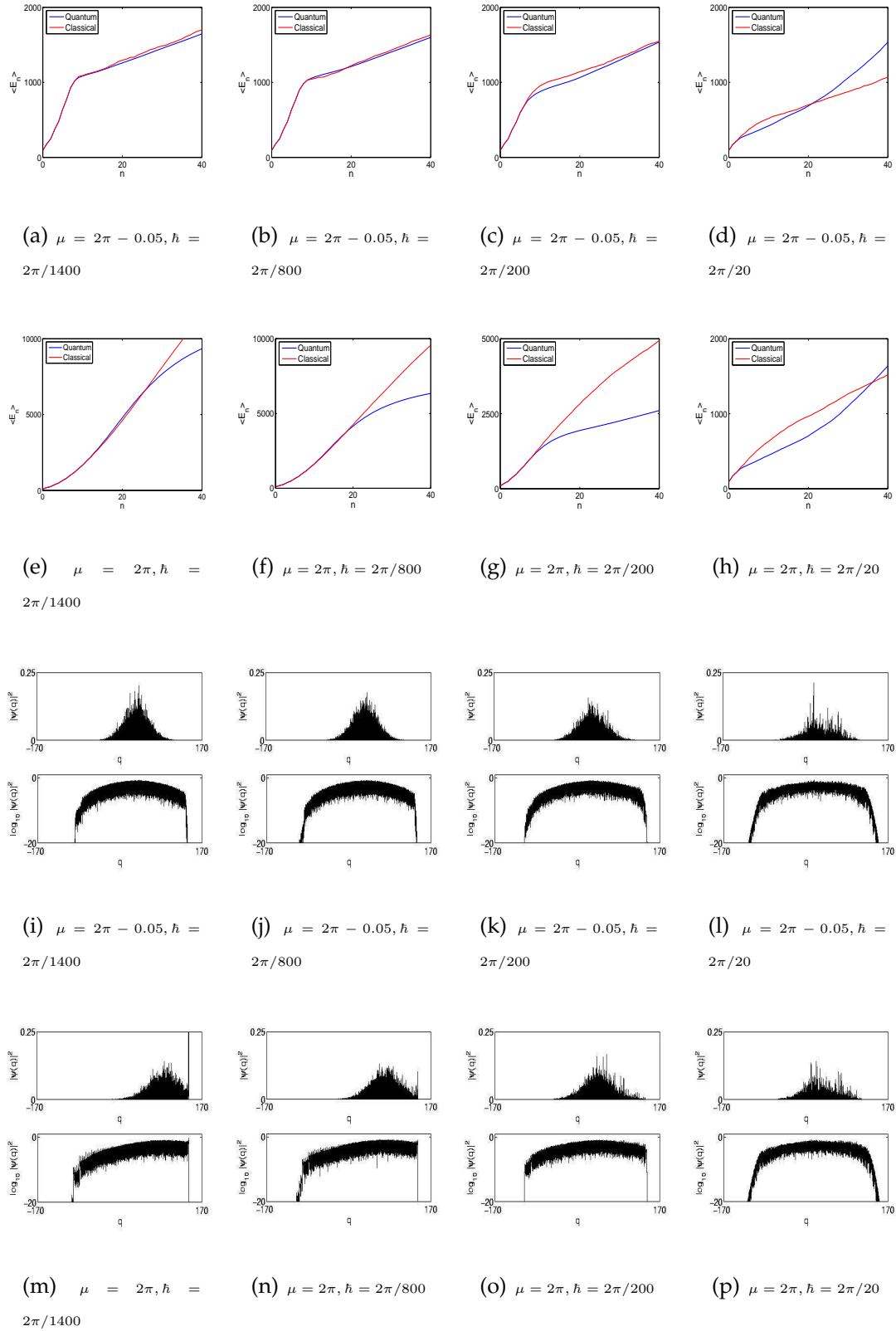


Figure 5.36. (a)-(h) E - v - n . (i)-(p) Final probability distribution in position basis after 40 iterations of the quantum map. We use a discretised Hilbert space of 2^{22} dimensions in all calculations

that whether the initial state is placed over the center of the island or over one of the stable points does not seem to make a difference either. However when we increase the value of \hbar we see that the quantum state placed over the center of the island, that is on the unstable line between the two classical stable islands, has a lesser energy growth rate than that of the classical system, see Figure 5.37(b). Only when we increase \hbar further do we see this effect when the quantum system is placed exactly over an elliptic stable point. The two classical and the two quantum diffusion curves are nearly identical when $\hbar = 2\pi/20$, see 5.37(d) and 5.37(h). This is expected as the initial distributions, relative to the size of the classical islands, are quite broad.

We next consider the situation when $\mu = 6.349972$. This is where Iomin and Zaslavsky found rapid growth in the kicked Harper model [20,21]. We see some evidence of the centered quantum system diffusing more rapidly than the classical system with $\hbar = 2\pi/1400$. Comparing this with the same situation with $\mu = 2\pi + 0.5$ we have no evidence to suggest anything fundamentally different occurring with this particular value of μ as the quantum system diffuses almost exactly as fast. However, comparing Figures 5.37(f) and 5.38(f) we do see a difference. With $\mu = 2\pi + 0.05$ the quantum energy growth seems to slow down. However, with $\mu = 6.349972$ this growth appears more quadratic. We have confirmed this with simulations over 80 time steps although we do not show this here. It also must be said however that the situation is much different when $\hbar = 2\pi/200$. Indeed, at these values the energy growth with $\mu = 2\pi + 0.5$ is greater than with $\mu = 6.349972$. This has also been checked over 80 time steps.

We also see little evidence of significant increases in the energy growth rates when the states are placed exactly over the stable islands. In fact the energy growth is nearly the same or higher when $\mu = 2\pi + 0.05$. This is perhaps not unexpected as the reason given for the increase in the quantum diffusion is related to the self similarity and stickiness inside the chaotic regions. Placing a state primarily around a stable elliptical fixed point is not the best way to examine this phenomena.

We finally examine the situation when $\mu = 2\pi + 0.1$. At this point the two stable islands that make up each accelerator mode have moved quite far apart, see Figure 2.15 and there is a significant difference between diffusion curves placed on a stable point and that placed on the unstable center of the island. We see that, as expected, in both the classical and quantum cases the subsequent diffusion rates are far less for initial states centered on the unstable center. We see

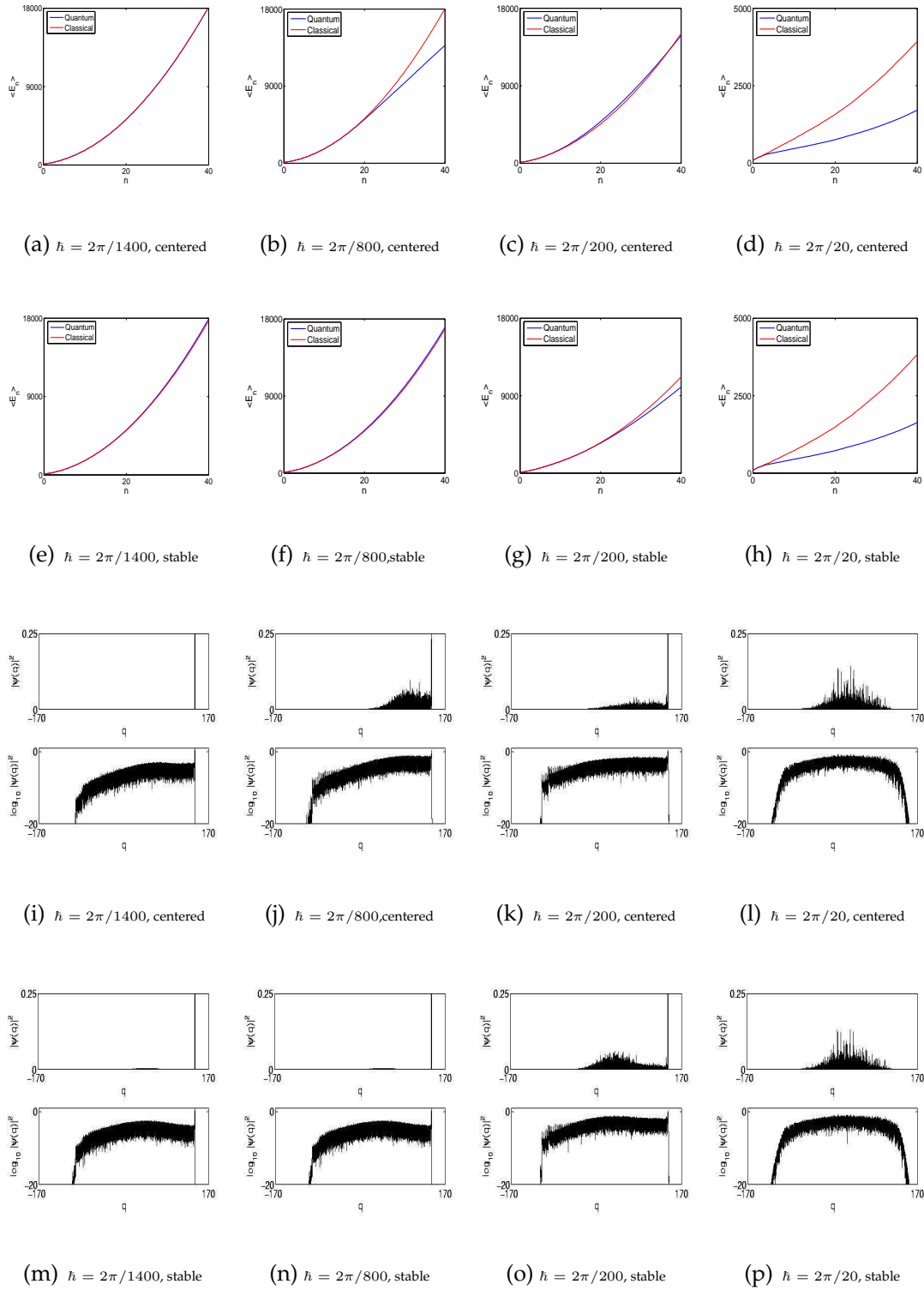


Figure 5.37. $\mu = 2\pi + 0.05$, (a)-(h) E - v - n . (i)-(p) Final probability distribution in position basis after 40 iterations of the quantum map. We use a discretised Hilbert space of 2^{22} dimensions in all calculations

however that in this case, as in the last, the quantum growth is greater than the classical growth when $\hbar = 2\pi/1400$. Moreover, unlike when $\mu = 6.349972$, the quantum growth is also greater than the classical growth when $\hbar = 2\pi/800$. This is hardly conclusive but it does at least suggest once again that there is really nothing special quantum mechanically about diffusion rates at $\mu = 6.349972$.

In all of the figures with $\mu \geq 2\pi$ we have evidence of a hard boundary preventing tunneling to higher energy accelerator modes. There is a very obvious rapid drop in the probability distribution to below $10^{1/20}$ on the right hand side. In all cases this drop off seems to end at around $10^{1/24}$. Since this is the wavefunction squared this means that the wavefunction beyond these edges is zero down to the twelfth decimal. This is just above the machine precision of $10^{1/16}$ that we have been using. This is not to say that the energy growth of the quantum system cannot grow faster than the classical ensemble under certain conditions. However, the fastest possible classical growth is found when we place the ensemble with very small marginals inside one of the stable islands. In none of the cases shown, and the hundreds of other simulations which we have not shown, have we ever seen the quantum system diffuse faster than this classical rate.

This is not conclusive proof of course. In order to fit the coherent states and classical ensemble inside the island we have had to make \hbar very small. This in turn reduces the amount of time over which we can evolve the system before we run into boundary effects while simultaneously making the quantum system behave more classically. However this leaves open the possibility that, after time, some quantum effects may begin to take over and we may get tunneling and therefore faster than classical energy growth. In order to lend perhaps some weight to possibility we plot in Figure 5.40 the logarithm of the wavefunction initially on a stable island with $\mu = 2\pi + 0.05$ and $\hbar = 2\pi/200$. We use an effective grid size of 2^{23} and evolve then system over 100 time-steps. Of course the wavefunction has begun to spread out and the diffusion is much less than the highest rate of classical diffusion we have found. However, we do have the possibility that the quantum system can reach areas of the phase space faster than that of the classical ensemble. Indeed it is not unreasonable to assume that were we able to evolve the quantum system for long enough and with small enough \hbar so that the quantum system can tunnel to other islands of higher energy while remaining entirely on accelerator modes. However it must be stressed that there is a significantly greater probability for the state to tunnel to modes of lesser energy. We shall leave any further speculation until the conclusion.

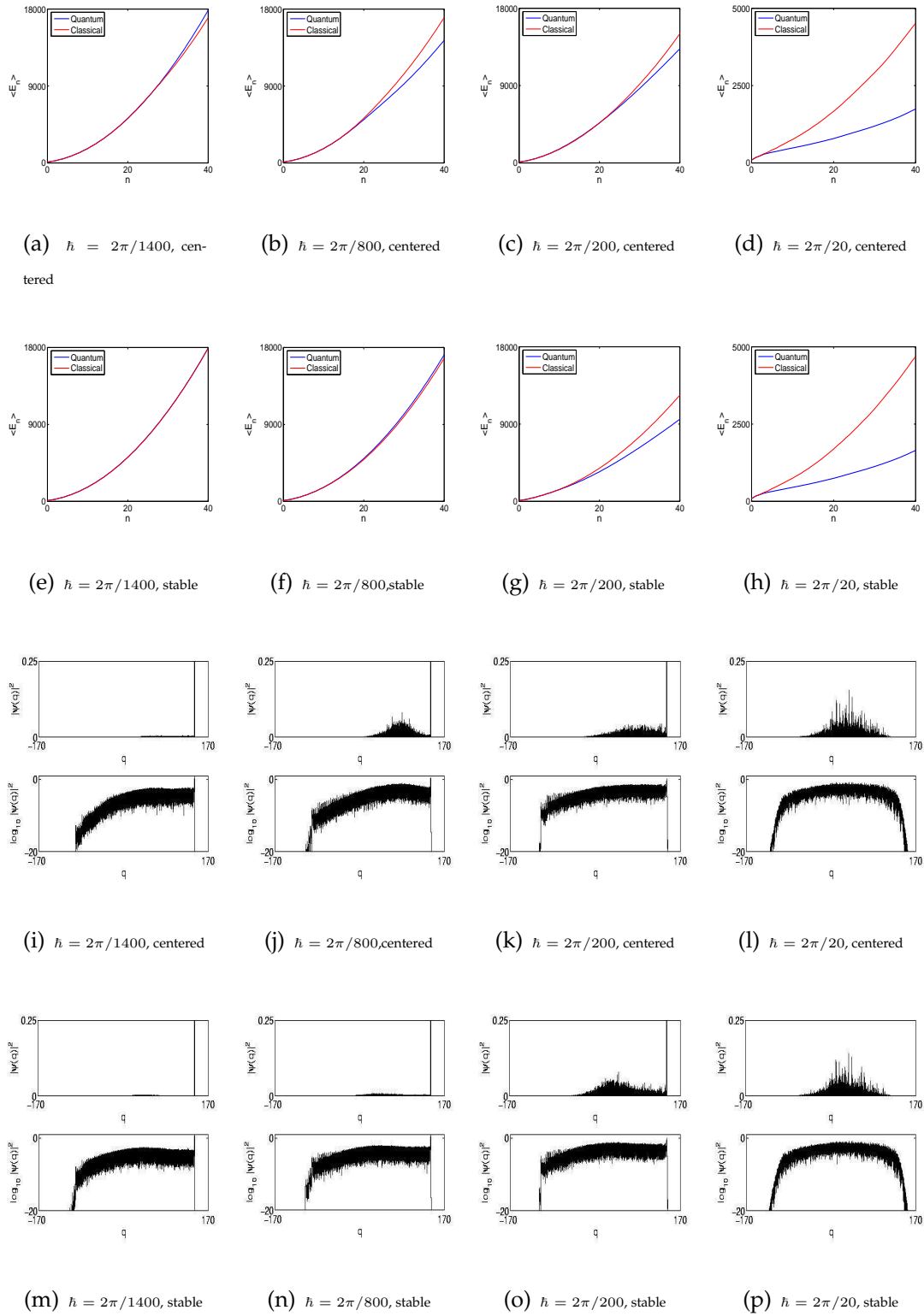


Figure 5.38. $\mu = 6.349972$, (a)-(h) E -v- n . (i)-(p) Final probability distribution in position basis after 40 iterations of the quantum map. We use a discretised Hilbert space of 2^{22} dimensions in all calculations

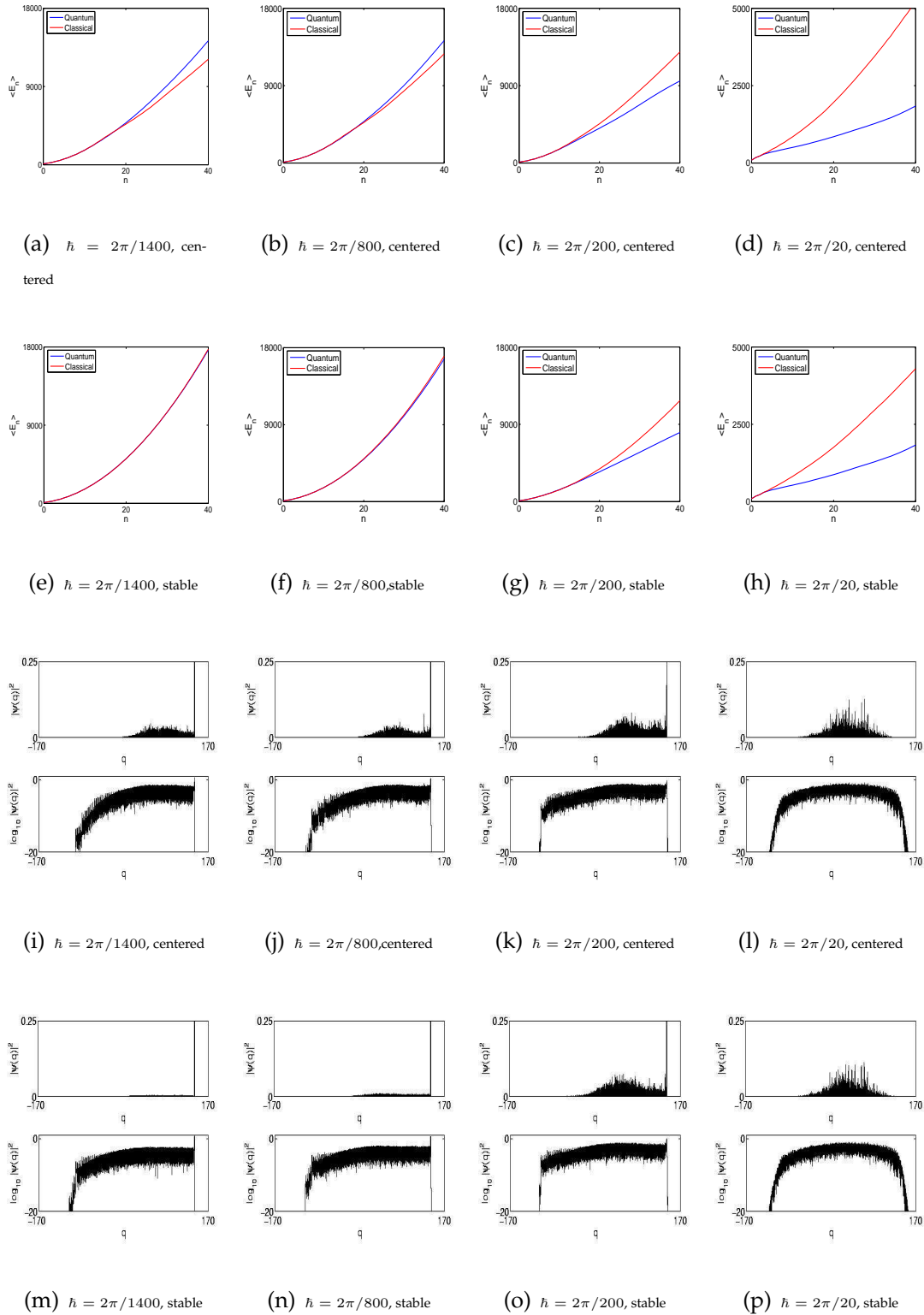
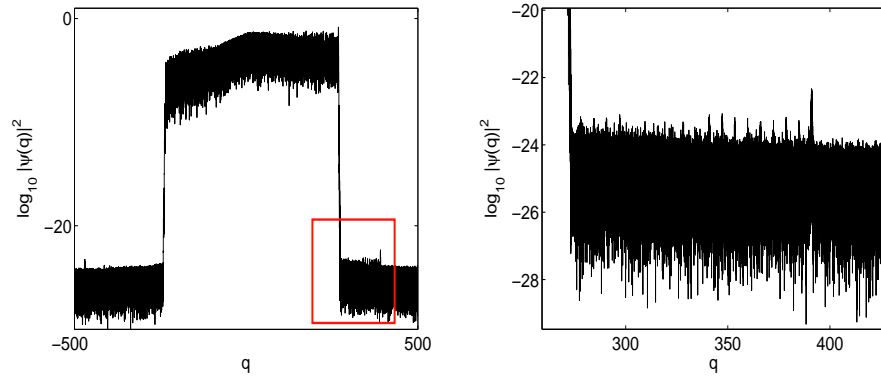


Figure 5.39. $\mu = 2\pi + 0.1$ (a)-(h) E -v- n . (i)-(p) Final probability distribution in position basis after 40 iterations of the quantum map. We use a discretised Hilbert space of 2^{22} dimensions in all calculations



(a) The state has a significant probability of tunneling to lower energy accelerator modes

(b) There is some evidence of tunneling to higher energy modes.

Figure 5.40. $\log_{10} |\psi(q', 100)|^2$ versus q' with $\hbar = 2\pi/200$ and $\mu = 2\pi + 0.05$ after 100 iterations of the quantum map. There seems to be barrier that prevents tunneling to higher energy modes. However, it is not possible to rule out tunneling to higher energy modes altogether.

5.4 Conclusion

We began this chapter by visually comparing the evolution of a quantum coherent state with that of a normally distributed classical ensemble. We then emphasised the effect that \hbar had on the simulations for the delta kicked harmonic oscillator with irrational frequency ratio. We determined that an initial minimum uncertain state would remain localised even after the a classical ensemble had begun to diffuse throughout the phase plane. However, we saw that this did not remain the case when we increased the value of the kicking parameter μ and reduced \hbar .

The diffusional properties of the quantum system with irrational frequency ratio were then examined and compared them with those of the classical system. The quantum system was shown to display some localisation at values of μ for which all effective KAM boundaries had vanished. We also showed that this suppression is somewhat linearly dependent on \hbar and has effectively vanished for $\hbar = 0.25$. These numerical calculations also show that the localisation effect also depends on the kick strength μ being small enough. The results agreed with our additional comments on the limit of the accuracy of the tight-binding approximation in section 3.4.1.

The new fractional Fourier transform method was then used to calculate a matrix representation of the Floquet operator in the position basis. We used a brute force LAPACK method of diagonalizing these matrices to see what information we could gather about the systems stationary states and quasi-energies. We visually examined the Husimi distributions of the stationary states and found remarkable structural similarity between these distributions and the classical Poincaré surface of section.

We then used the some standard techniques to analyse the systems stationary states and examine the extent of their extended nature. The results suggested clearly that as we increased μ and decreased \hbar the stationary states became more extended. We also examined the systems nearest neighbour quasi-energies level distribution and found a clear drift from the Poissonian level statistics to the Wigner statistic associated with quantum chaos and extended states as we increased μ and decreased \hbar . This once again suggested there was a limit to the validity of the tight-binding approximation.

We then turned our attention to the case where the two frequencies of the system were resonant and in particular where $1/R = 1/4$. Using the same method as in the irrational case we numerically calculated the systems stationary states. We showed that, in the cases of quantum resonance, the eigenstates have the periodic delta train structure predicted in section 3.4.2. The Husimi distributions for these states in resonance also show that the periodicity extends in many different quadratures in the phase plane. We also tried to show some particular examples of some stationary states that resembled superpositions of displaced Fock states analysed briefly in section 3.5.2. We also provided examples of completely localised states on the period 1 islands and examples where, under quantum resonance, this broke down. These situations we're all predicted analytically in section 3.5.2.

We also found evidence of eigenstates existing primarily around the classical ballistic islands that were also predicted in section 3.5.2. We were unable to find any evidence of eigenstates on accelerator modes when \hbar was not resonant with 2π . This point was also predicted in our analysis.

The diffusive behaviour of the quantum system as a function of \hbar was then examined. This was done for several initial conditions and with several different values of the kicking strength μ . We showed the well known tunneling effect and established that it is profoundly affected by the value of \hbar . Indeed we found that the quantum resonance effect is all round much more obvious than

had previously been shown. We have provided significant evidence suggesting that the value of \hbar need not fulfill the resonant condition, (3.61), exactly for significant increases in diffusion rates to take place. This effect was observed regardless of initial condition and value of μ . It was to try and explain this effect in a more quantitative way that led us to study the Self Fourier Functions in section 3.5.

The diffusion rates of the quantum system placed initially on the classical period 1 islands was also examined. In particular we wanted to see if the quantum system could tunnel to other periodic islands. We established that this could indeed happen but noticed that we were unable to see any definitive quantum resonance effects.

We finally gave a detailed examples of the initial behaviour of the quantum system placed around the classical accelerator modes. It was demonstrated that under certain conditions the quantum system could diffuse faster than the classical ensemble. It was seen that the quantum system could easily tunnel to other accelerator modes provided they had a lower energy than the main part of the wave-packet. There is a significant barrier preventing quantum diffusion at a faster rate than that of a classical ensemble entirely contained within the ballistic islands stable structure. Despite this we did however demonstrate that there was some evidence of tunneling to higher energy modes but that this was many orders of magnitudes less than that of the tunneling to lower energy modes.

I believe that the overall worth of the numerical method has been effectively demonstrated. It has confirmed, sometimes spectacularly, with all of the analytical tests we had time to compare it with. It has also, when asked to do so, agreed with any of the other numerical examples given in the literature.

In what I feel is one of the biggest tests of the numerical setup we have shown the exact periodicity of stationary states when $1/R = 1/4$ and $\hbar = 2m\pi/k^2n$. As well as this, these states are made up of trains of delta functions as predicted and their Husimi distributions are translationally invariant in many different directions in phase space. The procedure also clearly shows the existence of the quantum resonance and quadratic energy growth but also shows that this type of growth can also occur for values of \hbar near resonance. The final demonstration of analysing the quantum dynamics on the accelerator modes over 40 time-steps with $\hbar = 2\pi/1400$ can only be done using an effective grid size of 2^{22} and took approximately 7 minutes on a *Pentium4*. While the split step method, see section B.1, could possibly have performed a similar calculation it would have to have

taken thousands of times longer to achieve the same accuracy. Indeed, using our technique the same simulation using effective grid sizes of 2^{23} takes about an hour and would take weeks to accomplish using the split step method. Of course the differences are much less pronounced when we are dealing with the irrationally kicked system as the fast fractional Fourier transform takes up more time than the ordinary fast Fourier transform. However, as we have seen there is at most linear growth in the quantum system and the memory and efficiency requirements are therefore not the same.

In conclusion, we now have a technique that hand in hand with a reasonably fast computer can now analyse the dynamics of the kicked harmonic oscillator several orders of magnitude more efficiently than has previously been possible. We have tested this method and found that it has confirmed and improved upon much of the numerical data already available as well as placing limits on some of the available analytical results. I believe that this can become a very valuable tool in the general study of stochasticity in non KAM quantum systems.

References

- [1] F. Borgonovi and L. Rebuzzini, *Translational invariance in the kicked harmonic oscillator*, Phys. Rev. E **52**, 2302 (1995).
- [2] G. Kells, J. Twamley and D. Heffernan, *Dynamical Properties of the delta kicked harmonic oscillator*, Phys. Rev. E **70**, 015203 (2004).
- [3] M. Engel, *On Quantum chaos, Stochastic Webs and Localization in a Quantum Mechanical Kick system*. Ph. D Thesis, 2003.
- [4] G. P. Berman, V. Yu. Rubaev and G. M. Zaslavsky, *The problem of the quantum chaos in the kicked harmonic oscillator* Nonlinearity **4**, 543 (1991).
- [5] Go. Torres-Vega, Klaus B. Møller, and A. Zúñiga-Segundo, *Role that separatrices and stochastic webs play in quantum dynamics*, Phys. Rev. A **57**, 771 (1998).
- [6] I. Dana, Phys. Rev. Lett. **73**, 1609 (1994).
- [7] R. Ketzmerick, K. Kruse and T. Geisel, *Efficient diagonalization of kicked quantum systems* Physica D **131** 247 (1999).
- [8] A. R.R. Carvalho and A. Buchleitner, *Web-Assisted Tunneling in the Kicked Harmonic Oscillator*, Phys. Rev. Lett. 204101 (2004)
- [9] D. Shepelyansky and C. Sire, *Europhys. Lett.* **20** (2) 95 (1992).
- [10] M. Frasca, *Quantum kicked dynamics and classical diffusion*. Physics Lett. A **231**, 344 (1997).
- [11] D.R. Grempel, S. Fishman and R.E. Prange, *Localization in an incommensurate potential: An exactly solvable model*. Phys. Rev. Lett. **49**, 833 (1982).

- [12] P. W. Anderson, *Absence of diffusion in certain in random lattices*. Phys. Rev. **109**, 1492 (1958).
- [13] P. W. Anderson, *Localized magnetic fields in metals*. Phys. Rev. **124**, 41 (1961).
- [14] F. Haake, *Signatures of Quantum Chaos* vol. 54 of *Springer Series in Synergetics*, (Springer-Verlag, Berlin, 2nd edition 2001).
- [15] H. -J. Stöckman, *Quantum Chaos. An Introduction.*, (Cambridge University Press, Cambridge 1999).
- [16] R. Badrinarayanan and J. V. José, *Spectral properties of a Fermi Accelerating disk* pg 589 of *Quantum Chaos* [17].
- [17] G. Casati and B. Chirikov, *Quantum Chaos: between order and disorder* (Cambridge University Press 1995)
- [18] F. M. Israilev, J. Phys. **A22**, 865 (1989).
- [19] M. L. Mehta, *Random Matrices (2nd eddition)*, (Acedemic Press, San Diego, California 1991).
- [20] A. Iomin and G.M. Zaslavsky, *Heirarchical structures in the phase space and fractional kinetics: Immense delocalizaton in quantized systems* Chaos **10**, 147 (2000).
- [21] A. Iomin and G.M. Zaslavsky, *Quantum manifestation of Lévy-type flights in a chaotic system*, Chemical Physics **284**, 3 (2002)

Chapter 6

Conclusion and perspectives

I will conclude the manuscript with a general review of what has been achieved in this thesis. I will highlight what I feel are its major accomplishments as well as pointing out where there is room for further studies.

In Chapter 2 I examined the classical problem from a slightly different perspective. I tried to be mostly original in my analysis of the system's general properties. However originality can sometimes come at the expense of clarity. With this in mind I tried to find a balance between other authors material and my own.

There are a few contributions that I believe to be noteworthy. Firstly I feel that that by moving to a coordinate system where the momentum and position scales are the same is extremely useful. I also feel that it is important for this transformation to be canonical if the solutions are to be ever related to physical reality. Many authors find it useful to move to a dimensionless coordinate system but the transformations used to do this are no longer canonical.

Secondly is the discussion on the behaviour of the system with irrational frequency ratio. It was stressed that the KAM theorem cannot be applied in this case yet the system for all intents and purposes behaves exactly like a KAM system. This is an interesting contradiction and one that could be further explored.

Several attempts to apply simple stability analysis to the problem have been made. The analysis showing the instantaneous organisation of the phase space pattern under infinitesimal perturbation is, as far as I know, original. The stability analysis of the ballistic modes is also original and I believe gives a result that was previously unknown. It might be possible to find the exact stability conditions for other structures of the map but I do not see any real need for this to be done.

As I have repeatedly mentioned in Chapter 3, the problem of the quantum kicked delta harmonic oscillator is deceptively difficult. I felt that in order to be able understand the quantum manifestations of classical problems it would be useful to try work in the same coordinates as the classical mapping. This eventually led us to the Fractional Fourier transform method which was the basis of the entire thesis. The derivation connecting the transform with the evolution operator of the SHO at the start of Chapter 3 is entirely my own.

With regards to actually studying the perturbed quantum system it was felt that like all quantum problems, the dynamics would be best understood by examining the eigensolutions. We started by giving a detailed review of the work by Frasca and independently by Engle for irrational frequency ratios. It was pointed out that the tight-binding approximation could only be valid under certain conditions. We later backed up this assertion with concrete numerical evidence.

The work of Borgonovi and Rebuzzini, showing translational invariance for certain rational frequency ratios and the relationship between one and two parameter translation groups and linear and quadratic energy growth, was reviewed. The analysis of Engle was relied upon here also. Our approach to the problem was to try to take some property of the system, e.g. the classical phase structure, quantum resonance/translational invariance, and try to find an analytical function that was an approximate eigensolution and could be used to explain that property. This led us to consider three separate but related functional forms, namely the Dirac delta comb, the superpositions of Fock states and the hybrid double Gaussian states. While we were able to give specific instances where these functions were approximate eigenstates of the system we were unable to find any general solution to the problem or, except in special limiting cases, show that any of the functions could be used to form a complete basis. It was hoped that a general function could be found that would have each of the above functional forms as a special case. Unfortunately we were unable to establish the relationships in the correct context and in this respect the chapter is incomplete. However, I have established definite links between the different functions and I believe that a more concentrated effort in this direction may provide more satisfying results.

The most important aspect of this study was the realisation that the Fast Fourier transform and the Fast Fractional Fourier transform were precisely the evolution operators of the free evolution of the harmonic oscillator written in the position basis. Using this method we were able to develop a numerical algorithm

to simulate the quantum dynamics of the kicked system with greater accuracy and for longer times than were previously possible. This allowed us to accurately probe the kicked system with smaller values of the quantum parameter \hbar than other studies.

In this way the effects of certain classical structures could be seen in the actual quantum dynamics. As well as this, the simple control that we have over the parameter \hbar has also allowed us to illuminate purely quantum phenomena in much more detail than before. Among other things, the model clearly shows the \hbar dependence of the quantum suppression of energy growth in the irrational frequency ratio case. The model also suggests that linear energy growth in the $1/4$ quantum system is more the exception than the norm and that quantum suppression may even exist for certain specific values of \hbar .

We have given a comprehensive numerical analysis of the quantum system in the situations that have attracted most attention in the field. Namely the system with rational frequency ratio $1/4$ and with irrational frequency ratio $2/(\sqrt{5} + 1)$. We examined the actual dynamics as well as the numerically calculated eigen-solutions. It could be argued that I would have been better served by concentrating more specifically on some particular property like the quantum manifestation of classical resonance. However, it was strongly felt that we should try to demonstrate the applicability of the algorithm to a wide range of quantum and classical phenomena.

The numerical explorations of this fascinating system are sparse and are scattered throughout the literature. This thesis attempts to provide a fuller, self contained and more detailed exploration of the system. It is comforting to know that in specific situations where we have been able to compare our results with others they have been of a similar nature. However, due to the power of our algorithms we have been able to present these previous results in a broader context. While doing this was at times tedious it will hopefully provide a useful starting point to anyone wishing to understand the global behaviour of the quantum system.

Appendix A

The Simple Harmonic Oscillator

A.1 The Simple Harmonic Oscillator

The problem of finding the energy eigensolutions for the simple harmonic oscillator is included in all introductory text books on quantum mechanics. Our analysis here follows closely that found in [1] only using the more symmetrical Hamiltonian operator derived in chapter 2. This symmetry is essential for easily understanding many of the properties of the KHO and the numerical methods outlined in chapter 4. We begin with the symmetrical Hamiltonian derived in chapter 2:

$$\mathcal{H}_0(q, p) = \frac{\omega_0}{2} (p^2 + q^2). \quad (\text{A.1})$$

In this case \mathcal{H}_0 , p and q are understood to be operators. The next step is to introduce the slightly different annihilation and creation operators

$$a = \sqrt{\frac{1}{2\hbar}}(q + ip) \quad a^\dagger = \sqrt{\frac{1}{2\hbar}}(q - ip) \quad (\text{A.2})$$

or equivalently

$$q = \left(\sqrt{\frac{\hbar}{2}}\right) (a^\dagger + a) \quad p = \left(\sqrt{\frac{\hbar}{2}}\right) i(a^\dagger - a) \quad (\text{A.3})$$

Using the canonical commutation relation

$$[q, p] = i\hbar \quad (\text{A.4})$$

we can easily show that

$$[a, a^\dagger] = \left(\frac{1}{2\hbar}\right) (-i[q, p] + i[p, q]) = 1. \quad (\text{A.5})$$

With the introduction of the the number operator

$$N = a^\dagger a, \quad (\text{A.6})$$

with eigenvectors and eigenvalues defined by

$$N|n\rangle = n|n\rangle, \quad (\text{A.7})$$

we can write

$$\mathcal{H}_0 = \omega_0 \left(\frac{p^2 + q^2}{2}\right) = \frac{\hbar\omega_0}{2}(aa^\dagger + a^\dagger a) = \hbar\omega_0(N + 1/2), \quad (\text{A.8})$$

where we used (A.3), (A.5) and (A.6).

We now solve the Schrödinger equation (SE) in the usual way to find the time evolution operator. The state vector for the system must obey the SE , that is

$$i\hbar\frac{\partial}{\partial t}|\psi(t)\rangle = \mathcal{H}_0|\psi(t)\rangle. \quad (\text{A.9})$$

Integrating from $t = 0$ to T we have

$$|\psi(T)\rangle = \mathcal{U}_0(T)|\psi(0)\rangle = \exp(-i\mathcal{H}_0T/\hbar)|\psi(0)\rangle, \quad (\text{A.10})$$

where $\mathcal{U}_0(T)$ is called the evolution operator. Substituting in our Hamiltonian for the simple harmonic oscillator we have for the evolution operator

$$\mathcal{U}_0(T) = \exp\left(-\frac{i\theta}{2\hbar}(p^2 + q^2)\right) = \exp(-i(N + 1/2)\theta), \quad (\text{A.11})$$

with $\theta = \omega_0 T$.

We finally derive some results which will be needed later on. From (A.5) we can derive the commutation relations

$$\begin{aligned} [a, a^\dagger a] &= [a, N] = a, \\ [a^\dagger, a^\dagger a] &= [a^\dagger, N] = -a^\dagger. \end{aligned} \quad (\text{A.12})$$

Now, by definition, an operator in the Heisenberg picture may be gotten from one in the Schrödinger picture by virtue of the following relation

$$A_H = \mathcal{U}_0^\dagger A \mathcal{U}_0 \quad (\text{A.13})$$

where \mathcal{U}_0 is the time evolution operator defined above. We now note that the equations of motion for a and a^\dagger in the Heisenberg picture are given by

$$\frac{da_H}{dt} = \frac{1}{i\hbar} [a_H, \mathcal{H}_H] = \frac{1}{i\hbar} [a_H, \hbar\omega_0(a_H^\dagger a_H + 1/2)] = -i\omega_0 a_H \quad (\text{A.14})$$

$$\frac{da_H^\dagger}{dt} = \frac{1}{i\hbar} [a_H^\dagger, \mathcal{H}_H] = \frac{1}{i\hbar} [a_H^\dagger, \hbar\omega_0(a_H^\dagger a_H + 1/2)] = i\omega_0 a_H^\dagger, \quad (\text{A.15})$$

where we used the commutation relations in (A.12), valid in both the Schrödinger and Heisenberg pictures. We have also denoted the Heisenberg picture with the subscript H . These equations of motion may be easily solved to get

$$\begin{aligned} a_H(t) &= a(0)e^{-i\omega_0 t} = ae^{-i\omega_0 t} = \mathcal{U}_0^\dagger a \mathcal{U}_0, \\ a_H^\dagger(t) &= a^\dagger(0)e^{i\omega_0 t} = a^\dagger e^{i\omega_0 t} = \mathcal{U}_0^\dagger a^\dagger \mathcal{U}_0. \end{aligned} \quad (\text{A.16})$$

where we have used (A.13). These relations will be very useful later on.

A.1.1 Energy-eigenvalue problem

In the last section we introduced the annihilation operator a and the creation operator a^\dagger in (A.2) and derived the commutation relations (A.12). We may substitute these relations into the eigenvalue equation (A.7) to get

$$N[a|n'\rangle] = (n' - 1)[a|n'\rangle], \quad (\text{A.17})$$

$$N[a^\dagger|n'\rangle] = (n' + 1)[a^\dagger|n'\rangle]. \quad (\text{A.18})$$

We now examine the scalar product

$$\langle n' | N | n' \rangle = \langle n' | a^\dagger a | n' \rangle = n' \langle n' | n' \rangle. \quad (\text{A.19})$$

This is the norm of the vector $a | n' \rangle$ which is ≥ 0 . This and the fact that $\langle n' | n' \rangle > 0$ means that $n' \geq 0$, or the eigenvalues n' are real and nonnegative. If we let $n' = 0$ then we must have

$$a | 0 \rangle = 0, \quad (\text{A.20})$$

since the norm of that vector is zero by (A.19). The expressions in (A.18) show that $a | n' \rangle$ is an eigenket of N with eigenvalue $n' - 1$ and that $a^\dagger | n' \rangle$ is an eigenket of N with eigenvalue $n' + 1$. This means that $a | n' \rangle$ can differ from $| n' - 1 \rangle$ by only a constant and also that $a^\dagger | n' \rangle$ can differ from $| n' + 1 \rangle$ by a constant. We can therefore have

$$a | n' \rangle = c_n | n' - 1 \rangle \quad (\text{A.21})$$

The norm of this vector from (A.19) is

$$\langle n | a^\dagger a | n \rangle = n \langle n | n \rangle = |c_n|^2 \langle n - 1 | n - 1 \rangle. \quad (\text{A.22})$$

Since $\langle n | n \rangle$ and $\langle n - 1 | n - 1 \rangle$ are both normalized to unity we choose $|c_n|$ to be \sqrt{n} . We set the arbitrary phase to zero. We can therefore write

$$a | n \rangle = \sqrt{n} | n - 1 \rangle. \quad (\text{A.23})$$

A similar calculation for the creation operator a^\dagger gives

$$a^\dagger | n \rangle = \sqrt{n + 1} | n + 1 \rangle. \quad (\text{A.24})$$

For convenience we now collect these results into one set:

$$N | n \rangle = n | n \rangle \quad (\text{A.25a})$$

$$a | 0 \rangle = 0 \quad (\text{A.25b})$$

$$a | n \rangle = \sqrt{n} | n - 1 \rangle \quad (\text{A.25c})$$

$$a^\dagger | n \rangle = \sqrt{n + 1} | n + 1 \rangle. \quad (\text{A.25d})$$

It can easily be seen that the eigenkets $|n\rangle$ of N are also eigenkets of the Hamiltonian \mathcal{H}_0 . Using (A.8) we can write for the energy eigenvalue equation

$$\mathcal{H}_0|n\rangle = E_n|n\rangle = \hbar\omega_0(n + 1/2)|n\rangle. \quad (\text{A.26})$$

To see what these vectors look like in the position basis we use (A.25b) as a starting point. Writing this out but in terms of q and p we have

$$q + ip|0\rangle = 0 \quad (\text{A.27})$$

If we take the inner product of this with eigenbra $\langle q'|$ of q we have

$$\langle q'|q + ip|0\rangle = \left(q' + \hbar\frac{d}{dq'}\right)u_0(q') = 0, \quad (\text{A.28})$$

with $u_0(q') = \langle q'|0\rangle$. Here we have used the fact that

$$\langle q'|V(p)|\psi\rangle = V\left(\frac{\hbar}{i}\frac{\partial}{\partial q'}\right)\langle q'|\psi\rangle = V\left(\frac{\hbar}{i}\frac{\partial}{\partial q'}\right)\psi(q'), \quad (\text{A.29})$$

for any smooth function V . The normalised solution to (A.28) is

$$u_0(q') \equiv \langle q'|0\rangle = \left(\frac{1}{\pi\hbar}\right)^{1/4} \exp\left(\frac{-q'^2}{2\hbar}\right). \quad (\text{A.30})$$

This is the vacuum state written in the position representation. Using (A.25d) and (A.2) we can write

$$\langle q'|a^\dagger|0\rangle = \frac{1}{\sqrt{2\hbar}}\langle q'|q - ip|0\rangle = \langle q'|1\rangle. \quad (\text{A.31})$$

Using (A.29) and (A.30) we can write

$$u_1(q') \equiv \langle q'|1\rangle = \frac{1}{\sqrt{2\hbar}}\left(q' - \hbar\frac{d}{dq'}\right)u_0(q') = \left(\frac{2}{\hbar}\right)\left(\frac{1}{\pi\hbar}\right)^{1/4}q'\exp\left(-\frac{q'^2}{2\hbar}\right). \quad (\text{A.32})$$

By doing this repeatedly we may generate all the eigenfunctions u_0, u_1, \dots in the position representation. The energy eigenfunctions of the simple harmonic oscillator are then given by

$$u_n(q') = \langle q'|n\rangle = \left(\frac{1}{(\pi\hbar)^{1/2} 2^n n!} \right)^{1/2} \exp\left(\frac{-q'^2}{2\hbar}\right) H_n\left(\frac{q'}{\sqrt{\hbar}}\right). \quad (\text{A.33})$$

where H_n represent the Hermite polynomials. We will refer to $u_n(q')$ as the Hermite-Gauss (HG) polynomials.

A.1.2 Coherent States

We define the coherent state as the eigenvector of the non-hermitian operator a . We write down the eigenvalue problem

$$a|\alpha\rangle = \alpha|\alpha\rangle \quad (\text{A.34})$$

We expand out this expression using the completeness relation for the Fock basis:

$$|\alpha\rangle = \sum_{n=0}^{\infty} |n\rangle \langle n|\alpha\rangle \equiv \sum_{n=0}^{\infty} c_n(\alpha) |n\rangle. \quad (\text{A.35})$$

where $c_n(\alpha) = \langle n|\alpha\rangle$ is the transformation between number and coherent state representations. Substitution of (A.35) into (A.34) gives

$$a|\alpha\rangle = \sum_{n=1}^{\infty} c_n(\alpha) \sqrt{n} |n-1\rangle = \sum_{n=0}^{\infty} \alpha c_n(\alpha) |n\rangle, \quad (\text{A.36})$$

where we have also used (A.25c). We may shift indices to write this as

$$\sum_{n=0}^{\infty} c_{n+1}(\alpha) \sqrt{n+1} |n\rangle = \sum_{n=0}^{\infty} \alpha c_n(\alpha) |n\rangle. \quad (\text{A.37})$$

We now multiply both sides from the left by $\langle m|$ to obtain

$$c_{n+1}(\alpha) \sqrt{n+1} = \alpha c_n. \quad (\text{A.38})$$

Iterating forward from c_0 we can therefore write

$$c_n(\alpha) = \frac{\alpha^n}{\sqrt{n!}} c_0. \quad (\text{A.39})$$

Looking back to (A.35) we can therefore write out the coherent state $|\alpha\rangle$ as a summation of number states, that is

$$|\alpha\rangle = c_0 \sum_{n=0}^{\infty} \frac{\alpha^n}{\sqrt{n!}} |n\rangle. \quad (\text{A.40})$$

The value of c_0 is chosen so that

$$\begin{aligned} \langle\alpha|\alpha\rangle = 1 &= |c_0|^2 \sum_{n=0}^{\infty} \sum_{m=0}^{\infty} \frac{\alpha^{*m} \alpha^n}{\sqrt{n!m!}} \langle m|n\rangle \\ &= |c_0|^2 \sum_{n=0}^{\infty} \frac{(|\alpha|^2)^n}{n!} \\ &= |c_0|^2 \exp |\alpha|^2. \end{aligned} \quad (\text{A.41})$$

We then have for the coefficients c_n :

$$\langle n|\alpha\rangle = c_n(\alpha) = \exp(-1/2|\alpha|^2) \frac{\alpha^n}{\sqrt{n!}}. \quad (\text{A.42})$$

The final form for the coherent state in the number basis is

$$|\alpha\rangle = e^{-1/2|\alpha|^2} \sum_{n=0}^{\infty} \frac{\alpha^n}{\sqrt{n!}} |n\rangle. \quad (\text{A.43})$$

To write out the coherent state in the position basis we start with the definition of a in terms of position and momentum (A.2) and the eigenvalue equation (A.34),

$$\begin{aligned} a|\alpha\rangle &= \alpha|\alpha\rangle \\ &= \frac{1}{\sqrt{2\hbar}}[q + ip]|\alpha\rangle. \end{aligned} \quad (\text{A.44})$$

Taking the scalar product with the bra $\langle q' |$ we have

$$\langle q' | q + ip | \alpha \rangle = \sqrt{2\hbar} \alpha \langle q' | \alpha \rangle. \quad (\text{A.45})$$

We again evoke (A.29) to get

$$\left[\frac{q'}{\hbar} + \frac{d}{dq'} \right] \langle q' | \alpha \rangle = \sqrt{\frac{2}{\hbar}} \alpha \langle q' | \alpha \rangle. \quad (\text{A.46})$$

This can be manipulated to get

$$\frac{d\langle q'|\alpha\rangle}{\langle q'|\alpha\rangle} = \left[\sqrt{\frac{2}{\hbar}}\alpha - \frac{q'}{\hbar} \right] dq', \quad (\text{A.47})$$

which on integration yields

$$\langle q'|\alpha\rangle = C \exp \left[-\frac{q'^2}{2\hbar} + \sqrt{\frac{2}{\hbar}}\alpha q' \right], \quad (\text{A.48})$$

where C is a constant of integration. We find this constant C by requiring that the state $\langle q'|\alpha\rangle$ be normalised. That is,

$$\int_{-\infty}^{\infty} |\langle q'|\alpha\rangle|^2 dq' = 1. \quad (\text{A.49})$$

We first calculate $|\langle q'|\alpha\rangle|^2$. From (A.48) we have

$$\begin{aligned} |\langle q'|\alpha\rangle|^2 &= |C|^2 \exp \left[-\frac{q'^2}{\hbar} + \sqrt{\frac{2}{\hbar}}(\alpha + \alpha^*)q' \right] \\ &= |C|^2 \exp \left\{ -\left[\sqrt{\frac{q'}{\hbar}} - \frac{(\alpha + \alpha^*)}{\sqrt{2}} \right]^2 + \frac{(\alpha + \alpha^*)^2}{2} \right\}, \end{aligned} \quad (\text{A.50})$$

where we complete the square in the exponent. We now use the well known result

$$\int_{-\infty}^{\infty} e^{-(x-\zeta)^2} dx = \sqrt{\pi}. \quad (\text{A.51})$$

to get

$$|\langle q'|\alpha\rangle|^2 = |C|^2 \sqrt{\pi\hbar} e^{1/2(\alpha+\alpha^*)^2} = 1. \quad (\text{A.52})$$

We therefore have for the constant C ,

$$C = \left(\frac{1}{\pi\hbar} \right)^{1/4} e^{-1/4(\alpha+\alpha^*)^2 + i\theta}. \quad (\text{A.53})$$

where θ is an arbitrary real phase. We can choose the phase $\theta = \frac{i}{4}(\alpha^2 - \alpha^{*2})$ so that

$$C = \left(\frac{1}{\pi\hbar}\right)^{1/4} e^{-1/2(|\alpha|^2 + \alpha^2)}. \quad (\text{A.54})$$

If we substitute this expression into (A.48) we have the final and very useful expression for a coherent state in the position representation

$$\langle q'|\alpha\rangle = \left(\frac{1}{\pi\hbar}\right)^{1/4} \exp\left[-\frac{q'^2}{2\hbar} + \sqrt{\frac{2}{\hbar}}\alpha q' - \frac{1}{2}|\alpha|^2 - \frac{1}{2}\alpha^2\right]. \quad (\text{A.55})$$

This expression is most important. In chapter 5 we numerically compare the classical evolution of an ensemble of particles with the quantum evolution of a coherent state. It is also used in section 3.5.2 when we look for approximate eigenstates of the kicked system.

References

- [1] W. H. Louisell, *Quantum statistical properties of radiation*. (Wiley & Sons 1990).

Appendix B

The Split Step Method

B.1 The Split Step Method

The Split Step Procedure is a way of accurately evolving a quantum state in a complicated potential extremely efficiently. The key to this method is the invention of Fast Fourier Transform which allows one to jump between discrete position and momentum bases with minimum effort. As an example we consider the evolution operator of the SHO, see (A.11), written in terms of position and momentum operators

$$\mathcal{U}_0(t) = \exp\left(\frac{-i\omega_0(p^2 + q^2)t}{2\hbar}\right) \quad (\text{B.1})$$

The difficulty with the evolution of the quantum harmonic oscillator arises because the Hamiltonian of the system is dependent on both the position q and the momentum p . Therefore, \mathcal{U}_0 contains terms of both the position basis and momentum basis and is consequently diagonal in neither. However, it is well known that changing between the position and momentum basis can be done through Fourier Transforms. This fact is used to great advantage in the split step method [2]. In this method the exact operator \mathcal{U}_0 , applied for the small duration Δt , can be approximated by

$$\mathcal{U}'_0(\Delta t) = \exp\left(\frac{-i\Delta t p^2}{4\hbar}\right) \exp\left(\frac{-i\Delta t q^2}{2\hbar}\right) \exp\left(\frac{-i\Delta t p^2}{4\hbar}\right) \quad (\text{B.2})$$

where we use the Fast Fourier Transform (FFT) [1], to perform the change of basis, see section 4.4. Although this method is not exact, the error is $O(\Delta t)^3$,

and can therefore be made acceptably small by an appropriate choice of Δt . The number of operations needed to evolve the system from time t to time $t + \Delta t$ is $O(N \log N)$. However, using the stability condition for the Split-Step method [3], $\Delta t < \frac{l^2}{\pi}$, where l is the grid spacing, we roughly estimate the number of operations needed to accurately evolve the system over a finite time to be of $O(N^2 \log N)$.

References

- [1] J. W., Cooley, J.W. Tukey, *An Algorithm for Machine computation of Complex Fourier Series*, Mathematics of Computation, **19**, 297 (1965).
- [2] M. D. Feit, J.A. Fleck, Jr., and A. Steiger, *J. Comput. Phys.* **47**, 412 (1982).
- [3] J. A. C. Weideman and B. M. Herbst, *Split-Step Methods for the Solution of the Nonlinear Schrödinger Equation*, SIAM J. Numer. Anal., **23** 485 (1986).

Appendix C

Quasi-Probability Distributions

C.1 Quasi-probability Distributions

In chapter 2 we use the idea of the phase space map to describe a systems global behavior. It is visually the most powerful tool we have. The idea of the phase space map stems naturally from Hamiltonian mechanics in that the two axis represent the conjugate momentum and position variables. Classically we can know a particles position and momentum exactly and therefore at any one instant we plot with a point the particles exact configuration. This particular way of examining a particles dynamics highlights the fundamental difference between quantum and classical mechanics. The Heisenberg uncertainty principle in one of its many forms asserts that we cannot know exactly the position and momentum of a particle. It therefore is impossible to speak of a quantum state existing at a certain point in phase space. However it is possible to represent quantum states as quasi-probability distribution functions that depend simultaneously on both the position q and momentum p . These functions are extremely useful for studying classical quantum correspondence.

There are a several reviews quasi-probability distributions in the literature. In particular see [1,2]. We also found useful introductions to the subject in [3–5]. However, we will concentrate solely on the numerical algorithms used to generate reliable distributions from discrete vector arrays defined in the position basis. We start form the definition of the Wigner function

$$W(q', p') = \frac{1}{\pi\hbar} \int dx e^{\frac{-2ip'x}{\hbar}} \langle q' + x | \rho | q' - x \rangle \quad (\text{C.1})$$

where $\rho = |\psi\rangle\langle\psi|$. Suppose we have a vector in our discretised position basis

$\langle q[j]|\psi\rangle$, the density matrix in the position basis is therefore

$$\langle q'[j]|\rho|q'[k]\rangle = \langle q'[j]|\psi\rangle\langle\psi|q'[k]\rangle. \quad (\text{C.2})$$

On close inspection of (C.1) we see that each integration is similar to that of a Fourier transform but with an extra factor of 2 in the exponential. Much of the work from section 4.2 is also directly applicable here. In particular we can simulate what was originally a continuous Fourier transform with a FFT. Ignoring the factor of 2 for the moment we need to be clear about what vectors we are performing the *FFT's* on. The limits on the integration over x are now the maximum and minimum values of the vector $q[j]$, see (4.12). This means that some of the elements $\langle q'+x|\rho|q'-x\rangle$ fall outside the range for which ρ is defined. We illustrate this in Figure C.1 for a simplistic 8×8 density matrix. These extra values are set to zero, this is called *padding* in the literature.

In order to incorporate the factor of 2 into the exponential we oversample the vectors. The vectors are indicated in the figure by arrows. If the input vector, that for which we are trying to compute the Wigner function, is smooth then this oversampling is performed by simple interpolation. In many instances however we are attempting to find distributions for stationary states of the Floquet operator for the KHO with frequency ratio $1/4$. We have shown that under the right conditions the numerically calculated eigenstates are periodic trains of delta functions. In these cases simple interpolation is erroneous. It makes sense that the extra elements in these special cases should be set to zero.

Of course, as is always the case unless otherwise stated, the vectors on which we operate with the FFT must be correctly *fftshifted* before and after operating to give the correct results. This aspect of the algorithm is dealt with in detail in section 4.2.

The Husimi distribution can be defined as

$$H(q', p') = \frac{1}{\pi\hbar} \int dq'' \int dp'' \exp \left[\frac{m\kappa(q'' - q')^2}{\hbar} - \frac{(p'' - p')^2}{\hbar m\kappa} \right] W(q'', p'') \quad (\text{C.3})$$

where κ can be any arbitrary constant [2]. This is nothing more than a 2-dimensional Gaussian smoothing using a minimum uncertainty wave-packet. In order to calculate the Husimi distribution we then calculate the discrete Wigner distribution of the harmonic oscillator ground state, which we denote as W_0 . The Gaussian

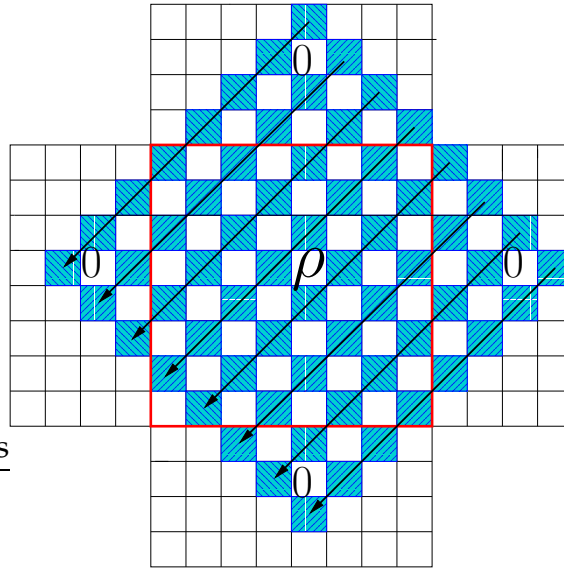


Figure C.1. Schematic showing the how the Wigner function may be calculated from the density matrix ρ . The matrix elements of the density matrix are inside the red square. All other highlighted squares are set to 0. We obtain the correct Wigner distribution by oversampling the highlighted squares by interpolation and then performing a FFT along the vectors indicated by the arrows.

smoothing can be performed by getting the digital convolution of the two Wigner distributions. The convolution can be rapidly performed using the 2-dimensional FFT's via the 2-dimensional convolution theorem [6,7].

$$W * W_0 = F_{\frac{\pi}{2}} \left[F_{-\frac{\pi}{2}} [W] F_{-\frac{\pi}{2}} [W_0] \right]. \quad (\text{C.4})$$

References

- [1] M. Hillery, R. F. O'Connell, M. O. Scully and E. P. Wigner, *Phys. Rep.* **106**, 121 (1984).
- [2] H.-W.Lee, *Theory and application of the quantum phase-space distribution functions*, *Physics Reports* **259**, 147 (1995)
- [3] W. H. Louisell, *Quantum statistical properties of radiation*, (Wiley & Sons 1990).
- [4] M. Engel, *On Quantum chaos, Stochastic Webs and Localization in a Quantum Mechanical Kick system*, Ph. D Thesis(2003)
- [5] R. R. Puri, *Mathematical Methods of Quantum Optics* Springer Series in optical sciences, (Springer-Verlag, Germany 2001)
- [6] R. Bracewell, *The Fourier Transform and Its Applications*, 3rd ed. (McGraw-Hill, New York ,1999).
- [7] <http://mathworld.wolfram.com/Convolution.html>

Declaration

I hereby declare that the work carried out in this thesis is my own except where otherwise stated.

Graham Kells